Assessing the ability of DNA damage response inhibitors to prevent escape from a telomere crisis

A thesis submitted for the degree of Doctor of Philosophy (PhD) by

Angelos Damo

December 2023

Division of Cancer and Genetics

School of Medicine

Cardiff University

Summary

Telomere crisis is a cellular state induced by telomere deprotection and characterised by genomic instability and cell death. Escape from telomere crisis is linked with the development of malignant tumours. Previous work in our lab has demonstrated that inhibition of the PARP1-induced DNA damage response can selectively kill cells undergoing crisis. The aim of this thesis is to examine if inhibition of other DNA damage response pathways can affect the ability of cells to escape a telomere induced crisis and to examine how this would influence cell cycle progression, apoptosis, telomere length and dynamics and DNA damage.

We used colorectal cancer cells expressing a dominant-negative telomerase (DN-hTERT) that undergo a well-defined period of crisis from which they escape and we treated them with DNA damage response inhibitors (RAD51, RAD52, ATR, CHK1, DNA-PK, WEE1, ATM, DNA Ligase I, III and IV). We selected three inhibitors (ATR, CHK1, DNA-PK) and treated primary fibroblasts that undergo a well-defined period of crisis from which they do not escape. We assessed how the inhibitors affected cellular functions before and during crisis.

Among the DNA damage response inhibitors tested, 50nM Rabusertib (CHK1i) consistently prevented cells escaping crisis and 50nM AZD6738 (ATRi) dramatically slowed down escape from crisis in colorectal cancer cells. The inhibitors activated the DNA damage response and they reduced cell growth, increased apoptosis and altered cell cycle progression during crisis. They did not affect the rate of telomere erosion before and during crisis, but Rabusertib increased telomere fusion during deep crisis. Primary fibroblasts undergoing telomere crisis were sensitive to 50nM Rabusertib but not to 50nM AZD6738.

We propose that the ATR-CHK1 pathway is crucial in keeping cells alive during crisis and suggest further clinical evaluation of Rabusertib as a potential treatment for patients with tumours that exhibit short dysfunctional telomeres.

List of Contents

List of Figures

List of Tables

Acknowledgements

I am extremely grateful to my project supervisor Duncan for giving me the opportunity to do this research. I deeply appreciate his guidance, feedback and expertise. I have felt greatly supported by his assistance at every stage of the research project.

I would like to thank Cardiff University and Cancer Research Wales for funding my project.

I would like to say a very big thank you to my supervisor Greg for his mentorship, support, patience and empathy. Our regular interaction allowed me to ask questions, share ideas, discuss the experimental design and receive feedback.

Many thanks to the STELA group: Julia, Kate, Sara, Kez, Kevin and Harsh for being supportive and providing me with assistance throughout my project.

I am grateful to my family for their continued love and encouragement. I greatly appreciate their endless support, faith in my abilities and interest in my project.

I would also like to acknowledge my friends Sania, Liza, Robin, Merula, Alonso, Yassir, Annabel, Carlos, Damjan and Dan for our meaningful experiences and memories during my PhD years.

I dedicate this work to all those who aspire to inspire others and create their own life story.

Abbreviations

ALT: Alternative lengthening of telomeres

A-NHEJ: Alternative non-homologous end joining

ATM: Ataxia telangiectasia mutated protein

ATR: Ataxia telangiectasia and Rad3-related protein

BER: Base excision repair

BFB cycles: Breakage-fusion-bridge cycles

BRCA 1 and 2: Breast cancer gene 1 and 2

CHK1: Checkpoint kinase 1

CHK2: Checkpoint kinase 2

C-NHEJ: Classical non-homologous end joining

DAPI: 4',6-diamidino-2-phenylindole

DDR: DNA-damage response

DMEM: Dulbecco's modified Eagle's medium

DMSO: Dimethyl sulfoxide

DNA: Deoxyribonucleic acid

DNA-PK: DNA-dependent protein kinase

DN-hTERT: Dominant negative hTERT

dNTP: Deoxyribonucleotide triphosphate

DSB: Double-strand break

DSBR: Double-strand break repair

EXO1: Exonuclease 1 protein

G1 phase: Growth phase 1

G2 phase: Growth phase 2

H2AX: H2A histone family member X

HCl: Hydrochloric acid

HDR: Homology-directed repair

HR: Homologous recombination

hTERT: Human telomere reverse transcriptase

kDa: kilodalton

LIG: DNA ligase

LOH: Loss of heterozygosity

M phase: Mitosis phase

MMEJ: Microhomology-mediated end joining

MMR: Mismatch repair

MRE11: Meiotic recombination 11 protein

NER: Nucleotide excision repair

PD: Population doubling

RAD51: DNA repair protein RAD51 homolog 1

RAD52: DNA repair protein RAD52 homolog

Rb: Retinoblastoma

ROS: Reactive oxygen species

S phase: Synthesis phase

SSBR: Single-strand break repair

ssDNA: Single-strand DNA

STELA: Single telomere length analysis

TEN buffer: Tris-EDTA-NaCl buffer

t-loop: Telomeric loop

TMEJ: Theta-mediated end joining

TMM: Telomere maintenance mechanism

TP53: Tumour protein 53

TRIS: Trisaminomethane

WT: Wild-type

γH2AX: Phosphorylated H2AX

Chapter 1

Introduction

1.1 Telomeres

A telomere is a structure of DNA and proteins that cap the end of eukaryotic linear chromosomes (Giardini et al, 2014). Its name originates from the Greek nouns τέλος (telos), meaning 'end' and μέρος (meros), meaning 'part'. Its role is to prevent the ends of chromosomes from being recognised as double-strand DNA breaks, hence preventing the activation of the DNA damage response, which would lead to fusions between chromosomes and genomic instability (Jafri et al, 2016). They are important for cellular survival and they drive the health span and propagation of the species (Chakravarti et al, 2021). Their loss of function has been linked with ageing, progeria syndromes, inflammatory diseases and carcinogenesis (Fouquerel and Opresko, 2017). Dysfunction in genes that maintain telomeres are associated with germline and somatic diseases like dyskeratosis congenita, ulcerative colitis and idiopathic pulmonary fibrosis (Chakravarti et al, 2021).

Telomeres are composed of repetitive G-rich DNA sequences, such as the sequence 5'-TTAGGG-3' in vertebrates, tandemly repeated into arrays of several kilobases in length and they display considerable length variation within human tissues (Giardini et al, 2014; Chakravarti et al, 2021). They are made of 1-20 kb of double-strand repeats and terminate at the 3' end in a single-strand overhang of approximately 50-200 nucleotides in humans. The telomeric DNA folds back on itself to create a structure that resembles a lariat called the Telomere loop or T-loop (Jafri et al, 2016; Fouquerel and Opresko, 2017; Nassour et al, 2021). Telomere length varies considerably between individuals, with heritability established by numerous studies and also exhibits variability across diverse human tissues (Demanelis et al, 2020; Barrett et al, 2015). A multimer of six protein subunits (TRF1, TRF2, TPP1, POT1, TIN2 and RAP1) forms the shelterin complex. This complex binds to telomeres and acts to suppress DNA damage repair signalling from the chromosome ends in order to prevent aberrant DNA activity leading to telomere end fusion via homologous recombination or non-homologous end-joining (Shay, 2016; Gunes et al, 2018; Chakravarti et al, 2021). Shelterin also stabilises the tertiary structure of telomeres as TRF2 contributes

to T-loop formation, which protects telomeres by concealing the ends from DDR proteins (Maciejowski and de Lange, 2017; Jafri et al, 2016; Sobinoff and Pickett, 2017). The affinity of shelterin for telomeres relies on three of its components that recognise the TTAGGG repeats: TRF1, TRF2 and POT1. TRF1 and TRF2 bind the double stranded region of telomeres and recruit TIN2 and RAP1 respectively. POT1 binds to the single-stranded 3' overhang with oligonucleotide-/oligosaccharide-binding folds to protect it (Sobinoff and Pickett, 2017; Nassour et al, 2021). A bridge connecting the single and double-stranded regions of the telomeres is formed by POT1, TPP1 and TIN2 interaction (Nassour et al, 2021). Shelterin suppresses activation of ATM (via TRF2), ATR (via POT1 and TPP1) and PARP1 and inhibits three double-strand repair pathways: homologous recombination (via RAP1, POT1, Ku70, and Ku80) , classical NHEJ (TRF2 and RAP1) and alternative end-joining (via TRF2, TPP1, and POT1; Ku70 and Ku80) (de Lange, 2018; Nassour et al, 2021). There are other proteins present at telomeres, such as nucleases and helicases that are not part of the shelterin complex, but they have an auxiliary function in maintaining telomere stability (Palm and de Lange, 2008). The shelterin complex also modulates the access and activity of telomerase, an enzyme that elongates telomeres (Mir et al, 2020). Mutations in the shelterin complex have been linked to activation of the DNA damage response at the chromosome ends (Sobinoff and Pickett, 2017; Chakravarti et al, 2021).

Due to the fact that DNA polymerases synthesise DNA in one direction with leading and lagging strands, referred by Olovnikov and Watson as the 'end replication problem', telomeres progressively become shorter by approximately 50 bp with each cell division (Olovnikov, 1996; Giardini et al, 2014). This can be counterbalanced by a ribonucleoprotein enzyme called telomerase, which adds hexameric nucleotide repeats at the end of the chromosomes, using an RNA template (Sobinoff and Pickett, 2017). The telomerase reverse transcriptase (TERT), which is the catalytic component of telomerase, creates a complex with the telomerase RNA component (TERC), which acts as a template for addition of telomeric repeats (Shay and Wright, 2019; Roake and Artandi, 2020). Telomerase is highly expressed in germ cells and undifferentiated stem and progenitor cells found in tissues such as skin, intestine, haematopoietic system, hair bulge and testes (Chakravarti et al, 2021). Unlike the stem cells of proliferating tissues which highly express telomerase, somatic cells do not express sufficient levels of the enzyme. This means that telomeres in these cells

erode with ongoing cell division, resulting in the loss of telomere function and imposing a limit on the number of times that cells can divide (known as the Hayflick limit). This is because the loss of telomere function at a few chromosome ends in a cell is sufficient to trigger replicative senescence, characterised by the absence of net growth (Maciejowski and de Lange, 2017; Capper et al, 2007; Nassour et al, 2021). This might have evolved as a tumour suppressive mechanism in long lived species, as almost all human cancers exhibit elevated expression of telomerase (Roake and Artandi, 2020). Telomerase is active during early human development but is inactivated between 12 and 18 weeks of gestation, probably due to alternative splicing of TERT and epigenetic alterations (Shay and Wright, 2019). Germline mutations in genes resulting in reduction of telomerase activity, cause diseases such as dyskeratosis congenita, aplastic anaemia and idiopathic pulmonary fibrosis, so cells need to express a specific amount of telomerase, which is low enough to reduce the chance of cancer, but enough to preserve tissue homeostasis (Roake and Artandi, 2020).

When telomeres become too short due to incomplete replication, they are not able to sustain the T-loop structure and the chromosomal ends are exposed as substrates to the DNA damage response machinery (Nassour et al, 2021). A model proposed by Cesare and Karlseder (2012) suggests that linear telomeres can exist in either an ‘intermediate state’ or an ‘uncapped state’. These linear telomeric states can lead to at least two growth plateaus which aim to prevent cell proliferation and act as barriers to malignant transformation: a growth plateau that is characterised by p53-dependent G1/S cell cycle arrest (replicative senescence) and another which is characterised by cell death (telomere-driven crisis) (Cesare and Karlseder, 2012). Telomeres in an ‘intermediate state’ are in a partly protective state as chromosome ends are exposed to DNA damage response factors but TRF2 still inhibits non homologous end joining (replicative senescence). However, telomeres in an ‘uncapped state’ are no longer protected by TRF2 which results in end-to-end fusions (telomere-driven crisis).

1.2 Replicative senescence

The first barrier to cell proliferation is replicative senescence, which is activated when one or more telomeres are identified as broken DNA ends. Senescence is a tumour-protective mechanism which prevents cells with considerable DNA damage to continue dividing (Nassour et al, 2021). Activation of oncogenes, DNA double-strand breaks, oxidative stress,

nutrient deficiency, epigenetic alterations and telomere dysfunction are all thought to trigger senescence (Kumari and Jat, 2021). Replicative senescence is activated by telomere shortening due to the end replication problem and senescent cells exhibit heterogeneity in their telomere length profiles, suggesting that just a few telomeres can drive the onset of senescence (Harley et al, 1990). Baird et al (2003) showed that telomeres at senescence were less than 4kb and some were nearly devoid of telomere repeats. They also demonstrated that telomere erosion at each telomere happens due to end replication, combined with occasional mutations such as telomere deletion events. This results in cells with both shorter telomeres, inducing replicative senescence, and longer telomeres. Deckbar et al (2007) showed that one double-strand break is enough to activate cell cycle arrest.

Replicative senescence is characterised by irreversible cell cycle arrest, predominantly in G1 phase and is activated by two main pathways: the p53/p21 and p16/RB pathways (Chakravarti et al, 2021). Both pathways are interlinked and they maintain senescence by altering gene expression, since p53 and pRB are transcriptional regulators (Kumari and Jat, 2021). In the p53/p21 pathway, once p53 is phosphorylated and activated, it upregulates p21. This, in turn, suppresses CDK2, leading to phosphorylation of RB, which binds to cell cycle regulator E2F resulting in cell cycle arrest (Gonzalez-Gualda et al, 2020). In the p16/RB pathway, p16 suppresses the CDK4-CyclinD complex leading to the dephosphorylation and stabilisation of the RB-E2F complex and suppression of the cell cycle (Gonzalez-Gualda et al, 2020). p53, p21, p16, pRB are the four most important components of the pathways and overexpression of any of these factors is enough to promote senescence (Kumari and Jat, 2021).

Senescent cells remain metabolically active and are resistant to some apoptotic signals, probably by upregulation of BCL-W and BCL-XL, as inhibiting them was shown to activate apoptosis in senescent cells (Nassour et al, 2021). When expression of these antiapoptotic Bcl-2 members is elevated, the release of cytochrome C is inhibited and as a result, the apoptosome, which induces intrinsic apoptosis, cannot assemble (Gonzalez-Gualda et al, 2020). Senescent cells also generate a range of immune and inflammatory mediators, referred to as Senescence-Associated Secretory Phenotype (SASP), which includes cytokines, chemokines, growth factors, metalloproteases and extracellular vesicles (Gonzalez-Gualda

et al, 2020). These factors can impact neighbouring cells by activating cell-surface receptors and signal transduction pathways that may contribute to cancer (Coppe et al, 2010). Some of the tumour-promoting effects of the SASP include the promotion of epithelial cell proliferation, migration, invasion and alteration of the differentiation status of surrounding cells (Coppe et al, 2010). In addition to these deleterious effects, SASP factors play a role in eliminating unnecessary cells during development and participating in tissue repair (Ohtani, 2022). Morphologically, senescent cells increase in size, which is thought to delay protein diffusion and binding needed for translation, because of cytoplasmic dilution. Hence, this process is thought to contribute to cell cycle arrest (Neurohn et al, 2019). Other morphological changes include multinucleation and granularity, which is likely because of the increase in the size and number of lysosomes (Kumari and Jat, 2021).

Senescence is a mechanism which can be beneficial for the health of an organism by promoting tumour suppression, wound healing and tissue homeostasis. However, the accumulation of senescent cells can promote aging and age-related diseases, such as atherosclerosis, diabetes, lung disease and cardiovascular diseases, via two mechanisms (Chakravarti et al, 2021). In the first mechanism, the replicative potential of tissue stem cells, immune cells and stromal cells is compromised and in the second mechanism, release of pro-inflammatory factors, such as IL-6 and TFN-α by senescent cells impairs organ function (Chakravarti et al, 2021).

1.3 Telomere crisis

When cells fail to undergo cell cycle arrest required for replicative senescence due to mutations in the p53/RB pathway, they keep dividing until the telomeres become critically short, after approximately 15-20 cell division cycles (Jafri et al, 2016; Gunes et al, 2018). As already mentioned, shelterin shields telomeres from activation of DNA damage signalling by ATM, ATR and PARP1, as well as DNA repair through homologous recombination, non-homologous end joining and alternative end joining. However, cells that continue dividing past replicative senescence have very short telomeres, with some ends eroded to subtelomeric regions, and they are unable to bind shelterin, thus they are no longer protected (Nassour et al, 2021; Capper et al, 2007).

These cells enter a second proliferation barrier, which is called a telomere-driven or replicative crisis. This state is characterised by a balance between signals of cell death and cell division and aims to eliminate cells from the population that have escaped replicative senescence (Jafri et al, 2016; Counter et al, 1992). While these cells have lost their p53 and RB pathways, they utilise other pathways, including the cGAS-STING DNA-sensing pathway, to induce cell death (Nassour et al, 2021). Telomere crisis is characterised by shorter (uncapped) and more linear chromosomes than senescence and a delayed progression to mitosis that involves activation of the spindle assembly checkpoint, where Aurora B-mediated removal of TRF2 amplifies telomere dysfunction, resulting in cell death (Nassour et al, 2021; Hayashi et al, 2015).

Autophagy is believed to play an important role in cell death during crisis, as cells undergoing crisis show biochemical and morphological characteristics of autophagy, such as a build-up of autophagic vacuoles, increased autophagic flux and enhanced expression of autophagy-related proteins (Nassour et al, 2021). The cGAS-STING DNA-sensing pathway is activated by the release of nuclear DNA from critically short telomeres in the cytosol. In combination with telomeric-repeat-containing RNA (TERRA), this process activates Z-DNA binding protein 1 (ZBP1), which in turn, activates the innate immune adapter protein mitochondrial antiviral-signalling protein (MAVS), leading to an interferon response and cell death by autophagy (Nassour et al, 2019; Nassour et al, 2023).

While shortening of telomeres can lead to proliferation arrest via telomere crisis and exert anti-tumour activity, it may also encourage cancer growth through a state of enhanced genomic instability. This instability arises from various mechanisms, including deletions, amplifications, translocations, the creation of dicentric chromosomes, chromothripsis and kataegis (von Morgen and Maciejowski, 2018). When telomere crisis is induced, the DNA repair pathways are activated at the termini of the chromosomes, leading to chromosome fusions between sister chromatids and the formation of dicentric chromosomes (von Morgen and Maciejowski, 2018). The dicentric chromosomes will continue through mitosis and lead to breakage-fusion-bridge cycles (BFB cycles) through production of anaphase bridges with successive chromosome breakage (Chakravarti et al, 2021). BFB cycles can result in three outcomes that play a role in cancer: loss of heterozygosity (LOH), non-reciprocal translocations and gene amplification. LOH can happen after breakage of a

dicentric chromosome, where one of the daughter cells inherits a chromosome with a terminal deletion and non-reciprocal translocations can happen when fractured chromosomes are repaired by a DNA repair mechanism known as Break-induced replication (Anand et al, 2013; Maciejowski and de Lange, 2017). Gene amplification can happen through multiple BFB cycles between sister chromatids, resulting in multiple amplicons of inverted repeats (Lo et al, 2002). Chromothripsis involves the fragmentation of chromosomes and the ligation of the fragments in a random way, probably through c-NHEJ, in a single event and has a frequency of over 50% in several cancer types (Cortes-Ciriano et al, 2020; von Morgen and Maciejowski, 2018; Nassour et al, 2021). Maciejowski et al (2015) suggested that chromothripsis may be triggered by TREX1-regulated resection and fragmentation of dicentric chromosomes through repair. Cleal et al (2019) proposed that chromothripsis induced during telomere crisis is caused by a replicative repair process that performs template switching by using microhomology and error-prone DNA polymerases. Kataegis involves clusters of cytosine mutations which are probably caused by cytosine deamination catalysed by APOBEC3 (Nik-Zainal et al, 2012). In addition, endoreduplication and mitotic failure during telomere crisis, when the p53 and Rb pathways are inactive, can trigger tetraploidisation, which promotes tumorigenesis in early cancers (Davoli and de Lange, 2012).

1.4 Telomere crisis and cancer

1.4.1 Escape from crisis

A very small percentage of cells (approximately 1 in 10,000-10,000,000 cells) undergoing a telomere crisis escape and are able to continue their growth gaining cellular immortality (Jafri et al, 2016) (figure 1.1). Loss of autophagy is likely to trigger escape from crisis (Nassour et al, 2019). When the cGAS-STING pathway is inactivated, cells avoid cell death by autophagy and continue dividing to escape crisis. These cells enter one last barrier to cancer development, which is defined by extensive cell death (Nassour et al, 2021). To overcome this, cells rely on two pathways to achieve cellular immortality: telomerase reactivation and alternative lengthening of telomeres.

Escape from telomere crisis is associated with the development of malignant tumours, as telomerase has been found to be expressed in 85-90% of malignant cancers (Shay, 2016). Lin et al (2010) showed that the recurrence of short telomeres and fusions increased as chronic lymphocytic leukaemia progressed, highlighting the role of a telomere crisis in cancer progression. Norris et al (2019) also showed that telomere length is predictive of progression free survival and overall survival in chronic lymphocytic leukaemia, as patients with shorter telomeres showed poorer prognosis. Overall, telomere erosion is linked to increased tumorigenesis, particularly when the p53 pathway is not functional, by enabling genetic and epigenetic changes that will permit cells to escape crisis and progress to cancer (Nassour et al, 2021; Artandi et al, 2000). Telomere shortening marks the transition of premalignant condition to malignant cancer (Gunes et al, 2018) and activation of telomerase contributes to malignant progression (Chakravarti et al, 2021).

1.4.2 Telomere maintenance mechanism activation

The re-activation or increase of the telomerase reverse transcriptase (TERT) is essential for the escape of the cells from telomere crisis, because it lengthens telomeres by synthesizing new telomeric nucleotide repeats and restores their function (Barthel et al, 2017). Telomerase activation is thought to occur by mutations in the TERT promoter, which contributes to healing the shortest telomeres (Chiba et al, 2017). In addition, mutations close to the binding site for the MYC-MAC-MAD1 family of proteins are also associated with telomerase activation (Mitchell et al, 2018). Alternative splicing of the TERT gene, gene amplification of TERT and epigenetic changes are also among the mechanisms that can activate telomerase (Shay, 2014). c-MYC can bind the TERT promoter and lead to TERT transcription and increase of its activity, as can WNT signalling with the help of KLF4 (Chakravarti et al, 2021). The cells that have escaped telomere crisis have a functional telomerase that can replenish telomeres and a highly altered genome with potentially tumorigenic properties (von Morgen and Maciejowski, 2018).

It should be noted that there is also an alternative mechanism to extend telomeres called alternative lengthening of telomeres (ALT), which is based on homologous recombination, it is observed in approximately 10-15% of tumours and it is correlated with a poor prognosis

(Dilley and Greenberg, 2015). ALT cells utilise two repair pathways, RAD51-dependent homologous recombination and RAD52-dependent homology directed repair (Hoang and O'Sullivan, 2020). Other crucial components of ALT include MRE11, RAD50, NBS1, FEN1, MUS81, and FANCD2 (Chakravarti et al, 2021). Alterations in telomeric chromatin assist accessibility of telomeres and recombination, contributing to ALT. The decrease of the histone chaperone ASF1 promotes ALT in cells expressing telomerase and possessing long telomeres (O'Sullivan et al, 2014). While ALT is significant in promoting tumorigenesis when telomerase is inactive, it is less likely to promote aggressive malignancy and metastasis (Chakravarti et al, 2021). Interestingly, Hu et al (2012) showed that telomerase inactivation in lymphoma cells initially led to reduced growth with re-establishment of crisis, but growth resumed as tumours switched to utilising ALT to maintain their telomeres.

Approximately 22% of 6,835 studied cancers do not show evidence of any telomere maintenance mechanism (TMM), either due to detection limitations or the absence of additional TMMs (Barthel et al, 2017). It is possible that these tumours have not undergone telomere crisis or in some cells, epigenetic or genetic alterations are sufficient to drive tumorigenesis without activation of a TMM (Nassour et al, 2019). This raises questions about whether TMM activation is an absolute requirement for escaping crisis. Overall, for the transition of normal cells to cancerous cells lots of genetic and epigenetic events take place, such as inactivation of tumour suppressors and activation of proto-oncogenes in a multistep process (Nassour et al, 2021). Nassour et al (2021) suggest that besides TMM activation, cells escape crisis by suppressing autophagy or the cytosolic DNA-sensing pathway to avoid cell death, although the mechanisms are not yet understood.

A

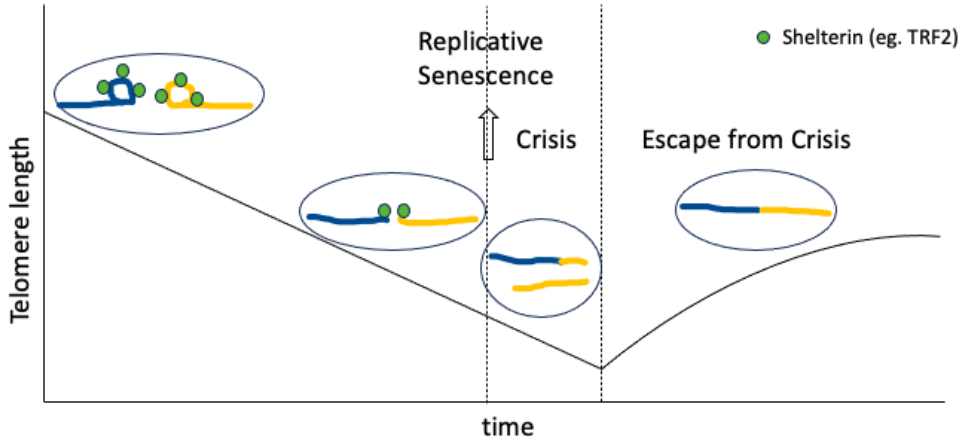

B

Characteristic	Replicative senescence	Crisis
Spontaneous escape	No	Yes
Activation of p53/Rb pathways	Yes	No
G1 cell cycle arrest	Yes	No
Fused telomeres	No	Yes
Genomic Instability	No	Yes

Figure 1.1 Senescence and Crisis A. When telomeres are long, they are protected by shelterin and are resistant to DNA damage repair. When telomeres become critically short, the p53 and Rb pathways are activated leading to senescence, which is characterised by irreversible cell cycle arrest. At this stage, the telomeres are still protected from fusion. Bypass of senescence by suppression of p53 and Rb pathways leads to further cell division and erosion of telomeres. This triggers crisis, a state characterised by telomere fusion, genomic instability and extensive cell death. Escape from crisis by the activation of a telomere maintenance mechanism results in the progression of a malignant phenotype due to acquired genomic instability. B. Summary of characteristics of human fibroblasts in replicative senescence compared to crisis. Adapted from Karlseder 2020; Narita 2019; Nassour et al, 2021.

1.5. The DNA Damage Response

1.5.1 Introduction

Although the DNA is a stable molecule, DNA damage happens continuously in our cells due to endogenous and exogenous factors. Because of that, they have evolved a DNA damage response, which contains multiple highly coordinated interconnected pathways crucial to cell survival (Pilie et al, 2019). The DNA damage response (DDR) is a network of signalling pathways that are activated after the detection of DNA damage and serve to preserve genome stability by increasing the likelihood of DNA being passed on intact to the following

generation (O'Connor, 2015). Different outcomes after DDR is activated include transient cell cycle arrest, apoptosis, senescence, chromatin remodelling, transcription, pre-mRNA splicing modifications, differentiation and DNA repair (Matt and Hoffman, 2016). DNA damage can occur as mismatches during replication, single-strand breaks (SSBs), which are relatively easy to repair and double-strand breaks (DSBs), which are more lethal (Pilie et al, 2019). Single-strand breaks, DNA lesions and mismatches can be repaired via the base excision repair, nucleotide excision repair and mismatch repair pathways (Huang and Zhou, 2021).

DSBs can occur from replication errors, reactive oxygen species or ionising radiation (Cannan and Pederson, 2016). There are two major pathways that are activated after the induction of DSBs: homologous recombination repair (HRR) and non-homologous end joining (NHEJ). HRR is dependent on a sister chromatid and is slower and more accurate, while NHEJ is independent of a homologous template, is faster, less accurate and prone to cause DNA re-arrangements (Moynahan and Jasin, 2010; Lieber, 2010). NHEJ includes two pathways: classical NHEJ and alternative end joining, also known as microhomology-mediated end joining (MMEJ), which encompasses theta-mediated end joining (TMEJ) (Pismataro et al, 2023). The DSB DNA repair pathway choice is dependent on the cell cycle stage, as cells in G1 phase do not have a sister chromatid to perform HRR, thus, NHEJ is the predominant repair mechanism (O'Connor, 2015). HRR is restricted to the S and G2 phases of the cell cycle, when sister chromatids are available (Mjelle et al, 2015). While NHEJ and HRR are both repressed during mitosis, MMEJ is the predominant DSB repair pathway, facilitated by RHINO accumulation promoting Polθ recruitment to DSBs (Brambati et al, 2023). In addition, NHEJ is inhibited at replication forks because when they collapse during S phase, they have one-ended DSBs and by linking DNA ends on different chromosomes, NHEJ would produce chromosomal rearrangements (Groelly et al, 2022). In this case, cells use HRR to repair DSBs at replication forks (Nickoloff et al, 2021).

Another important component of the DNA damage response is DNA damage checkpoint activation. G1/S checkpoint ensures the DNA damage is repaired before DNA replication, with the key regulators of this checkpoint being ATM, CHK2 and p53. The intra-S phase checkpoint delays start of replication in case of unrepaired DNA, using checkpoint factors ATR, CHK1, and WEE1 (O'Connor, 2015). G2/M checkpoint delays mitosis in case of

unrepaired or under-replicated DNA, with CHK1, MYT1 and WEE1 being key factors in this stage (O'Connor, 2015). Overall, some of the most crucial kinases in DDR are ATR and ATM, which are the kinases that regulate the response to DSBs and replication stress by phosphorylating many downstream targets (Pilie et al, 2019; Huang and Zhou, 2021).

1.5.2 Base excision repair

Base excision repair (BER) is activated in response to small DNA lesions that do not distort the DNA helix. In this pathway, a DNA glycosylate such as OGG1, an enzyme that identifies mutated bases in DNA, breaks the bond between the mutated base and deoxyribose (Choi and Lee, 2022). Following this, an apurinic or apyrimidinic site is created and is detected by AP endonuclease (APE1), which cleaves the phosphodiester backbone (Beard et al, 2019). This generates a SSB intermediate with a 3'-hydroxyl and 5'-deoxyribosephosphate (dRP) end (Abbotts and Wilson, 2018). Then, the dRP is deleted, PARP1 and XRCC1 drive the gathering of repair factors, Pol β fills the gaps and DNA ligase I or III performs the ligation in a process known as short patch or single-nucleotide BER, because it incorporates one nucleotide (Choi and Lee, 2022). There is an alternative process called long-patch BER that repairs and incorporates more than one nucleotide (2-12 nucleotides) and mostly takes place in proliferating cells. This process requires replication proteins after APE1 cleavage, such as RFC, PCNA, Pol ε and δ, FEN and LIG1 (Abbotts and Wilson, 2018). While the factors that determine the choice between short patch or long patch are not fully understood yet, the initiating glycosylate, the cell cycle phase, the replicative status of the cell and the ATP concentration are thought to play an important role (Abbotts and Wilson, 2018). BER is not an isolated repair pathway, as it interacts with other pathways and may even be regulated by them. Its deregulation could increase risk for cancer, aging-related diseases and other disorders (Huang and Zhou, 2021).

1.5.3 Single-strand break repair

Single-strand break repair (SSBR) is a DNA repair mechanism that repairs single-strand breaks (SSBs), which are discontinuities in one of the two DNA strands and can lead to genetic instability or cell death (Caldecott, 2008). SSBs are detected by PARP1, which binds to the 5'- hydroxyl DNA end and recruits XRCC1. XRCC1 functions as a scaffolding protein for SSBR factors, such as polynucleotide kinase phosphatase (PNKP) (Mei et al, 2020). PARP1

also binds to TDP1 and forms a TDP1-PARP1 molecular complex which releases the 3'-phosphate ends (Caldecott, 2008). PNKP hydrolyses the 3'-phosphate end and phosphorylates the 5'-hydroxyl end. Gap filling via short-patch or long-patch repair is performed and the nicks are sealed by ligation (LIG3 or LIG1) (Mei et al, 2020). If SSBs are not repaired in time, DNA replication forks during S phase collapse or become blocked, which produces DSBs (Mei et al, 2020). These DSBs will probably be repaired by homologous recombination, but SSB increase may saturate this pathway, resulting in genetic instability (Caldecott, 2008).

1.5.4 Nucleotide excision repair

Nucleotide excision repair (NER) is another more complex pathway to repair bulky DNA lesions that distort the DNA helix and it is mostly activated by chemical compounds or UV radiation (Choi and Lee, 2022). It corresponds to two different pathways: global genome repair NER (GG-NER), which happens anywhere in the genome and transcription-coupled NER (TC-NER), which repairs DNA in the transcribed strand of genes (Choi and Lee, 2022). In GG-NER, the DNA lesions are identified by XPC in complex with RAD23B and CERN2 and when the XPC complex binds to the damaged site, RAD23B detaches from the complex (Merteijn et al, 2014). In TC-NER, the lesions are identified by RNA polymerase II when it stalls at the lesion and the CSA-CSB complex is formed, which leads to reverse translocation of RNA polymerase II, making the damaged site accessible for repair (Merteijn et al, 2014). In both pathways, TFIIH is recruited to the lesion, XPG binds to pre-incision NER complex and the helicase activity of TFIIH unwinds the double helix close to the lesion, confirming the presence of DNA damage (Merteijn et al, 2014). Then, RPA is recruited to coat the non-damaged strand, XPA recruits the XPF-ERCC1 heterodimer which cuts 5' to the lesion and XPG is activated and cuts 3' to the lesion, resulting in the removal of the lesion within the strand, typically spanning 22 to 30 nucleotides (Merteijn et al, 2014). Then, PCNA recruits DNA polymerase δ, κ and ε to fill the gap of nucleotides and DNA ligase I or DNA ligase III complete the reaction by sealing the nick (Merteijn et al, 2014). Deficiency of NER is correlated with predisposition to cancer, neurodevelopmental diseases and xeroderma pigmentosum (Choi and Lee, 2022).

1.5.5 Mismatch repair

Mismatch repair (MMR) is a process that repairs replication errors, enhancing the fidelity of DNA replication (Huang and Zhou, 2021) and its main role is to rectify spontaneous base mispairing and small insertions-deletion loops (Pecina Slaus et al, 2020). In this pathway, the MSH2-MSH6 heteroduplex identifies the mismatch or the insertion and binds to the DNA at the damaged site (Huang and Zhou, 2021). The heterodimer MLH1-PMS2, PCNA and RFC are recruited to the complex to promote endonuclease activity of MS2, which creates SSBs close to the mismatch (Pecina Slaus et al, 2020). The nicked DNA generates entry sites for Exonuclease 1, which performs excision of the strand containing the mismatched bases generating a ssDNA and RPA binds to it to prevent its degradation (Pecina Slaus et al, 2020). The DNA is then re-synthesised by DNA polymerase δ and DNA ligase I performs the ligation (Huang and Zhou, 2021). When the MMR pathway is deficient, the rate of secondary mutations is elevated by 100 up to a 1000 times (Huang and Zhou, 2021).

1.5.6 Double-strand break repair

1.5.6.1 Homologous Recombination

As already mentioned, HR requires a homologous template for repair and is a more accurate pathway. It can be divided into different sub pathways, but the first steps are similar and require common factors. In this pathway, following the presence of a DSB break, nucleases such as the MRN complex (Mre11, Rad50 and Nbs1), together with CtIP, degrade the 5' ends of the DSBs through DNA-end resection, to create two 3' ssDNA overhangs, which are coated by RPA (Elbakry and Lobrick, 2021). RAD51 replaces RPA on ssDNA in a step that is facilitated by BRCA1 and BRCA2, as the latter loads RAD51 to the ends (Huang and Zhou, 2021). RAD51 forms a nucleoprotein filament which contributes to identification, binding and invasion to the homologous double-strand DNA and the formation of a displacement loop (D-loop) with the help of PALB2 and RAD51AP1 (Groelly et al, 2022). Then, DNA is synthesised across the break using the sister chromatid as a template.

DNA-end resection is strictly regulated because of its essential role in ensuring error-free HR (Zhao et al, 2020). It happens during S and G2 phase by phosphorylation of CtIP, although it can happen in G1 phase when breaks occur in the ribosomal or centromeric DNA (Groelly et al, 2022). The newly formed ssDNA is elongated through the action of nucleases and DNA

helicases, such as EXO1, DNA2 and BLM (Zhao et al, 2020). The 9-1-1 checkpoint clamp complex orchestrates resection by either promoting it, recruiting both DNA2-SGS1 and EXO1 to resection sites, or by recruiting an inhibitor (Ngo et al, 2014; Ngo and Lydall, 2015). The MRN complex contributes to the recruitment and activation of ATM at DSB sites, which leads to the phosphorylation of multiple factors involved in the DDR (Sun et al, 2020). RAD51 is a major molecule of the HR pathway, as it drives the formation of D-loops to promote DNA synthesis (Huang and Zhou, 2021). Once the DNA is synthesised, there are at least three different sub-pathways that can be used. In the first pathway, the invading strand can be displaced and anneal to the complementary strand and this is referred to as synthesis-dependent strand annealing (SDSA) (Krejci et al, 2012). In the second pathway, the second end of the DSB can be used to stabilise the D-loop structure, generating a structure called double-Holliday junction (dHJ) (Krejci et al, 2012). In the third pathway, which is termed break-induced replication (BIR), DNA is synthesised from the invading one-ended DSB end without the requirement of the second end (Elbakry and Lobrick, 2021).

1.5.6.2 Non-homologous end joining

As mentioned, NHEJ does not require a homologous template and even though it is accurate most of the times, it can be mutagenic. While it causes loss of nucleotides at the ligated site, changing the sequence, most DSBs in human cells are repaired by this pathway (Huang and Zhou, 2021). In this pathway, DSBs are recognised by Ku70-Ku80 heterodimer, which binds with a high affinity to the broken ends via its central domain (KU core). Ku70-80 complex protects DNA ends from degradation and recruits DNA-PKcs (Ghosh and Raghavan, 2021). DNA-PKcs interacts with KU80, which enhances the DNA-binding affinity of DNA-PKcs and it forms the DNA-PKcs/Ku/DSB complex (Ghosh and Raghavan, 2021). It also recruits ARTEMIS, PNKP, APE1, TDP1 and the XRCC4-XLF-LIG4 complex. Following activation, DNA-PKcs is auto-phosphorylated and phosphorylates Artemis nuclease, resulting in its activation (Huang and Zhou, 2021). End resection is catalysed by endonuclease Artemis and DNA polymerases μ and λ add nucleotides to the DNA ends (Huang and Zhou, 2021). Ligation of these DNA ends is catalysed by DNA ligase IV, the only eukaryotic ligase involved in NHEJ, and XRCC4. This step also utilises two additional factors, XLF and PAXX (Groelly et al, 2022). XRCC4 has no enzymatic activity but functions as a scaffold protein, stabilises DNA ligase IV and drives its activity by promoting its adenylation (Ghosh and Raghavan, 2021). XLF plays an important

role in NHEJ as it drives the ligation of numerous mismatched ends whereas 53BP1 promotes the terminal linking of DNA (Ghosh and Raghavan, 2021).

1.5.6.3 Alternative end joining

Alternative end joining, also known as microhomology-mediated end joining (MMEJ) is essential for the survival of cells with impaired HR and NHEJ and contributes to genomic instability, particularly at telomeres (Jiang, 2022; Brambati et al, 2023). It is a mutagenic process and is associated with the production of chromosomal deletions and translocations (Ghosh and Raghavan, 2021). It is similar to classical NHEJ, but without relying on the NHEJ factors (DNA-PKcs, Ku70 and DNA ligase IV) and requires a microhomology region of 4 to 25 bp (Huang and Zhou, 2021). PARP1, which competes with Ku for DNA binding, binds to the DSB ends and the MRN complex or CtIP perform DNA resection, which leads to a 3' ssDNA tail that can anneal with the microhomologous sequence (Ghosh and Raghavan, 2021). The annealing process is not well-understood and results in the annealed DNA and 3' flaps, which are cleaved by XPF/ERCC1 and FEN1 (Ghosh and Raghavan, 2021). The flap removal results in DNA sequence loss, Polθ extends annealed intermediates and DNA ligase III/XRCC1 performs the ligation of the ends (Huang and Zhou, 2021). Polθ, encoded by the POLQ gene, is central to MMEJ and its mutagenic effects contribute to genomic alterations (Brambati et al, 2020). During the M phase, the activity of MMEJ is aided by the accumulation of RHINO, which promotes the recruitment of Polθ to damage sites (Brambati et al, 2023).

Table 1.1: The table lists some important DDR components and the pathways in which they participate.

DDR molecule	DDR Pathway Network
ATR	ATR-CHK1, HR, NHEJ, NER
RAD52	HR
ATM	ATM-p53, HR, NHEJ
DNA Ligase I (LIG1)	MMR, BER, NER, SSBR, HR
DNA Ligase III (LIG3)	BER, NER, SSBR, NHEJ, HR
DNA Ligase IV (LIG4)	NHEJ
DNA-PK	NHEJ
CHK1	ATR-CHK1, HR, NHEJ, NER
WEE1	ATR-CHK1, HR
RAD51	HR

1.5.7 The DNA Damage Response and cancer

A major hallmark of cancer cells is genomic instability, which is caused by accumulation of mutations in the DNA of dividing cells and the deregulation of DDR machinery (Choi and Lee, 2022). DDR components (table 1.1) can be used by cancer cells to drive their growth via bypassing apoptosis and producing genetic heterogeneity within tumours (Pilie et al, 2019). Interestingly, deficiencies in the DDR machinery can also create therapeutic opportunities. Therapies that target the DDR aim to block cell cycle checkpoints, leading to accumulation of DSBs and enhance replication stress, resulting in an increase in DSBs and subsequent cell death (Pilie et al, 2019). In addition, impairing HR, which is a faithful DDR process means that the cancer cell will rely more on auxiliary error-prone DDR pathways, accumulating further DNA damage (Pilie et al, 2019). A characteristic hallmark of cancer cells is the loss of one or more DDR pathways, which means that cancer cells are mainly dependent on the remaining pathways (Carrassa and Damia, 2017). Inhibition of the active pathways in cancer cells that have lost one DNA repair pathway will kill them, as they cannot use alternative pathways, unlike normal cells which can compensate for the inhibited pathways (O'Connor, 2015; Carrassa and Damia, 2017). This strategy is known as

synthetic lethality. In addition, DDR is activated by cancer cells to reduce the effectiveness of chemotherapy and radiotherapy and can even lead to resistance to cancer therapy after an initial response (Weber and Ryan, 2015). Therefore, DDR pathways appear to be a promising target in cancer research and currently the most studied DDR molecules as therapeutic targets include ATM, ATR, WEE1, CHK1 and DNA-PKcs among others (Jin and Oh, 2019).

Here we describe a successful example of synthetic lethality. The poly(ADP-ribose) polymerase (PARP) family consists of 17 nuclear proteins involved in many DDR pathways and chromatin remodelling. The most well-defined member is PARP1 which has a main role in the identification and repair of SSBs, stabilising replication forks and enlisting the DNA repair machinery (Pilie et al, 2019). Recent studies indicate that it is also involved in many DNA repair pathways, such as NER, classical and alternative NHEJ, HR and DNA mismatch repair (Rose et al, 2020). PARP inhibitors are some of the most well-studied DDR inhibitors with several preclinical and clinical studies for breast, ovarian, prostate and pancreatic cancers being carried out. Currently, olaparib, rucaparib, niraparib, talazoparib, veliparib and AZD5305 are in clinical use or trials (Hopkins et al, 2022). Most PARP inhibitors target PARP1 by competing with nicotinamide (NAD^+) for the catalytically active site of PARP molecules, although they may also inhibit PARP2 and PARP3 (Rose et al, 2020; Nambiar et al, 2023).

Suppressing PARP1/2 increases the formation of SSBs and DSBs during DNA replication (Groelly et al, 2022). BRCA1 and BRCA2 are essential genes for genome stability, as they contribute to accurate DNA repair within the HR pathway, following treatment with DNA-damaging agents. In the absence of DNA damage, they protect stalled replication forks (Groelly et al, 2022). Cells carrying BRCA1/2 mutations cannot perform homologous recombination, leading to accumulation of SSBs and DSBs and rendering them sensitive to PARP inhibitors (Hopkins et al, 2022). The discovery of the synthetic lethal interaction between PARP inhibition and BRCA1/2 deficiency was first shown in 2005 (Bryant et al, 2005) and has given us one of the best characterised examples of synthetic lethality, which offered a promising strategy for cancer therapy (Groelly et al, 2022).

1.6. Targeting the DNA Damage Response

1.6.1. ATM

1.6.1.1 Role of ATM

Ataxia telangiectasia mutated (ATM) is a large serine/threonine kinase (370kDa) and a major initiator of the DNA damage response in mammalian cells (Phan and Rezaeian, 2021). The ATM canonical pathway is activated in response to double-strand breaks. It is recruited to the DNA damage site and binds to the MRN complex, resulting in its conformational change and activation (Carrassa and Damia, 2017). Once activated, it phosphorylates downstream targets, which induce cell cycle arrest or cell death via apoptosis (Phan and Rezaeian, 2021). The ATM pathway is essential for the activation of the G1/S checkpoint, so that cells with damaged DNA do not proceed to the S phase. This is achieved by the phosphorylation of CHK2 by ATM, which, in turn, phosphorylates p53, leading to activation of p21 and facilitating cell cycle arrest (Carrassa and Damia, 2017; Tian et al, 2015). ATM can also be activated by chromatin changes in non-canonical signalling pathways by ATMIN, instead of the MRN complex, leading to phosphorylation of downstream targets (Phan and Rezaeian, 2021).

ATM also takes part in DSB repair by playing a role in the initiation of HR and it is further involved in metabolic regulation, chromatin remodelling and migration (Matt and Hoffman, 2016; Jin and Oh, 2019). It is needed for fork restart and prevention of accumulation of double-strand breaks during normal replication and after external induction of replication stress (Carrassa and Damia, 2017). In addition, it is important in sensing oxidative stress (Guo et al, 2010). Exposure to oxygen or reactive oxygen species (ROS) activates ATM, which activates TSC2, resulting in mTOR signalling and leading to a reduction of ROS levels (Phan and Rezaeian, 2021). ATM (and ATR) is also activated by hypoxia and phosphorylates HIF2α to stabilise it and contribute to cell survival. Following ROS production, ATM also regulates pexophagy, a process that involves the autophagic degradation of peroxisomes, contributing to cellular homeostasis. Lastly, ATM can be activated by starvation or reactive nitrogen species, it regulates mitophagy which is a process involving the elimination of mitochondria and it induces autophagy after being activated by oxidative stress (Phan and Rezaeian, 2021).

ATM signalling interferes with chemotherapy and radiation therapy in cancer cells, as it repairs the damage that has been induced and therefore it is of great importance to inhibit ATM signalling in order to improve response in cancer patients (Jin and Oh, 2019). Hypoxia and elevated ROS commonly develop in solid tumours, meaning that ATM may encourage cancer cell survival by stabilising HIF1α to decrease the amount of ROS (Phan and Rezaeian, 2021). ATM can activate AkT, NF-KB and the pentose phosphate pathway to increase cancer cell survival (Phan and Rezaeian, 2021). ATM signalling is upregulated in some cancer cells (i.e. prostate, pancreatic and melanoma cancer cells), possibly because they have evolved mechanisms to escape apoptosis (Phan and Rezaeian, 2021). Elevated ATM activity is correlated with increased metastasis, invasion and epithelial-mesenchymal transition of breast cancer cells (Phan and Rezaeian, 2021). These findings suggest that inhibiting ATM may be useful for targeting cancer cells.

1.6.1.2 KU-60019 (ATM inhibitor)

Several ATM inhibitors have been developed and studied in both human and animal cancer cells. KU-60019 was developed in 2009 and it is an improved analogue of another ATP-competitive ATM inhibitor (KU-55933), which has similar target specificity with almost no non-specific target effects. However, KU-60019 is more potent and has increased bioavailability, although bioavailability remains relatively weak (Golding et al, 2009). It supressed p53, H2AX and CHK2 phosphorylation and it completely inhibited basal and radiation-induced AKT (S473) phosphorylation, which is performed by ATM, therefore supressing signalling that would lead to survival in several glioma cell lines (Golding et al, 2009). KU-60019 also supresses migration, invasion and growth of human glioma cells, possibly by inhibiting MEK/ERK signalling (Golding et al, 2009).

A study showed that KU-60019 sensitised glioma cells to radiation, while KU-60019 and radiation treatment was not toxic to normal mouse brain tissue outside the radiation field (Biddlestone-Thorpe et al, 2013). The glioma cells that did not have a functional p53 were much more sensitive to KU-60019 compared to wild type cells (Biddlestone-Thorpe et al, 2013). Another study demonstrated that KU-60019 radio-sensitised adult and paediatric glioblastoma-initiating cells with high expression of TP53 and low PI3K activity, with the strongest effect taking place 96hr after delivery of the inhibitor (Vecchio et al, 2015). PTEN is

involved in the DNA repair process and McCabe et al (2015) demonstrated that KU-60019 caused particular toxicity in PTEN-deficient cancer cells in tumour xenografts compared to wild-type cells. Li et al (2018) also reported that KU-60019 made PTEN-deficient MDA-MB-468 breast cancer cells more sensitive to cisplatin, by elevating DNA damage accumulation and increasing apoptosis. KU-60019 entered clinical trials in 2017, with an estimated completion date in 2024, to assess the combination of KU60019 with a CK2 inhibitor in organotypic cultures of Human Renal Tumours (Lavin and Yeo, 2020; Jin and Oh, 2019).

1.6.2 ATR-CHK1 pathway

1.6.2.1 Role of ATR and CHK1

The kinase ataxia telangiectasia and Rad-3 related (ATR) is activated by many types of genotoxic stress and the production of single-strand DNA (ssDNA), which is a result of either stalled and collapsed replication forks (replicative stress) or resected DNA double-strand breaks (Carrassa and Damia, 2017). Replication stress is generated by intrinsic factors, such as reactive oxygen species or external stressors and it occurs when DNA polymerase activity is uncoupled from replisome helicase activity, which results in ssDNA production (Carrassa and Damia, 2017; Neizer-Ashun and Bhattacharya, 2021). ATR is crucial for cell viability and plays an important role in cell cycle arrest and DNA repair by activating CHK1, a Ser/Thr protein kinase which is located downstream of ATR in the same pathway (Carrassa and Damia, 2017). Following the formation of ssDNA, replication protein A (RPA) binds to prevent a break and recruits the RAD17/9-1-1 and ATR/ATRIP complexes (Carrassa and Damia, 2017). The formation of this multi-subunit complex promotes ATR activity, which phosphorylates CHK1 at S317 and S345, leading to CHK1 activation (Zhang and Hunter, 2014). Phosphorylation at S317 is necessary for phosphorylation at S345 and mutation of S345 to Ala caused loss of checkpoints and cell death (Zhang and Hunter, 2014). Phosphorylation of these sites are initiating events and this is followed by autophosphorylation at S296, which is needed for full kinase activity (Neizer-Ashun and Bhattacharya, 2021). It is likely that after CHK1 is activated, it dissociates from the chromatin to phosphorylate its substrates that are mostly in the nucleoplasm (Neizer-Ashun and Bhattacharya, 2021).

ATR and CHK1 supress origin firing, stabilise replication forks and promote their repair (Saldivar et al, 2017). ATR and CHK1 regulate origin firing negatively to prevent its excessive activation even during normal S phase progression (Saldivar et al, 2017). Following replication stress, they block replication origin firing to reduce DNA replication. This is regulated by the phosphorylation and degradation of CDC25A through CHK1 and it allows time for repair (Carrassa and Damia, 2017). Stabilising replication forks entails preserving the ability of stalled polymerases to proceed DNA synthesis after replication elongation is hindered (Saldivar et al, 2017).

The ATR/CHK1 pathway is a mediator of the intra S-phase checkpoint, slowing down DNA synthesis after DNA damage to ensure accurate replication. It is also a mediator of the G2/M cell cycle checkpoint, preventing the entry of cells with incomplete DNA replication or DNA damage into mitosis (Carrassa and Damia, 2017). The arrest in S phase is regulated by Claspin, which aids to bring CHK1 nearby ATR at the replication fork, so it can be phosphorylated (Saldivar et al, 2017). Once activated, CHK1 phosphorylates and inactivates the three CDC25 phosphatases, with CDC25A being the most important target. These phosphatases are responsible for cyclin-CDK activation, a process needed for cell cycle progression (Saldivar et al, 2017). ATR is also involved in other functions, such as inter-strand crosslink repair, meiosis and responds to mechanical and osmotic stress (Saldivar et al, 2017). In addition, ATR activation following telomere shortening contributes to a tumour-suppressive effect by inducing cell proliferation arrest. This effect remains unless the p53 and RB tumour suppressor pathways are compromised, allowing continued growth past the senescence barrier (Maciejowski and de Lange, 2017). CHK1 is important in the mitotic spindle checkpoint, which safeguards the precision of mitotic segregation during mitosis to avoid chromosomal instability and aneuploidy (Carrassa and Damia, 2017). CHK1 also modulates other functions such as embryo development, gene transcription and somatic cell viability maintenance (Zhang and Hunter, 2014). Recent findings have also demonstrated that CHK1 is crucial for regulating hematopoietic stem and progenitor cell development and expansion (Neizer-Ashun and Bhattacharya, 2021).

During DNA replication in human cells, CHK1 is phosphorylated by ATR (Saldivar et al, 2017). Both ATR and CHK1 are active during S phase progression in the absence of DNA damage and inhibiting CHK1 leads to DNA damage during S phase (Carrassa and Damia, 2017). While

CHK1 is essential for arresting cells at the G2 phase following DNA damage, it is not active during the normal G2/M phase transition in the absence of DNA damage or when the damage is repaired (Zhang and Hunter, 2014). However, CHK1 localises to interphase chromosomes to block premature entry to mitosis during normal cell cycle progression (Neizer-Ashun and Bhattacharya, 2021). CHK1 has essential functions in the absence of damage that are not related to its role in the DDR, yet these functions are not well-understood (Neizer-Ashun and Bhattacharya, 2021). ATR activity can also differ depending on the different biological responses. For example, there are particular chromosomal regions called common fragile sites, which need ATR to preserve their stability even during normal replication (Saldivar et al, 2017).

ATR, ATM and DNA-PK share sequence and functional homology, but ATM and DNA-PK are activated mainly by DNA double-strand breaks and are not crucial for cell survival (Saldivar et al, 2017). CHK1 is also involved in homologous recombination by phosphorylating RAD51 (Thr309) leading to its recruitment to the DNA damage site and aiding the interaction between RAD51 and BRCA2 (Carrassa and Damia, 2017). If CHK1 is supressed, the double-strand breaks cannot be repaired by homologous recombination, resulting in cell death. Studies show that the ATR and ATM pathways cross-talk and modulate each other when there is DNA damage to preserve genomic stability by coordinating cell cycle progression with DNA repair (Matt and Hoffman, 2016; Jin and Oh, 2019; Carrassa and Damia, 2017). As ssDNA is often an intermediate of dsDNA breaks, ATM also promotes CHK1 activation by phosphorylation at both S17 and S345 through RPA/ATR-ATRIP complex recruitment (Carrassa and Damia, 2017). Multiple studies have demonstrated that ATM also plays a role in the activation of the intra S-phase and the G2/M cell cycle checkpoints (Weber and Ryan, 2015). In conclusion, ATM and ATR pathways (figure 1.2) partially overlap and if one pathway is defective, the other pathway may compensate (at least to a certain degree) for that loss of function (Weber and Ryan, 2015).

Several studies have shown that ATR loss prevents the activation of the G2/M cell cycle arrest checkpoint, impeding DNA repair and leading to increased sensitivity of cancer cells to ionizing radiation and chemotherapy (Weber and Ryan, 2015). Cancer cells exhibit higher replication stress and therefore, may be more reliant on ATR than normal cells (Saldivar et al, 2017). Because of that, they need to sustain a functional ATR-CHK1 pathway and CHK1

inhibition leads to collapse of the fork as DNA replication is incorrectly initiated from numerous origins (Carrassa and Damia, 2017). CHK1 has been found to be overexpressed in a range of tumours and its expression is positively correlated with the grade of the tumour and shorter overall survival (Zhang and Hunter, 2014). CHK1 also contributes to therapy resistance and findings have shown that increased CHK1 expression provides an advantage in cell survival, as cells are better able to deal with replicative stress (Zhang and Hunter, 2014). These findings suggest that ATR and CHK1 inhibition may be useful for targeting cancer cells with elevated levels of replication stress.

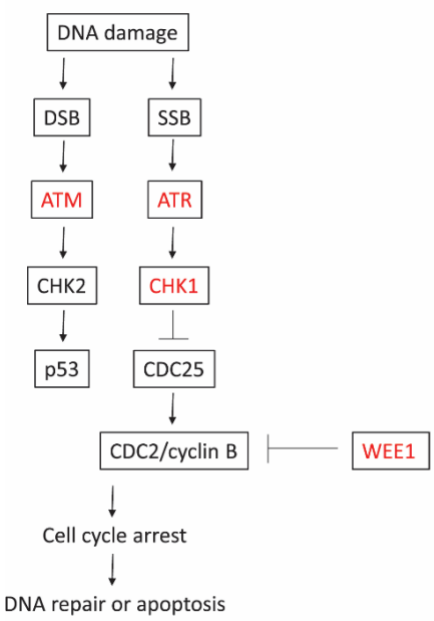

Figure 1.2: A simplified illustration of the ATR-CHK1 and ATM-p53 pathways. ATR is commonly activated by ssDNA breaks and phosphorylates its effector CHK1, while ATM is commonly activated by dsDNA breaks and phosphorylates its effector CHK2. The pathways eventually lead to cell cycle arrest, which allows for DNA repair, or results in apoptosis. Adapted from Weber and Ryan, 2015.

1.6.2.2 AZD6738 (ATR inhibitor)

The first specific ATR inhibitors were reported after some CHK1 inhibitors had already progressed to clinical trials. This delay in their development was due to difficulties in obtaining the pure active form of the ATR kinase and the lack of structural information (Barnieh et al, 2021). AZD6738 is an ATR inhibitor and an improved analogue of AZ20, the first ATR inhibitor to be described with *in vivo* data (Foote et al, 2018). It was developed by AstraZeneca, it is orally administered, it has great solubility and bioavailability and it is highly

potent and selective (Foote et al, 2018). AZD6738 inhibits the G2 checkpoint by supressing activation of ATR and phosphorylation of CHK1 (S345) (Suzuki et al, 2022). P53 deficient cancers are expected to be particularly sensitive to AZD6738 treatment. P53 is the main regulator of the G1/S checkpoint, meaning that cancer cells that are P53 deficient are dependent on CHK1 (which regulates the S and the G2 checkpoint) for survival (Suzuki et al, 2022).

AZD6738 has been extensively studied preclinically across a variety of tumour types. It induced cell death and senescence as a single agent and increased cytotoxicity of cisplatin and gemcitabine in non-small cell lung cancer cells, regardless of P53/ATM status (Vendetti et al, 2015). It also resulted in accumulation of unrepaired DNA damage, cell death by mitotic catastrophe and tumour growth inhibition in ATM and P53-deficient chronic lymphocytic leukemia cells (Kwok et al, 2016). Another study showed that AZD6738 had an intense synergistic cytotoxic effect in B-cell lymphoma when used in combination with both AZD7762 (CHK1i) and Adavosertib (WEE1i), irrespective of the TP53, MYC, and ATM mutational status of the cells (Restelli et al, 2019). When combined with gemcitabine, it increased cytotoxicity in pancreatic ductal adenocarcinoma cell lines (Wallez et al, 2018). Combined treatment of AZD6738 and Adavosertib (WEE1i) led to Triple-Negative Breast Cancer growth inhibition and sensitised cells to chemotherapy (Jin et al, 2018). The increased cell death was ascribed to supressed DNA damage repair, elevated replication stress and mitotic catastrophe.

AZD6738 first entered clinical trials in 2013 and there are numerous phase I and II studies, currently recruiting or preparing to recruit, either as monotherapy or combined with radiotherapy, olaparib, acalabrutinib, gemcitabine, durvalumab, carboplatin and paclitaxel, in a variety of cancers (i.e. breast cancer, small cell lung cancer, ovarian cancer, melanoma, gastric adenocarcinoma and leukaemia) including those that are ATM-deficient (Foote et al, 2018). As most of these trials are currently underway or recruiting, the data is not revealed and the full clinical potential of AZD6738 is not reported yet. However, results so far are encouraging. A phase I study of AZD6738 as monotherapy in advanced solid tumours showed that it was well-tolerated (Dillon et al, 2019). Kim et al (2021) reported that the inhibitor can be safely combined with paclitaxel and this combination showed promising activity against tumours with durable responses (phase I study). A phase II trial showed that

AZD6738 and durvalumab exhibited antitumour activity and durable responses in refractory advanced gastric cancer patients, while common toxicities could be controlled with dose modification (Kwon et al, 2022).

1.6.2.3 Rabusertib (CHK1 inhibitor)

As CHK1 is needed for proliferation, survival and appropriate cell cycle progression, cells with no CHK1 activity are not tumorigenic in general (Gorecki et al, 2021). CHK1 inhibitors for cancer therapy have been investigated for more than twenty years and have longer history than ATR inhibitors (Gorecki et al, 2021). While they have been very promising in preclinical studies, clinical translation has been more challenging. There have been seven CHK1 inhibitors that have entered clinical phases I/II, one of which is Rabusertib. Klaeger et al (2017) established that Rabusertib is by far the most selective CHK1 inhibitor in the panel of CHK1 inhibitors they tested, with high potency and no off-target effects. Treatment with Rabusertib produces a cellular phenotype identical to that deriving from genetic knockdown of CHK1 (King et al, 2014). It reduces CHK1 autophosphorylation on Serine 296 and blocks phosphorylation of CHK1 substrates without supressing direct phosphorylation of CHK1 by ATR (King et al, 2014). Rabusertib was developed by Eli Lilly and Company and completed seven trials, three of which were phase I/II. Completed Phase I studies have evaluated the safety and maximum tolerable dose of Rabusertib when combined with pemetrexed, cisplatin and gemcitabine (Weiss et al, 2013; Calvo et al, 2016; Doi et al, 2015).

Several studies have shown promising results for Rabusertib treatment as monotherapy or in combination with other drugs. CHK1 inhibition with Rabusertib killed specifically both sensitive head and neck squamous cell carcinomas cell lines by apoptosis in S-phase and more resistant cell lines by accumulating chromosomal breaks that are detrimental during mitosis (van Harten et al, 2019). Zhao et al, (2016) showed that treatment with Rabusertib abolished the G2/M checkpoint and raised DNA damage in acute myeloid leukemia cells and combination treatment of Rabusertib and Bcl-2-selective inhibitor ABT-199 increased apoptosis. Alcaraz-Sanabria et al, (2017) demonstrated that Rabusertib combined with alisertib (mitotic aurora kinase A inhibitor) increased apoptosis and decreased the stem cell population in ovarian cancer cells.

While phase I studies showed that Rabusertib was well tolerated when combined with pemetrexed and gemcitabine, phase II trials of Rabusertib combined with these drugs appeared less promising. There was no significant effect in the overall survival of pancreatic cancer patients from a combination treatment of Rabusertib and gemcitabine compared to gemcitabine alone (Laquente et al, 2017). There was also no significant effect in advanced NSCLC patients from a combination treatment of Rabusertib and pemetrexed (Scagliotti et al, 2016). Lastly, the combination treatment of Rabusertib and pemetrexed and cisplatin increased the risk of thromboembolic events in non-squamous NSCLC patients (Wehler et al, 2017). Because the intended clinical use of Rabusertib was to be combined with DNA damaging agents and in light of the aforementioned results, Rabusertib was discontinued in 2013.

1.6.3 WEE1

1.6.3.1 Role of WEE1

WEE1 is a serine-threonine kinase that is essential for G2/M checkpoint regulation to inhibit mitotic entry after DNA damage (figure 1.2). When no DNA damage is present, CDK1 is dephosphorylated by CDC25C phosphatase which leads to CDK1(CDC2)-cyclin B complex activation and progression to mitosis (Bukhari et al, 2022). WEE1 is phosphorylated during G2/M transition by PLK1 leading to its degradation via the ubiquitin proteasome system (Bukhari et al, 2022). However, in the presence of DNA damage, WEE1 phosphorylates CDK1- cyclin B complex (on Tyr15) which results in its inactivation, leading to G2 cell cycle arrest to allow time for DNA repair (Matheson et al, 2016). It also regulates CDK1 and CDK2 activity during S phase and maintains genome stability during DNA replication (Carrassa and Damia, 2017).

Many cancers have an impaired G1 checkpoint, particularly P53-deficient cells, which prevents them from repairing DNA damage before S-phase, hence leading to increased mutations (Matheson et al, 2016). Because of that, these cancer cells depend on the G2/M checkpoint to avoid further DNA damage. Since normal cells have both the G1 and the G2 checkpoints functioning, inhibition of the G2 checkpoint will selectively affect cancer cells (Matheson et al, 2016). Therefore, WEE1 inhibition would lead to elevated CHK1 activity which abrogates the G2 checkpoint, causing cancer cells to enter mitosis with DNA damage

and resulting in apoptosis via mitotic catastrophe (Kong and Mehanna, 2021). Supressing WEE1 would also accelerate CHK2 phosphorylation and activation, leading to inappropriate DNA replication and DNA double-strand breaks (Kong and Mehanna, 2021).

It should be noted that WEE1 is over-expressed in many types of cancer (breast, lung, melanoma, leukaemia, osteosarcoma and squamous cell carcinoma) and this over-expression is correlated with tumour development and poorer prognosis, but in some other cancers the loss of WEE1 is associated with poorer prognosis (Matheson et al, 2016). As a consequence, WEE1 inhibitors would be effective in cancers that over-express WEE1 and rely on a functional G2 checkpoint.

1.6.3.2 Adavosertib (WEE1 inhibitor)

Adavosertib (also called AZD1775 or MK1775) is the first potent and selective WEE1 inhibitor, it was developed by AstraZeneca and it was discovered from a compound library. It inhibits WEE1 kinase in an ATP-competitive manner and can abrogate the G2/M checkpoint by blocking phosphorylation of CDC2 at tyrosine 15, hence activating it (Hirai et al, 2009; Meng et al, 2021).

Out of all the WEE1 inhibitors, Adavosertib has been used the most in preclinical studies, which have showed promising results. Adavosertib combined with chemotherapy agents (gemcitabine, carboplatin, cisplatin) selectively increased apoptosis in cells lacking P53 functionality, without significant increase in toxicity from the combination treatment (Hirai et al, 2009). However, a later study showed that Adavosertib sensitised hematologic and solid tumours cell lines to cytarabine (chemotherapy agent) irrespective to P53 functionality (Van Linden et al, 2013). Another study showed that Adavosertib blocked cell proliferation, caused cell cycle arrest and increased apoptosis in gastric cancer cells, particularly in cells expressing high amounts of WEE1 (Kim et al, 2016). The same study showed that combination treatment of Adavosertib and Paclitaxel or 5-fluorouracil suppressed proliferation of gastric cancer cells and in gastric cancer orthotopic-transplanted mice. It was also demonstrated that Adavosertib treatment promoted premature entry to mitosis and delayed mitotic exit by inducing arrest at metaphase with a 12-hour delay to transition to anaphase (Lewis et al, 2017). The WEE1 inhibitor caused mitotic arrest leading to cell death irrespective of the cell cycle phase before treatment, making it also an anti-mitotic

agent. The same study also demonstrated that combination treatment of Adavosertib and paclitaxel lowered survival in different breast cancer cell lines compared to monotherapy.

A phase I trial established the safety and maximum tolerable dose of Adavosertib as monotherapy in patients with BRCA mutations (Do et al, 2015). Another phase I study showed that combined treatment of Adavosertib with cisplatin and docetaxel is safe, tolerable and with promising antitumour activity in head and neck cancer cells (Mendez et al, 2018). In a Phase II study, Adavosertib enhanced the activity of carboplatin in TP53-mutated tumors and showed manageable toxicity (Leijen et al, 2016). Another phase II study showed that combined Adavosertib and gemcitabine treatment in women with platinum resistant epithelial ovarian cancer improved the overall survival from 7.2 to 11.5 months, with manageable toxicity which was mostly haematological (Lheureux, 2019). There are several phase I and phase II trials with Adavosertib either currently recruiting or preparing to recruit being used as monotherapy or in combination with other treatments (i.e. temozolomide, olaparib, belinostat, radiation) in a variety of cancers (i.e. glioblastoma, ovarian cancer, leukaemia, cervical cancer). Interestingly, Adavosertib also inhibits other kinases (i.e. PLK1) so future results will show if the off-target effects impact positively or negatively on cancer cell survival (Matheson et al, 2016).

1.6.4 DNA-PK

1.6.4.1 Role of DNA-PK

The DNA-dependent protein kinase (DNA-PK) is a serine/threonine protein kinase that is made up of a catalytic subunit (DNA-PKcs) and a Ku heterodimer and belongs to a family of proteins called phosphatidylinositol 3-kinase-related kinase (PIKK), along with ATM and ATR (Yue et al, 2020). The KU heterodimer consists of the Ku70 and Ku80 subunits and heterodimerisation is crucial to preserve the stability of both subunits, as loss of one subunit would result in reduced amounts of the other (Mohiuddin and Kang, 2019). DNA-PK is involved in many additional functions besides double-strand break repair, some of which are yet to be discovered.

DNA-PK is a major component of non-homologous end joining. Following DNA damage, the Ku heterodimer recognises the double-strand breaks and binds to the free ends and recruits the NHEJ components (DNA-PKcs, XRCC4-DNA ligase IV complex, XLF), which are brought

together at the broken ends (Blackford and Jackson, 2017). The DNA-PKcs is activated, possibly by Caspase-2-mediated cleavage of Ku80 at Asp726, phosphorylates NHEJ factors, promotes tethering of broken DNA strands and recruits the endonuclease ARTEMIS (Blackford and Jackson, 2017). This leads to DNA-end processing and ligation by the XRCC4-DNA ligase IV complex and finally the NHEJ machinery is uncoupled (Mohiuddin and Kang, 2019). Ku80 is essential in restricting the broken ends of chromosomes in the nucleus to allow appropriate alignment at the site of repair (Mohiuddin and Kang, 2019).

The factors that determine which DDR pathway (HR or NHEJ) is chosen are not fully understood yet and DNA-PKcs phosphorylation status is one of these factors. BRCA1 blocks NHEJ in the S and G2 phases of the cell cycle by supressing DNA-PKcs autophosphorylation at S2056 (Yue et al, 2020). It is also possible that cells with activated/phosphorylated DNA-PKcs choose NHEJ as their primary DDR pathway, while cells with inactive/unphosphorylated DNA-PKcs choose HR, although contradictory findings imply a more complicated mechanism (Mohiuddin and Kang, 2019).

DNA-PK is also involved in telomere integrity and maintenance by protecting telomeres from being processed and fused. When phosphorylated at S2056, DNA-PKcs promotes telomere end-capping by interacting with KIP and TRF2, preventing them from being seen as double- strand breaks, which would lead to their inappropriate processing (Mohiuddin and Kang, 2019). The Ku70/Ku80 heterodimer is involved in the silencing of telomere-proximal genes and shielding telomeres from nucleolytic degradation (Mohiuddin and Kang, 2019).

DNA-PKcs also contributes to growth arrest and mitotic entry delay by phosphorylating P53 at S15 and S37 and RPA32 at S4 and S8 (Mohiuddin and Kang, 2019). It is involved in the regulation of mitosis by localising to centrosomes and associating with PLK1 in the mitotic phase, which modulates mitotic entry and exit (Mohiuddin and Kang, 2019). It also phosphorylates downstream components that play a role in regulation of mitosis. Lastly, it phosphorylates CHK2 at Thr68, which is important in organising the mitotic spindle (Mohiuddin and Kang, 2019). DNA-PKcs is also important in the DNA replication stress response, where ATR phosphorylates DNA-PKcs at stalled replication forks, resulting in transcriptional activation of Claspin, needed for activation of the S phase checkpoint (Yue et al, 2020).

DNA-PK activity is increased in hepatocellular carcinoma and multiple myeloma and DNA-PKcs activity has been found to promote angiogenesis, tumour migration and secretion of pro-metastatic proteins (Mohiuddin and Kang, 2019). Several studies have shown that inhibiting DNA-PKcs can potentiate radiotherapy and chemotherapy (Yue et al, 2020).

1.6.4.2 NU7441 (DNA-PK inhibitor)

NU7441 is amongst the most potent and selective DNA-PKcs inhibitors. It has a hundred times higher selectivity for DNA-PK than other kinases from the PI3KK family (ATM and ATR) (Zhao et al, 2006). It enhanced the activity of doxorubicin, etoposide and radiation in tumour cells and delayed the repair of DNA double-strand breaks (Zhao et al, 2006). While NU7441 is a well-characterised DNA-PK inhibitor that has been used in many studies, the restricted aqueous solubility and oral bioavailability have limited its further development (Zhao et al, 2006).

NU7441 has been shown in several studies to enhance radiosensitivity in different cancers including lung, colon, breast, liver and prostate. Zhang et al, (2020) observed that phosphorylation of DNA-PKcs and consequent NHEJ events were significantly overexpressed in uveal melanoma cells that are resistant to ionising radiation and Selumetinib (MEK 1/2 inhibitor). They demonstrated that NU7441 made these cells susceptible to radiation and Selumetinib (a MEK 1/2 inhibitor) *in vitro* and *in vivo* by enhancing DNA damage and significantly delayed DNA double-strand break repair, which was used as a mechanism of resistance. Another study showed that NU7441 treatment sensitised non-small cell lung cancer cells to X-ray and carbon ion radiation, while the same NU7441 concentration (0.3μM) was not toxic to tumour cells as monotherapy (Sunada et al, 2016). The combination treatment did not suppress double-strand break repair, due to the low NU7441 concentration, but it induced G2/M arrest, increased DNA fragmentation and elevated senescence. Lastly, when NU7441 was combined with CK2 inhibitor CX-4945, it made gastric cancer cells more sensitive to radiotherapy and elevated apoptosis, compared to NU7441 treatment as monotherapy (Geng et al, 2019).

NU7441 rendered glioma cell lines more susceptible to two Topoisomerase 2 inhibitors (NK314 and VP-16) by postponing DNA damage repair (NHEJ) (Kopa et al, 2020). The combination treatment also caused high double-strand break accumulation, altered cell

cycle distribution and increased apoptosis. When combined with the CHK1 inhibitor PF-477736 in neuroblastoma cell lines, the cells were sensitised to CHK1 inhibition, as double-strand breaks were induced and NHEJ was suppressed (Ando et al, 2019). Combination treatment of NU7441 and topoisomerase inhibitors (amrubicin and irinotecan) had a synergistic effect against the growth of non-small cell lung carcinoma cells by suppressing DNA repair and enhancing apoptosis (Yanai et al, 2017). The inhibitor has also been demonstrated to enhance the effects of chemotherapy in other cancers (i.e. breast, lung, CLL, nasopharyngeal carcinoma) (Mohiuddin and Kang, 2019). NU7441 is not currently in clinical trials, but newly developed DNA-PKcs inhibitors that offer increased specificity have entered clinical trials (Dylgjeri and Knudsen, 2022).

1.6.5 RAD51 and RAD52

1.6.5.1 Role of RAD51

RAD51 is the principal catalyst of homologous recombination and an important protector of genomic stability (Wassing and Esashi, 2021). Following DNA damage, the MRN complex identifies and binds to DSBs, leading to resection of the 5' strands of the DNA and generating the 3' ssDNA overhangs, which are coated with RPA that prevents secondary structure formation or degradation (Bonilla et al, 2020). RAD51 displaces RPA and BRCA2 contributes to the assembly of RAD51 nucleoprotein filament, which searches for homology and invades a homologous region, forming a DNA intermediate. This intermediate is processed by DNA synthesis using one of three pathways: gene conversion, synthesis-dependent strand annealing and RAD51-dependent break-induced replication (Bonilla et al, 2020).

RAD51 plays an important role in overcoming replication stress and is essential for cell viability. RAD51 possibly has a structural role in fork protection, while its enzymatic function is needed for homologous recombination (Bonilla et al, 2020). Following fork stalling, the newly generated strands undergo annealing during fork reversal, contributing to genome stability by restricting the accumulation of ssDNAs (Wassing and Esashi, 2021). This process allows replication to restart by homologous recombination, avoiding the error-prone mechanism of NHEJ, which would generate genomic instability. The mechanism is not known yet, but it is hypothesised that RAD51 binds and stabilises the reversed arm of the

fork. RAD51 forms a nucleoprotein filament to shield the newly created DNA end from nucleolytic attack (Wassing and Esashi, 2021). This promotes genomic stability, as the reversed fork is a stable intermediate formation and it prevents generation of double-strand breaks. To activate fork reversal, RAD51 is recruited to the stalled replication forks and it interacts with the extended ssDNA. BRCA2, BRCA1, FANCD2 and BOD1L stabilise the RAD51 filament, preventing the production of double-strand breaks and promoting its repair by faithful DNA repair mechanisms, such as nucleotide excision repair to enable replication continuation (Wassing and Esashi, 2021). However, when RAD51 is not stabilised at the reversed fork, breakage might occur, which can lead to RAD51-dependent homologous recombination, where the DNA intermediate is extended by break-induced replication (Bonilla et al, 2020). This is a DSB repair mechanism at broken replication forks that allows continuation of replication, but as it may start at sites with partial homology or repeats, it can have mutagenic repercussions and cause genomic instability (Wassing and Esashi, 2021). In this case, RAD51-mediated fork reversal can cause genomic instability instead of protecting the genome. In conclusion, RAD51 at stalled forks can either preserve or impede genomic stability, which is dependent on the nature and strength of the genotoxic stress, the modulation of RAD51 activity at the fork and the surrounding DNA sequence (Wassing and Esashi, 2021).

RAD51 is overexpressed in several cancer cell lines, including those from the prostate, pancreas, breast and lung, as a result of RAD51 promoter activation, which is approximately 840 times more than in normal cells. RAD51 overexpression is correlated with resistance to anticancer therapy, lymph node and distant metastases and a poorer prognosis (Gachechiladze et al, 2017). Hence, RAD51 emerges as an attractive therapeutic target, since inhibiting homologous recombination might specifically affect cancer cells that are highly dependent on it (Budke et al, 2012).

1.6.5.2 Role of RAD52

RAD52 is a DNA/RNA-binding protein that promotes homology identification and annealing of strands, playing an important role in DNA repair and the preservation of genomic integrity. Its interaction with DNA is regulated by its N-terminal domain, which is essential to its activity (Balboni et al, 2023). Post-translationally, RAD52 is acetylated, which is an essential modification that modulates protein-protein interactions with proteins involved in

homologous recombination (Rossi et al, 2021). In addition, phosphorylation of RAD52 at Tyr104 decreases its binding ability with dsDNA but increases its binding activity with ssDNA (Balboni et al, 2023).

RAD52 is an important component of homologous recombination in yeast, but in vertebrates it is a non-essential supplementary factor and its lack of activity does not impair cell survival (Balboni et al, 2023). It has been shown that BRCA2-deficient cells need RAD52 to survive, indicating that RAD52 regulates RAD51 loading and helps to displace RPA, assuming the role of BRCA2 when the activity of the latter is absent (Balboni et al, 2023). However, more research is needed to shed light on the role that RAD52 has in homologous recombination.

RAD52 plays an important role in single strand annealing (SSA), which is an error prone process for repairing DNA double-strand breaks. RAD52 is recruited on the broken DNA ends to contribute to their annealing and identify the region of homology (Rossi et al, 2021). Following that, the ERCC1-XRF complex is tethered to the N-terminal domain of RAD52 and cleaves the ssDNA ends (Rossi et al, 2021). Again, the full role of RAD52 in SSA is not fully understood yet.
There is also a substitute homologous recombination pathway that utilises RNA transcripts for DSB repair, is active in G0/G1 phase and is thought to be RAD52 dependent (Balboni et al, 2023). It promotes the creation of an RNA-DNA heteroduplex complex (R-loop), where the RNA is used as a template for DSB repair and links both ends of a homologous double-strand break with RNA, allowing strand exchange between ssRNA and dsDNA (Balboni et al, 2023).

RAD52 also acts during DNA replication, as it is involved in recognition and repair of stalled replicated forks. It activates break-induced replication, which is a pathway that fixes single-ended double-strand breaks, by pairing homologous sequences (Gottifredi and Wiesmuller, 2020). RAD52 interacts with numerous nucleases during this pathway, promoting continuation of DNA replication (Gottifredi and Wiesmuller, 2020). However, studies indicate that break-induced replication activated by RAD52, drives genome instability in human cancers (Rossi et al, 2021).

RAD52 has been found to be deregulated in cancer. Specifically, it is upregulated in some cancers, such as liver and rectal and downregulated in others, such as cervical and urothelial (Balboni et al, 2023). PARP inhibitors are clinically approved to be used against specific BRCA2-deficient cancers and RAD52 may also be a promising therapeutic target in cancers that RAD52 is overexpressed.

1.6.5.3 RI-1 (RAD51 inhibitor)

Budke et al (2012) identified RI-1, a RAD51 inhibitor, from a high throughput screen of a library with 10,000 compounds. It suppresses RAD51 activity by binding irreversibly and directly to RAD51 at cysteine-319, near a protein-protein interface which is needed for RAD51 filament formation on ssDNA and recombinase activity, therefore disrupting them. They showed that the inhibitor suppresses homologous recombination efficiency and made human cancer cells more susceptible to inter-strand DNA cross-linking chemotherapy drug mitomycin C.

Berte et al, (2016) demonstrated that RI-1 enhanced double-strand breaks, chromosomal alterations, apoptosis and necrosis in glioblastoma cells and increased the anticancer effect of chloroethylating nitrosoureas (alkylating agents) in a glioma xenograft model. Chen et al, (2017) demonstrated that RI-1 supressed cell growth in cervical cancer cells *in vitro* and *in vivo* (tumour xenografts) and blocked their transition from G1 to S phase. They also showed that RI-1 sensitised cervical cancer cells to both cisplatin and ionizing radiation. PTEN promotes DNA repair through homologous recombination, which is RAD51 dependent and RI-1 sensitised breast cancer cells with wild type PTEN to olaparib by causing four times more γH2AX foci than either of them (Zhao et al, 2017). In addition, RI-1 radio sensitised radioresistant glioblastoma stem cells delaying repair up to 180 min after IR and increasing apoptosis (Balbous et al*,* 2016).

However, RI-1 has a short half-life, due to reactivity that promotes irreversible binding and has restricted its development in preclinical animal studies (Budke et al, 2013). RI-2, an analogue of RI-1, was developed shortly afterwards and is an optimised RAD51 inhibitor, as it binds to RAD51 reversibly and lacks reactivity while it still inhibits homologous recombination repair in human cells (Budke et al, 2013). To date, neither of them has entered clinical trials.

1.6.5.4 6'-OH-DOPA and AICAR (RAD52 inhibitors)

Drug discovery targeting the RAD52 C-terminal domain has been challenging due to the absence of knowledge regarding its superstructure and protein interactions. Only a few small molecule inhibitors have been described and there are issues regarding specificity and toxicity (Balboni et al, 2023). Chandramouly et al, (2015) discovered 6-OH-DOPA, a small molecule inhibitor of RAD52 that damages its ring structures and inhibits single strand annealing, but it has little effect on HR or NHEJ in cells with functional BRCA. It preferentially suppressed cell proliferation in BRCA1-deficient triple-negative breast cancer cells and in BRCA-defective AML and CML cells (Chandramouly et al, 2015). Aguilar-Morante et al, (2018) reported significantly higher RAD52 mRNA levels in malignant gliomas compared to normal brain, which is negatively associated with survival. They showed that inhibition of RAD52 with 6-OH-DOPA impaired Glioblastoma cell survival because of accumulation of DNA damage. However, some challenges surrounding the inhibitor include lack of high specificity and the fact that it promotes Parkinson's disease and degeneration of mitral neurons, as it is a dopaminergic toxin, making it inappropriate for anticancer treatment (Balboni et al, 2023).

5-Aminoimidazole-4-carboxamide ribonucleotide (AICAR) is another RAD52 inhibitor, which was identified via virtual screenings of a drug-like compound library and functions by inhibiting RAD52-ssDNA interaction, without affecting RAD51-ssDNA complex formation (Sullivan et al, 2016). As it is a permeable molecule, it diffuses into cells and is phosphorylated intracellularly to produce large amounts of ZMP, which is the active and not permeable form (Sullivan et al, 2016). It is placed between two monomers of RAD52 and interacts with its DNA-binding domain to form an H-bond interaction with Thr148 (Sullivan et al, 2016). It selectively killed BRCA1 and BRCA2-mutated breast and pancreatic carcinoma cells by exerting synthetic lethality (Sullivan et al, 2016). However, there is very limited research on this inhibitor and its full potential is yet to be explored. Currently, there are no RAD52 inhibitors in clinical trials or in the market.

1.6.6 DNA Ligases

1.6.6.1 Role of DNA ligases

DNA ligases play a crucial role in all DNA-containing life forms, as they are essential for DNA repair events and have specialised roles in cell growth and DNA maintenance (Ellenberger and Tomkinson, 2008). They catalyse phosphodiester bond formation in a process that involves three steps by using a high energy cofactor (NAD^+ or ATP) (Tomkinson et al, 2013). There are three human genes coding DNA ligases (DNA ligase I, III and IV), which have distinct yet overlapping roles.

The first step of the multistep reaction that DNA ligases catalyse involves AMP transfer from ATP (eukaryotes and archaea) or NAD^+ (bacteria) to an active-site lysine residue of the DNA ligase enzyme (Ellenberger and Tomkinson, 2008). The second step involves AMP transfer from the ligase to the 5' phosphate of the DNA substrate producing an intermediate product (Tomkinson et al, 2013). In the third step, the 3' OH of another DNA strand attacks the 5' phosphate, AMP is displaced and the ends of the two DNA strands are linked (Ellenberger and Tomkinson, 2008).

DNA ligase I is the replicative ligase, it is recruited to nuclear DNA replication via its interaction with PCNA and it performs Okazaki fragment joining (Tomkinson et al, 2013). DNA ligase I becomes increasingly phosphorylated during S phase and dephosphorylated following DNA damage or replication blockage (Ellenberger and Tomkinson, 2008). Complex posttranslational modifications regulate its interactions with different proteins and its participation in different DNA reactions (Ellenberger and Tomkinson, 2008). In its absence, Okazaki fragment synthesis is performed through a single-strand break repair mechanism which requires DNA ligase III and XRCC1 (Tomkinson et al, 2013). It is also involved in base excision repair, nucleotide excision and single-strand break repair (Tomkinson et al, 2013).

The LIG3 gene encodes numerous polypeptides via alternative splicing and produces mitochondrial and nuclear DNA ligase IIIα via alternative translation (Tomkinson et al, 2013). This gene is crucial for cell viability as it encodes the only mitochondrial DNA ligase and is required in the replication and repair of the mitochondrial genome (Tomkinson et al, 2013). Nuclear DNA ligase III interacts with XRCC4, a DNA repair protein, forming a complex. Studies in human cells have shown that DNA ligase III/XRCC4 is crucial for DNA replication

when DNA ligase I is absent (Tomkinson et al, 2013). It is also involved in base excision repair, single-strand break repair and nucleotide excision repair (Tomkinson et al, 2013). It is also a major component of alternative NHEJ, which is active in low amounts in wild type cells and generates several chromosomal translocations, and functions independently of XRCC4 (Tomkinson et al, 2013).

DNA ligase IV is an important factor for NHEJ, it links double-strand DNA breaks and completes V(D)J recombination (Ellenberger and Tomkinson, 2008). It forms a complex with XRCC4 and interacts with DNA-PK. The ligase also participates in the repair of endogenous DNA damage that would otherwise lead to apoptosis (Ellenberger and Tomkinson, 2008).

Studies have found increased DNA ligase I levels in cancer cells, probably due to their elevated proliferation compared to normal cells (Tomkinson et al, 2013). In addition, a pattern of increased DNA ligase III and decreased DNA ligase IV levels has been found in a lot of cancer cells, because of reduced NHEJ and elevated alternative NHEJ in these cells (Tomkinson et al, 2013).

1.6.6.2 L189 (Ligase inhibitor)

L189 is an inhibitor of DNA ligase I, III and IV that was identified from a computer-aided drug design approach (Chen et al, 2008). It suppressed the ligase reaction by more than 90% but did not have a strong effect on T4 DNA ligase. Specifically, it inhibited the second step of the ligation reaction, when the ligase is supposed to interact with nicked DNA, by competing with DNA for binding to its DNA binding pocket and consequently preventing DNA binding. L189 also suppressed NHEJ in HeLa cells, as it inhibited DNA ligase IV, which is an essential factor of NHEJ (Chen et al, 2008).

It should be expected that once L189 enters human cells, it will suppress growth and may be cytotoxic as it inhibits all human ligases. Chen et al, (2008) showed that the inhibitor reduced cell growth and viability in both human cell lines and cancer cell lines in a concentration-dependent way. However, when sub-toxic concentrations of L189 were used in combination with DNA alkylating agent MMS, cytotoxicity was increased in cancer cell lines, but not normal breast epithelial cells. L189 combined with ionizing radiation also increased cell death in colon cancer cells, but not in normal breast epithelial cells (Chen et al, 2008). This is because DNA ligase I levels were increased in cancer cell lines compared to

normal cells. Interestingly, ligase III levels were increased while ligase IV levels were decreased in three cancer cell lines (breast, cervical and colon) compared to normal cells (Chen et al, 2008). L189 also reduced cell growth of HeLa cells and combination treatment of L189 and Temozolomide decreased cell growth and proliferation by potentiating growth arrest of HeLa cells (probably in G2/M phase), without activating cell death mechanisms (Jahagirdar et al, 2018). The inhibitor has not entered clinical trials yet.

Table 1.2: The table provides a summary of the nine inhibitors used in this study

Inhibitor	Target	Clinical Trials
AZD6738	ATR	Yes
AICAR	RAD52	No
KU-60019	ATM	Yes
L189	DNA Ligase I, III and IV	No
6-OH-DOPA	RAD52	No
NU7441	DNA-PK	No
Rabusertib	CHK1	Yes
Adavosertib	WEE1	Yes
RI-1	RAD51	No

1.7 The DNA Damage Response and Crisis

In 2014, our lab showed that deletion of LIG3, but not LIG4, inhibited escape from telomere crisis and implicated LIG3-dependent A-NHEJ in the processing of telomere fusion during crisis (Jones et al 2014). In fact, LIG3-dependent A-NHEJ leads to significantly more inter-chromosomal fusions compared to intra-chromosomal fusions and the study found that cells failing to escape crisis showed higher proportions of inter-chromosomal fusions. This result suggests that inhibition of the A-NHEJ pathway may prevent escape from telomere crisis.

In support of this hypothesis, Ngo et al (2018) showed that olaparib and rucaparib, both of which inhibit PARP1, which is an important component of the A-NHEJ pathway, selectively killed human cells undergoing a telomere crisis. That was the first demonstration that it is

possible to pharmacologically inhibit escape from a telomere crisis. Suppression of PARP did not change cell growth before crisis or the rate of telomere erosion, but led to accumulation of intra-chromosomal telomere fusion, elevated activation of DNA damage checkpoints and increased apoptosis (Ngo et al, 2018). The authors suggest that the addition of the inhibitors prevented cells from escaping a telomere-driven crisis by impeding the repair of dysfunctional telomeres and contributing to replicative stress at telomeres. They propose that inhibiting PARP1 results in an increase of SSBs and replicative stress, which would increase apoptosis. They also suggested that PARP inhibition may affect HR, which may increase sister telomere fusion (intra-chromosomal fusion) and subsequently apoptosis. Overall, the paper indicates that increasing DNA damage may be sufficient to prevent escape from crisis with a promising potential for targeting cells with short dysfunctional telomeres and suppressing cancer development.

Following on from this study, we aimed to test if other DDR inhibitors have the same effect on cells undergoing a telomere-driven crisis and to identify their mechanism of action. This type of 'crisolytic' drugs would have the potential to kill pre-cancerous tumours with short dysfunctional telomeres (figure 1.3).

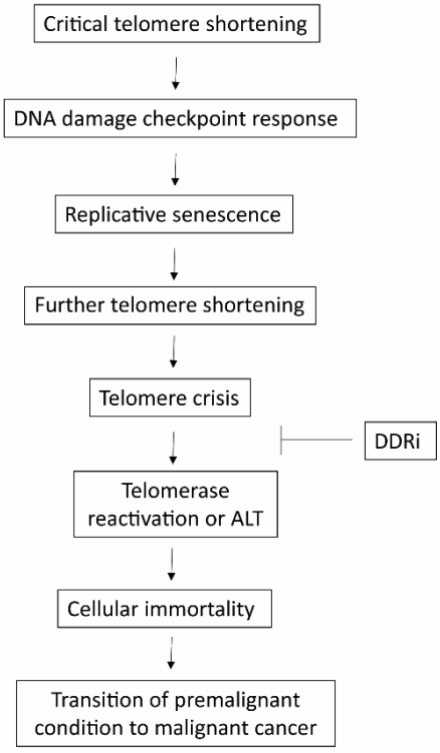

Figure 1.3: The path from critical telomere shortening to malignant tumorigenesis. Increasing DNA damage during telomere crisis may prevent escape from crisis thus inhibiting malignant transformation. Adapted from Nassour et al, 2021.

1.8 Aims of the project

This study investigated the ability of nine DNA damage response inhibitors [AZD6738 (ATR), KU-60019 (ATM), L189 (LIG1, LIG3, LIG4), 6-OH-DOPA (RAD52), NU7441 (DNA-PK), Rabusertib (CHK1), Adavosertib (WEE1), RI-1 (RAD51) and AICAR (RAD52)] to prevent cells from escaping a telomere-driven crisis and their impact on cellular properties (Table 1.2). Our hypothesis was that the DNA damage inhibitors will specifically affect cells undergoing a telomere crisis (pre-cancerous cells), while having no or low toxicity on the healthy cells.

The individual aims of the study are presented below:

- Identify an appropriate range of DDRi concentrations to treat HCT116 cells
- Determine how the nine DDRi influence cell growth, cell cycle progression and apoptosis in WT-HCT116 cells and DN-hTERT HCT116 cells
- Assess the impact of DDRi on the rate of telomere erosion before and during crisis
- Assess the impact of DDRi on telomere fusion before and during crisis
- Examine how the DDRi affect the DNA damage response before and during crisis
- Establish which DDRi inhibit escape from a telomere-drive crisis
- Evaluate how the selected DDRi influence cell growth, cell cycle progression and apoptosis in human primary fibroblasts
- Determine if the selected DDRi can selectively target and kill cells with short dysfunctional telomeres in a population of cells with both long and short telomeres

Chapter 2

Materials and Methods

2.1 Cell culture

WT HCT116 human colorectal cancer cells were cultured in Gibco McCoy's 5A medium (Thermo Fisher Scientific) supplemented with 10% v/v fetal calf serum (FCS) (Thermo Fisher Scientific), 2mM L-glutamine (Sigma) and 1 % *Penicillin*/*Streptomycin* (stock 10000U/ml & 10mg/ml; Sigma). DN-hTERT HCT116 colorectal cancer cells were made by introducing a dominant-negative hTERT construct into WT-HCT116 cells through retroviral transfection, which abrogated telomerase activity (Jones et al, 2014). DN-hTERT HCT116 cells were cultured as above but additionally supplemented with 1% puromycin (stock 250 µg/ml; Calbiochem). HCA2 WT and IMR90 WT fibroblast cells were cultured in Gibco Dulbecco's Modified Eagle's Medium (DMEM) (Thermo Fisher Scientific) supplemented with 10% v/v fetal calf serum (FCS) (Thermo Fisher Scientific), 2mM glutamine (Sigma), 1 % *Penicillin*/*Streptomycin* (stock 10000U/ml & 10mg/ml; Sigma). All cell cultures were incubated at 37°C in 5% CO2.

WT HCT116 cells were treated with nine different DDR inhibitors (AZD6738, KU-60019, L189, 6-OH-DOPA, NU7441, Rabusertib, Adavosertib, RI-1 and AICAR) at different concentrations in order to determine the most appropriate inhibitor concentration range for the treatment of DN-hTERT HCT116 (table 2.1). DN-hTERT HCT116 were treated with eight different DDR inhibitors (AZD6738, KU-60019, L189, 6-OH-DOPA, NU7441, Rabusertib, Adavosertib and RI-1) at different concentrations. HCA2 and IMR90 cells were treated with three different DDR inhibitors (NU7441, AZD6738, Rabusertib) at different concentrations. A control sample treated with DMSO (or HCl for cells treated with 6-OH-DOPA) was used for all the experiments. The inhibitor was added once every two or three days. Table 2.1 shows the different inhibitors used in the experiments.

Table 2.1: The table lists the nine inhibitors used in this study

Inhibitor	Product Number	Company	Stock Concentration
AZD6738	S7693-SEL	Selleck Chemicals	10mM
AICAR	S1802-SEL	Selleck Chemicals	150mM
KU-60019	S1570-SEL	Selleck Chemicals	10mM
L189	3561	Tocris Bioscience	50mM
6-OH-DOPA	5740	Tocris Bioscience	50mM
NU7441	S2638-SEL	Selleck Chemicals	5mM
Rabusertib	S2626-SEL	Selleck Chemicals	10mM
Adavosertib	S1525-SEL	Selleck Chemicals	10mM
RI-1	S8077-SEL	Selleck Chemicals	100mM

The cells were passaged once a week, when the flasks were approximately 80% confluent. After aspirating the medium, cells were washed off with 1 x trypsin (Thermo Fisher Scientific; 600µl for 6-well plates; 1ml for T25 flasks; and 2ml for T75 flasks). Trypsin was immediately removed, then it was added again (same amount) and trypsinised cells were incubated for 5 minutes. After incubation, cells, which were detached from the plate, were mixed in fresh medium (2.4ml for 6-wells; 4ml for T25 flasks; and 8ml for T75 flasks).

2.2 Cell counting

After cells were trypsinised, the cells were counted through fluorescence image cytometry on the NucleoCounter® NC-3000™ system (Chemometec). A 50µl aliquot of cell suspension was collected and 2.62µl of Solution 13 (30µg/ml Acridine Orange, Sigma; 100µg/ml DAPI, Sigma) was added to it. 11µl of the mixture was transferred to an A8 chamber slide from ChemoMetec and counted using the cell counter. After passaging, cell samples were collected for DNA extraction (to be used for STELA and telomere fusion analysis), Western Blot (only in the fibroblast cultures) or frozen for further cell culture experiments.

2.3 2-step Cell Cycle Analysis

A 2-step cell cycle analysis was performed according to the protocol for the NucleoCounter® NC-3000™ system (Chemometec), an advanced image cytometer that uses fluorescence imaging to analyse cell properties. Briefly, $2x10^5$ cells from each sample were centrifuged at

400g for 5 minutes, washed once with PBS and resuspended in 50µl of Solution 10 (lysis buffer) containing 10µg/ml DAPI. Following that, the cells were incubated at 37^0 C for 5 minutes and 50µl of Solution 11 (stabilisation buffer) was added. A volume of 10µl of cell suspension was loaded into an 8-chamber slide, which was placed on the tray of NucleoCounter® NC-3000™ for analysis. Fluorescence emitted by cells is quantified and DNA content histograms are generated. Markers in these histograms can be employed to categorise cells into various cell cycle stages.

2.4 Annexin V Apoptosis Assay

Annexin V Apoptosis Assay was performed according to the protocol for the NucleoCounter® NC-3000™ system (Chemometec). Briefly, $4x10^5$ cells from each sample were centrifuged at 400g for 5 minutes, resuspended in 100µl Annexin V binding buffer, 2µl Annexin V-CF488A conjugate (490/515nm) and 2µl Hoechst 33342 (10µg/ml) and incubated at 37 °C for 15 minutes. After that, the cells were centrifuged as before and resuspended in 300µl Annexin V binding buffer. This step was repeated, cells were centrifuged as before, resuspended in 100µl Annexin V binding buffer supplemented with 10µg/ml PI and 30µl of cell suspension was loaded into the 2-chamber slide which was placed on the tray of NucleoCounter® NC-3000™ for analysis.

2.5 Cell freezing and thawing

Cells were centrifuged at 1,000 rpm for 5 minutes and the supernatant was removed to obtain a volume of 0.5ml cells in medium. A volume of 0.5ml freezing mix (80% FCS; 20% DMSO, Sigma) was added to the cells to make up a total of 1ml and cells were thoroughly mixed and transferred to a cryovial. The cryovial was transferred to a Mr Frosty, which contained isopropyl alcohol and stored at -80 °C. For long-term storage, cells were kept in liquid nitrogen.

Cells were rapidly thawed in a 37 °C water bath and transferred to a 15ml tube and 9ml growth medium was added drop-wise. After that, the cells were centrifuged at 1,000 rpm for 5 minutes and the medium was replaced with fresh medium.

2.6 DNA extraction and quantification

After trypsinization, cells were centrifuged at 3000 rpm for 5 minutes, washed twice with 1xPBS, the supernatant was removed and a ''wet'' pellet was stored at -20°C. For DNA extraction the cells were thawed, resuspended in 300µl lysis buffer (100nM NaCl, 100mM Tris HCl pH8, 5mM EDTA pH8, 0.5% SDS) containing 3µl RNase (stock concentration 10mg/ml; Sigma) and 3µl Proteinase K (stock concentration 20mg/ml; Sigma) and incubated overnight at 45°C. The following day, the cells were briefly centrifuged, mixed with 300µl of ultra-high purity phenol/chloroform (Sigma) and placed in a tube rotator for 30 minutes. Following that, the cells were centrifuged at 13000 rpm for 5 minutes, the aqueous phase and interphase were transferred to a tube containing 300µl of phenol/chloroform and placed in a tube rotator for 20 min. After that, the cells were centrifuged as before and the aqueous phase was transferred to a screwcap tube. 25µl of 3M Sodium Acetate (pH5.2; Sigma) and 900µl of ice cold 100% ethanol was added to the cells and they were centrifuged as before. The pellet was washed in 1ml ice cold 70% ethanol and the tubes were left to air-dry in the fume cabinet for 1 hour. Lastly, the cells were resuspended in 100µl of Tris buffer (10mM, pH8), incubated at 37^{o} C for 30 minutes and quantified with the QuantiFluor-ST fluorometer (Promega).

The fluorometer was calibrated using 10µl calf thymus DNA (100µg/ml; Bio-Rad) with 2ml of 1 x TEN buffer [ddH2O, 0.1µl/ml Hoechst dye and 10 x TEN stock buffer (100mM Tris, 10mM EDTA and 2M NaCl, pH 7.4)]. The samples were quantified by adding 2µl of the sample in a cuvette containing 2ml of 1xTEN buffer. Each sample was read three times and an average was calculated.

2.7 STELA (Single Telomere Length Analysis)

17p6, XpYpC, XpYpE2, XpYp-427G/415C and XpYp-427A/415T STELA (table 2.3) were performed as stated by standard protocols (Jones et al, 2014). Briefly, DNA was diluted to 10ng/µl with TRIS-HCl (10mM, PH 8) and 1µl of 10ng/µl DNA was mixed with 1µl of telorette 2 (10µM) and 38µl of TRIS-HCl. Each PCR reaction contained 4.98µl H_2O, 1µl 10xbuffer (75 mM Tris HCl at pH 8.8, 20mM (NH4)SO4 and 0.01% Tween20; Thermo Fisher Scientific), 0.8µl $MgCl_2$ (25mM; Thermo Fisher Scientific), 0.12µl dNTPs (100mM; Promega), 1µl Teltail (5µM), 1µl telomere specific primer (5µM), 0.1µl Taq/PWO DNA polymerases (10:1)

(Thermo Fisher Scientific and Roche) and 1µl of Tel2/DNA mix. A SimpliAmp Thermal Cycler (Thermofisher Scientific) was used for PCR (table 2.2).

Table 2.2: Cycling conditions for STELA

Oligonucleotides	Conditions
XpYpC	20 seconds at 94°C, 30 seconds at 65°C and 8 minutes at 68°C for 22 cycles
17p6	20 seconds at 94°C, 30 seconds at 59°C and 8 minutes at 68°C for 22 cycles
XpYpE2	15 seconds at 94°C, 30 seconds at 65°C and 10 minutes at 68°C for 22 cycles
XpYp-427G/415C	15 seconds at 94°C, 30 seconds at 66.5°C and 10 minutes at 68°C for 25 cycles
XpYp-427A/415T	15 seconds at 94°C, 30 seconds at 66.5°C and 10 minutes at 68°C for 25 cycles

In each reaction, 2µl of 6 x Ficoll gel loading solution (5% bromophenol blue, 5% xylene and 15% Ficoll) was added and a 0.5% TAE agarose gel electrophoresis was used to resolve the PCR products. The gel was run at 110V for approximately 16 hours at 4 °C. This was followed by a Southern blotting hybridization with a random-primed α-^{33}P-labeled (GE Healthcare) TTAGGG repeat probe. A transilluminator was used to cut the gel and the gel was washed twice for 6 minutes in depurination buffer (0.25M HCl) and 15 minutes in denaturation buffer (1.5M NaCl, 0.5M NaOH). A positively charged membrane (Hybond-XL GE healthcare) was used to transfer the DNA for 4-5 hours. After that, the membrane was hybridised in Church buffer (0.5M sodium phosphate dibasic, 7% SDS, 1% BSA, 1mM EDTA) with 25µl of the radiolabelled probe overnight at 56 °C. The probe was denatured at 96 °C for 5 minutes before it was added to the bottle with the blot. After hybridisation, the blot was washed with wash buffer (0.1% SDS and 0.1 x SSC) three times with 20 minute intervals. Then, the STELA blot was dried at 56°C, exposed to a phosphor screen (Amersham) overnight and imaged using a Typhoon FLA 9500 imager (GE Healthcare). The analysis was performed using ImageQuantTL software (GE Healthcare).

2.8 Telomere Fusion Assay

DNA was diluted to 25ng/µl and 6 reactions of 10µl were set up, each containing 1.98µl H_2O, 1 µl 10xbuffer (75mM Tris HCl at pH 8.8, 20mM (NH4)SO4 and 0.01% Tween20; Thermo Fisher Scientific), 0.8µl $MgCl_2$ (25mM; Thermo Fisher Scientific), 0.12µl dNTPs (100mM; Promega), 1µl forward primer (10µM), 1µl reverse primer (10µM), 0.1µl Taq/PWO (10:1) (Thermo Fisher Scientific and Roche) and 5µl of DNA. A SimpliAmp Thermal Cycler (Thermofisher Scientific) was used to cycle the reactions at 94 °C for 20 seconds, 62 °C for 30 seconds and 68 °C for 8 minutes for 25 cycles. The gel was prepared in the same way as in STELA, but run at 50 V for approximately 16 hours at 4 °C. Southern blot hybridisation with a random-primed α-^{33}P-labeled (GE Healthcare) TTAGGG repeat probe and imaging were performed as in STELA, except that the blot was wrapped in cling film before being exposed to a phosphor screen.

Table 2.3. This table lists the primers used in STELA and telomere fusion analysis

Oligonucleotides	**Sequences**
Teltail	5'-TGCTCCGTGCATCTGGCATC-3'.
XpYpC	5'-CAGGGACCGGGACAAATAGAC-3'
XpYpM	5'-ACCAGGTTTTCCAGTGTGTT-3'
17p6	5'-GGCTGAACTA TAGCCTCTGC-3'
17pseqrev1	5'-GAATCCACGGATTGCTTTGTGTAC-3'
XpYpE2	5'-TTGTCTCAGGGTCCTAGTG-3'
XpYp-427G/415C	5'-GGTTATCGACCAGGTGCTCC-3'
XpYp-427A/415T	5'-GGTTATCAACCAGGTGCTCT-3'

2.9 Protein extraction and quantification

Cell pellets were washed in 1 x PBS three times and resuspended in 50µl lysis buffer (135mM NaCl, 20mM Tris, 5mM EDTA, 0.1% (v/v) Triton X-100, 5% (v/v) Glycerol dissolved in water pH 7.6) containing 3mM PMSF (Sigma), 1/100 Protease Inhibitor Cocktail III (Calbiochem) and 1/100 Phosphatase Inhibitor Cocktail II (Calbiochem). They were left on ice for 5 minutes to lyse and then centrifuged at 20,000 g at 4 °C for 30 minutes. The

supernatant was aliquoted to a fresh tube and stored at -80 °C, while 5µl were diluted in 45µl ddH2O for protein quantification.

For protein quantification, a series of standards was prepared with different dilutions (0.1, 0.2, 0.3, 0.4mg/ml) of BSA (Thermo Fisher Scientific). The standards and the samples were measured in triplicates after adding 300µl Coomassie Plus (Thermo Fisher Scientific) and incubated for 10 minutes at room temperature. The protein was quantified on the Cytation 3 imaging reader (Biotek) using a 96-well plate by measuring the absorbance at the wavelength of 595nm and calculating the concentrations using a standard curve generated by plotting the values of the standards.

2.10 Western Blotting

Once the protein concentration was determined, the appropriate protein volume was mixed with lysis buffer to make a final volume of 12µl and 4µl of :4x laemmli loading buffer (Biorad) containing beta-mercaptoethanol (1/10) was added to it. Samples were incubated at 100 °C for 5 minutes and then loaded onto Mini-PROTEAN III TGX precast gel (15 wells; Bio-Rad). The gel was run in 1 x running buffer (0.25M glycine, 24mM Tris base, 3.4mM SDS at pH 8.3) at 100V for approximately 1 hour and 15 minutes.

After gel electrophoresis, the protein was transferred onto PVDF membrane (Immobolin-P Millipore) in transfer buffer (25mM Tris base, 0.19M glycine, 20% methanol at pH 8.1-8.4) at 100V for 1hr. The membrane was firstly immersed in methanol for 3 seconds and then washed in ddH2O for 2 minutes. The order of the components is as follows: black face of clamp, pad, 2 x 3MM paper, gel, membrane, 2 x 3MM paper, pad, white face of clamp which faced the red side of holder.

After protein transfer, the membrane was blocked in 1xTBST (20mM Tris, 150mM NaCl, 0.1% (w/v) Tween® 20 detergent) and 5% milk/Bovine serum albumin (BSA) for 1 hour. Then, the membrane was washed 3 times for 10-15 minutes in 1xTBST and incubated in a 50ml falcon with 3ml 1xTBST, 5% milk/BSA and primary antibody (1 in 1000) (Table 2.4) at 4°C overnight. After that, the membrane was washed 3 times for 10-15 minutes in 1xTBST and incubated in a 50ml falcon with 3ml 1xTBST, 5% milk/BSA and secondary antibody (1 in 2000) at room temperature for 1-1.5 hour. Finally, the membrane was covered in detection

solution (Thermo Scientific™ Pierce™ ECL Plus Western Blotting Substrate; Thermofisher) for 5 minutes, wrapped in saran and developed (Amersham ImageQuant 800 GxP biomolecular imager; cytiva). To strip the membrane, the membrane was washed for 10 minutes in ddH2O, another 10 minutes in 0.2M NaOH and another 10 minutes in ddH2O.

Table 2.4: This table lists the antibodies used in Western Blot analysis

Primary Antibody	**Product Number**	**Secondary Antibody**	**Supplier**
Phospho-Chk1 (S345)	2348T	Rabbit mAb	Cell Signalling Technology
Phospho-Chk2 (Thr68)	2661T	Rabbit mAb	Cell Signalling Technology
Phospho-Chk1 (S296)	2349S	Rabbit mAb	Cell Signalling Technology
LC3B (D11) XP	3868T	Rabbit mAb	Cell Signalling Technology
Chk1 (2G1D5)	2360S	Mouse mAb	Cell Signalling Technology
H2AX	A300-083A-M	Rabbit mAb	Cambridge Bioscience
gamma-H2AX	A300-081A-M	Rabbit mAb	Cambridge Bioscience
Recombinant Chk2 [EPR4325]	ab109413	Rabbit mAb	ABCAM
p53	MABE327	Mouse mAb	Sigma-Aldrich

2.11 Statistical Analysis

Statistical significance was assessed using Student's two-tailed t-test (equal variances), which was performed with GraphPad Prism 8. The samples analysed had a sample size of 3 (biological replicates). To determine statistical significance, a threshold of $p<0.05$ (*) was set. Data from STELA and telomere fusion assays are shown as means ± standard error of the mean (SEM), calculated from at least four repeats.

Chapter 3

Assessing the effect of DNA damage response inhibitors on HCT116 cells

3.1 Abstract

Telomere crisis is a cellular state induced after critical telomere shortening and bypass of senescence due to loss of cell-cycle checkpoints. Escape of cells from crisis, which is marked by cell death and genomic instability, is linked to cancer development. It has been previously demonstrated that inhibition of the PARP1-induced DNA damage response (DDR) can prevent the escape of cells from crisis. In this chapter we examine how nine DDR inhibitors (DDRi), targeting proteins required for DDR, affect the ability of cells to escape from crisis.

We used a colorectal cancer cell line (HCT116) expressing a dominant-negative telomerase (DN-hTERT) that undergoes a well-defined period of crisis from which they consistently escape. We treated these cells with different concentrations of DDR inhibitors in a series of three experiments and the effects of these drugs on cell cycle, apoptosis, telomere erosion and progression through crisis were monitored.

NU7441 (DNA-PKi), Rabusertib (CHK1i) and AZD6738 (ATRi) prevented cells from escaping crisis in these experiments. In the chosen concentrations, the inhibitors increased apoptotic levels in the cells prior to crisis, without strongly affecting their cell cycle progression. The addition of these inhibitors did not affect the rate of telomere erosion in DN-hTERT HCT116 cells during telomere crisis.

We have thoroughly investigated the effect of nine DDR inhibitors on cells undergoing a telomere crisis and identified three promising inhibitors: NU7441, Rabusertib and AZD6738 that prevent cells from escaping a telomere driven crisis.

3.2 Introduction

Telomeres are DNA-protein structures that cap the end of eukaryotic linear chromosomes (Barnes et al, 2020). They protect the chromosomes by preventing the activation of the DNA damage response, which would recognise chromosome ends as double-strand DNA breaks and potentially degrade them. DNA polymerases synthesise DNA in one direction, with leading strands that are completely synthesised to the end and lagging strands that cannot be fully replicated at the terminal of the chromosomes (end replication problem) (Olovnikov, 1996; Watson, 1972). As a result, telomeres gradually become shorter by losing 20-50 base pairs with each cell division (Barnes et al, 2020). Stem cells of proliferating tissues express a ribonucleoprotein enzyme called telomerase, which synthesises nucleotide repeats (5'-TTAGGG-3') at the end of the chromosomes, but somatic cells do not express it sufficiently (Maciejowski and de Lange, 2017; Capper et al, 2007).

Critical telomere shortening in somatic cells, mainly caused by the 'end replication problem', activates P53-dependent DNA damage response and G1/S cell cycle arrest (replicative senescence) (Shay, 2016). However, mutations in the P53/RB pathway prevent cells from undergoing cell cycle arrest and they continue to divide until the telomeres become severely short. When this happens, the DNA damage response will become activated and process the chromosome ends, leading to chromosome fusions and chromosomal instability, which kills most cells (Barnes et al, 2020). This state, which is characterised by telomere fusion-induced genomic instability and cell death is called telomere crisis (Jafri et al, 2016). 1 in 10^5 to 1 in 10^7 cells escape telomere crisis and continue to grow by re-activating/increasing telomerase reverse transcriptase or engaging alternative lengthening of telomeres (ALT) mechanisms for unlimited proliferation (von Morgen and Maciejowski, 2018; Shay et al, 1993). As cells that have escaped telomere crisis have a highly modified genome, escape from telomere crisis is linked to the development of malignant tumours (Shay, 2016).

The DNA damage response (DDR) is a network of the signalling pathways that are activated following the generation of DNA damage (O'Connor, 2015). It is responsible for detecting and repairing DNA damage by inducing cell cycle arrest, modulation of DNA replication, senescence or cell death. There are at least 450 essential proteins involved in the DDR and

different forms of DNA damage lead to different repair mechanisms (Pearl et al, 2015; O'Connor, 2015). DDR activation in cancer cells decreases the effectiveness of chemotherapy and radiotherapy, which can lead to development of resistance to cancer therapy (Weber and Ryan, 2015). Moreover, a unique mark of cancer cells is loss of one or more DDR pathways, meaning that cancer cells rely on the remaining pathways (Carrassa and Damia, 2017). Inhibiting these remaining pathways in cancer cells would be lethal, unlike in normal cells, which can use alternative existent pathways (O'Connor, 2015; Carrassa and Damia, 2017). This novel approach in cancer therapy is called synthetic lethality. Thus, DDR is gaining increased interest in cancer research and offers potential targets for drug development.

Ngo et al (2018) demonstrated that two PARP inhibitors, olaparib and rucaparib, selectively killed colorectal cancer cells undergoing crisis, by impeding the repair of dysfunctional telomeres and/or inducing replicative stress at telomeres. This suggests that increasing DNA damage can selectively eliminate cells undergoing a telomere crisis. It was the first demonstration that a drug can prevent cellular escape from crisis, offering the potential to target tumours with dysfunctional telomeres. Following that study, we aimed to investigate whether other DDR inhibitors (DDRi) could have a similar effect during crisis. In this chapter, nine DDRi, including AZD6738 (ATRi), KU-60019 (ATMi), L189 (LIG1i, LIG3i, LIG4i), 6-OH-DOPA (RAD52i), NU7441 (DNA-PKi), Rabusertib (CHK1i), Adavosertib (WEE1i), RI-1 (RAD51i) and AICAR (RAD52i), were assessed in their ability to prevent cells from escaping a telomere crisis. Their impact on cell cycle progression, apoptosis and telomere dysfunction was also studied.

In this chapter, we conducted four main experiments. In the first experiment, wild type (WT) HCT116 cells were treated with the nine inhibitors in order to detect the most appropriate range of drug concentrations to be used in HCT116 cells undergoing a telomere crisis. In the second experiment, HCT116 cells that undergo crisis, following the expression of a dominant negative hTERT construct, were treated with the pre-determined inhibitor concentrations to study their effect on cell growth, cell cycle progression and apoptosis, as well as their ability to prevent cells from escaping a telomere crisis. Inhibitors that may prevent cells from escaping crisis were selected to be further studied in the third (six inhibitors) and fourth

experiment (four inhibitors). Lastly, telomere length analysis was used to test whether these DDRi impact telomere dynamics during crisis.

3.3 Aims

In this chapter, we hypothesise that increased DNA damage, induced by the inhibition of the cellular DNA damage response, may synergise with telomere damage, induced by telomere erosion, to eliminate cells undergoing crisis. As a result, we also hypothesise that increasing DNA damage by inhibiting the DNA damage response will specifically sensitise cells with short dysfunctional telomeres, but not cells with long telomeres. To test this hypothesis, we used DDR inhibitors with different molecular targets to treat colorectal cancer cells (HCT116) expressing a dominant-negative telomerase (DN-hTERT HCT116).

The aims of this chapter are to:

- Identify the most appropriate DDRi concentrations to treat DN-hTERT HCT116 cells
- Assess how nine DDRi affect cell growth, cell cycle progression and apoptosis levels in WT-HCT116 cells
- Identify DDRi that prevent DN-hTERT HCT116 cells from escaping crisis
- Evaluate the effect of DDRi on cell growth, cell cycle progression and apoptosis levels in DN-hTERT HCT116 cells
- Assess if the DDRi used in this study affect the rate of telomere erosion during crisis

3.4 Results

3.4.1. Assessing the effect of DNA damage response inhibitors on WT- HCT116 cells

WT-HCT116 colorectal cancer cells were treated with nine DDR inhibitors to determine the most appropriate range of concentrations to be used for subsequent experiments with HCT116 cells expressing DN-hTERT. The duration of the cell treatment was for two weeks, the cells were passaged at the beginning of the second week and the inhibitors were added every two or three days. Different drug concentrations, covering a broad range of concentrations, were used to treat WT-HCT116 cells. WT-HCT116 cells treated with dimethyl sulfoxide (DMSO) at a concentration of 0.1% served as a control for all the inhibitors, except for 6-OH-DOPA, which was dissolved in 1M HCl , due to better solubility. The final concentration of HCl for 6-OH-DOPA-treated or control cells was 1mM. The inhibitors were first dissolved in an appropriate amount of DMSO/HCl before addition to the cells to ensure that the concentration of DMSO/HCl was the same for all inhibitors. At the end of the first and second week of the cell culture the cell counts were recorded and cell-cycle and apoptosis assays were carried out to determine the growth rate, cell cycle progression and cell death, respectively.

The aim of the experiment was to identify the two most appropriate concentrations to treat DN-hTERT HCT116 cancer cells in order to study the ability of the inhibitors to prevent escape from telomere crisis. The two concentrations to be used in DN-hTERT HCT116 cancer cells, should not be potent enough to significantly affect growth or kill the DN-hTERT HCT116 cells before entering crisis. Initially, five concentrations were chosen for each inhibitor to cover a wide range of values. When possible, the decision for the five concentration values was guided by their use in the literature.

3.4.1.1 Assessing the effect of NU7441, AICAR, Rabusertib and Adavosertib on WT-HCT116 cells

Cell treated with 5µM NU7441 (DNA-PK inhibitor) showed a very slow cell growth in the first week and were not passaged at the end of the week, however their growth rate increased in the second week (figure 3.1.A). Cells treated with 0.15µM and 0.5µM NU7441 showed a decrease in growth compared to the control, but this was possibly a result of an experimental error, as cells treated with 1.5 µM NU7441 showed a growth pattern similar to

the control. It was decided that the two concentrations that would be used in subsequent experiments with DN-hTERT HCT116 cells would be 0.5µM and 1.5µM.

None of the concentrations of AICAR (RAD52 inhibitor) dramatically affected the growth rate of the cells, with only the higher concentration of 300µM slightly slowing down cell growth in the second week (figure 3.1.B). Concentrations greater than 300µM were not tested, as these would be too high to be administered in the clinical setting. However, a follow-up experiment was conducted to examine the effect of the higher AICAR concentration (300µM) in combination with two concentrations of a DNA damaging agent, bleomycin, in WT-HCT116 cells (figure 3.1.C). This experiment was performed to test whether any evidence of biological effect could be determined. 300µM AICAR in combination with 20µg/ml of Bleomycin had a slight effect on cell growth (PD, Population Doubling 6,) compared to the control cells (PD7). Due to the inability of the inhibitor to have a strong effect on cell growth at such a high concentration, the inhibitor was not used for subsequent experiments.

As even the lowest of the selected concentrations (0.2µM) of Rabusertib (CHK1 inhibitor) appeared to slow the rate of cell growth (figure 3.1.D), a follow up experiment with lower concentrations was set up (figure 3.1.E). All the three lower concentrations of Rabusertib showed a growth pattern similar to the control cells. It was concluded that the two concentrations that would be used in subsequent experiments using DN-hTERT HCT116 cells would be 25nM and 50nM.

Similarly to Rabusertib, as the lowest of the selected concentrations (0.1µM) of Adavosertib (WEE1 inhibitor) appeared to slow down cell growth (figure 3.1.F), a follow up experiment with lower concentrations was set up (figure 3.1.G). In the new experiment, the same concentration of 0.1µM (100nM) Adavosertib only slightly slowed down cell growth (PD17) compared to the control cells (PD18). Concentrations lower than 0.1µM did not have any effect on the growth rate. It was decided that the two concentrations to be used in subsequent experiments with DN-hTERT HCT116 cells would be 50nM and 100nM.

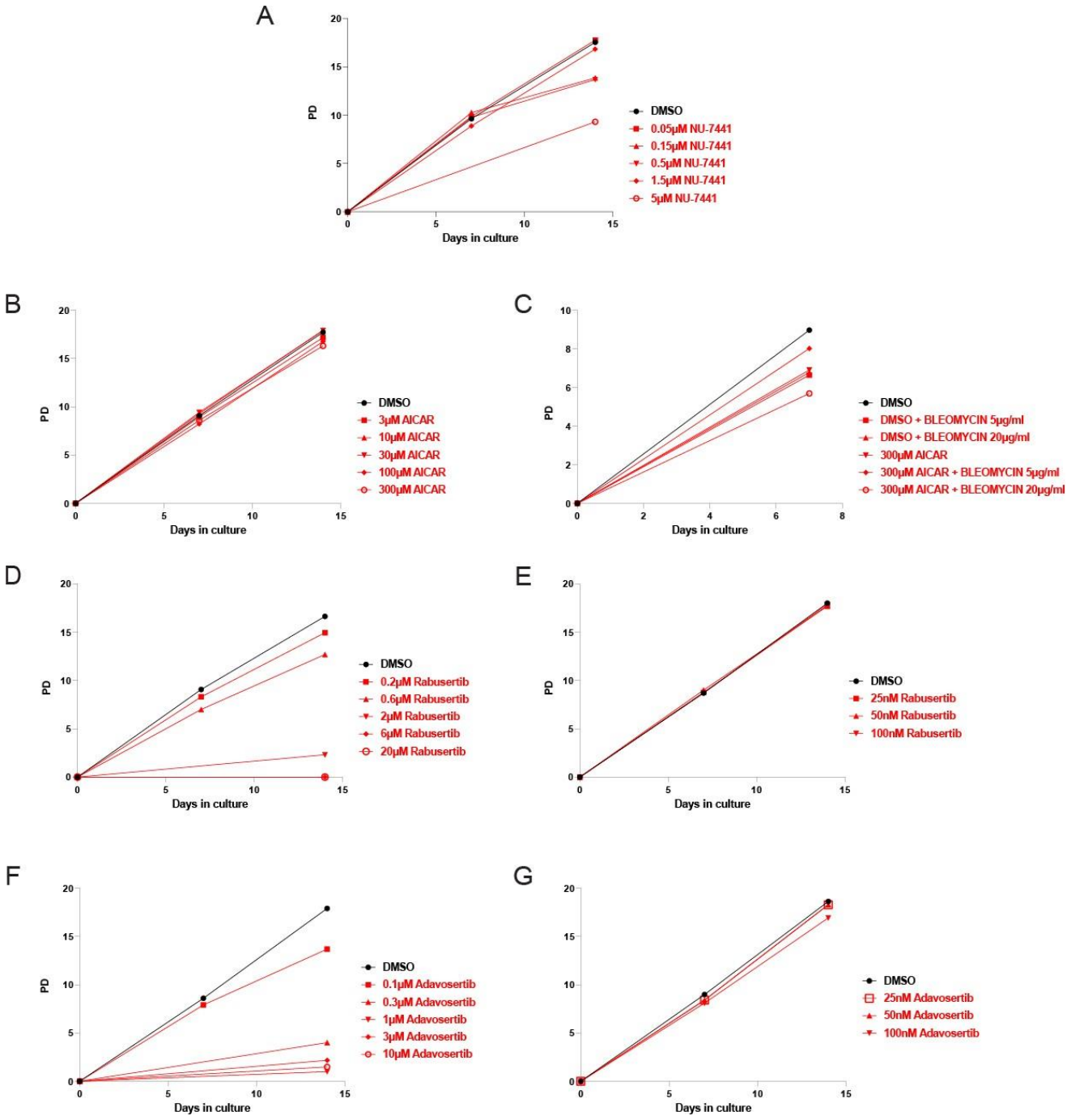

Figure 3.1: Cell growth of WT HCT116 cells treated with different concentrations of DDR inhibitors. Growth curve of WT HCT116 cells during two weeks of treatment with NU-7441 (A), AICAR (B and C), Rabusertib (D and E) and Adavosertib (F and G). The cells were passaged at day 7 of treatment except for cells with low confluency (5µM NU-7441, 2-20µM Rabusertib, 0.3-10µM Adavosertib). PD=population doubling

3.4.1.2 Assessing the effect of AZD6738, RI-1, KU-60019, L189 and 6-OH-DOPA on WT-HCT116 cells

The cells treated with 0.05µM AZD6738 (ATR inhibitor) displayed a growth rate similar to the control cells, but 0.5µM AZD6738 slowed cell growth (PD15) compared to the control cells (PD18) (figure 3.2.A). Higher concentrations strongly inhibited cell growth. These results are confirmed by literature, as 0.5µM AZD6738 evidently slowed down WT-HCT116 growth, while concentrations higher than 1µM had a very dramatic effect on WT-HCT116 growth (Dillon et al, 2017). It was decided that the two concentrations to be used in DN-hTERT HCT116 cells would be 0.05µM and 0.1µM.

0.5µM RI-1 (RAD51 inhibitor) did not affect cell growth and 1.5 µM RI-1 only slightly slowed down cell growth at the second week (figure 3.2.B). 5 µM RI-1 or higher strongly affected cell growth. It was decided that the two concentrations to be used in subsequent experiments with DN-hTERT HCT116 cells would be 0.5µM and 1µM.

KU-60019 (ATM inhibitor) concentrations of 0.05µM, 0.15µM and 0.5µM displayed a very similar growth rate to the control cells, with only a slight decrease in cell growth at the concentration of 0.5µM (PD17) compared to the control cells (PD18) (Figure 3.2.C). It was decided that the two concentrations to be used in subsequent experiment using DN-hTERT HCT116 cells would be 0.15µM and 0.5µM.

As the five concentrations (0.5-5µM) of L189 (LIG1, LIG3, LIG4 inhibitor) did not have an effect on cell growth during the first week, three additional concentrations were included in the second week (figure 3.2.D). While 10µM L189 did not appear to have an important effect on cell growth, 25µM and 50µM L189 dramatically affected cell growth. These results are confirmed by literature, as 5 µM L189 treatment of WT-HCT116 cells had almost no effect on cell growth, while 10µM L189 treatment only slightly affected cell growth (Chen et al, 2008). It was decided that the two concentrations to be used in DN-hTERT HCT116 cells would be 5µM and 10µM.

While concentrations 0.1-1 µM 6-OH-DOPA (RAD52 inhibitor) had a growth rate similar to the control cells, there was only a slight decrease in cell growth in 3µM 6-OH-DOPA-treated cells and a dramatic decrease in cell growth in 10µM 6-OH-DOPA-treated cells (figure 3.2.E).

It was decided that the two concentrations to be used in subsequent experiments using DN-hTERT HCT116 cells would be 0.3µM and 1µM.

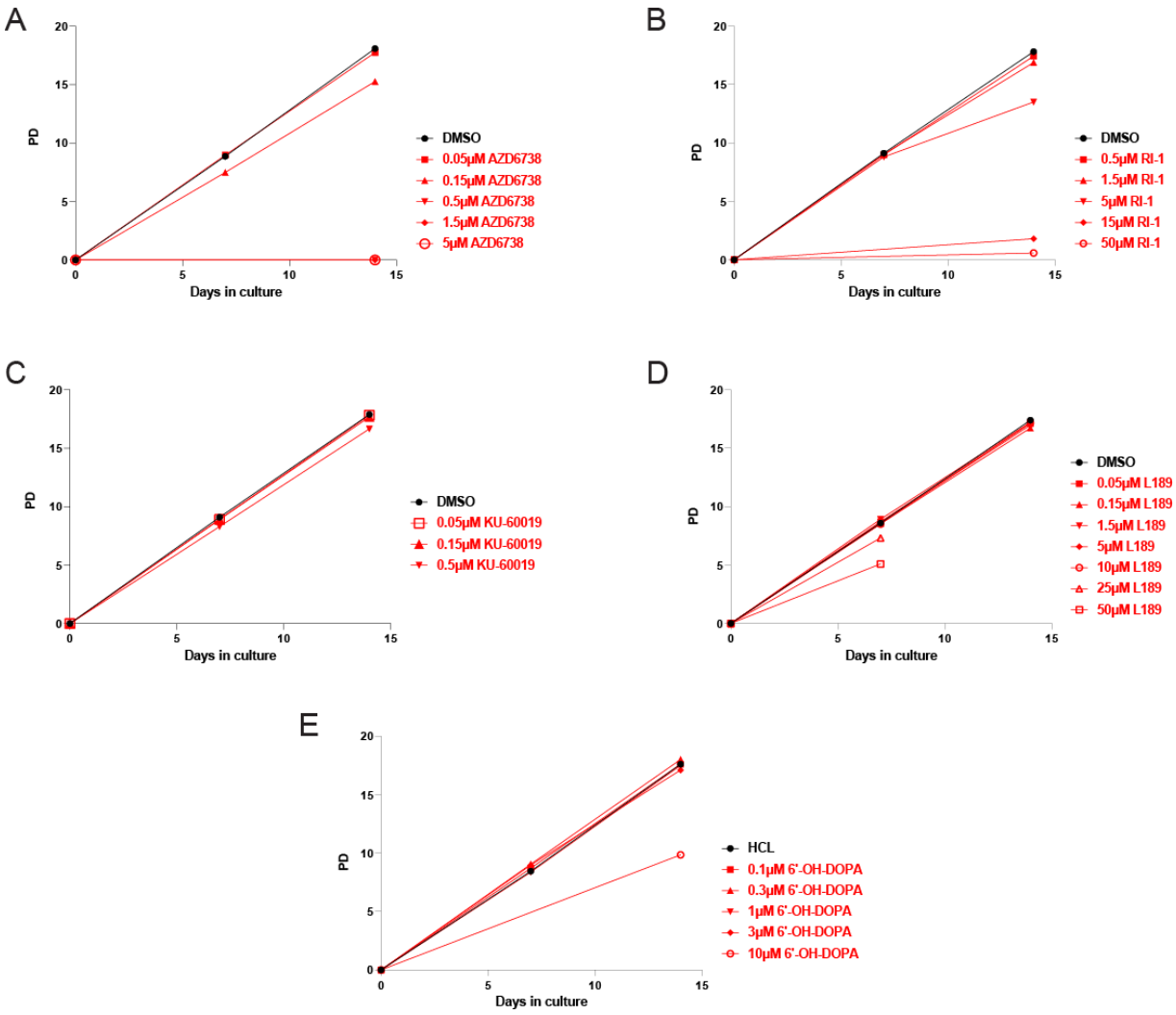

Figure 3.2: Cell growth of WT HCT116 cells treated with different concentrations of DDR inhibitors. Growth curve of WT HCT116 cells during two weeks of treatment with AZD6738 (A), RI-1 (B), KU-60019 (C), L189 (D) and 6-OH-DOPA (E). The cells were passaged at day 7 of treatment except for cells with low confluency (0.5-5µM AZD6738, 15-50µM RI-1, 10µM 6'-OH-DOPA). Cells treated with 10µM, 25µM and 50µM L189 were treated only for one week.

3.4.2 Assessing the effect of eight DNA damage response inhibitors on DN-hTERT-HCT116 cells

To study the potential of the DDR inhibitors to modulate the ability of cells to escape a telomere-driven crisis, a clonal population of HCT116 cells expressing DN-hTERT was used. These cells have been extensively characterised (Ngo et al, 2018; Jones et al, 2014). The expression of DN-hTERT abrogates telomerase activity such that telomeres erode and they have a well-defined onset of replicative crisis, but are consistently able to escape crisis. These cells were cultured in the same conditions as WT HCT116, as described in the previous section, but with the addition of puromycin to select for the presence of the DN-hTERT construct. They were treated with eight DDR inhibitors (without AICAR) and fresh inhibitor was added every two or three days. Two different drug concentrations, as determined from the previous experiments, were used to treat the DN-hTERT HCT116 cells along with a DMSO or a HCl control (for the 6-OH-DOPA). At the end of each week, the cells were counted and cell-cycle and apoptosis assays were carried out to determine the growth rate, cell cycle progression and cell death respectively. Every time the cells were harvested, a sample of cells was collected to be cryopreserved and an experiment sample was taken to be used for DNA extraction for subsequent telomere length analysis (STELA) (figure 3.3).

The inhibitor experiments were divided into two sets and the treatment started at PD36. In the first experiment DN-hTERT HCT116 cells were treated with AZD6738, KU-60019, L189 and 6-0H-DOPA (Set 1) and in the second experiment DN-hTERT HCT116 cells were treated with NU7441, Rabusertib, Adavosertib and RI-1 (Set 2). The second experiment was started one and a half weeks after the first experiment.

After the start of each experiment, the cells were counted each week until the third week, when cell growth stopped, the cells appeared large and vacuolated and there was increased apoptosis. These are the characteristics of cells undergoing a telomere-driven crisis (Ngo et al, 2018). The cells entered a crisis state after about 54 population doublings from the point of single-cell cloning. Before the onset of crisis there was no detectable difference in the growth rates of the treated cells and differences only became apparent as the cells entered crisis. DN-hTERT HCT116 cells treated with HCl, 0.3µM 6-OH-DOPA and 1µM 6-OH-DOPA from Set 1 (figure 3.11) and 0.5µM NU7441 (figure 3.4) and 50nM Adavosertib (figure 3.6) from Set 2 escaped the crisis state, after approximately 40 days.

The growth of these cells increased, and the rates of apoptosis decreased, compared to the week before they entered crisis (Week 3). The cells that escaped from Set 1 were passaged four or five times after they escaped crisis, in a time period of approximately 30 days and a final PD of 70, when the experiment was intentionally terminated. Cells treated with 0.5µM NU7441 showed an increased cell growth, but cells treated with 50nM Adavosertib appeared as small and dense colonies that were far apart from each other.

Unfortunately, neither of the DMSO-treated control cells in Set 1 or Set 2 escaped (figures 3.4-3.10). The failure of the DMSO-treated cells to escape crisis was unexpected as numerous previous experiments demonstrate that these cells reliably escape. It was considered that the control cells did not escape crisis because only a small number of cells entered crisis due to the passage point being too close to the point at which the cells entered crisis, hence these cells may have had a lower chance to escape. In the next section, the effects of each inhibitor on DN-hTERT cells experiencing telomere crisis are described.

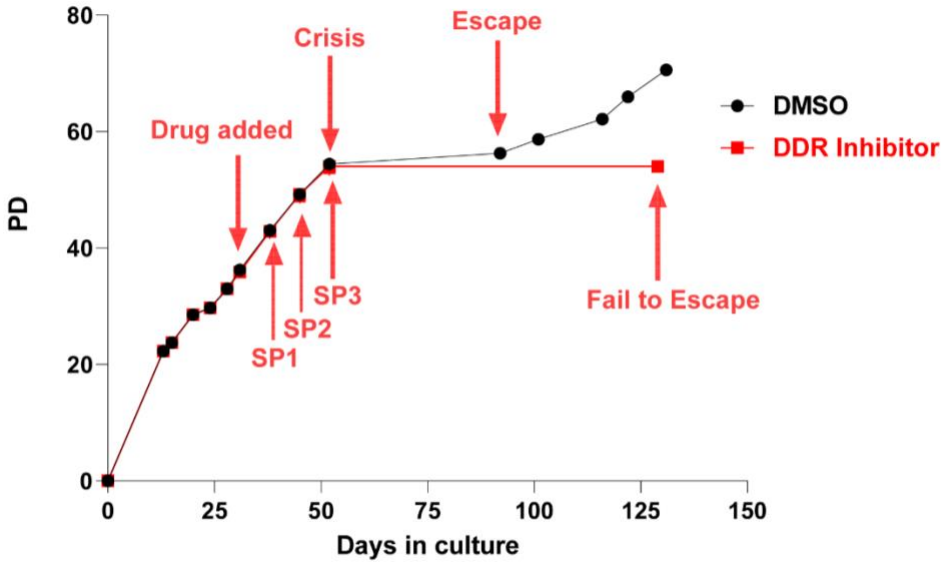

Figure 3.3. Crisis and escape PD curve. This figure shows a representative growth curve of DN-hTERT HCT116 cells treated with a DDR inhibitor that prevents escape from crisis. DN-hTERT HCT116 cells enter crisis after about 54 population doublings from the point of single-cell cloning. At the end of each week after the addition of the drug (Sampling Points 1, 2 and 3), the cells are counted, cell-cycle and apoptosis assays are carried out, a sample is cryopreserved and another sample is collected for STELA. While cells treated with DMSO enter crisis and escape, cells treated with the DDR inhibitor enter crisis and fail to escape.

3.4.2.1 Assessing the effect of NU7441 on DN-hTERT-HCT116 cells

Cells treated with 0.5µM NU7441 (DNA-PK inhibitor) escaped crisis at PD54 (day 90) and were passaged five times for 44 days after crisis, reaching PD70, while cells treated with 1.5 µM NU7441 were passaged once after crisis but died (figure 3.4A). DMSO-treated control cells did not escape crisis.

Cells treated with both concentrations of NU7441 showed an increased accumulation of cells in G2/M, S, and >4n phase as they approached crisis, in a similar way to the control cells (figure 3.4B). At day 45 and 52, there were more inhibitor-treated cells in S, G2/M, >4n phase and less in G1 phase compared to control cells. 0.5µM NU7441-treated cells showed a reduced accumulation in G2/M and S phase and an increased accumulation in G1 phase as they were recovering from escaping crisis (days 90-116).

Apoptosis levels increased by ~30% (compared to control cells) in both concentrations of NU7441-treated cells at day 45 of treatment (figure 3.4.C). There was also an increase in early apoptotic 1.5µM NU-7441-treated cells at day 52 of treatment compared to control cells. In the weeks after crisis 0.5µM NU7441-treated cells maintained similar levels of apoptosis to the last week before crisis (day 52), with approximately 35% cell death.

In conclusion, NU7441 did affect strongly cell cycle progression (<15% compared to the control cells at day 45) in DN-hTERT HCT116 cells, but it had a strong effect on apoptotic levels at day 45. Since cells treated with the lower concentration of NU7441 managed to escape crisis and recover, while those treated with the higher concentration of the inhibitor failed to escape crisis, NU7441 may influence the ability of the cells to escape a telomere crisis.

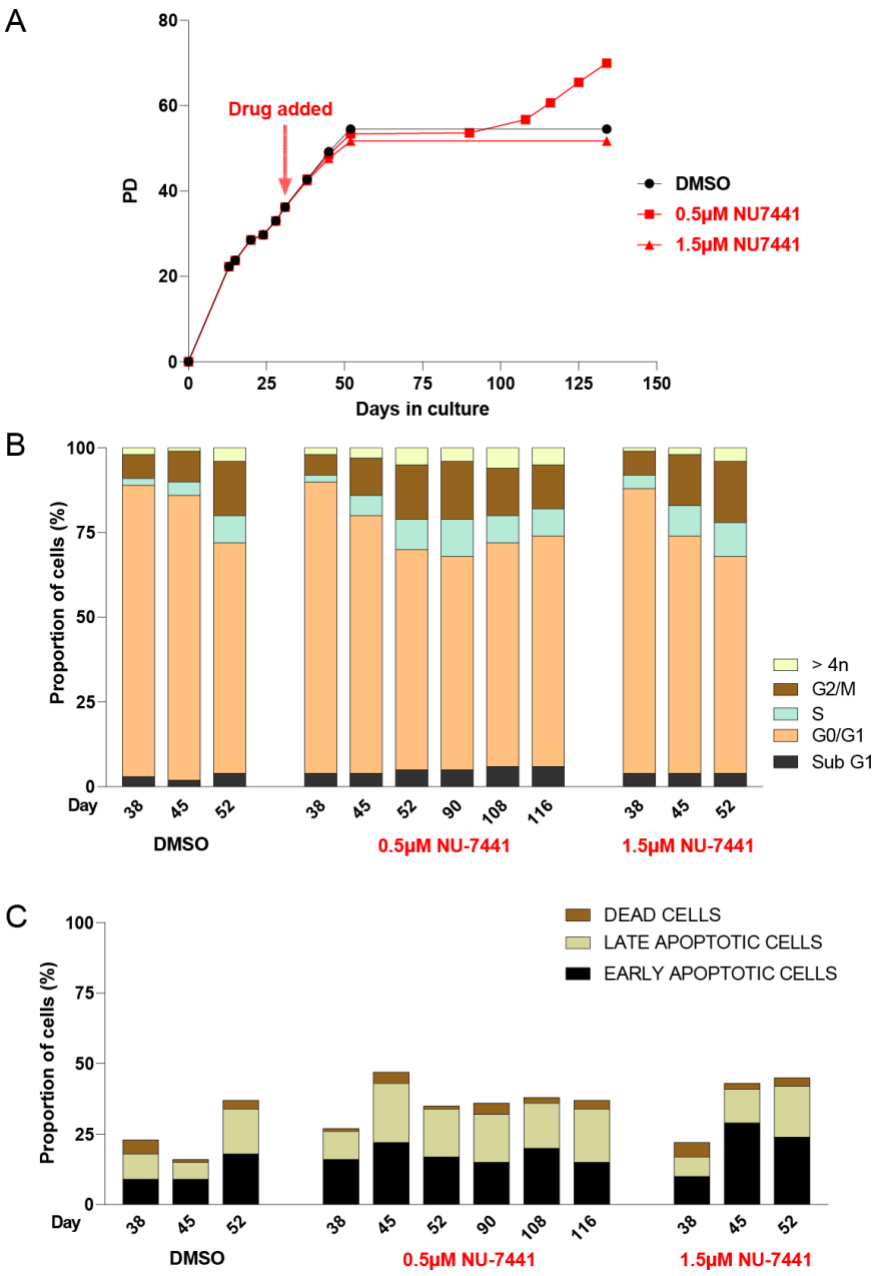

Figure 3.4: Cell growth, cell cycle and apoptosis analysis of DN-hTERT HCT116 cells treated with two different concentrations of NU7441. The figure shows the growth curve (A), cell cycle progression (B) and apoptotic levels (C) of DN-hTERT HCT116 treated with DMSO and NU7441. Cells were passaged three times after the addition of the inhibitor and entered crisis after ~54 population doublings from the point of single-cell cloning. A 2-step cell cycle analysis was carried out to determine the cell cycle state before (days 38, 45, 52) and after crisis (days 90, 108 and 116) for escapees. Apoptosis was analysed at the same days using Annexin-V/propidium iodide (PI) staining. Cells were classified as early apoptotic when they were Annexin V positive and PI negative, late apoptotic when they were Annexin V and PI positive and dead when they were Annexin V negative and PI positive.

3.4.2.2 Assessing the effect of Rabusertib on DN-hTERT-HCT116 cells

Cells treated with both concentrations of Rabusertib (CHK1 inhibitor) failed to escape crisis (figure 3.5.A). Unfortunately, this was also the case with the control DMSO-treated cells.

Cells treated with both concentrations of Rabusertib showed an increased accumulation of cells in G2/M, S, and >4n phase as they approached crisis, in a similar way to the control cells (figure 3.5.B). There were no differences in the cell cycle distribution between inhibitor-treated and control cells.

There was not an increase in the apoptotic levels of 25nM Rabusertib-treated cells compared to the DMSO-treated cells, but there was increased apoptosis (early and late) in 50nM Rabusertib-treated cells at days 45 and 52 (figure 3.5.C).

In conclusion, Rabusertib did not strongly affect cell cycle progression in DN-hTERT HCT116 cells, but it increased apoptosis at the higher concentration (by approximately 20%). However, since both the control cells and inhibitor-treated cells failed to escape, no conclusion could be reached about whether this inhibitor can prevent escape from a telomere crisis.

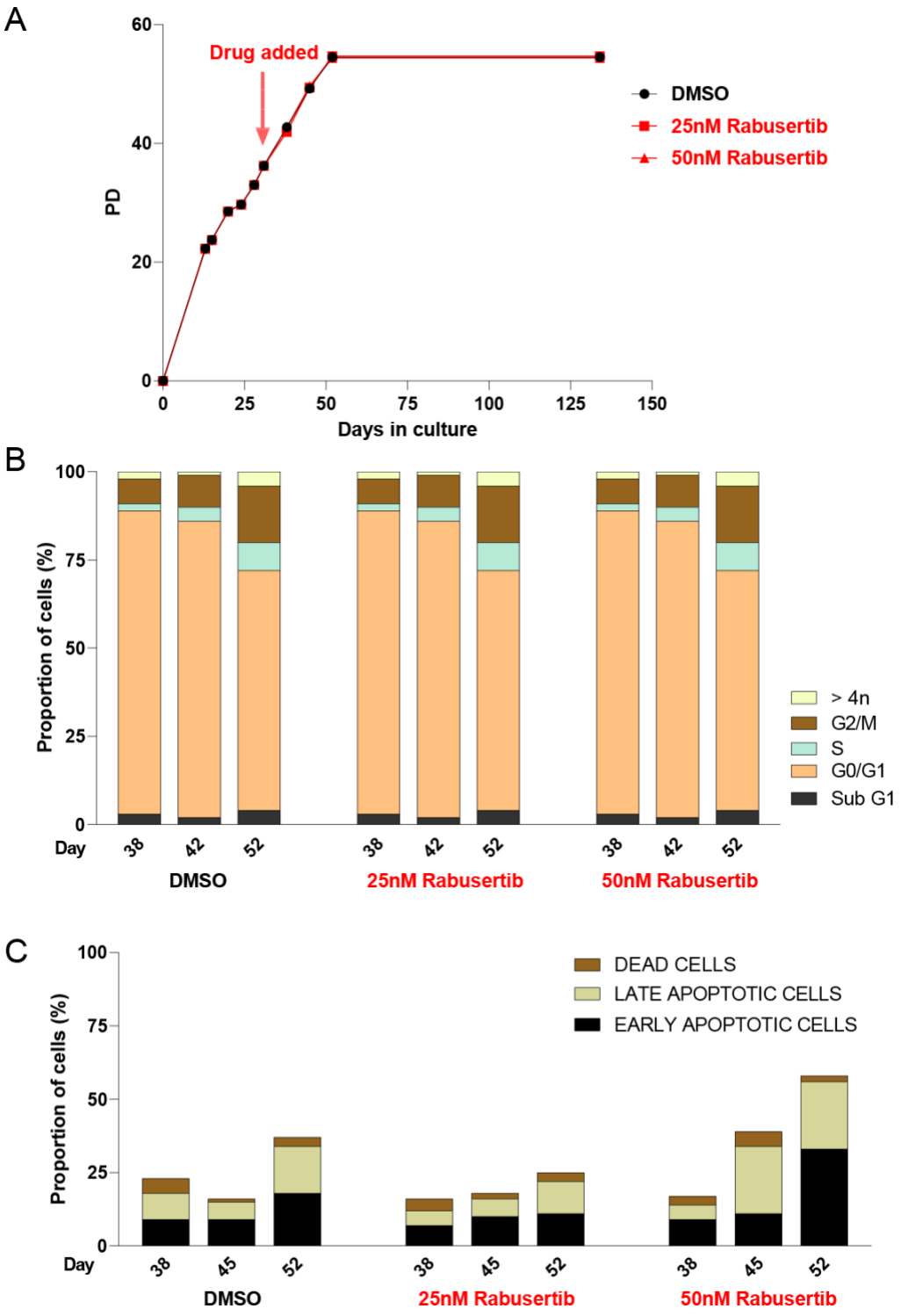

Figure 3.5: Cell growth, cell cycle and apoptosis analysis of DN-hTERT HCT116 cells treated with two different concentrations of Rabusertib. The figure shows the growth curve (A), the cell cycle progression (B) and apoptotic levels (C) of DN-hTERT HCT116 treated with DMSO and Rabusertib. Apoptosis was analysed using Annexin-V/propidium iodide (PI) staining. Cells were classified as early apoptotic when they were Annexin V positive and PI negative, late apoptotic when they were Annexin V and PI positive and dead when they were Annexin V negative and PI positive.

3.4.2.3 Assessing the effect of Adavosertib on DN-hTERT-HCT116 cells

Cells treated with 50nM Adavosertib (WEE1 inhibitor) escaped crisis at PD54 (day 87) (figure 3.6.A). Under the microscope the cells appeared to grow in small colonies with packed centers (not shown). In contrast, the cells treated with 100nM Adavosertib failed to escape crisis, but they exhibited slower cell growth prior to crisis.

Cells treated with both concentrations of Adavosertib showed an increased accumulation of cells in G2/M, S and >4n phase as they approach crisis, in a similar way to the control cells (figure 3.6.B). There were differences in the cell cycle distribution between 50nM Adavosertib-treated and control cells at day 52 (more cells in S, G2/M, >4n phase and less cells in G1 phase) and between 100nM Adavosertib-treated and control cells at day 45 (more cells in S and >4n phase and less cells in G1 phase). No sample of cells treated with 100nM Adavosertib was collected for analysis at day 52, because there was limited cell growth. After cells treated with 50nM Adavosertib escaped crisis, the vast majority of the cells (> 61%) was in the G2/M phase.

There was increased (early and late) apoptosis in Adavosertib-treated cells (for both concentrations) compared to the control cells at day 45 (figure 3.6.C). This increase was higher in cells treated with 100nM Adavosertib. After cells treated with 50nM Adavosertib escaped crisis, apoptotic levels were reduced (20% lower apoptosis between day 161 and 180).

In conclusion, Adavosertib affected cell cycle progression in DN-hTERT HCT116 cells and it increased apoptosis (by approximately 25% at day 45). Since the lower concentration of Adavosertib-treated cells managed to escape crisis and reached a PD of 70, while the higher concentration of the inhibitor failed to escape crisis, Adavosertib may affect the ability of the cells to escape a telomere crisis.

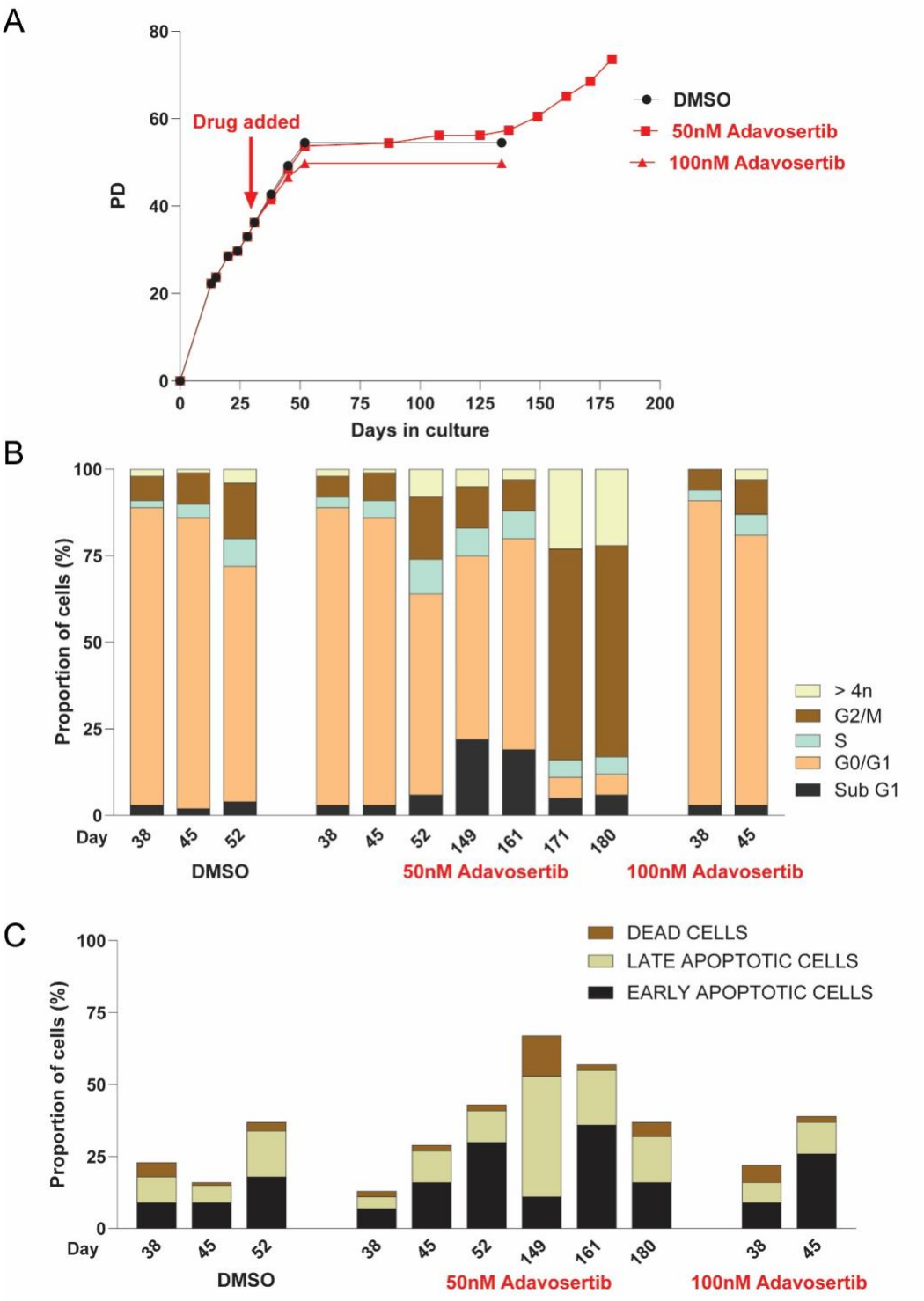

Figure 3.6: Cell cycle and apoptosis analysis of DN-hTERT HCT116 cells treated with two different concentrations of Adavosertib. The figure shows the growth curve (A), the cell cycle progression (B) and apoptotic levels (C) of DN-hTERT HCT116 treated with DMSO and Adavosertib. Apoptosis was analysed using Annexin-V/propidium iodide (PI) staining. Cells were classified as early apoptotic when they were Annexin V positive and PI negative, late apoptotic when they were Annexin V and PI positive and dead when they were Annexin V negative and PI positive.

3.4.2.4 Assessing the effect of RI-1 on DN-hTERT-HCT116 cells

Cells treated with RI-1 (RAD51 inhibitor) failed to escape crisis and so did the control cells (figure 3.7.A).

Cells treated with both concentrations of RI-1 showed an increased accumulation of cells in G2/M, S, and >4n phase as they approached crisis, in a similar way to the control cells (figure 3.7.B). There were differences in the cell cycle distribution between inhibitor-treated and control cells at day 52 (more cells in subG1 and >4n phase and less cells in G1 phase). The differences were more pronounced in cells treated with the higher concentration (1μM).

While RI-1-treated cells did not exhibit higher apoptotic levels at days 38 and 52 compared to the control cells, they showed increased early and late apoptosis at day 45 (figure 3.7.C).

In conclusion, RI-1 affected cell cycle progression only at day 52 and slightly affected apoptotic levels (<20% at day 45) in DN-hTERT HCT116 cells. Since both the control and the inhibitor-treated cells failed to escape crisis, no conclusion could be reached as to whether this inhibitor can prevent the escape from a telomere crisis.

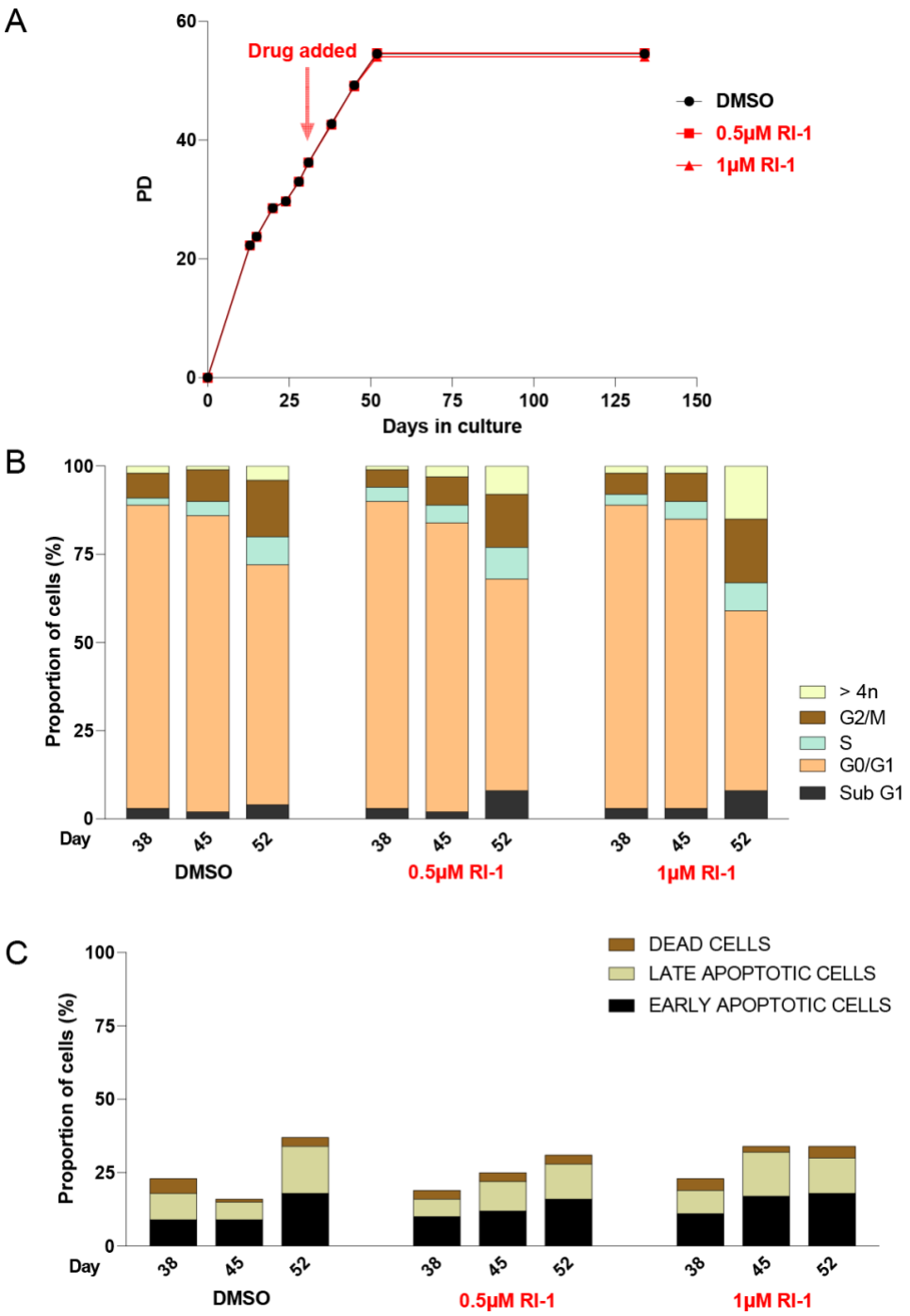

Figure 3.7: Cell growth, cell cycle and apoptosis analysis of DN-hTERT HCT116 cells treated with two different concentrations of RI-1. The figure shows the growth curve (A), the cell cycle progression (B) and apoptotic levels (C) of DN-hTERT HCT116 treated with DMSO and RI-1. Apoptosis was analysed using Annexin-V/propidium iodide (PI) staining. Cells were classified as early apoptotic when they were Annexin V positive and PI negative, late apoptotic when they were Annexin V and PI positive and dead when they were Annexin V negative and PI positive.

3.4.2.5 Assessing the effect of AZD6738 on DN-hTERT-HCT116 cells

As the two concentrations of the inhibitor were very potent, because they affected cell growth before crisis, it was decided to reduce the concentration of AZD6738 to one fourth of the original concentration in the subsequent experiments. Cells treated with AZD6738 (ATR inhibitor) failed to escape crisis and so did the control cells (figure 3.8.A).

Cells treated with both concentrations of AZD6738 showed an increased accumulation of cells in G2/M and S phase as they approached crisis, in a similar way to the control cells (figure 3.8.B). However, cells treated with both concentrations of AZD6738 showed a slightly increased accumulation in S phase and a decrease in G1 phase compared to the control cells. No samples were collected for analysis at day 52, because there was limited cell growth, so the cells were not passaged.

Although there was only a slight increase in apoptosis at days 38 and 45 in 0.05 μM AZD6738-treated cells, the inhibitor severely affected cell growth at day 52 (figure 3.8.C).

In conclusion, AZD6738 only slightly affected cell cycle progression and apoptotic levels in DN-hTERT HCT116 cells at days 38 and 45 (as data from day 52 is not available). Since both the control and the inhibitor-treated cells failed to escape crisis, no conclusion could be reached as to whether this inhibitor can prevent the escape from a telomere crisis.

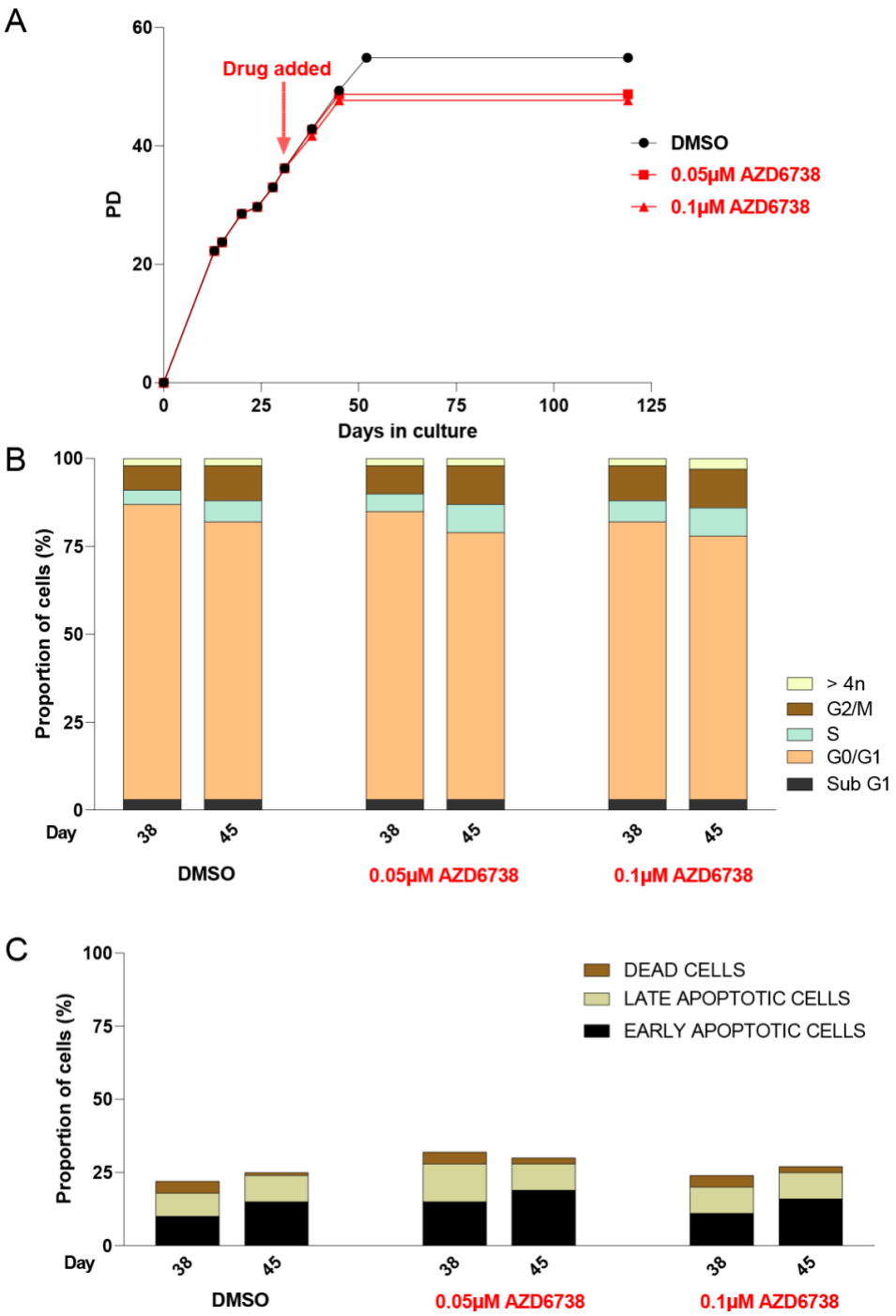

Figure 3.8: Cell growth, cell cycle and apoptosis analysis of DN-hTERT HCT116 cells treated with two different concentrations of AZD6738. The figure shows the growth curve (A), the cell cycle progression (B) and apoptotic levels (C) of DN-hTERT HCT116 treated with DMSO and AZD6738. Apoptosis was analysed using Annexin-V/propidium iodide (PI) staining. Cells were classified as early apoptotic when they were Annexin V positive and PI negative, late apoptotic when they were Annexin V and PI positive and dead when they were Annexin V negative and PI positive.

3.4.2.6 Assessing the effect of KU-60019 on DN-hTERT-HCT116 cells

Cells treated with KU-60019 (ATM inhibitor) failed to escape crisis and so did the control cells (figure 3.9.A).

Cells treated with both concentrations of KU-60019 showed an increased accumulation of cells in G2/M and >4n phase as they approached crisis, in a similar way to the control cells (figure 3.9.B). There were differences in the cell cycle distribution between inhibitor-treated and control cells at all days (more cells in S and G2/M phase and less cells in G1 phase). The differences were more pronounced at days 45 and 52.

There was no increase in the apoptotic levels of KU-60019-treated cells compared to the control cells (figure 3.9.C).

In conclusion, KU-60019 affected cell cycle progression, but not apoptotic levels in DN-hTERT HCT116 cells. Since both the control and the inhibitor-treated cells failed to escape crisis, no conclusion could be reached as to whether this inhibitor can prevent the escape from a telomere crisis.

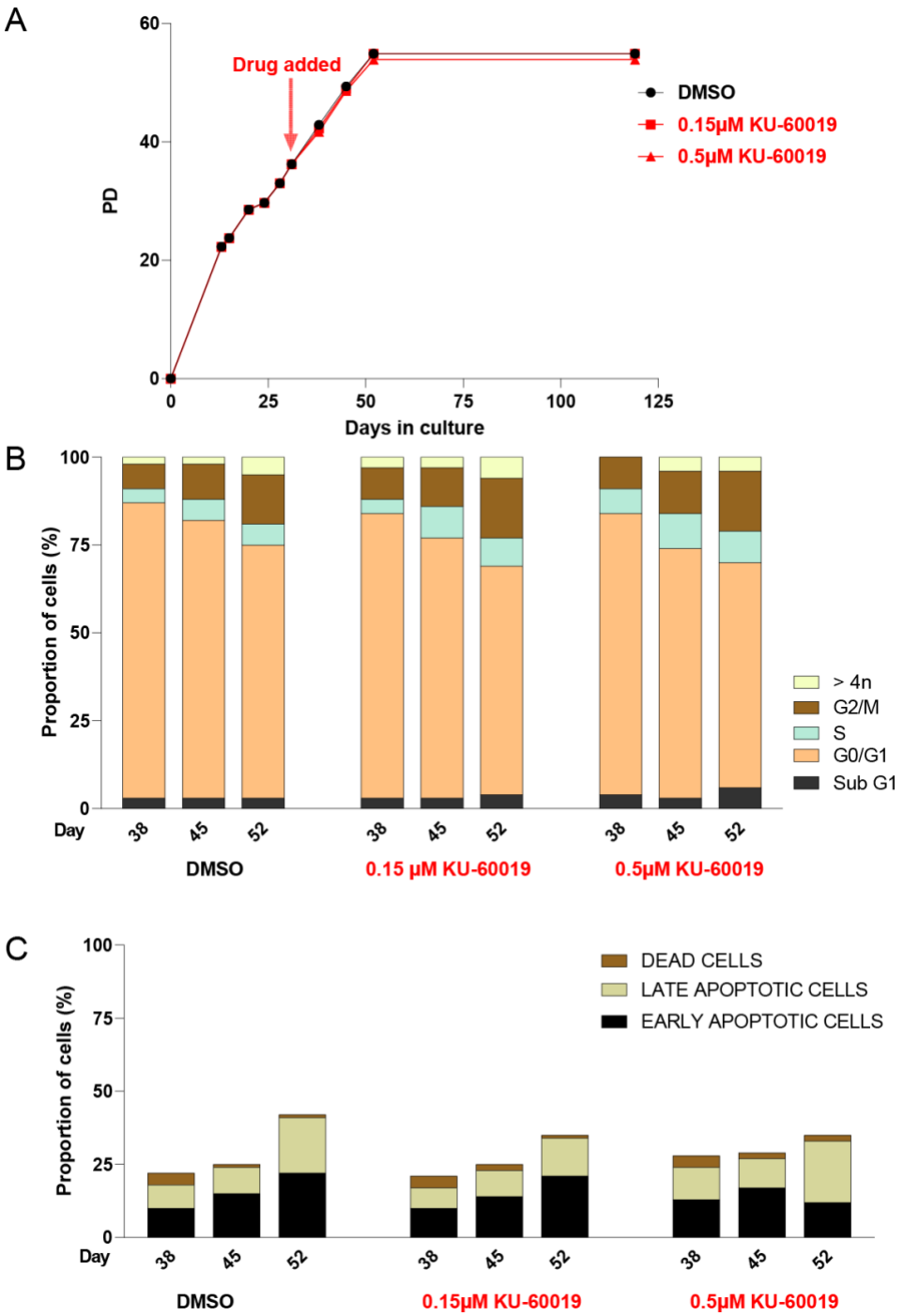

Figure 3.9: Cell growth, cell cycle and apoptosis analysis of DN-hTERT HCT116 cells treated with two different concentrations of KU-60019. The figure shows the growth curve (A), the cell cycle progression (B) and apoptotic levels (C) of DN-hTERT HCT116 treated with DMSO and KU-60019. Apoptosis was analysed using Annexin-V/propidium iodide (PI) staining. Cells were classified as early apoptotic when they were Annexin V positive and PI negative, late apoptotic when they were Annexin V and PI positive and dead when they were Annexin V negative and PI positive.

3.4.2.7 Assessing the effect of L189 on DN-hTERT-HCT116 cells

Cells treated with L189 (DNA Ligase I, III and IV inhibitor) failed to escape crisis and so did the control cells (figure 3.10.A).

Cells treated with both concentrations of L189 showed an increased accumulation of cells in G2/M and >4n phase as they approached crisis, in a similar way to the control cells (figure 3.10.B). There were no significant differences in the cell cycle distribution between inhibitor-treated and control cells.

There was no increase in the apoptotic levels of 5μM L189-treated cells compared to the control cells. However, there was an increase in the apoptotic levels of 10μM L189-treated cells compared to the control cells at day 38 (~10% increase) and 52 (~20% increase in early apoptotic cells) (figure 3.10.C).

In conclusion, L189 did not affect cell cycle progression but affected apoptotic levels in DN-hTERT HCT116 cells. Since both the control and the inhibitor-treated cells failed to escape crisis, no conclusion could be reached as to whether this inhibitor can prevent the escape from a telomere crisis.

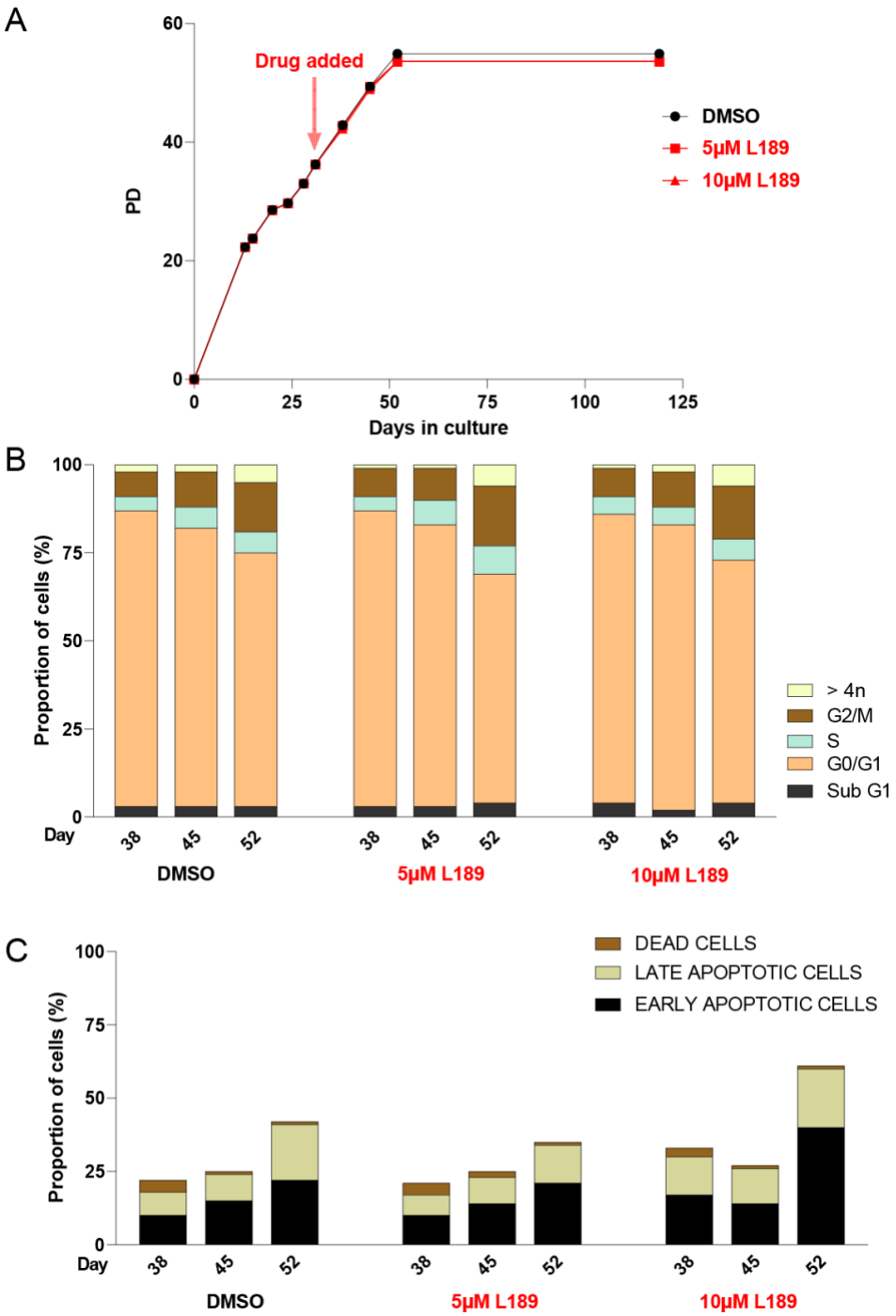

Figure 3.10: Cell growth, cell cycle and apoptosis analysis of DN-hTERT HCT116 cells treated with two different concentrations of L189. The figure shows the growth curve (A), the cell cycle progression (B) and apoptotic levels (C) of DN-hTERT HCT116 treated with DMSO and L189. Apoptosis was analysed using Annexin-V/propidium iodide (PI) staining. Cells were classified as early apoptotic when they were Annexin V positive and PI negative, late apoptotic when they were Annexin V and PI positive and dead when they were Annexin V negative and PI positive.

3.4.2.8 Assessing the effect of 6-0H-DOPA on DN-hTERT-HCT116 cells

Control cells treated with HCl escaped crisis first (PD57, day 89) followed by the cells treated with the two concentrations of 6-0H-DOPA (RAD52 inhibitor) (PD56, day 94) (figure 3.11.A).

Cells treated with both concentrations of 6-OH-DOPA showed an increased accumulation of cells in G2/M and >4n phase as they approached crisis and after crisis the cells in G2/M phase were either reduced (cells treated with the lower concentration) or remained almost the same (cells treated with the higher concentration) (figure 3.11.B). There were no significant differences in the cell cycle distribution between inhibitor-treated and control cells prior to crisis (days 38-52). After cells had recovered from crisis at day 110, the cell cycle distribution was similar between the control and inhibitor-treated cells.

There was no increase in the apoptotic levels of 6-OH-DOPA-treated cells compared to the control cells before crisis (figure 3.11.C). After crisis (day 110), 0.3µM and 1µM 6-OH-DOPA increased apoptotic levels by 8% and 10% respectively, but the apoptotic levels remained <30%.

In conclusion, 6-OH-DOPA did not affect cell cycle progression and apoptotic levels in DN-hTERT HCT116 cells. Since the 6-0H-DOPA-treated cells behaved in a similar way to the control cells, entering crisis at the same PD point and escaping crisis at a similar PD point, it can be concluded that 0.3µM 6-OH-DOPA and 1µM 6-OH-DOPA do not prevent cells from escaping a telomere crisis.

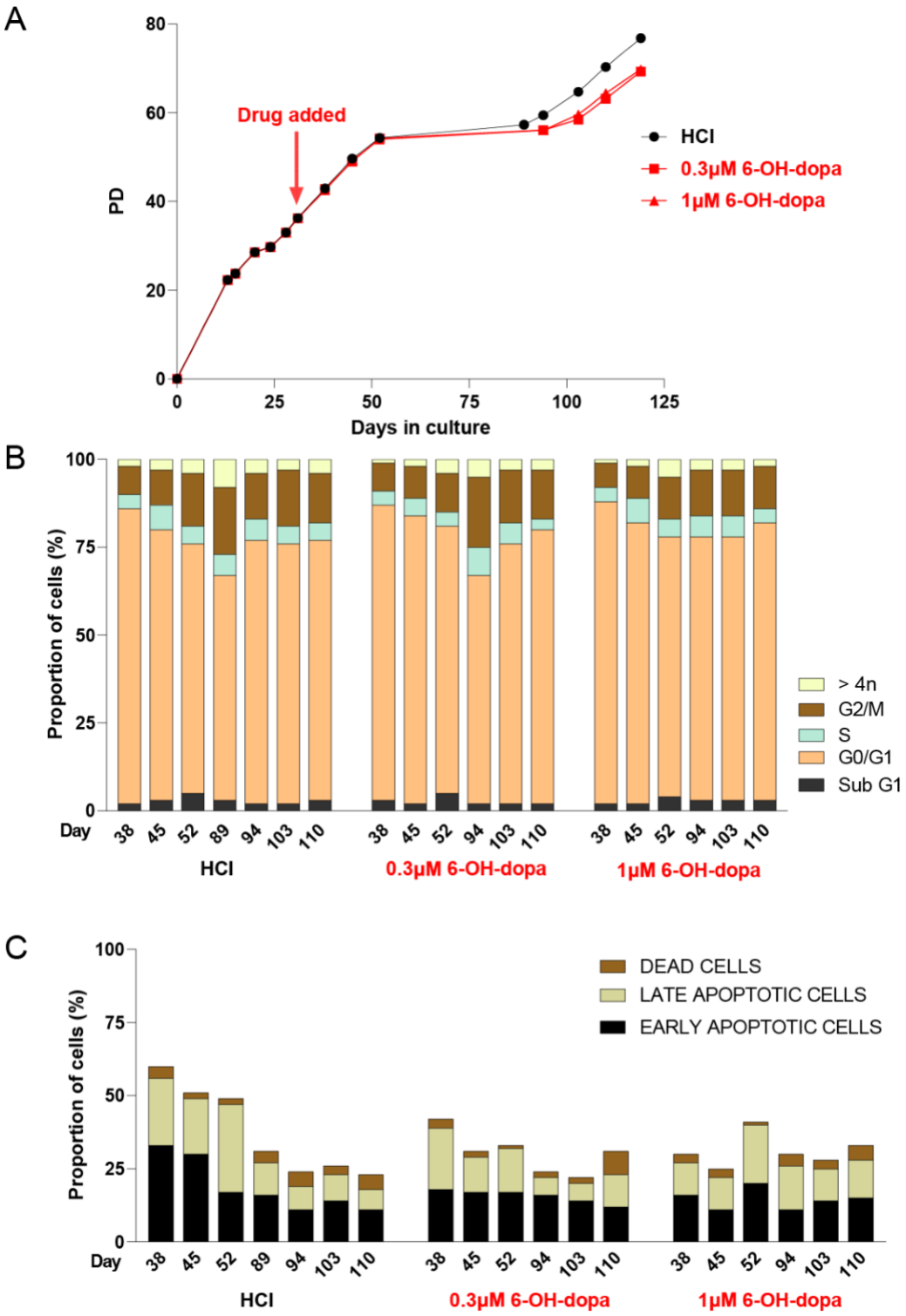

Figure 3.11: Cell growth, cell cycle and apoptosis analysis of DN-hTERT HCT116 cells treated with two different concentrations of 6-OH-DOPA. The figure shows the growth curve (A), the cell cycle progression (B) and apoptotic levels (C) of DN-hTERT HCT116 treated with HCl and 6-OH-DOPA. Apoptosis was analysed using Annexin-V/propidium iodide (PI) staining. Cells were classified as early apoptotic when they were Annexin V positive and PI negative, late apoptotic when they were Annexin V and PI positive and dead when they were Annexin V negative and PI positive.

2.4.2.9 STELA analysis

Single-telomere length analysis (STELA) is a PCR-based technique that precisely measures telomere length on individual chromosomes (Baird et al, 2003). It allows for the detection of very short telomeres and uses primers that are specific to sub telomeric sequences of a chromosome (Baird et al, 2003; Montpetit et al, 2014).

Telomere length analysis was undertaken to assess if any of the inhibitors affected the rate of erosion or telomere stability during crisis. The telomere length of the DN-hTERT HCT116 cells before the administration of the inhibitor (Week 0, PD36) was compared to the inhibitor-treated cells at the end of Week 3 of treatment (day 52), when they started entering crisis (PD54). Figure 3.12 shows the analysis of the 17p telomeres of the cells treated with the inhibitors in Set 1 and figure 3.13 shows the analysis of the 17p telomeres of the cells treated with the inhibitors in Set 2. Figure 3.12 shows that the telomeres of all the inhibitor-treated cells are equally short to the control cells and shorter than the telomeres from the non-treated cells at PD36 (W0). AZD6738 was not included as no sample was obtained from day 52, due to the slow growth of AZD6738-treated cells.

Figure 3.13 shows that the telomeres of all the inhibitor-treated cells are shorter than the telomeres from the non-treated cells at PD36 (W0). In addition, it shows a slightly shorter mean telomere length (up to 0.23kb) for the cells treated with the lower concentration of NU7441, both concentrations of Adavosertib and both concentrations of RI-1 compared to the control cells. To further test the ability of the inhibitors in this set to alter the rate of telomere erosion, a further analysis of the XpYp telomeres from these cells was conducted. STELA of the XpYp telomeres revealed that the telomeres of all the inhibitor-treated cells are equally short to the control cells and shorter than the telomeres from the non-treated cells at PD36 (W0) (Figure 3.14). STELA analysis of the 17p telomeres in HCT116 cells shows a bimodal distribution of telomeres, due to allelic variation as a consequence of different paternal and maternal telomeric contributions (Baird et al, 2003; Britt-Compton et al, 2006) whereas only one telomeric allele is detected at XpYp.

In conclusion, HCT116 DN-hTERT cells entered crisis induced by telomere erosion and none of the inhibitors affected the rate of telomere erosion during crisis.

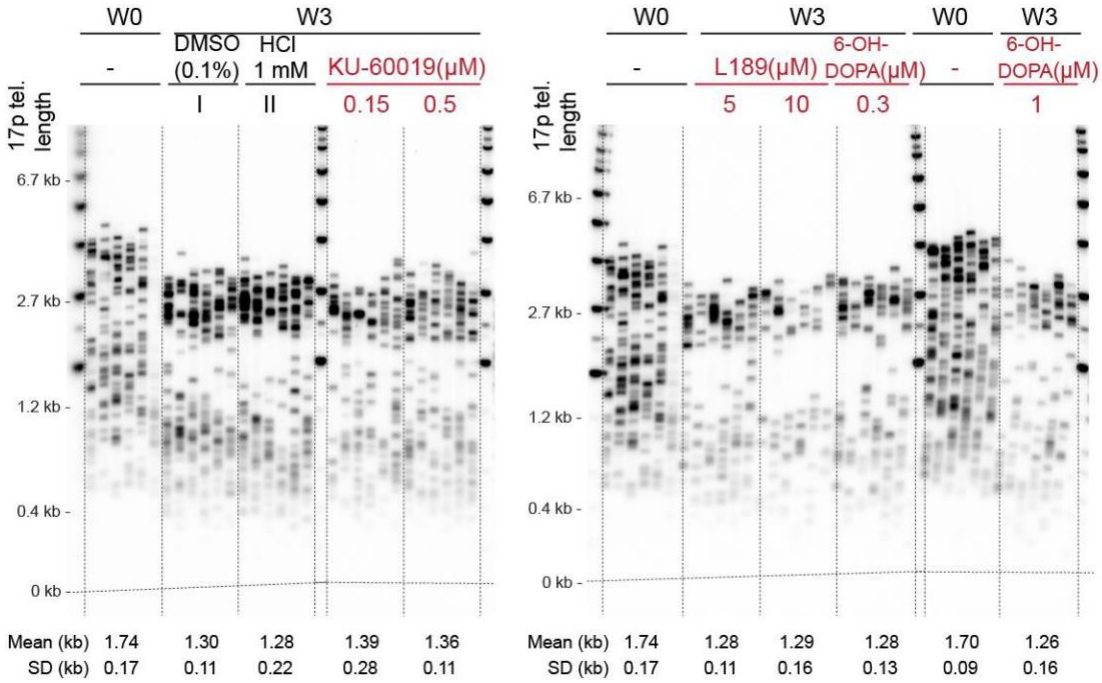

Figure 3.12: STELA of the 17p telomeres from DN-hTERT HCT116 cells treated with two different concentrations of KU-60019, 6-0H-DOPA and L189. DNA from DN-hTERT HCT116 cells was extracted before the experiment (Week 0) and at the end of the third week of the inhibitor treatment (day 52). DMSO and HCl are used as control samples.

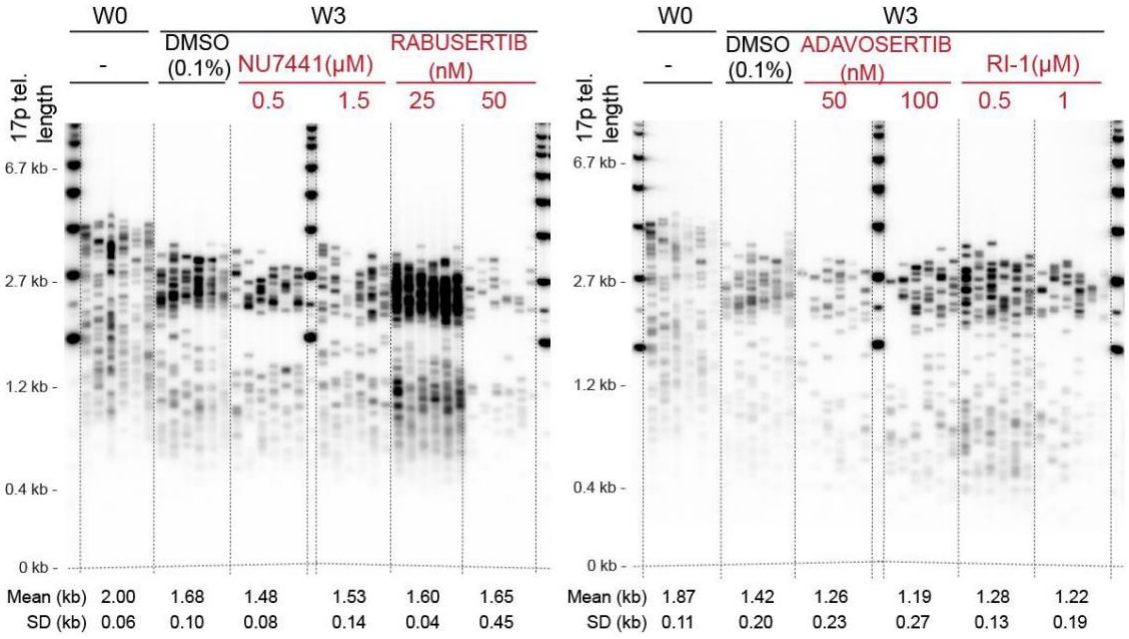

Figure 3.13: STELA of the 17p telomeres from DN-hTERT HCT116 cells treated with two different concentrations of NU7441, Rabusertib, Adavosertib and RI-1. DNA from DN-hTERT HCT116 cells was extracted before the experiment (Week 0) and at the end of the third week of the inhibitor treatment (day 52). DMSO is used as a control sample.

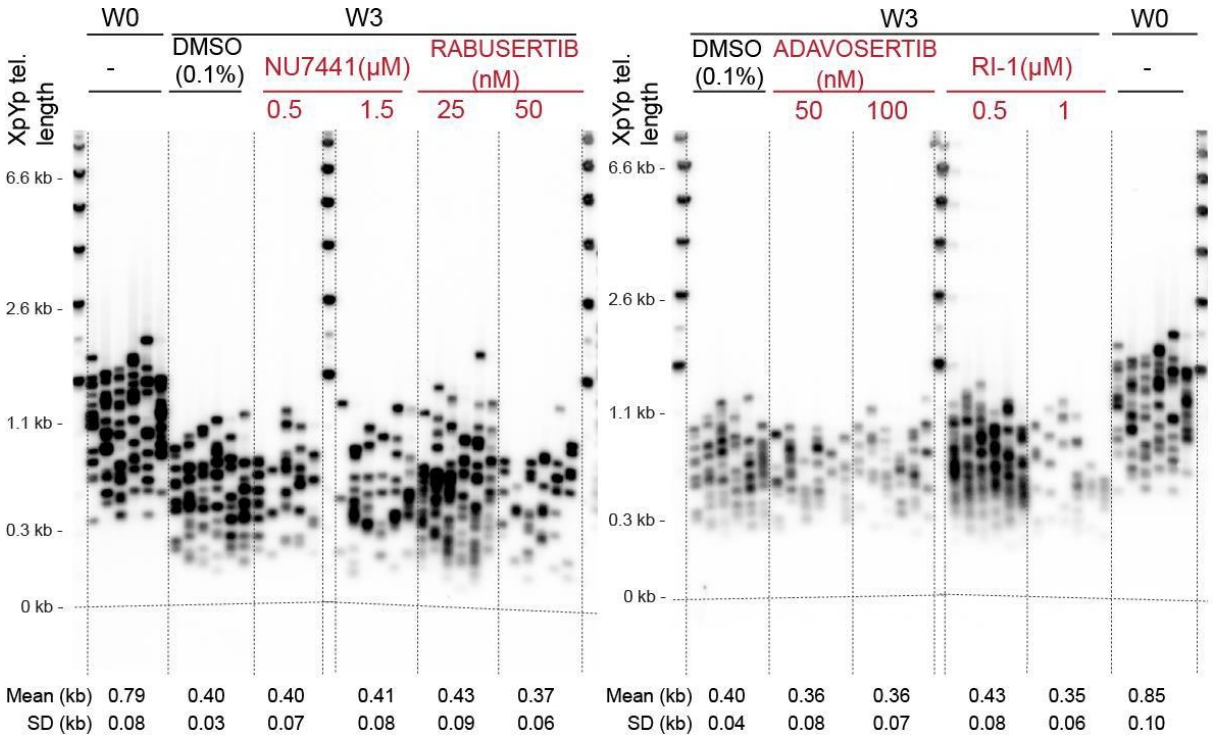

Figure 3.14: STELA of the XpYp telomeres from DN-hTERT HCT116 cells treated with two different concentrations of NU7441, Rabusertib, Adavosertib and RI-1. DNA from DN-hTERT HCT116 cells was extracted before the experiment (Week 0) and at the end of the third week of the inhibitor treatment (day 52). DMSO is used as a control sample.

3.4.3 Assessing the effect of six DNA damage response inhibitors on DN-hTERT-HCT116 cells

As the control DMSO-treated cells failed to escape crisis in the previous experiment, a follow-up experiment was conducted, in which a higher number of cells was passaged before crisis. The follow-up experiment studied the effect of the six most promising inhibitors (Rabusertib, Adavosertib, NU7441, AZD6738, KU-60019 and RI-1) on DN-hTERT-HCT116 cells**.** 6-OH-DOPA was dropped because the previous experiment showed it failed to prevent cells from escaping crisis. L189 was also dropped because of the high concentration used in this study (5µM and 10µM), which would make it challenging to administer it to patients. The experiment was performed in two sets named Set 3 and Set 4: Set 3 consists of cells treated with NU7441, Rabusertib and KU-60019 and Set 4 consists of cells treated with AZD6738, RI-1 and Adavosertib. The conditions were the same as the previous experiment, but the number of cells passaged was increased in Week 3 (onset of crisis, day 52) from $1x10^5$ to $2x10^5$, to increase the chance of the DMSO-treated cells escaping (control cells). The control cells escaped in Set 3 (figures 3.15-3.17), but failed to escape in Set 4 (figures 3.18-3.20). Set 3 showed that all three concentrations of NU7441 and Rabusertib used in the study prevented cells from escaping crisis, while KU-60019 did not. Set 4 showed that RI-1 did not prevent cells from escaping crisis. Adavosertib and AZD6738-treated cells in Set 4 failed to escape crisis. However, since the control cells also failed to escape crisis, no conclusion can be made regarding whether they prevent escape from crisis.

The treatment started at PD36 and the cells entered a crisis state after 54 population doublings for Set 3 and 53 population doublings for Set 4 from the point of single-cell cloning. Control cells and KU60019-treated cells with the second highest concentration spent 40 days in crisis (Set 3) and RI-1-treated cells with the highest concentration spent 42 days in crisis (Set 4). The experiment was terminated when the cells that escaped crisis surpassed a PD of 70 at day 129 for Set 3 and at day 122 for Set 4.

A cell cycle and apoptosis assay were performed to evaluate the effect of the inhibitors on cell cycle progression and apoptosis before and after crisis. DMSO-treated cells were used as a control to compare cell cycle progression and apoptotic levels relative to the inhibitor-treated cells with the indicated concentrations. In the next section, the effects of each inhibitor on DN-hTERT cells in Set 3 and Set 4 are described.

3.4.3.1 Assessing the effect of NU7441 on DN-hTERT-HCT116 cells

The cells treated with all three concentrations of NU7441 (DNA-PK inhibitor) failed to escape crisis (figure 3.15.A). As shown by the growth curve, cell growth was reduced as the concentration increased, with the lower concentration having visibly lower cell growth compared to the control cells. Cells treated with the highest concentration of NU7441 were not passaged at the end of Week 3 (day 52). These cells were passaged three times after crisis but did not survive.

Cell cycle progression of 1µM and 1.5µM NU7441-treatrd cells differed to control cells at day 38, as there were more cells in sub G1 and >4n phase and less cells in G1 phase (figure 3.15.B). Also, at day 45, there were more cells in sub G1, S phase and G2/M phase and less cells in G1 phase.

The apoptosis assay showed that the apoptotic levels of the inhibitor-treated cells increased as the cells approached crisis and compared to the control cells at day 45 and 52, but there was not a strong difference between the different concentrations (figure 3.15.C).

In this experiment, NU7441 prevented cells from escaping crisis, affected cell cycle progression and increased apoptosis in DN-hTERT HCT116 cells prior to crisis.

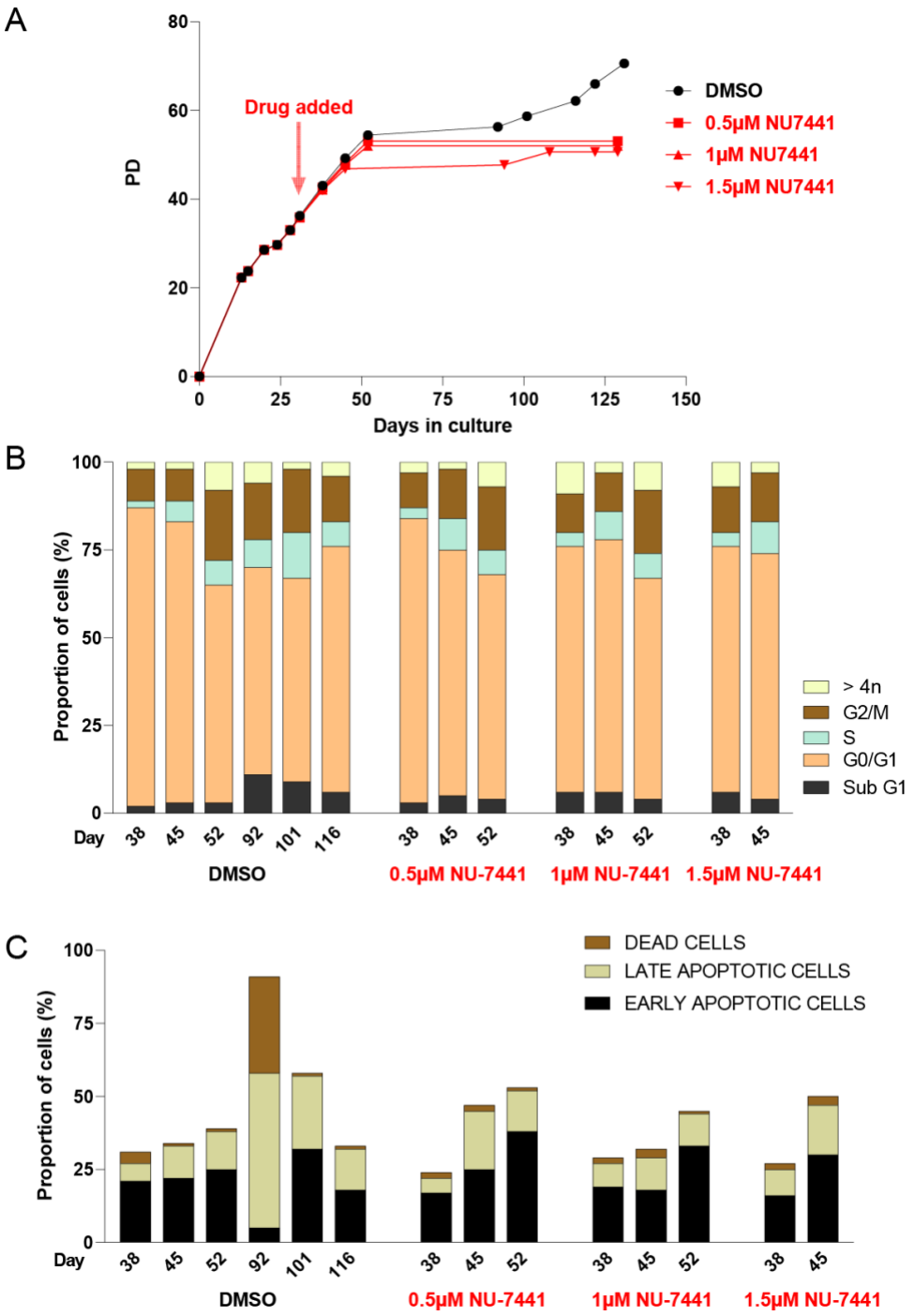

Figure 3.15: Cell growth, cell cycle and apoptosis analysis of DN-hTERT HCT116 cells treated with three different concentrations of NU7441. The figure shows the growth curve (A), the cell cycle progression (B) and apoptotic levels (C) of DN-hTERT HCT116 treated with DMSO and NU7441. Apoptosis was analysed using Annexin-V/propidium iodide (PI) staining. Cells were classified as early apoptotic when they were Annexin V positive and PI negative, late apoptotic when they were Annexin V and PI positive and dead when they were Annexin V negative and PI positive.

3.4.3.2 Assessing the effect of Rabusertib on DN-hTERT-HCT116 cells

The cells treated with all three concentrations of Rabusertib (CHK1 inhibitor) failed to escape crisis (Figure 3.16.A). According to the growth curve, all three concentrations lead to a similar cell growth rate before crisis compared to DMSO control, but failed to escape after entering crisis.

All cells showed an increased accumulation in sub G1, G2/M, S, >4n phase and a decrease in G1 phase as they approached crisis (Figure 3.16.B). However, there was no difference in cell cycle progression between the different concentrations of Rabusertib or compared to the control.

Figure 3.16.C shows that the apoptotic levels increased as the cells approached crisis. The higher the concentration of Rabusertib, the higher the increase in apoptosis at day 52, which was over 50% in the two higher concentrations.

In this experiment, Rabusertib prevented cells from escaping crisis, did not affect cell cycle progression but increased apoptosis in DN-hTERT HCT116 cells prior to crisis.

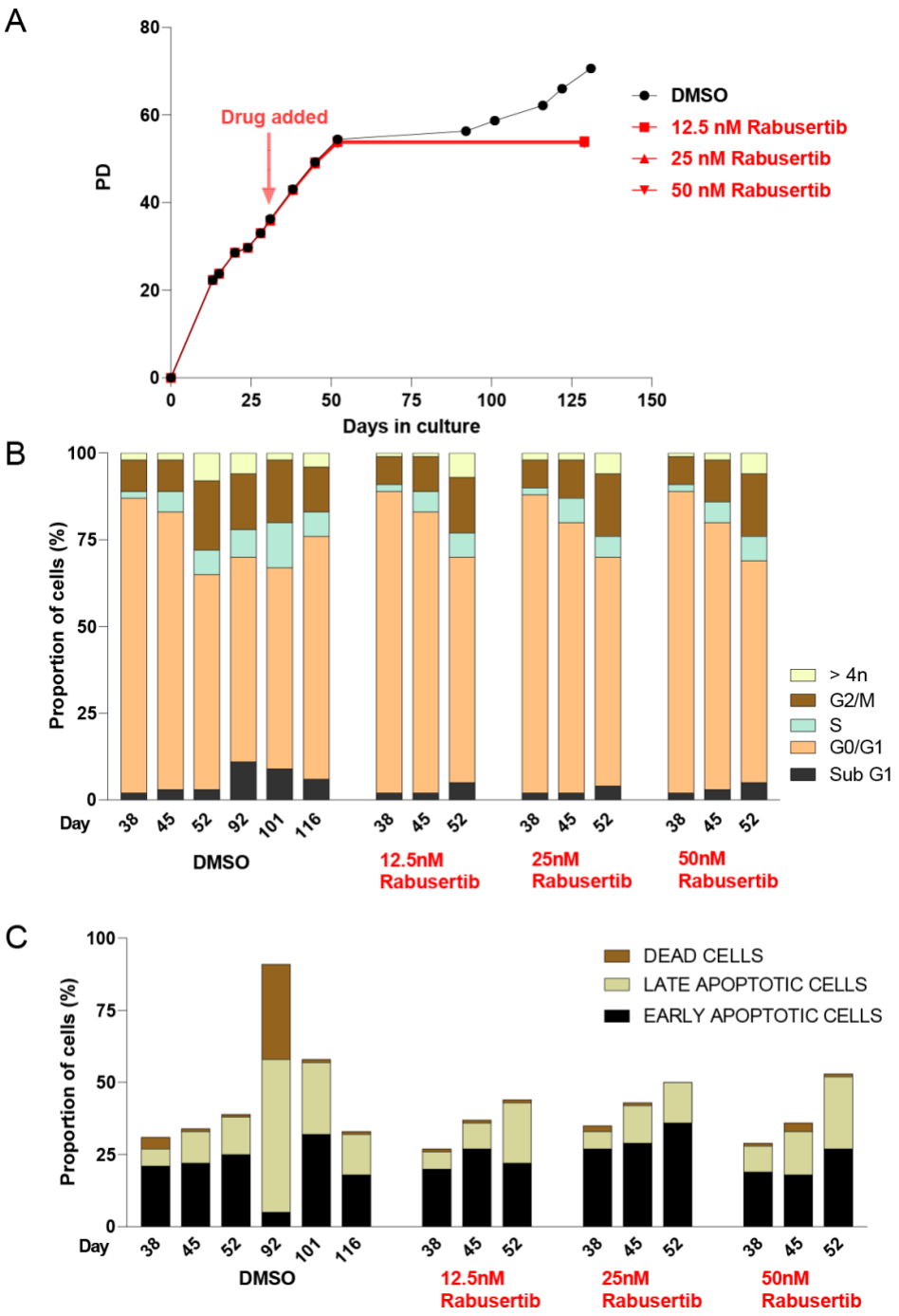

Figure 3.16: Cell growth, cell cycle and apoptosis analysis of DN-hTERT HCT116 cells treated with three different concentrations of Rabusertib. The figure shows the growth curve (A), the cell cycle progression (B) and apoptotic levels (C) of DN-hTERT HCT116 treated with DMSO and Rabusertib. Apoptosis was analysed using Annexin-V/propidium iodide (PI) staining. Cells were classified as early apoptotic when they were Annexin V positive and PI negative, late apoptotic when they were Annexin V and PI positive and dead when they were Annexin V negative and PI positive.

3.4.3.3 Assessing the effect of KU-60019 on DN-hTERT-HCT116 cells

The cells treated with the second highest concentration of KU-60019 (ATM inhibitor) escaped crisis (Figure 3.17.A). Cells treated with the lower concentration failed to escape crisis, while cells treated with the highest concentration were passaged after crisis and while they survived, they were growing very slowly (≈5PD) over a long period of time (≈35 days). According to the growth curve, cells treated with the highest concentration had a reduced cell growth compared to the control cells and the other concentrations and were not passaged at the end of Week 3 (day 52).

Figure 3.17.B shows that there was no difference in cell cycle progression in cells treated with 0.05µM KU-60019 compared to the control cells. However, cells treated with higher concentrations (0.15µM and 0.5µM), accumulated more in the G2/M and S phase at day 45 compared to the control cells. After cells had recovered from crisis (day 116), 0.15µM KU-60019-treated cells had a similar cell cycle progression pattern to that before crisis (day 45).

While cells treated with the two lower concentrations of the inhibitor had similar apoptotic levels to each other and higher than those of the control cells at day 52, cells treated with the highest concentration had very high apoptotic levels (>60%) at day 45 compared to control cells (Figure 3.17.C). After 0.15µM KU-60019-treated cells started recovering from crisis (days 92-116), apoptosis decreased (with the exception of day 108).

In this experiment, 0.15µM KU-60019 did not prevent cells from escaping crisis, but at a lower and a higher concentration (0.05µM and 0.5µM), KU-60019 prevented these cells from escaping crisis or growing, respectively. KU-60019 mildly affected cell cycle progression, but strongly increased apoptosis in DN-hTERT HCT116 cells prior to crisis.

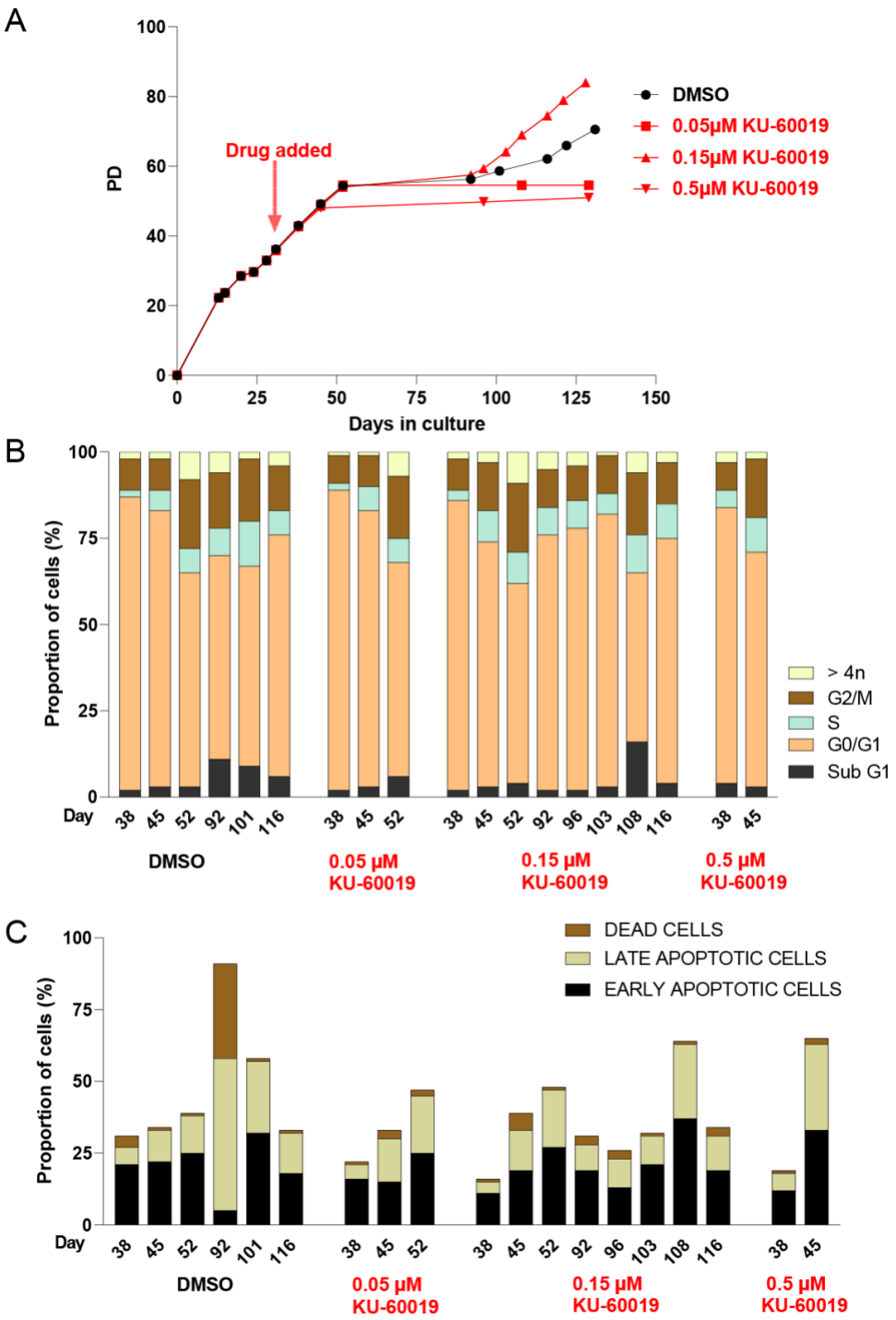

Figure 3.17: Cell growth, cell cycle and apoptosis analysis of DN-hTERT HCT116 cells treated with three different concentrations of KU-60019. The figure shows the growth curve (A), the cell cycle progression (B) and apoptotic levels (C) of DN-hTERT HCT116 treated with DMSO and KU-60019. Apoptosis was analysed using Annexin-V/propidium iodide (PI) staining. Cells were classified as early apoptotic when they were Annexin V positive and PI negative, late apoptotic when they were Annexin V and PI positive and dead when they were Annexin V negative and PI positive.

3.4.3.4 Assessing the effect of RI-1 on DN-hTERT-HCT116 cells

The cells treated with the highest concentration of RI-1 (RAD51 inhibitor) escaped crisis, while those treated with DMSO and the lower concentrations did not. (Figure 3.18.A). According to the growth curve, cell growth before crisis did not change depending on the inhibitor concentration and was similar to the control cells.

Figure 3.18.B shows that as cells approached crisis they accumulated in sub G1, G2/M, S, >4n phase and decreased in G1 phase. After crisis, cells treated with the highest concentration of RI-1 follow the same pattern for the first two weeks (day 94 and 103) and then the distribution of the cells became similar to how it was before they reached crisis (day 45). There was no difference in cell cycle progression compared to the control or between the concentrations.

Figure 3.18.C shows that there was no difference in apoptotic levels in RI-1-treated cells compared to the control cells. Cells treated with the highest concentration of RI-1 had high apoptotic levels when they escaped crisis (day 103), which decreased afterwards.

In this experiment, the high concentration of RI-1 (1.5 μM) did not prevent cells from escaping crisis, but surprisingly the lower concentrations (0.5μM, 1μM) prevented cells from escaping. RI-1 did not affect cell cycle progression or apoptosis in DN-hTERT HCT116 cells prior to crisis.

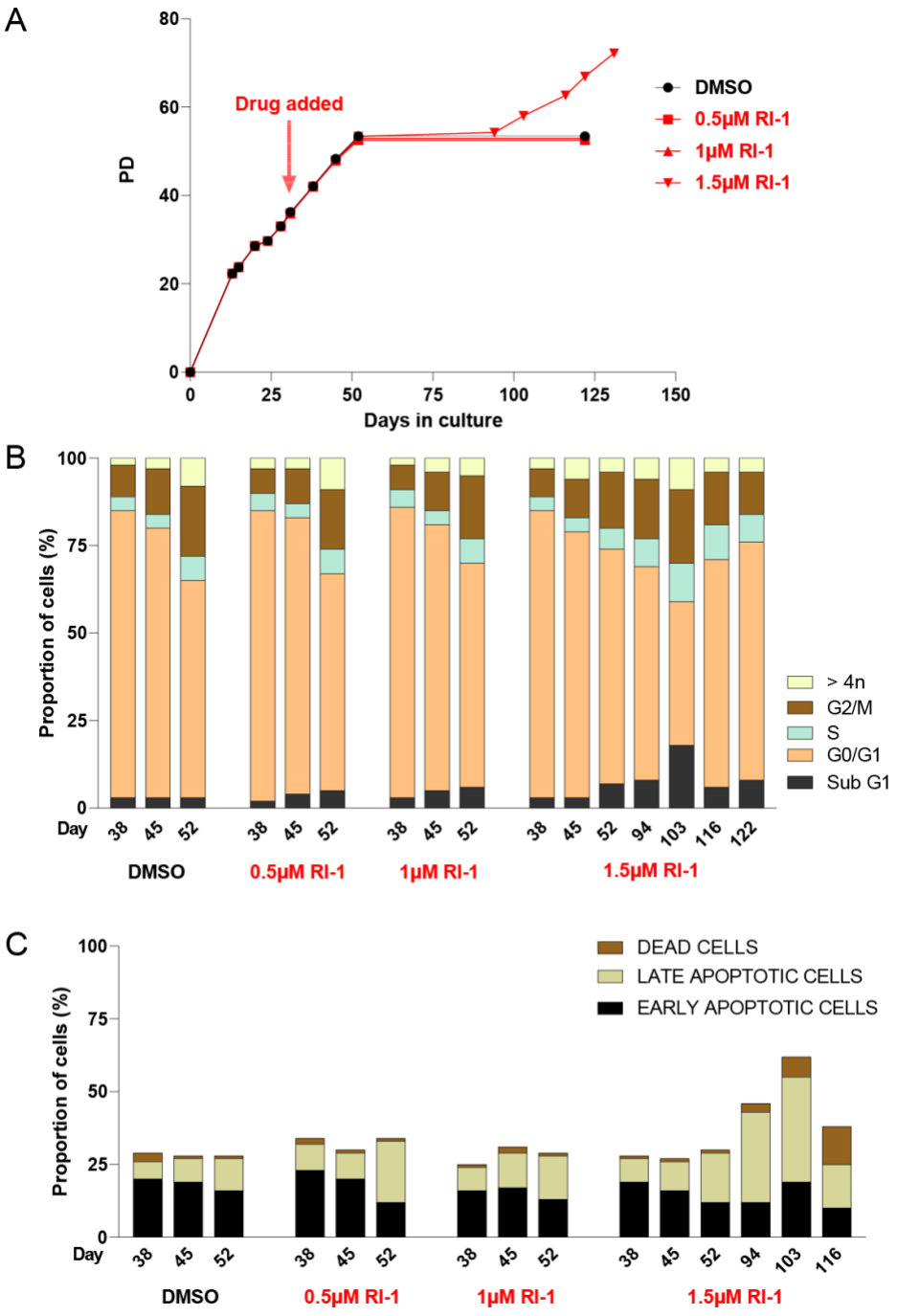

Figure 3.18: Cell growth, cell cycle and apoptosis analysis of DN-hTERT HCT116 cells treated with three different concentrations of RI-1. The figure shows the growth curve (A), the cell cycle progression (B) and apoptotic levels (C) of DN-hTERT HCT116 treated with DMSO and RI-1. Apoptosis was analysed using Annexin-V/propidium iodide (PI) staining. Cells were classified as early apoptotic when they were Annexin V positive and PI negative, late apoptotic when they were Annexin V and PI positive and dead when they were Annexin V negative and PI positive.

3.4.3.5 Assessing the effect of Adavosertib on DN-hTERT-HCT116 cells

The cells treated with all three concentrations of Adavosertib (WEE1 inhibitor) failed to escape crisis (Figure 3.19.A), but as the control cells also failed to escape crisis, no conclusion can be reached regarding whether the inhibitor can prevent escape from crisis. According to the growth curve, the cell growth rate depended on the concentration of the inhibitor, with a lower cell growth as the concentration increases.

Cells treated with Adavosertib showed an increased accumulation of cells in G2/M, S, >4n and a reduction of cells in G1 phase compared to the control cells (Figure 3.19.B). There was also a difference in cell cycle progression between the different concentrations of Adavosertib. At higher concentrations, more cells accumulated in G2/M and >4n phase, while less cells accumulated in G1 phase.

There was an increase in apoptosis (both early and late) at day 45, with the highest concentration having the highest increase and reaching apoptotic levels over 60% (figure 3.19.C).

In this experiment, Adavosertib-treated cells did not escape crisis and the inhibitor affected both cell cycle progression and apoptosis in DN-hTERT HCT116 cells prior to crisis.

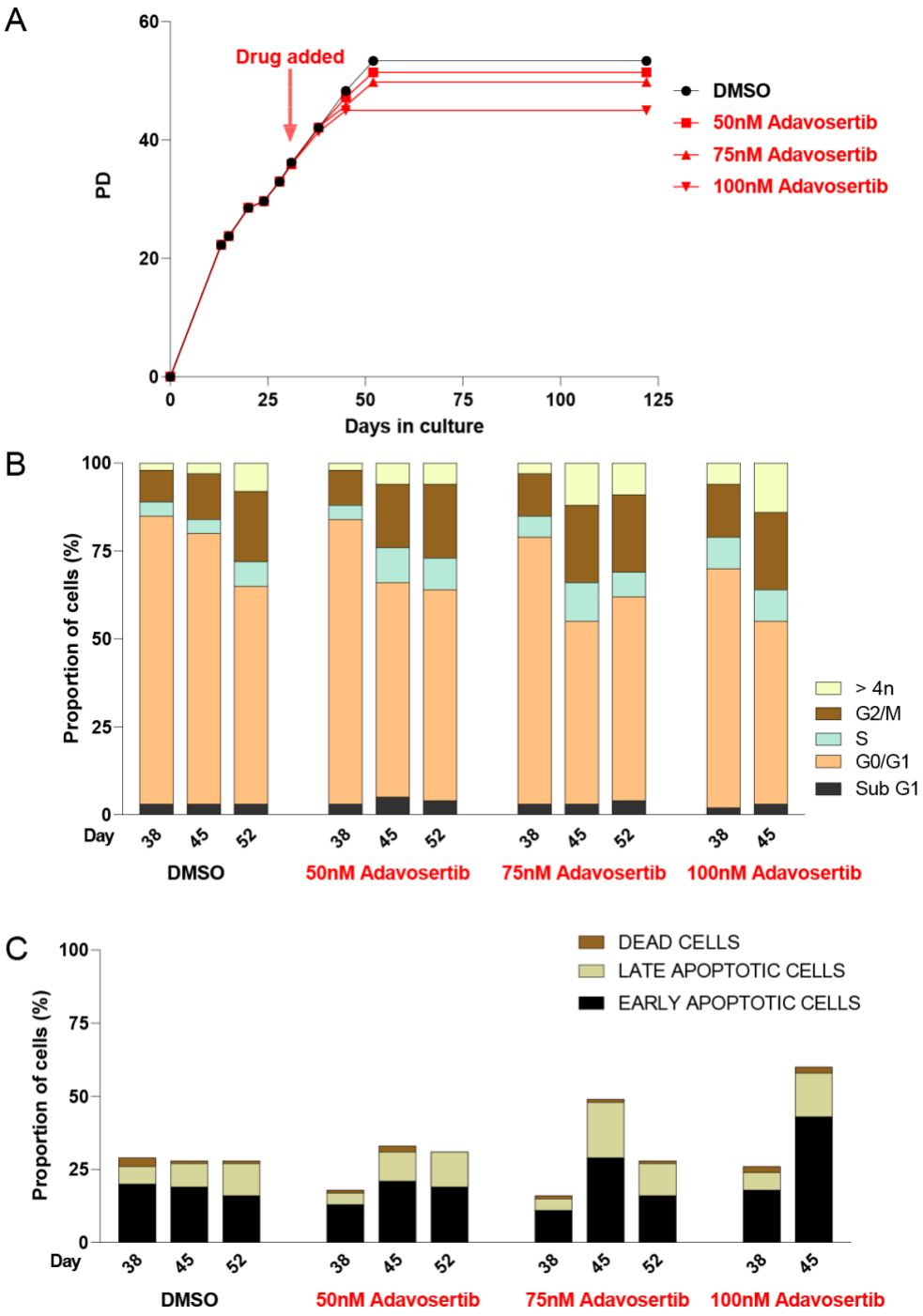

Figure 3.19: Cell growth, cell cycle and apoptosis analysis of DN-hTERT HCT116 cells treated with three different concentrations of Adavosertib. The figure shows the growth curve (A), the cell cycle progression (B) and apoptotic levels (C) of DN-hTERT HCT116 treated with DMSO and Adavosertib. Apoptosis was analysed using Annexin-V/propidium iodide (PI) staining. Cells were classified as early apoptotic when they were Annexin V positive and PI negative, late apoptotic when they were Annexin V and PI positive and dead when they were Annexin V negative and PI positive.

3.4.3.6 Assessing the effect of AZD6738 on DN-hTERT-HCT116 cells

The cells treated with all three concentrations of AZD6738 (ATR inhibitor) failed to escape crisis (Figure 3.20.A), but as the control cells also failed to escape crisis, no conclusion can be reached regarding whether the inhibitor can prevent escape from crisis. According to the growth curve, all three concentrations of AZD6738 result in a similar cell growth rate before crisis.

Cells treated with all three concentrations of AZD6738 showed an increased accumulation of cells in sub G1, G2/M, S, >4n and a reduction of cells in G1 phase as they approached crisis, in a similar way to the control cells (Figure 3.20.B). There was no difference in cell cycle progression compared to the control cells or between the different concentrations of AZD6738.

Apoptotic cells remained less than 50% and there was no difference in apoptosis compared to the control or between the three concentrations, with the exception of higher apoptosis in 25nM AZD6738-treated cells at day 45 (Figure 3.20.C).

In this experiment, AZD6738-treated cells did not escape crisis and the inhibitor did not affect cell cycle progression or apoptosis in DN-hTERT HCT116 cells prior to crisis.

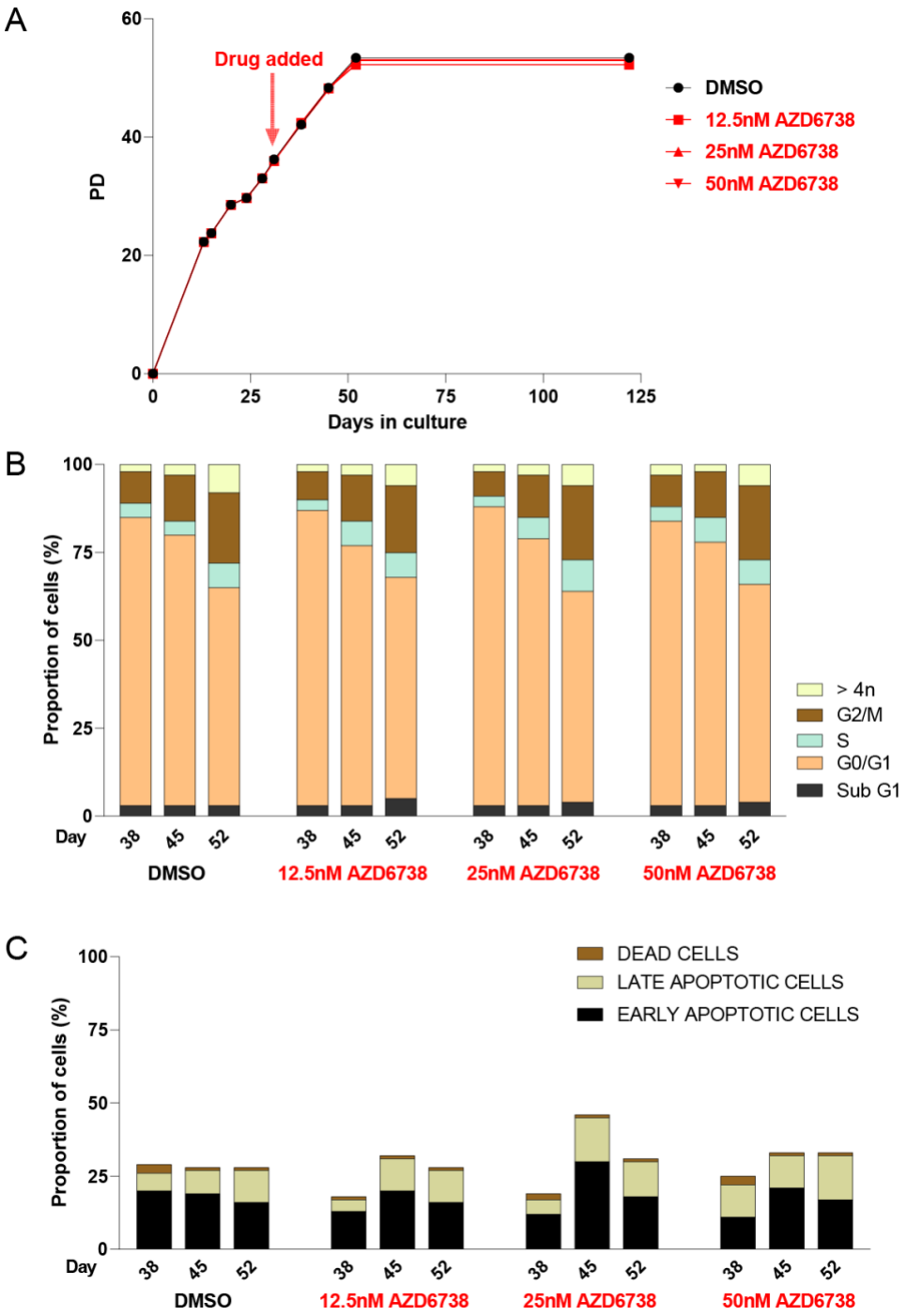

Figure 3.20: Cell growth, cell cycle and apoptosis analysis of DN-hTERT HCT116 cells treated with three different concentrations of AZD6738. The figure shows the growth curve (A), the cell cycle progression (B) and apoptotic levels (C) of DN-hTERT HCT116 treated with DMSO and AZD6738. Apoptosis was analysed using Annexin-V/propidium iodide (PI) staining. Cells were classified as early apoptotic when they were Annexin V positive and PI negative, late apoptotic when they were Annexin V and PI positive and dead when they were Annexin V negative and PI positive.

3. 4. 4 Assessing the effect of four DNA damage response inhibitors on DN-hTERT-HCT116 cells

The previous experiment showed that NU7441 and Rabusertib prevented DN-hTERT-HCT116 cells from escaping crisis (figures 3.15 and 3.16), while AZD6738 and Adavosertib may prevent these cells from escaping crisis (figures 3.20 and 3.19). RI-1 failed to prevent escape from crisis at the highest concentration used (figure 3.18) and KU-60019 failed to prevent cells from escaping crisis at the second highest concentration used, while cells treated with its highest concentration also managed to survive and grow slowly after crisis (figure 3.17).

A follow-up experiment was set up to further study the effect of the four most promising inhibitors identified in the previous experiment (Rabusertib, Adavosertib, NU7441, AZD6738) on DN-hTERT-HCT116 cells**.** The experiment was performed in two sets named Set 5 and Set 6: Set 5 consists of cells treated with Rabusertib and Adavosertib and Set 6 consists of cells treated with AZD6738 and NU7441. The conditions were the same as the previous experiment, but the number of cells passaged was increased in Week 3 (onset of crisis) from $2x10^5$ to $8x10^5$ (in a T75 flask), to increase the chance of the DMSO-treated cells escaping crisis (control cells). Set 6 cells were also passaged one more time before entering crisis, compared to the previous experiments and both experiments included three DMSO-treated samples and one untreated control. All control cells escaped in Set 6, but only one out of the three DMSO controls escaped in Set 5. Set 6 showed that all three concentrations of NU7441 and AZD6738 used in the study prevented cells from escaping crisis, while Set 5 showed that Adavosertib did not prevent cells from escaping crisis. In Set 5, Rabusertib-treated cells failed to escape crisis, but since some of the control cells also failed to escape crisis, no conclusion can be made regarding whether the inhibitor prevented escape from crisis in this experiment.

The treatment started at PD36, and the cells entered crisis after 53 population doublings from the point of single-cell cloning in both sets. Adavosertib-treated cells spent 33 days in crisis (Set 5) (figure 3.22) and control cells spent only 23 days in crisis (Set 6) (figures 3.23 and 3.24). The experiment was terminated when the cells that escaped crisis surpassed a PD of 70 at day 135 for Set 5 and at day 107 for Set 6.

Cell cycle and apoptosis assays were performed to evaluate the effect of the inhibitors on cell progression and apoptosis before and after crisis. DMSO-treated cells were used as a control to compare cell cycle progression and apoptotic levels relative to the inhibitor-treated cells with the indicated concentrations.

3.4.4.1 Assessing the effect of Rabusertib on DN-hTERT-HCT116 cells

The cells treated with all three concentrations of Rabusertib (CHK1 inhibitor) failed to escape crisis (Figure 3.21.A). However, two out of three DMSO-treated samples also failed to escape crisis, so no definitive conclusions regarding the ability of Rabusertib to prevent escape from crisis could be made. According to the growth curve, all three concentrations of Rabusertib lead to a similar cell growth rate before crisis.

Cells treated with all three concentrations of Rabusertib showed an increased accumulation of cells in G2/M and a reduction of cells in G1 phase as they approached crisis, in a similar way to the control cells (Figure 3.21.B). No apparent effect in cell cycle progression could be seen compared to the control or between the different concentrations of Rabusertib.

At day 38 of treatment with Rabusertib, apoptosis levels were low (<30% overall) and similar to the DMSO-treated cells (Figure 3.21.C). At day 45, there was increased apoptosis in 50nM Rabusertib-treated cells (>40% overall) compared to the control cells.

In this experiment, Rabusertib did not affect cell cycle progression in DN-hTERT HCT116 cells (during the first two weeks of treatment), but it increased apoptosis at the higher concentration. Although no conclusion could be reached about whether this inhibitor can prevent escape from a telomere crisis in this experiment, the fact that Rabusertib-treated cells failed to escape crisis verifies previous findings.

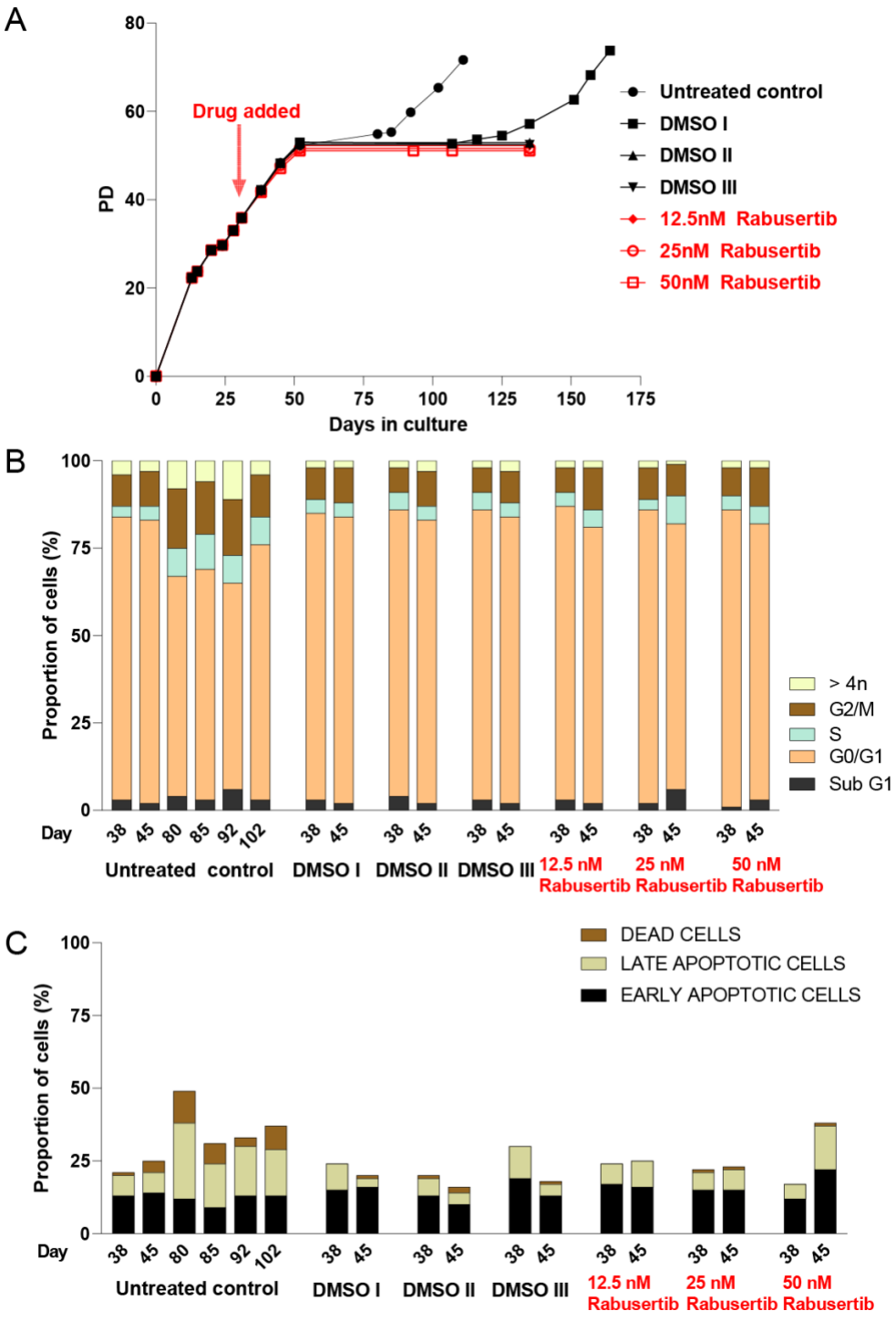

Figure 3.21: Cell growth, cell cycle and apoptosis analysis of DN-hTERT HCT116 cells treated with three different concentrations of Rabusertib. The figure shows the growth curve (A), the cell cycle progression (B) and apoptotic levels (C) of DN-hTERT HCT116 treated with DMSO and Rabusertib. The experiment contains three DMSO-treated replicates (DMSO I-III) and one untreated control. Apoptosis was analysed using Annexin-V/propidium iodide (PI) staining. Cells were classified as early apoptotic when they were Annexin V positive and PI negative, late apoptotic when they were

3.4.4.2 Assessing the effect of Adavosertib on DN-hTERT-HCT116 cells

The cells treated with the two highest concentrations of Adavosertib (WEE1 inhibitor) escaped crisis (Figure 3.22.A). Unexpectedly, cells treated with the lowest concentration of Adavosertib failed to escape crisis. According to the growth curve, the highest concentration of Adavosertib had a significant impact on cell growth before crisis, compared to the other two lower concentrations.

Figure 3.22.B shows that Adavosertib affected cell cycle progression before crisis. For example, at day 45, cells treated with the lower concentration of Adavosertib, accumulated less in the G1 phase and more in the S and G2/M phase, compared to the control. As the concentration of Adavosertib increased, more cells were in G2/M and >4n phase and less cells were in G1 phase at day 45.

Figure 3.22.C shows that Adavosertib strongly affected apoptosis with apoptotic levels increasing as the concentration of the inhibitor increased at day 45, with the highest concentration having over 50% apoptosis. In Adavosertib-treated cells that escaped, apoptosis increased as the cells approached crisis and while apoptosis was highest immediately after they escaped crisis (day 85), it decreased to reach the same levels of apoptosis as before crisis (75nM Adavosertib) or even lower (100nM Adavosertib).

In this experiment, the two highest concentrations of Adavosertib did not prevent cells from escaping crisis and the inhibitor affected both cell cycle and apoptotic levels in DN-hTERT HCT116 cells.

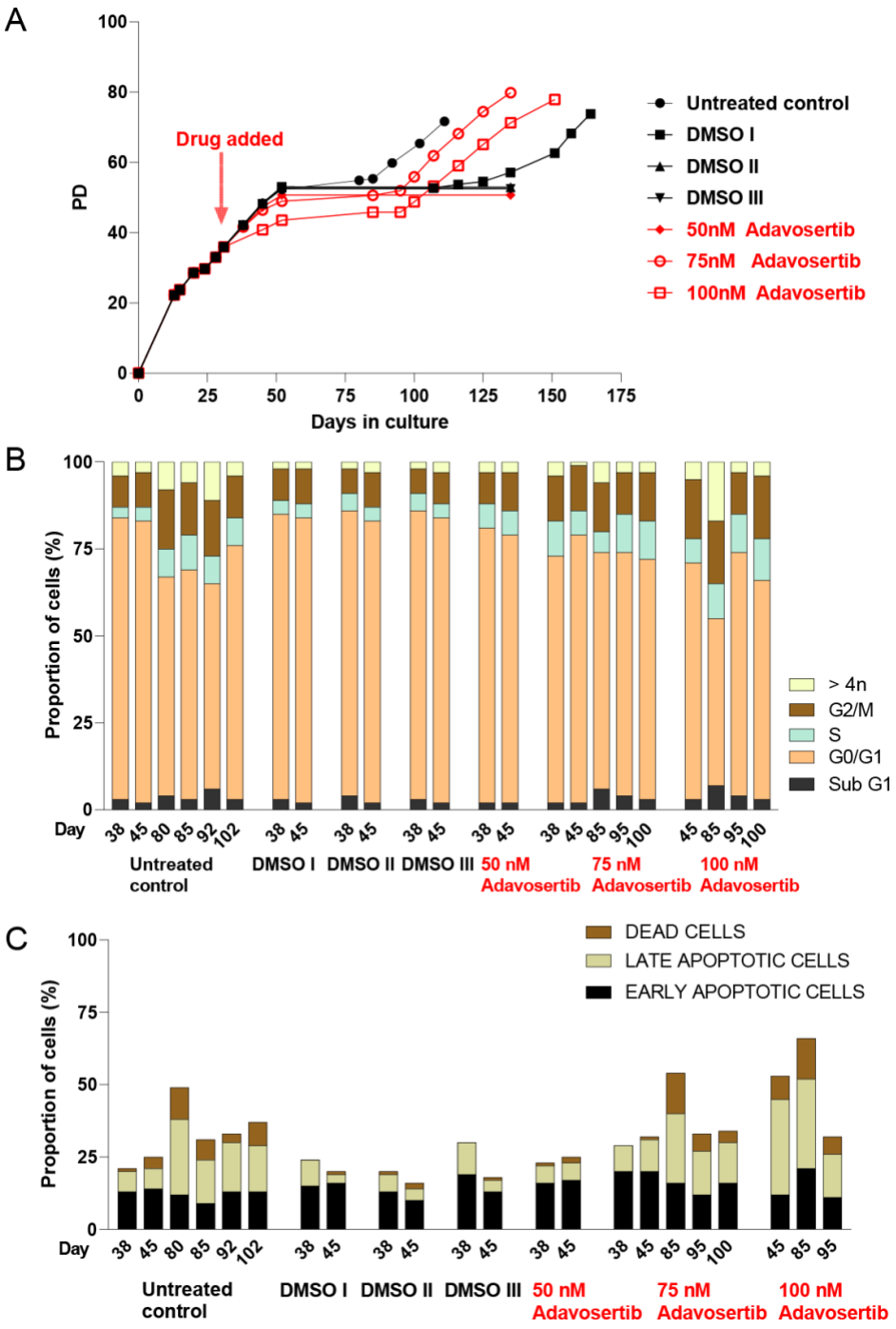

Figure 3.22: Cell growth, cell cycle and apoptosis analysis of DN-hTERT HCT116 cells treated with three different concentrations of Adavosertib. The figure shows the growth curve (A), the cell cycle progression (B) and apoptotic levels (C) of DN-hTERT HCT116 treated with Adavosertib. Apoptosis was analysed using Annexin-V/propidium iodide (PI) staining. Cells were classified as early apoptotic when they were Annexin V positive and PI negative, late apoptotic when they were Annexin V and PI positive and dead when they were Annexin V negative and PI positive.

3.4.4.3 Assessing the effect of AZD6738 on DN-hTERT-HCT116 cells

The cells treated with all three concentrations of AZD6738 (ATR inhibitor) failed to escape crisis (Figure 3.23.A), whereas all three of the DMSO-treated control cells escaped crisis. The growth rate of the cells before they reached crisis did not change considerably between the three concentrations.

As the cells got closer to deep crisis (day 59), there were less cells in the G1 phase and more cells in the sub G1, S, G2/M and >4n phase. As control (untreated and DMSO-treated) samples were escaping crisis, there were less cells in G2/M phase and more cells in G1 phase (figure 3.23.B). There was no difference in the cell cycle progression between the cells treated with the three different concentrations of AZD6738 and control cells.

During days 52 and 59, when the cells started entering deep crisis, there were very high apoptotic levels (>50% overall) and there was no difference in apoptosis between the three different concentrations or between the DMSO-treated and inhibitor-treated cells (Figure 3.23.C). As control (untreated and DMSO-treated) samples were escaping crisis, apoptosis levels were reduced. Interestingly, lower levels of apoptosis (both early and late) were seen when the cells were deeper into crisis.

In this experiment AZD6738 prevented cells from escaping crisis and it did not affect cell cycle progression or apoptosis in DN-hTERT-HCT116 cells.

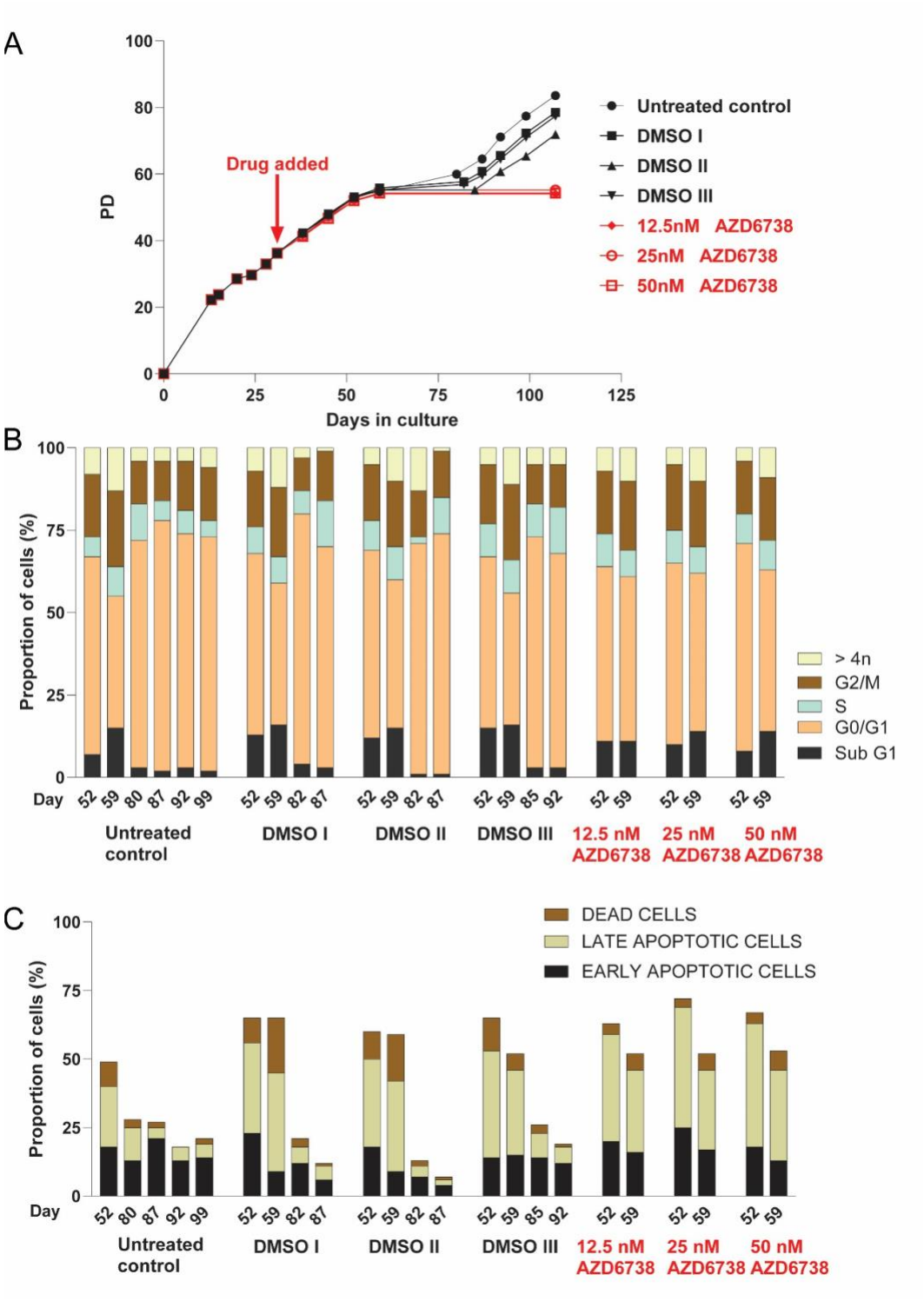

Figure 3.23: Cell growth, cell cycle and apoptosis analysis of DN-hTERT HCT116 cells treated with three different concentrations of AZD6738. The figure shows the growth curve (A), the cell cycle progression (B) and apoptotic levels (C) of DN-hTERT HCT116 treated with DMSO and AZD6738. Apoptosis was analysed using Annexin-V/propidium iodide (PI) staining. Cells were classified as early apoptotic when they were Annexin V positive and PI negative, late apoptotic when they were Annexin V and PI positive and dead when they were Annexin V negative and PI positive.

3.4.4.4 Assessing the effect of NU7441 on DN-hTERT-HCT116 cells

The cells treated with all three concentrations of NU7441 (DNA-PK inhibitor) failed to escape crisis (Figure 3.24), whereas all three DMSO-treated controls escaped. The graph shows that the growth rate of the cells before they reached crisis was affected by the concentration of the inhibitor, where the higher concentration reduced cell growth more compared to the lowest concentration. As the inhibitor strongly affected cell growth when it was added to the cells, there were not enough cells to perform a cell cycle and apoptosis analysis. In conclusion, NU7441 prevented cells from escaping crisis and had a concentration-dependent effect on cell growth.

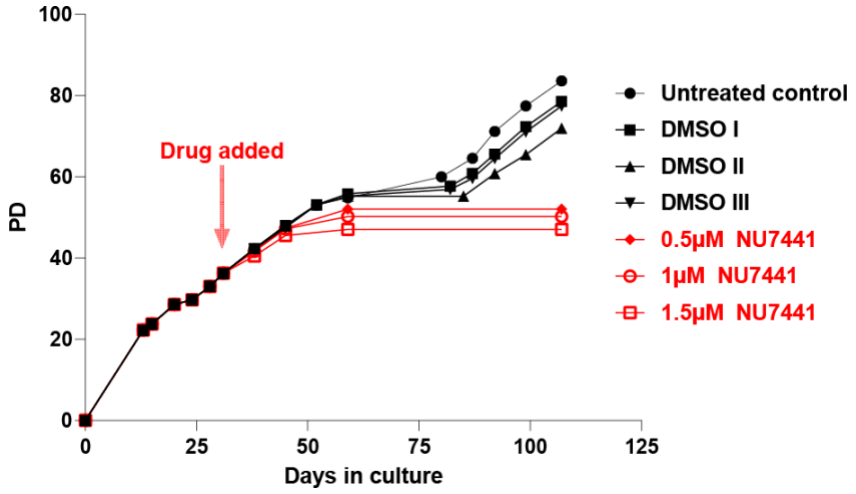

Figure 3.24: Cell growth of DN-hTERT HCT116 cells treated with three different concentrations of NU7441. The figure shows the growth curve of DN-hTERT HCT116 treated with DMSO and NU7441.

3.4.4.5 STELA analysis

Telomere length analysis was undertaken to assess if any of the inhibitors affected the rate of telomere erosion during crisis. The telomere length of the DN-hTERT HCT116 cells before the administration of the inhibitor (Week 0, PD36) was compared to the inhibitor-treated cells at day 52 (Set 5) or day 59 (Set 6), when they started entering crisis (PD53).

Figure 3.25 shows the analysis of the 17p telomeres of the cells treated with Rabusertib, Adavosertib and AZD6738. The telomeres of all the inhibitor-treated cells were equally short to the control cells and shorter than the telomeres from the non-treated cells at PD36 (W0). NU7441 was not included as no sample was obtained from day 52 or 59 due to the slow growth of NU7441-treated cells. This verifies that HCT116 DN-hTERT cells entered crisis induced by telomere erosion and none of the inhibitors affected the rate of telomere erosion during crisis, as shown from our previous findings (figure 3.14).

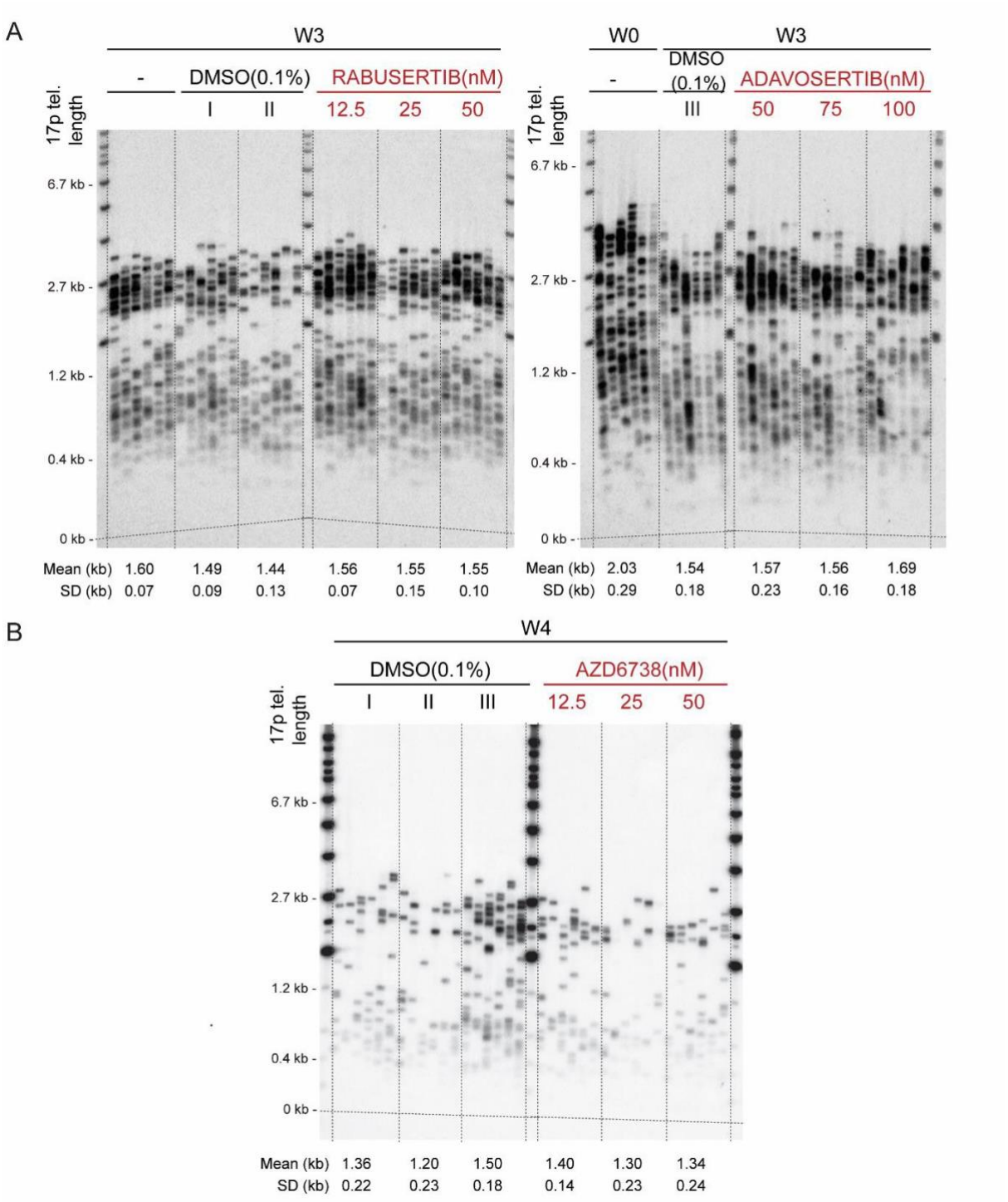

Figure 3.25: STELA of the 17p telomeres from DN-hTERT HCT116 cells treated with three different concentrations of Rabusertib, Adavosertib and AZD6738. DNA from DN-hTERT HCT116 cells was extracted before the experiment (Week 0) and at the end of the third (day 52) or fourth week (day 59) of the inhibitor treatment. DMSO treated samples are used as control samples.

3.5 Discussion

3.5.1 6-OH-DOPA, RI-1 and Adavosertib did not prevent HCT116 DN-hTERT cells from escaping crisis

In this study, DDR inhibitors previously demonstrated to impair cancer cell survival were used to treat both HCT116 WT and DN-hTERT expressing cells. The first part of the study, which consisted of one experiment, aimed to show that the inhibitors affected WT- HCT116 either in their cell growth or their cell cycle progression or their apoptotic levels and to establish a suitable range of concentrations to be tested in subsequent experiments. The second part of the study, which consisted of three experiments (named Set 1 to Set 6), aimed to assess the ability of each inhibitor to prevent escape from a telomere crisis and select the most promising ones for further investigation.

In the first experiment (Set 1), control HCT116 DN-hTERT cells (treated with 1mM HCl control), escaped crisis as expected, with the 6-OH-DOPA- treated cells (0.3µM, 1µM) escaping shortly after (figure 3.11). Neither of the concentrations influenced cell growth, cell cycle progression or apoptosis before crisis. After escape from crisis, the 6-OH-DOPA-treated cells had a reduced cell growth compared to control cells (by ~5PD) and the cells treated with the highest concentration had slightly higher apoptotic levels compared to control cells. This experiment showed that 6-0H-DOPA did not stop cells escaping crisis in the concentrations tested, although it had a small impact on cell growth after escape. Testing 6-OH-DOPA concentrations higher than 1µM or even higher than 3µM (which had no effect on cell growth in WT-HCT116), might be impractical, especially when other inhibitors might be effective at a much lower concentration.

In the first experiment (Set 2), RI-1 treated cells (0.5µM, 1µM) failed to escape crisis, but so did the control cells (figure 3.7). The higher concentration of the inhibitor (1µM RI-1) slightly affected both cell cycle progression (only at day 52) and apoptosis (only at day 45), while the lower concentration had no effect. In this experiment, no conclusion could be made as to whether this inhibitor affected escape from crisis, since the control cells failed to escape. In the second experiment (Set 4), we included an additional third concentration (1.5µM)

(figure 3.18). Cells treated with the highest RI-1 concentration (1.5µM) escaped crisis, while cells treated with the lower concentrations and control cells unexpectedly failed to escape crisis. In this experiment, there was no visible difference in cell cycle progression or apoptosis, compared to the control or between the concentrations. Neither of the concentrations tested affected cell growth prior to crisis, which is consistent with the previous findings in WT-HCT116 cells. This experiment showed that 1.5µM RI-1 did not stop cells escaping crisis. Testing RI-1 concentrations higher than 1.5µM but lower than 5µM (which reduced cell growth in WT-HCT116 cells), might not be practical due to the high concentration.

Adavosertib was one of the most potent inhibitors in our study. In the first experiment (Set 2), cells treated with 50nM Adavosertib escaped crisis, while cells treated with the higher concentration (100nM) failed to escape (figure 3.6). Cells treated with both concentrations had an altered cell cycle progression and increased apoptotic levels prior to crisis and the higher concentration slightly slowed down cell growth prior to crisis (also observed in the WT-HCT116 experiment). The fact that the lower concentration did not stop cells escaping crisis, but the cells treated with a higher concentration failed to do so, appeared promising. In the second experiment (Set 4), we added an intermediate concentration (75nM) (figure 3.19). None of the cells treated with the three concentrations escaped crisis, but unfortunately neither did the control cells. As observed in the previous experiment, all concentrations altered cell cycle progression and increased apoptosis. The inhibitor also affected cell growth prior to crisis, with a minimal effect for the lower concentration, but a noticeable effect for the higher concentration. In this experiment, no conclusion could be made, because control cells also failed to escape. In the third experiment (Set 5), cells treated with the highest (100nM) and intermediate (75nM) Adavosertib concentration escaped crisis, as did untreated cells and one out of the three DMSO-treated control cells (figure 3.21). Adavosertib increased apoptosis and affected cell cycle progression in all concentrations used, while it reduced cell growth prior to crisis in a concentration-dependent manner. The findings of this experiment, along with the previous finding (Set 2) showing that cells treated with 50nM Adavosertib also escaped crisis, confirmed that all tested Adavosertib concentrations did not prevent HCT116 escape from a telomere crisis.

The possibility of testing Adavosertib concentrations higher than 100nM but lower than 300nM (which dramatically reduced cell growth by ~14PD in WT-HCT116 cells), might prove challenging as 100nM already reduced cell growth prior to crisis, so higher concentrations might kill cells before entering crisis. Alternatively, Adavosertib can be further investigated in combination with other inhibitors. Adavosertib has been previously used in combination with Rabusertib to induce a more than additive effect in head and neck squamous cell carcinoma cell lines in similar concentrations we are using in this study (van Harten et al, 2019). Adavosertib has also been used in combination with AZD6738 to produce a synergistic effect in triple negative breast cancer cells (Jin et al, 2017) and multiple basal-like breast cancer cell lines (Brunner et al, 2020) in a higher concentration than the ones used in this study.

It is not exactly known why 6'-OH-DOPA, RI-1 and Adavosertib did not affect the ability of the cells to escape crisis, but a possible explanation for each of the inhibitors is offered below. We assume that the inhibitors functioned as expected. To the best of our knowledge, 6-OH-DOPA has not been previously tested on HCT116 cells. In a different study, treatment of HCT116 cells with 10μM RI-1 only slightly reduced cell growth, while treatment with 20μM RI-1 only slightly increased apoptosis, which is consistent with the fact that 1.5μM RI-1 did not influence cell growth or apoptosis in our study (figures 3.2, 3.18) (Liao et al, 2022). In addition, a different study showed that treatment of HCT116 with 100nM Adavosertib slightly reduced cell growth, while treatment with 500nM Adavosertib strongly reduced cell growth, which is consistent with our results (figures 3.1, 3.6, 3.19, 3.22) (Agostini et al, 2021). 6-OH-DOPA is a RAD52 inhibitor, which disrupts its ring structures, but it has little effect on HR or NHEJ (Chandramouly et al, 2015). In yeast, Rad52 is crucial in HR, by functioning as a RAD51 mediator but in humans this role is performed by BRCA2, while RAD52 has a back-up role (Lok and Powell, 2012; Balboni et al, 2023). RAD52 inhibition has been demonstrated to impair the growth of BRCA-deficient cancer cells, but not BRCA-proficient cells (Lok et al, 2013; Balboni et al, 2023). However, HCT116 cells are BRCA-proficient cells, meaning that RAD52 inhibition is not sufficient to disrupt HR and increase DNA damage during crisis. RI-1 inhibits RAD51 by inactivating it through binding to a protein surface that acts as an interface between protein subunits in RAD51 filaments (Budke et al, 2012). However, Lambert and Lopez (2000) showed that changes in the RAD51 pathway do

not significantly affect the efficiency of total double-strand break repair in mammalian cells, but instead change the ratio between HR and single strand annealing (SSA). So, it is likely that in our experiment, cells mostly shifted to a different DSBR pathway, such as SSA which is RAD51-independent. Adavosertib is a potent and selective WEE1 inhibitor which acts by evading the G2 cell cycle checkpoint and this does not allow cells to repair DNA damage. WEE1 is activated by CHK1, phosphorylates and inhibits CDK1/CDC2, regulates chromatin integrity and plays an important role in the G2 DNA damage checkpoint (Gorecki et al, 2021). Gomez et al. (2022) investigated resistance mechanisms to Adavosertib and discovered that resistance could emerge through reduction in the levels of CDK1, the target for WEE1 inhibition or the generation of a different resistant mechanism that involved increase of CHK1 activation to restore G2 arrest. Interestingly, after 50nM Adavosertib-treated samples escaped crisis, we observed a dramatic accumulation of cells in G2/M phase (>61%), indicating a G2 arrest (figure 3.6.C). Thus, it is possible that the afore-mentioned mechanism may have reduced the efficacy of the WEE1 inhibitor in our long-term cell culture experiment. Another possibility is that these pathways (RAD51, RAD52 and WEE1) are not important for cell survival during crisis.

The main limitation of this study is that the control DMSO-treated cells failed to escape crisis in several sets of this study (Sets 1, 2, 4 and 5), contrary to our previous findings (Ngo et al 2018). The reason for this is thought to be the low number of cells being passaged before crisis, with $1x10^5$ cells being passaged at day 52, when cells were entering crisis, meaning that they had a lower chance to escape (Set 1 and 2). The number of cells passaged was increased to $2x10^5$ in the following experiment (Set 3 and 4). In this experiment, the control cells for Set 3 managed to escape crisis but failed to do so in Set 4. Cells in Set 3 were more confluent prior to crisis than cells in Set 4, which might have influenced their ability to escape crisis. To overcome this limitation, $8x10^5$ cells were passaged in a T75 flask at day 52 and were passaged again in the same way at day 59 (Set 6). As the DMSO-treated cells managed to escape crisis in this set, control cells were passaged in the same way ($8x10^5$ cells in T75 flask) in following experiments in the next chapter.

In conclusion, 1µM 6-0H-DOPA, 1.5µM RI-1 and 100nM Adavosertib were not sufficient to prevent cells from escaping crisis. We decided it was not worth further investigating higher

concentrations of 6-0H-DOPA and RI-1 in cells undergoing crisis, as these concentrations might be too high for administration in patients. In addition, further investigating Adavosertib concentrations higher than 100nM, might kill cells before entering crisis, given the high potency of the drug, but Adavosertib can be investigated in combination with other inhibitors in future studies.

3.5.2 Studies of the effect of L189 and KU-60019 on escape from telomere crisis were inconclusive

Studies on L189 and KU-60019 were inconclusive in terms of their ability to influence escape from a telomere crisis. L189 (5μM and 10 μM) was tested in one experiment (Set 1), in which all treated cells failed to escape crisis, but so did the control cells (figure 3.10). The inhibitor did not significantly influence cell cycle progression, but it increased apoptosis (at 10μM) at day 38 and 52. We decided to not include this inhibitor in our following experiments, because the tested concentrations were high and it would make it impractical for patient administration. Jones et al (2014) showed that DNA ligase III is absolutely required for escape from telomere crisis, whereas DNA ligase IV is not. In future studies, it might be worth investigating other DNA ligase III inhibitors, such as L67 which had a more dramatic effect on HCT116 cell growth compared to L189 (Chen et al, 2018).

Cells treated with KU-60019 (0.15μM and 0.5μM) failed to escape crisis in the first experiment (Set 1) and so did control cells (figure 3.9). The inhibitor affected cell cycle distribution but did not increase apoptotic levels. In the second experiment (Set 3), cells treated with 0.15μM KU-60019 escaped crisis and recovered, but cells treated with 0.5μM escaped crisis and were growing very slowly (figure 3.17). The inhibitor affected cell cycle progression and increased apoptosis only at 0.5μM at day 45. We decided to not include this inhibitor in our following experiments, because we would have to test concentrations over 0.5μM and we preferred to focus on inhibitors that might be effective in much lower concentrations. However, KU-60019 is a highly specific improved analogue of another ATM inhibitor (KU55933) (Golding et al, 2009) and the fact that 0.5μM KU-60019 slowed down cell growth after escape from crisis appears promising, so it would be interesting to examine higher concentrations of KU-60019 in future studies.

3.5.3 NU7441, Rabusertib and AZD6738 prevented HCT116 DN-hTERT cells from escaping crisis

In the first experiment (Set 2), cells treated with 0.5μM NU7441 escaped crisis, while cells treated with 1.5μM NU7441 and control cells failed to do so (figure 3.4). The inhibitor had an effect on cell cycle progression, increased apoptosis at both concentrations and slightly reduced cell growth prior to crisis, as was the case in WT-HCT116 cells. The fact that the lower concentration did not stop cells escaping crisis, but cells treated with the higher concentration did not escape, appeared promising. In the second experiment (Set 3), an intermediate concentration (1μM) was added. All three NU7441 concentrations (0.5μM, 1μM and 1.5μM) prevented cells from escaping crisis, while the control cells escaped crisis, as expected (figure 3.15). As in the first experiment, all three concentrations altered cell cycle progression and increased apoptosis, while the higher concentration visibly slowed down cell growth prior to crisis. In the third experiment (Set 6), all three NU7441 concentrations (0.5μM, 1μM and 1.5μM) prevented cells from escaping crisis, while all four control cells (three DMSO-treated and one untreated) escaped crisis, as expected (figure 3.24). The inhibitor had a concentration-dependent effect on cell growth prior to crisis. All three experiments showed that NU7441 may influence the ability of DN-hTERT HCT116 cells to escape a telomere driven crisis, affected cell growth prior to crisis (particularly the higher concentration), affected cell cycle progression and increased apoptosis (cell cycle progression and apoptosis data not available in the last experiment).

NU7441 is a potent and specific inhibitor of DNA-PKcs (Yanai et al, 2017). Combined with radiation treatment, it increased accumulation of cells in the G2/M phase of the cell cycle and induced apoptosis, which is consistent with our results (figures 3.4 and 3.15) (Yang et al, 2016). DNA-PK is a protein kinase made of a catalytic subunit and a Ku heterodimer and is an essential component of NHEJ (Mohiuddin and Kang, 2019). It is recruited to double-strand breaks and plays a key role in the processing and ligation of the breaks. This function may be crucial for cells experiencing telomere crisis. When DNA-PK is inhibited, DNA damage repair is impeded, which results in apoptosis (Yanai et al, 2017). This is consistent with our data (figures 3.4C and 3.15C). Besides DDR, DNA-PK is crucial in other pathways that are involved in cell survival and proliferation (Mohiuddin and Kang, 2019). DNA-PK also

plays an important role in telomere maintenance by facilitating telomere end-capping and protecting against fusion (Mohiuddin and Kang, 2019). When DNA-PKcs activity was impeded in human cells, it led to significant telomere shortening (Mohiuddin and Kang, 2019), although we did not observe that in our STELA analysis. Therefore, another mechanism that DNA-PK inhibition may influence escape from crisis, is by increasing telomere damage.

In the first experiment (Set 2), 50nM and 100nM AZD6738 seemed to dramatically reduce cell growth in DN-hTERT HCT116 cells, as they weren't able to be passaged at day 52, prior to entering crisis (figure 3.8). In WT-HCT116 cells, 50nM had almost no effect on cell growth, but 150nM caused a significant reduction in cell growth. None of the AZD6738-treated cells or the control cells escaped crisis, leading to no conclusion. The higher concentration of AZD6738 influenced both cell cycle progression and (mildly) apoptosis. In the second experiment (Set 4), we reduced the concentrations to 12.5, 25 and 50nM, due to the strong effect of the inhibitor on cell growth prior to crisis in the last experiment (figure 3.20). Unfortunately, the control cells also did not escape crisis in this experiment, and neither did the AZD6738-treated cells, leading to inconclusive results. No visible effect was seen in cell cycle progression or apoptosis at the new concentrations. In the final experiment (Set 6), all AZD6738-treated cells failed to escape, while all control cells escaped, showing that AZD6738 may influence the ability of DN-hTERT HCT116 cells to escape crisis given that no AZD6738-treated cells have escaped so far (figure 3.23). AZD6738 did not influence cell cycle progression or apoptotic levels, confirming the results of the previous experiment. The potential of an inhibitor being effective at a concentration as low as 12.5nM appears exciting.

AZD6738 is an improved analogue of another ATRi (AZ20) and is highly selective and potent. It inhibits phosphorylation of CHK1 (Ser345) by ATR and has entered clinical trials (phase I and II) (Sundar et al, 2017). Harata et al (2023) showed that 500nM AZD6738 treatment (as a monotherapy) affected the cell growth of WT-HCT116 cells and did not alter cell cycle progression, which is consistent with our results (figure 3.8). ATR is a protein kinase with an essential role in stabilising genome integrity by regulating the DNA replication stress response (which leads to DNA breaks) and DNA damage activated-cell cycle checkpoints

(Sundar et al, 2017). It is activated by RPA-coated single-stranded DNA which is mostly generated by stalled DNA replication or during the early stages of HR (Sundar et al, 2017). It phosphorylates CHK1, which leads to G2/M cell cycle arrest, allowing for DNA repair. p53 is important in G1/S cell cycle arrest to allow for DNA damage repair, so p53-deficient cells would depend on G2/M cell cycle arrest for repair. Following AZD6738 treatment, p53-deficient cancer cells were not able to arrest to repair their DNA, leading to DNA damage accumulation and apoptosis (Harata et al, 2023). However, Harata et al (2023) demonstrated that AZD6738 was also functional in HCT116 cells with proficient p53 and hypothesised that in these cells, DNA damage happens in the S phase which would be repaired at the G2/M checkpoint, if ATR was functional. Hence, we speculate that in our experiment AZD6738 treatment did not allow cells to repair DNA damage accumulated in the S phase, as the G2/M checkpoint was not functional, leading to cell death. However, it is important to note that ATR is involved in multiple processes (protein modification, transcriptional regulation, developmental processes, cell structure, mobility, proliferation and differentiation), so it is challenging to pinpoint the exact mechanism in which AZD6738 might affect the ability of the cells to escape crisis (Kim et al, 2017).

DN-hTERT HCT116 cells treated with Rabusertib (25nM and 50nM) in the first experiment (Set 2) failed to escape crisis, as did control cells (figure 3.5). There was no effect on cell cycle progression or cell growth prior to crisis, but apoptosis was increased at the highest concentration. In the second experiment (Set 3), a lower concentration (12.5nM) was added and no Rabusertib-treated cells escaped crisis, while control cells escaped (figure 3.16). Similar to the previous experiment, Rabusertib did not influence cell cycle progression or cell growth prior to crisis, but increased apoptosis (even at 12.5nM). In the third experiment (Set 5), all Rabusertib-treated cells failed to escape crisis, while the untreated control and one out of three DMSO control cells escaped crisis (figure 3.21). As shown previously, Rabusertib did not affect cell cycle progression or growth before crisis and increased apoptosis (particularly at 50nM). As cells treated with Rabusertib continuously failed to escape crisis in all experiments, we conclude that it may influence the ability of the cells to escape telomere crisis. As with AZD6738, the potential of Rabusertib having a ‘crisolytic’ effect at a low concentration of 12.5nM appears promising.

Rabusertib (LY2603618) is a selective and potent CHK1 inhibitor *in vitro* and *in vivo* that entered clinical testing (phase I and II studies in combination with chemotherapy). Treatment with Rabusertib abolished the G2/M checkpoint in cells treated with DNA damaging agents (King et al, 2013). CHK1 is activated through phosphorylation by ATR and modulates cell cycle checkpoints (S and G2/M checkpoints) to prevent cells with damaged DNA from entering into mitosis. It is involved in the initiation of DNA replication, it stabilises replication forks and it coordinates mitosis (McNeely et al, 2010). P53 is a protein that also promotes cell cycle arrest (G1 phase) to allow time for DNA repair, so P53-deficient cells are expected to be hypersensitive to CHK1 inhibition due to synthetic lethality (King et al, 2013). This would lead to premature entry into mitosis, resulting in mitotic catastrophe. However, HCT116 cells have a functioning P53 pathway and Zenvirt et al (2010) showed that P53-proficient cells can activate DNA-damage checkpoints through the P53 pathway. Nonetheless, these cells cannot enter the cell cycle again when CHK1 is inhibited, because CHK1 is essential for the recovery of P53-proficient cells after cell cycle arrest. This leads to cell death by a different unknown mechanism (Tao et al, 2009), while Zenvirt et al (2010) reported that in their study cell death happened by caspase-3-dependent apoptosis. They showed that under DNA damage (which in this case is telomere damage), P53-proficient cells are no less sensitive to CHK1 inhibition compared to P53-deficient cells, but they just die by a different mechanism. Given that both AZD6738 and Rabusertib inhibit the ATR-CHK1 pathway, it is possible that this pathway is important for cell survival during crisis.

While the control cells failed to escape in some experiments, leading to inconclusive results, the results showed great consistency between the different repeats regarding cell growth, cell cycle progression and apoptosis patterns. The results also suggest no correlation between cellular apoptosis or cell cycle progression and the ability to escape a telomere crisis. However, apoptosis and cell cycle progression have only been monitored prior to crisis in our experiment. In the following chapter we will be investigating apoptotic levels and cell cycle progression during crisis. Our results also showed that none of the inhibitors affected the rate of telomere erosion during early crisis. In the following chapter, we will be investigating if the inhibitors affect the rate of telomere erosion during late crisis, to understand if there is a correlation between telomere length and the ability to escape a telomere crisis. In the sets that control cells behaved as expected, it was shown that

Rabusertib (12.5nM, 25nM and 50nM), AZD6738 (12.5nM, 25nM and 50nM) and NU7441 (1 µM, 1.5 µM) prevented cells from escaping crisis. While Rabusertib and AZD6738-treated cells did not escape crisis in any of the three experiments, 0.5µM NU7441 (the lowest concentration used) failed to prevent escape from crisis in one out of the three experiments. Rabusertib and AZD6738 have been selected to be further investigated in the following chapter.

3.5.4 Conclusion

In conclusion, three inhibitors that may eliminate cells during crisis have been identified in this stage of the study. Our experiments demonstrated that Rabusertib (12.5nM, 25nM and 50nM), AZD6738 (12.5nM, 25nM and 50nM) and NU7441 (1 µM, 1.5 µM) prevented cells from escaping crisis. They also showed that 1µM 6-0H-DOPA, 1.5µM RI-1 and 100nM Adavosertib did not prevent cells from escaping crisis. For the aforementioned concentrations, Rabusertib did not influence cell cycle progression or cell growth prior to crisis, but increased apoptosis. AZD6738 did not influence cell cycle progression or apoptotic levels and NU7441 had a concentration-dependent effect on cell growth prior to crisis and increased apoptosis. These novel findings provide fundamental clues for future studies on DDR inhibitors in cells undergoing a telomere crisis.

Chapter 4

Assessing the effect of Rabusertib (CHK1i) and AZD6738 (ATRi) on HCT116 cells

4.1 Abstract

Telomere crisis is a cellular state induced by critical telomere shortening and escape of cells from crisis is linked to cancer development. The ATR – CHK1 pathway plays a key role in genome protection by regulating DNA damage-induced cell cycle checkpoints. In this chapter we examine how two inhibitors, Rabusertib, which is a CHK1 inhibitor (CHK1i) and AZD6738, which is an ATR inhibitor (ATRi) affect the ability of cells to escape a telomere induced crisis.

We used colorectal cancer cells (HCT116) expressing a dominant-negative telomerase (DN-hTERT) that undergo a well-defined period of crisis from which they escape. We treated these cells with 50nM Rabusertib and 50nM AZD6738 and the effects of these inhibitors on cell growth, cell cycle progression, apoptosis, telomere erosion, fusion and DDR protein expression levels were monitored before and during crisis. We also assessed how the two inhibitors affected cell growth, cell cycle progression, apoptosis and DDR protein expression levels in WT-HCT116 cells, which do not undergo crisis.

50nM Rabusertib (CHK1i) consistently prevented cells from escaping crisis and 50nM AZD6738 (ATRi) dramatically slowed down escape from crisis. In the chosen concentrations, the inhibitors did not affect cell growth, apoptosis and cell cycle progression prior to crisis, but reduced the rates of cell growth, increased apoptosis and altered cell cycle progression during deep crisis. The addition of these inhibitors did not affect the rate of telomere erosion before and during crisis, but Rabusertib increased fusion events during deep crisis. Both inhibitors triggered the DNA damage response, likely by inhibiting DDR, causing DNA damage accumulation, which subsequently activated further DDR pathways. However, each inhibitor had a different effect on CHK1 activity.

In conclusion, we have shown that Rabusertib and AZD6738 reduce the ability of cells to escape a telomere driven crisis and affect the properties of the cells during crisis. We have

also provided evidence of the importance of the ATR-CHK1 pathway in keeping cells alive during crisis and propose further clinical evaluation of Rabusertib as a potential treatment for patients with tumours that have short dysfunctional telomeres.

4.2 Introduction

As previously described, telomere crisis is a state induced by severely short telomeres and characterised by telomere fusion and cell death. Only a very small percentage of cells undergoing a telomere crisis will escape and continue their growth by re-activation or up-regulation of telomerase activity (Shay, 2016). Due to the fact that escapee cells have accumulated extensive genomic mutations, escape from telomere crisis is linked to the progression of malignant tumours (Shay, 2016). In this study we investigate the use of DDR inhibitors to modulate the ability of cells to escape crisis and potentially impede the progression to malignancy.

The kinase ataxia telangiectasia and Rad-3 related (ATR) is induced by single-stranded DNA and double-stranded DNA junctions, which predominantly arise at stalled replication forks and is essential for cell viability, especially during the S-phase of the cell cycle (Lecona and Fernandez-Capetillo, 2018). It plays a key role in the replication stress response to ensure that the genome is precisely replicated once every cell cycle and it is essential for normal cell cycle progression (Saldivar et al, 2017). It inhibits the G2/M transition through the phosphorylation of CHK1 to limit mitotic entry when the genome is incompletely replicated (Saldivar et al, 2017). ATR has multiple functions during double-strand DNA break repair, inter-strand crosslink repair, meiosis, in response to mechanical and osmotic stress and at telomeres (Saldivar et al, 2017). ATR, which is a large protein (300kDa) shares sequence and functional homology with ATM, a DNA damage response kinase that is activated by the presence of double-strand DNA breaks (Marechal and Zou, 2013). The ATR pathway cross-talks with the ATM pathway and the two pathways modulate each other (Marechal and Zou, 2013). ATR is known to phosphorylate downstream ATM-specific substrates and activate the G1/S cell cycle checkpoint, which is a key function of ATM. This suggests that defects in one pathway may be compensated by the other pathway to some degree to protect the genome (Barnieh et al, 2021).

AZD6738 is an ATR inhibitor developed by AstraZeneca, which is an improved analogue of another ATR inhibitor (AZ20) and can be orally administered (Weber and Ryan, 2015). It is highly selective, it has been studied extensively and it entered clinical trials in 2013 (Barnieh

et al, 2021). A phase I study of AZD6738, as monotherapy in advanced solid tumours showed that it was well-tolerated (Dillon et al, 2019). There are currently at least 25 Phase I and II trials either recruiting or preparing to recruit and they are testing the drug either as monotherapy, or in combination with other agents in a variety of cancers. However, the data from clinical trials is not released yet, thus the full potential of the inhibitor is yet to be known (Barnieh et al, 2021).

Chk1 is a Ser/Thr protein kinase located downstream of ATR that phosphorylates downstream effectors, it plays an important role in cell cycle and DNA damage regulation and it is essential to cell survival (Gorecki et al, 2021). It is phosphorylated by ATR following replication stress and regulates the intra-S and G2/M checkpoints to slow down cell cycle progression and allow time for DNA damage repair (Neizer-Ashun and Bhattacharya, 2021). CHK1 is also important in the mitotic spindle checkpoint, ensuring correct assembly of chromatids on the mitotic spindle to prevent genomic instability and for controlling hematopoietic stem and progenitor cell development and expansion (Peddibhotla et al, 2009; Neizer-Ashun and Bhattacharya, 2021). If there is significant DNA damage, CHK1 can trigger apoptosis by suppressing caspases 2 and 3 (Gorecki et al, 2021).

Rabusertib is the first potent and highly selective Chk1 inhibitor, developed by Eli Lilly and Company. Completed phase I studies have evaluated the safety and maximum tolerable dose of Rabusertib when combined with pemetrexed and cisplatin (Calvo et al, 2014). Unfortunately, phase II trials appear to be less promising, as there was no significant effect in the overall survival of pancreatic cancer patients from a combination treatment of Rabusertib and gemcitabine compared to gemcitabine alone (Laquente et al, 2017). Rabusertib was eventually discontinued in 2013 after seven completed trials (Gorecki et al, 2021).

This study is divided into three stages. In the first stage, we treated DN-hTERT HCT116 with 50nM Rabusertib and 50nM AZD6738 to confirm that they affect the ability of cells to escape crisis. We assessed how the two inhibitors affected the properties of the cells, such as cell growth, cell cycle progression and apoptosis before crisis. In the second stage, we treated WT-HCT116 cells with 50nM Rabusertib and 50nM AZD6738 to examine how the two inhibitors affected cell growth, cell cycle progression and apoptosis compared to cells undergoing crisis. In the third stage, we treated DN-hTERT HCT116 with 50nM Rabusertib

and 50nM AZD6738 and harvested them during deep crisis for analysis. We compared how the two inhibitors affected cell growth, cell cycle progression and apoptosis in deep crisis compared to early crisis. We also compared how the two inhibitors affected telomere erosion and genomic instability in deep crisis compared to early crisis. Lastly, we performed Western Blot analyses to investigate how the two inhibitors affected protein expression levels in deep crisis compared to early crisis.

4.3 Aims

In this chapter, we focus on the DDR inhibitors Rabusertib (CHK1i) and AZD6738 (ATRi) which were shown to prevent cells from escaping crisis at selected concentrations in the previous chapter. We hypothesise that these inhibitors affect the ability of DN-hTERT HCT116 cells to escape telomere crisis, act specifically during telomere crisis by increasing DNA damage (which synergises with telomere damage) and do not affect cells that do not undergo telomere crisis or cells prior to entering telomere crisis. To test this, we treated DN-hTERT HCT116 and WT-HCT116 with the two inhibitors and the properties of the cells (cell growth, cell cycle progression, apoptosis, telomere erosion, genomic instability, protein expression) were studied before and during crisis.

The aims of this chapter are to:

- Confirm that Rabusertib and AZD6738 affect the ability of DN-hTERT HCT116 cells to escape crisis
- Assess how the two inhibitors affect cell growth, cell cycle progression and apoptosis before and during crisis
- Assess how the two inhibitors affect cell growth, cell cycle progression and apoptosis in WT-HCT116 cells
- Assess if the two inhibitors affect the rate of telomere erosion before or during crisis
- Determine how the two inhibitors influence genomic instability before and during crisis
- Evaluate the status of DDR proteins by Western blot analysis during crisis

4.4 Results

4.4.1. Assessing the effect of Rabusertib on DN-hTERT HCT116 cells

In the previous chapter, we showed that 12.5nM, 25nM and 50nM Rabusertib (CHK1i) prevented cells from escaping crisis (figure 3.16). To further examine if Rabusertib affects the ability of DN-hTERT HCT116 cells to escape a telomere-driven crisis we treated them with 50nM Rabusertib. The experiment included three control samples treated with DMSO and three samples treated with the CHK1 inhibitor under the same conditions (triplicate experiment). The inhibitor was added every two or three days at the same time for all samples. At the end of each week, the cells were counted and cell-cycle and apoptosis assays were carried out to determine the growth rate, cell cycle progression and cell death respectively. When the cells were harvested, a cell sample was collected for DNA extraction to perform telomere length (STELA) and telomere fusion analysis.

As expected, the rate of cell growth declined as the cells approached crisis (figure 4.1.A). Differences in cell growth between the samples became apparent only after cells entered crisis. During late crisis cell growth stopped, the morphology of the cells had changed, as cells appeared large and vacuolated and there was increased cell death. The cells entered a crisis state after ~53 population doublings from the point of single-cell cloning. Cells were passaged four times before they entered deep crisis. Control cells treated with DMSO escaped crisis and continued growing, as expected. They were passaged six times before they reached PD 70, when the experiment was intentionally terminated. The differences in cell growth between the three control samples before and after crisis were minimal. All three samples treated with Rabusertib failed to escape crisis. The inhibitor did not impact on cell growth prior to the onset of crisis. This experiment confirmed that 50nM Rabusertib affects the ability of cells to escape a telomere driven crisis.

Overall, as cells were approaching crisis (day 52), there was a higher number of cells in the sub G1, G2/M, S and >4n phase (~45% combined) and a lower number of cells in the G0/G1 phase (~55%) compared to day 38. At the end of the first week of treatment (day 38), there was a higher number of inhibitor-treated cells in the sub G1 phase ($p=0.025$) and a lower number in G1 phase ($p=0.01$) compared to control cells (Figure 4.1.B,D). At the end of the second week of treatment (day 45), there was a higher number of inhibitor-treated cells in

the G1 phase (p=0.04) and a lower number in G2/M phase (p=0.02) compared to control cells. At the end of the third week of treatment (day 52), there was a lower number of inhibitor-treated cells in the >4n phase (p=0.03) compared to control cells. In conclusion, there were a few differences in the cell cycle distribution between control and Rabusertib-treated samples, but the effect of Rabusertib on the cell cycle was inconclusive over the three week period as no specific pattern was observed (e.g. decreased G1 phase accumulation at day 38, but increased G1 population at day 45).

Apoptosis levels increased as cells approached crisis (Figure 4.1.C,E). In the DMSO-treated cells apoptotic levels increased approximately 10% between day 38 and day 52 of treatment (with an increase in late apoptotic cells). In Rabusertib-treated cells, there was a smaller increase (~5%) between day 38 and day 52 of treatment. Rabusertib-treated cells exhibited higher apoptotic levels at day 38 compared to control cells [both early (p=0.007) and late (p=0.016) apoptosis], but there were no noticeable differences at day 45 and 52. A possible explanation could be that the addition of the inhibitor mildly stressed the cells in the first week of treatment, but they recovered afterwards. Rabusertib did not impact on apoptotic levels prior to the onset of crisis, with approximately 25% apoptosis in both control and inhibitor-treated cells before entering deep crisis.

In conclusion, 50nM Rabusertib prevented DN-hTERT HCT116 cells from escaping a telomere-driven crisis but did not strongly affect cell growth, cell cycle progression and apoptosis prior to crisis.

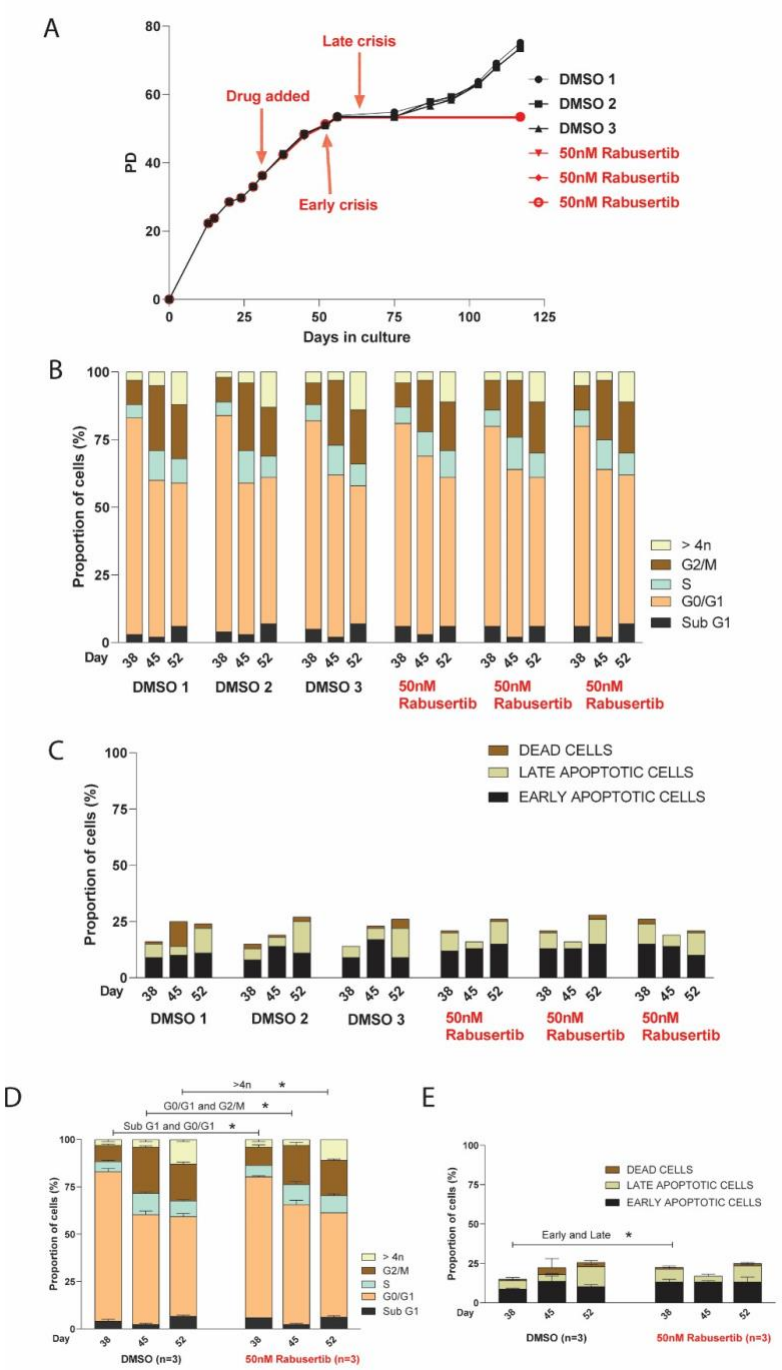

Figure 4.1: Cell growth, cell cycle and apoptosis analysis of DN-hTERT HCT116 cells treated with 50nM Rabusertib. The figure shows the growth curve (A), the cell cycle progression (B,D) and the apoptotic levels (C,E) of DN-hTERT HCT116 treated with DMSO and Rabusertib. Figures 4.1.D and 4.1.E show the mean cell cycle progression and apoptosis, respectively, calculated from the three biological replicates. Apoptosis was analysed using Annexin-V/propidium iodide (PI) staining. Cells are classified as early apoptotic when they are Annexin V positive and PI negative, late apoptotic when they are Annexin V and PI positive and dead when they are Annexin V negative and PI positive. P values were obtained using Student's t-test (2 tailed, equal variances, n=3) and * indicates $p < 0.05$.

4.4.2. Assessing the effect of AZD6738 on DN-hTERT HCT116 cells

In the previous chapter, we showed that 12.5nM, 25nM and 50nM AZD6738 (ATRi) prevented cells from escaping crisis (figure 3.20). To further test if AZD6738 affects the ability of DN-hTERT HCT116 cells to escape a telomere-driven crisis we treated them with 50nM AZD6738. The experiment included three control samples treated with DMSO and three samples treated with the ATR inhibitor under the same conditions (triplicate experiment).

As expected, the rate of cell growth declined as cell cultures approached crisis (figure 4.2.A). There was no difference in cell growth between the samples prior to the onset of crisis. The cells entered a crisis state after ~53 population doublings from the point of single-cell cloning. Cells were passaged four times before they entered deep crisis. Control cells behaved as expected, escaping crisis and continuing growing. They were passaged six times before they reached PD 70. All three samples treated with AZD6738 escaped crisis, but significantly more slowly compared to control cells. Cells had to be passaged up to nine times until they reached a PD of 70, when the experiment was intentionally terminated. This experiment showed that 50nM AZD6738 slows down escape from crisis in DN-hTERT HCT116 cells.

As previously shown, the percentage of cells in G0/G1 phase decreased, while the percentage of cells in sub G1, G2/M, S and >4n phase increased as cells approached crisis (day 52) (figure 4.2.B,D). There were minimal differences in the cell cycle distribution between control and AZD6738-treated cells before crisis (~day 56). The only significant difference observed was a decreased G2/M accumulation ($p=0.02$) in inhibitor-treated cells compared to control cells at day 45. We have showed that AZD6738 did not impact on cell cycle progression prior to crisis. During early crisis (day 56), there were differences amongst the control samples and inhibitor treated samples (although not statistically significant). Two DMSO samples had a low percentage of cells in sub G1, G2/M, S and >4n phase (<35% combined), while all three AZD6738-treated samples (and a control DMSO treated sample) had a higher percentage of cells in these phases (>45% combined). This suggests that AZD6738 might affect cell cycle progression (in G2/M phase) during crisis.

As previously shown, apoptotic levels increased as cells approached crisis (approximately a 10% increase between day 38 and day 52) (figure 4.2.C,E). No significant differences were observed in the apoptotic levels between control cells and inhibitor-treated cells prior to crisis. One of the AZD6738-treated samples had slightly higher apoptosis (~8% higher) at day 38 compared to the other samples, but at days 45 and 56 there were no differences. This showed that AZD6738 did not impact on apoptotic levels prior to the onset of crisis. During early crisis (day 56), all three DMSO samples had <49% apoptosis (two of which only had 23%), while all three AZD6738-treated samples had >55% apoptosis (two of which had >79%). These results indicate that AZD6738 affects apoptotic levels specifically during crisis [by increasing early apoptosis ($p= 0.045$) and dead cells ($p= 0.047$)].

In conclusion, 50nM AZD6738 dramatically slowed down DN-hTERT HCT116 cells from escaping a telomere-driven crisis but did not affect cell growth, cell cycle progression and apoptosis prior to crisis. The inhibitor might affect cell cycle progression and it increased apoptosis during early crisis.

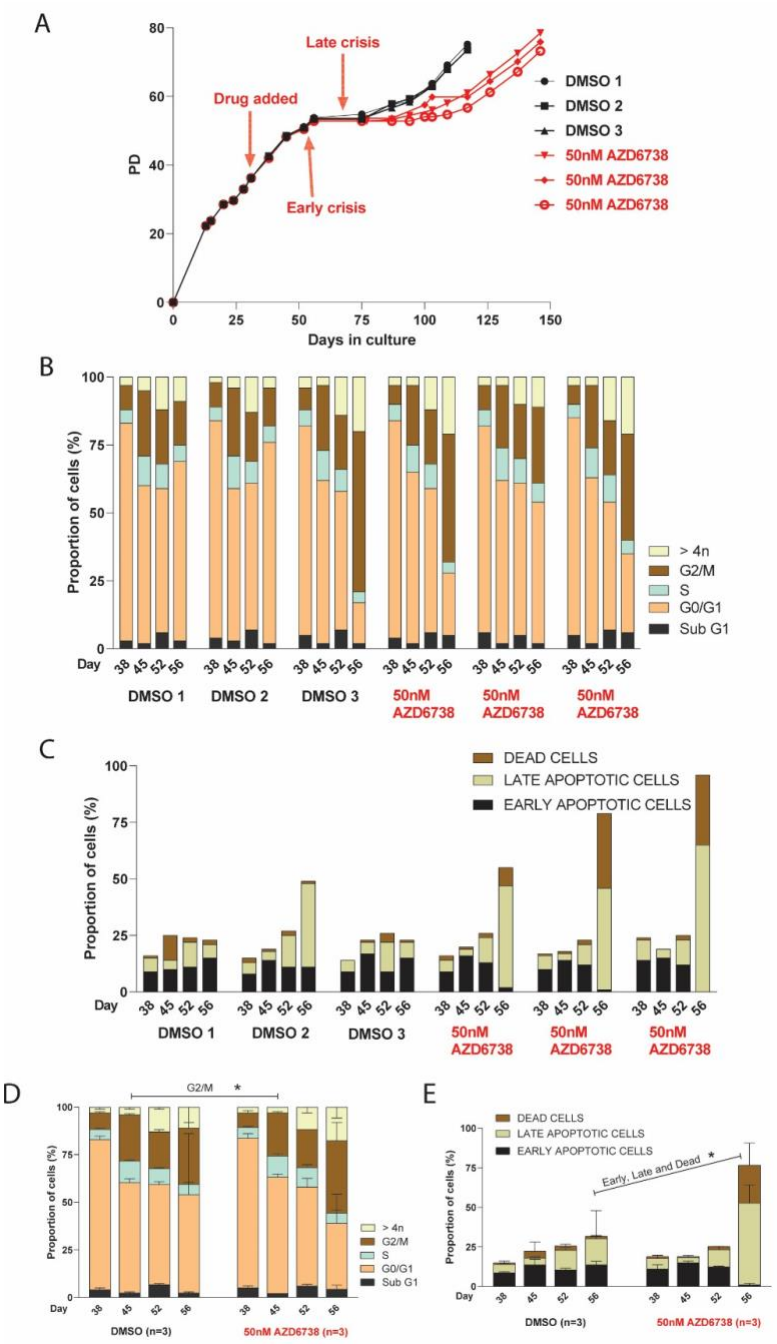

Figure 4.2: Cell growth, cell cycle and apoptosis analysis of DN-hTERT HCT116 cells treated with 50nM AZD6738. The figure shows the growth curve (A), the cell cycle progression (B,D) and the apoptotic levels (C,E) of DN-hTERT HCT116 treated with DMSO and AZD6738. Figures 4.2.D and 4.2.E show the mean cell cycle progression and apoptosis, respectively, calculated from the three biological replicates. Apoptosis was analysed using Annexin-V/propidium iodide (PI) staining. Cells are classified as early apoptotic when they are Annexin V positive and PI negative, late apoptotic when they are Annexin V and PI positive and dead when they are Annexin V negative and PI positive. P values were obtained using Student's t-test (2 tailed, equal variances, n=3) and * indicates $p < 0.05$.

To further test how AZD6738 affects the properties of DN-hTERT HCT116 cells after they escape crisis, we monitored the cell cycle progression and apoptosis until they reached a PD of 70. An analysis was performed only when there were enough cells available after passaging.

Overall, as cells recovered from crisis, the proportion of cell in G0/G1 phase increased, while their distribution in sub G1, G2/M, S and >4n phase decreased (figure 4.3.A). This is the opposite pattern observed compared to when cells approached crisis (figure 4.2.B). At day 117, two DMSO-treated samples (1,2) had a similar cell cycle distribution (74-79% in G0/G1) to that observed before crisis, while one DMSO-treated sample (3) only had 18% of cells in G0/G1 phase. It is not known what stressed the cells in DMSO-treated sample (3) as this was not reflected in the cell growth or the apoptotic levels and it was most likely an experimental outlier. At the same day (117), AZD6738-treated cells showed a lower accumulation in G0/G1 phase (42-55%) and a higher accumulation in sub G1 (2-5%) and >4n phase (8-13%) compared to control samples (1) and (2). However, by day 146 two out of the three AZD6738-treated samples (1,3) showed a similar cell cycle distribution (73-78% in G0/G1) to that observed before crisis. In conclusion, cells treated with AZD6738 required more time to restore the cell cycle distribution compared to control cells, which is expected given that their escape was more delayed.

Overall, as cells recovered from crisis, apoptotic levels were reduced (figure 4.3.B), which is the opposite pattern observed compared to when cells approached crisis (figure 4.2.C). At day 117, DMSO-treated samples had very low apoptosis (17-22%), while AZD6738-treated samples had very high apoptosis (57-96%). However, by day 146, apoptotic levels in AZD6738-treated samples were reduced dramatically (13-26%). In conclusion, cells treated with AZD6738 required more time to lower their apoptotic levels compared to control cells, which is expected given that their escape was more delayed.

To sum up, it took longer for AZD6738-treated cells to recover their cell cycle distribution and apoptotic levels compared to control cells. However, a conclusion cannot be made as to whether AZD6738 increased apoptosis and altered cell cycle progression after crisis because the difference could be due to a delayed escape from crisis.

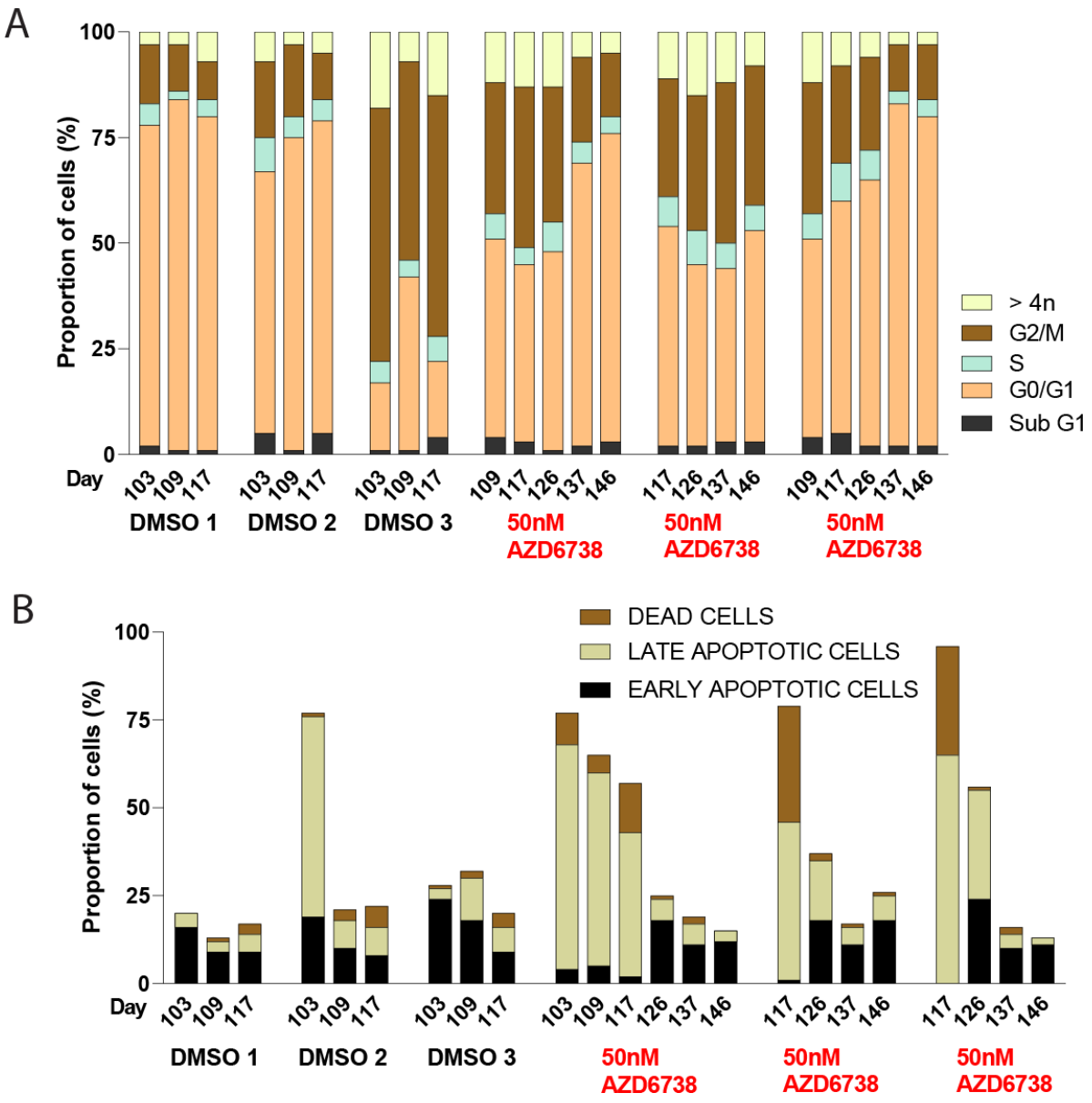

Figure 4.3: Cell cycle and apoptosis analysis of DN-hTERT HCT116 cells treated with 50nM AZD6738 after crisis. The figure shows the cell cycle progression (A) and the apoptotic levels (B) of DN-hTERT HCT116 treated with DMSO and AZD6738 after they escaped crisis. Apoptosis was analysed using Annexin-V/propidium iodide (PI) staining. Cells are classified as early apoptotic when they are Annexin V positive and PI negative, late apoptotic when they are Annexin V and PI positive and dead when they are Annexin V negative and PI positive.

4.4.3. Assessing the effect of Rabusertib and AZD6738 on WT-HCT116 cells

To investigate if the two inhibitors affect only cells undergoing a telomere crisis, we treated WT-HCT116 cells. These cells do not undergo telomere crisis, as they have a functional telomerase, which maintains the length of the telomeres. The experiment included three control samples treated with DMSO and three samples treated with the inhibitor under the same conditions (triplicate experiment). The inhibitor was added every two or three days at the same time for all samples. At the end of each week the cells were counted and at selected timepoints, cell-cycle and apoptosis assays were carried out to determine cell cycle progression and cell death respectively. We have previously tested the effect of these inhibitors on WT-HCT116 cells only for two weeks (figures 3.1.E, 3.2.A). In this experiment, the treatment lasted for 111 days.

4.4.3.1 Assessing the effect of Rabusertib on WT-HCT116 cells

In the previous chapter we showed that 14-day treatment of WT-HCT116 cells with 50nM Rabusertib had no impact on cell growth (figure 3.1.E). In this experiment, 50nM Rabusertib did not affect cell growth during the 111-day treatment (figure 4.4.A). There was a reduction in cell growth after day 21 in all cells, due to error when passaging the cells. A smaller amount of cells was passaged leading to cellular stress and a population reduction. However, the cells quickly recovered after day 28.

The stress induced in the cells by the passaging error was reflected in the cell cycle distribution at day 21, as there were more cells in the sub G1 and >4n phase compared to days 7 and 14 (figure 4.4.B). When cells were harvested at the last day of the experiment, a lot of them were in S phase, as cells had not reached high confluency yet. There were no differences in the cell cycle distribution between control and inhibitor-treated cells. This shows that 50nM Rabusertib did not affect cell cycle progression in WT-HCT116 cells.

Apoptotic levels in the first three weeks of treatment were relatively low (<25%) (figure 4.4.C). At day 21 there was a small increase in apoptosis (~10%) compared to day 7, which reflects the population decline shown in the growth curve. At the last day of the experiment (day 111), apoptotic levels were very low (~10%). There were no visible differences in the apoptotic levels between the control and the inhibitor-treated cells. This shows that 50nM Rabusertib did not affect apoptosis in WT-HCT116 cells.

In conclusion, 50nM Rabusertib did not affect cell growth, cell cycle progression and apoptosis in WT-HCT116 cells.

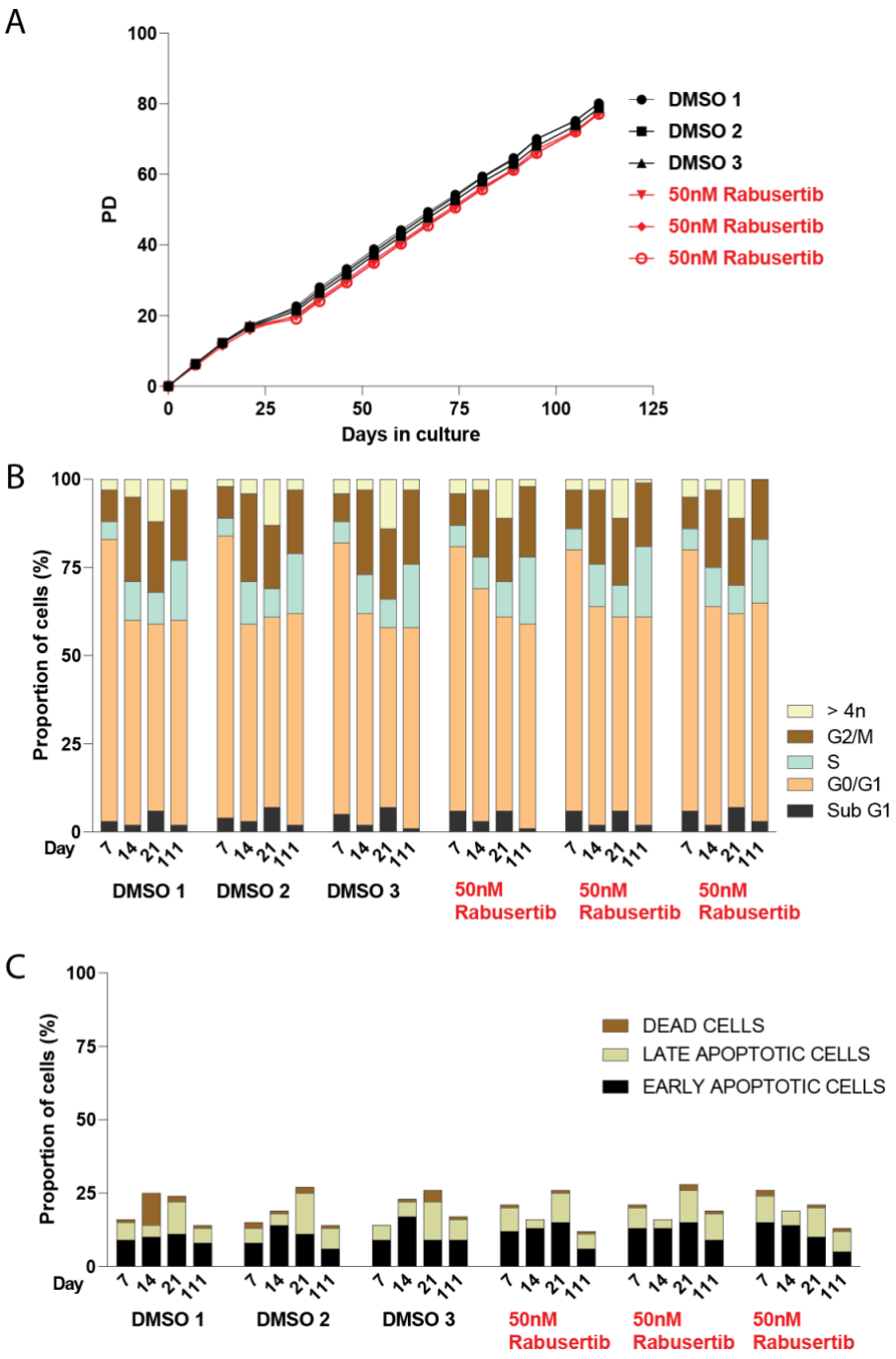

Figure 4.4: Cell growth, cell cycle and apoptosis analysis of WT-HCT116 cells treated with 50nM Rabusertib. The figure shows the growth curve (A), the cell cycle progression (B) and the apoptotic levels (C) of WT-HCT116 treated with DMSO and Rabusertib. Apoptosis was analysed using Annexin-V/propidium iodide (PI) staining. Cells are classified as early apoptotic when they are Annexin V positive and PI negative, late apoptotic when they are Annexin V and PI positive and dead when they are Annexin V negative and PI positive.

4.4.3.2 Assessing the effect of AZD6738 on WT-HCT116 cells

In the previous chapter we showed that 14-day treatment of WT-HCT116 cells with 50nM AZD6738 had no impact on cell growth (figure 3.2.A). In this experiment, 50nM AZD6738 did not affect cell growth during the 111-day treatment (figure 4.5.A). As already mentioned, there was a reduction in cell growth after day 21 in all cells, due to error when passaging the cells.

There were no differences in the cell cycle distribution between control and inhibitor-treated cells (figure 4.5.B). There was also no difference in the apoptotic levels between the control and the inhibitor-treated cells (figure 4.5.C). This shows that 50nM AZD6738 did not affect cell cycle progression and apoptosis in WT-HCT116 cells.

In conclusion, 50nM AZD6738 did not affect cell growth, cell cycle progression and apoptosis in WT-HCT116 cells.

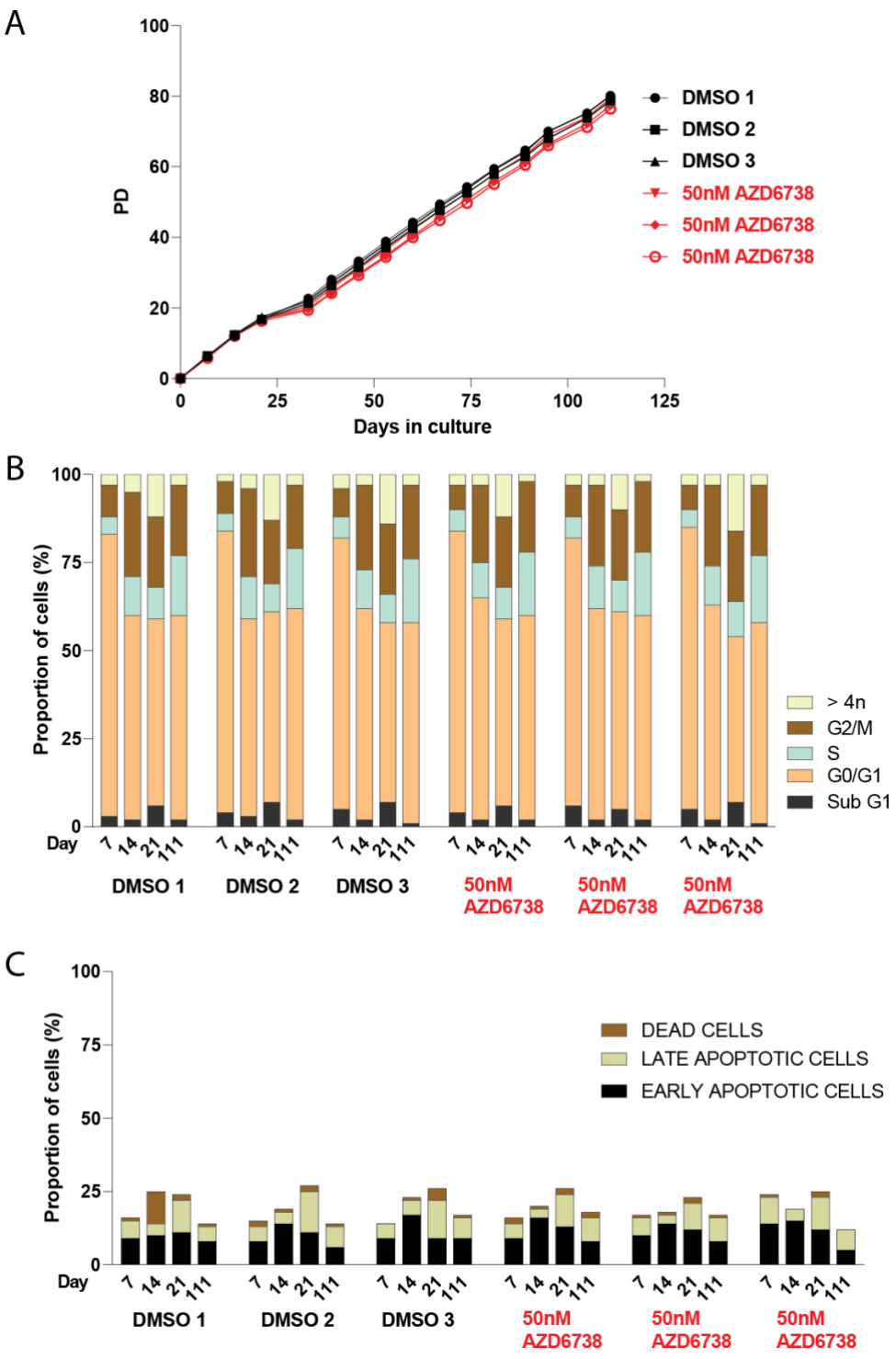

Figure 4.5: Cell growth, cell cycle and apoptosis analysis of WT-HCT116 cells treated with 50nM AZD6738. The figure shows the growth curve (A), the cell cycle progression (B) and the apoptotic levels (C) of WT-HCT116 treated with DMSO and AZD6738. Apoptosis was analysed using Annexin-V/propidium iodide (PI) staining. Cells are classified as early apoptotic when they are Annexin V positive and PI negative, late apoptotic when they are Annexin V and PI positive and dead when they are Annexin V negative and PI positive.

4.4.4 Assessing the effect of Rabusertib and AZD6738 on cell growth, cell cycle and apoptosis during crisis

We have shown that the two inhibitors do not affect the properties of cells that do not undergo crisis or cells before they enter crisis. To investigate further how these inhibitors affect the cells during crisis, we conducted three experiments using DN-hTERT HCT116 cells. Each experiment contained three control samples (treated with DMSO), three samples treated with 50nM AZD6738 and three samples treated with 50nM Rabusertib. All three samples in each experiment were treated under the same conditions (triplicate experiment, n=3) and harvested at the same timepoint (during deep crisis) for analysis. While in all experiments, the cells were harvested during late crisis for analysis, the timepoint of harvesting was different to study how the properties of cells were affected in different stages of crisis.

Cells cryopreserved from the experiments which confirmed that the two inhibitors alter the ability of the cells to escape crisis (figures 4.1, 4.2), were thawed at the end of the first week of treatment (day 38) to start Experiment 1. Once Experiment 1 was completed, cells from this experiment were thawed at the end of the third week of treatment (day 52) to start Experiments 2 and 3. The reason for thawing the cells just before the start of crisis in experiments 2 and 3 was to reduce variability between the experiments The inhibitor was added every two or three days at the same time for all samples. At the end of each week, the cells were counted and cell-cycle and apoptosis assays were carried out to determine the growth rate, cell cycle progression and cell death respectively. At the end of Week 3 (day 52) and Week 5 of treatment, a cell sample was collected for DNA extraction to perform STELA and fusion analysis and another cell sample was collected for lysis and Western blot analysis. Cells entered a crisis state after ~52 population doublings from the point of single-cell cloning. Cells were passaged three times before they entered deep crisis in Experiment 1 and one time in Experiments 2 and 3.

In the first experiment, there was a minimal difference in cell growth prior to the onset of deep crisis (Week 1 to Week 4 of treatment) amongst the samples (figure 4.6.A). From Week 1 to Week 2 cells grew approximately 2-3 PDs (as they were recovering from the mild stress of thawing), while from Week 2 to Week 3 cells grew approximately 4 PDs. From Week 3 to Week 4, there was a reduction in cell growth (approximately 2 PD growth), as cells had

entered the early stages of crisis. During deep crisis (Week 4 to Week 5), there was a reduction in cell growth in cells treated with 50nM Rabusertib (0.2 PD) and 50nM AZD6738 (0.43 PD) compared to the control cells (0.78 PD), but it was not statistically significant (p=0.05 and p=0.21). This showed that while the two inhibitors did not affect cell growth prior to crisis, they both reduced cell growth during crisis, particularly Rabusertib.

We compared cell cycle progression at the end of Week 3 (day 52) and Week 4 (day 60) of treatment (figure 4.6.B) and during deep crisis (day 66) (figure 4.6.C). Between Week 3 and Week 4, there was a reduction of cells in the G0/G1 phase and an increase of cells in the sub G1, S, G2 and >4n phase. During early crisis, there were no differences between the cell cycle distribution amongst the samples, except for a small increase in accumulation of AZD6738-treated cells in G1 phase (p=0.02) at Week 3 (day 52). During deep crisis, there was a change in cell cycle distribution between control cells and inhibitor-treated cells. There were more AZD6738-treated cells in >4n phase (p=0.03) and less Rabusertib-treated cells in G1 phase (p=0.017) compared to control cells. Although not statistically significant, there were also more Rabusertib-treated cells in >4n phase (p=0.06), less AZD6738-treated cells in G1 phase (p=0.06) and in both inhibitor-treated samples there were also more cells in sub G1 phase (3-3.7% increase, p=0.11, p=0.09). We have shown that while the two inhibitors had a minimal effect on cell cycle progression prior to deep crisis, they both changed the distribution during deep crisis.

We compared apoptosis at the end of Week 3 (day 52) and Week 4 (day 60) (figure 4.6.D) and during deep crisis (day 66) (figure 4.6.E). Before deep crisis, apoptotic levels were relatively low (<30%) and the only significant difference amongst the samples was observed at day 52 with an increase in late apoptotic AZD6738-treated cells (p=0.03). During deep crisis, there was a difference in the apoptotic levels between control cells (38%) and inhibitor-treated cells (45%), but it wasn't statistically significant (p=0.19 and p=0.35 for late apoptosis). This showed that while both inhibitors did not affect apoptosis considerably prior to deep crisis, they may increase apoptosis during deep crisis.

In conclusion, Experiment 1 showed that neither of the inhibitors affected cell growth and only had a minimal effect on cell cycle progression and apoptosis prior to crisis, but both inhibitors decreased cell growth and had a stronger effect on cell cycle progression and apoptosis during deep crisis.

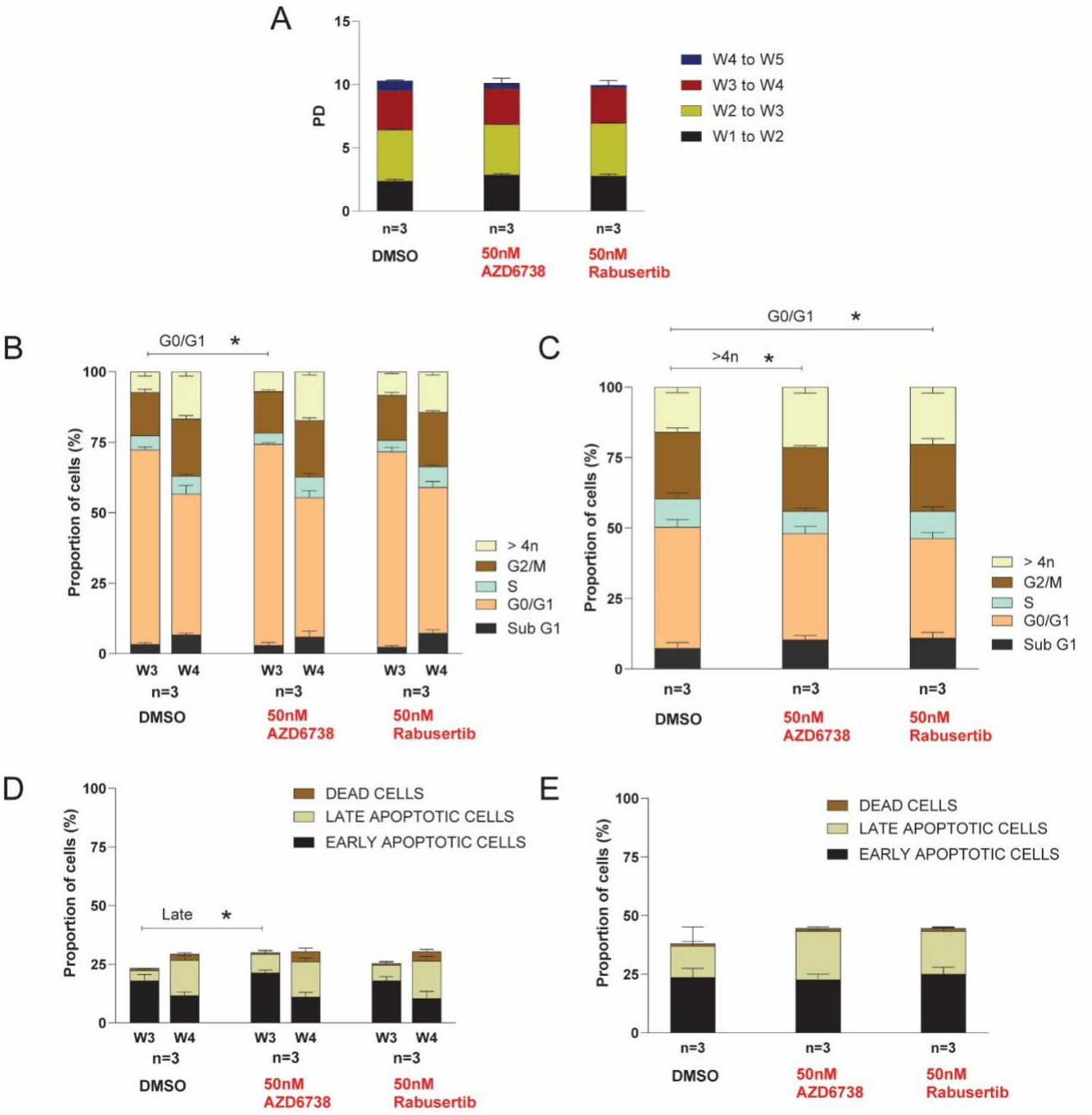

Figure 4.6: Cell growth, cell cycle and apoptosis analysis of DN-hTERT HCT116 cells treated with 50nM AZD6738 and 50nM Rabusertib in Experiment 1. The figure shows the PD each week of treatment (A), the cell cycle distribution at Week 3 and 4 of treatment (B), the cell cycle distribution at Week 5 of treatment (C), the apoptotic levels at Week 3 and 4 of treatment (D) and the apoptotic levels at Week 5 of treatment (E). Apoptosis was analysed using Annexin-V/propidium iodide (PI) staining. Cells are classified as early apoptotic when they are Annexin V positive and PI negative, late apoptotic when they are Annexin V and PI positive and dead when they are Annexin V negative and PI positive. P values were obtained using Student's t-test (2 tailed, equal variances, n=3) and * indicates $p < 0.05$.

In the second experiment, there was a significant difference in cell growth between the control cells (~2.8 PD) and cells treated with 50nM Rabusertib (~1.3 PD) during deep crisis (W4 to W5, p=0.003), and to a lesser degree, during early crisis (~0.5PD reduction, W3 to W4, p=0.02) (figure 4.7.A). Cells treated with AZD6738 (~1.7 PD) also exhibited slower growth compared to control cells (~2.8 PD) during deep crisis, but it was not significant (p=0.057). This showed that the two inhibitors reduced cell growth during crisis, particularly Rabusertib.

We compared cell cycle progression at the end of Week 4 of treatment (day 59) (figure 4.7.B) and during deep crisis (day 70) (figure 4.7.C). During early crisis (figure 4.7.B), there was no difference between cell cycle distribution amongst the samples, except for an increased accumulation of Rabusertib-treated cells in S phase (p=0.007). Most cells were in G0/G1 phase (>50%), a lower percentage of cells were in the S phase, G2/M phase and >4n phase (~45% combined) and a very low percentage of cells were in sub G1 phase (~2%). During deep crisis (figure 4.7.C), there was a small difference in cell cycle distribution between control cells and AZD6738-treated cells, while there was a dramatic difference between control cells and Rabusertib-treated cells. For the cells treated with AZD6738, there was an increased accumulation in S phase (3% increase) and sub G1 phase (1% increase) and less cells in G1 phase (5% decrease) compared to control cells, but there was no difference in the number of the cells that were in >4n phase (~8%) and G2/M phase (12.7%). For the cells treated with Rabusertib, there was an increased accumulation in sub G1 phase (5% increase, not significant, p=0.16), S phase (~5% increase, p=0.01), G2/M phase (4% increase, p=0.01) and >4n phase (11.6% increase, p=0.049) and a decreased accumulation in G1 phase (~24% decrease, p=0.03) compared to control cells. This showed that while the two inhibitors did not affect cell cycle progression prior to deep crisis, they both changed the distribution during deep crisis, particularly Rabusertib.

We compared apoptosis at the end of Week 4 of treatment (day 59) (figure 4.7.D) and during deep crisis (day 70) (figure 4.7.E). Before deep crisis, there was a reduction in early apoptosis in cells treated with AZD6738 (p=0.01) and Rabusertib (p=0.01), although total apoptotic levels were similar and relatively low (~20%). During deep crisis, there was a difference in the apoptotic levels between control cells (35%) and Rabusertib-treated cells (46%), but not between control cells and AZD6738-treated cells, which had lower apoptotic

levels. The increase in apoptosis in Rabusertib-treated cells was due to an increase in late apoptotic cells, but it wasn't significantly different (p=0.067). This showed that while Rabusertib did not increase apoptosis prior to deep crisis, it slightly increased apoptosis during deep crisis.

In conclusion, Experiment 2 showed that neither of the inhibitors affected cell growth, cell cycle progression and apoptosis prior to crisis. It also showed that both inhibitors decreased cell growth and affected cell cycle progression (particularly Rabusertib) during crisis, while only Rabusertib increased apoptosis during deep crisis.

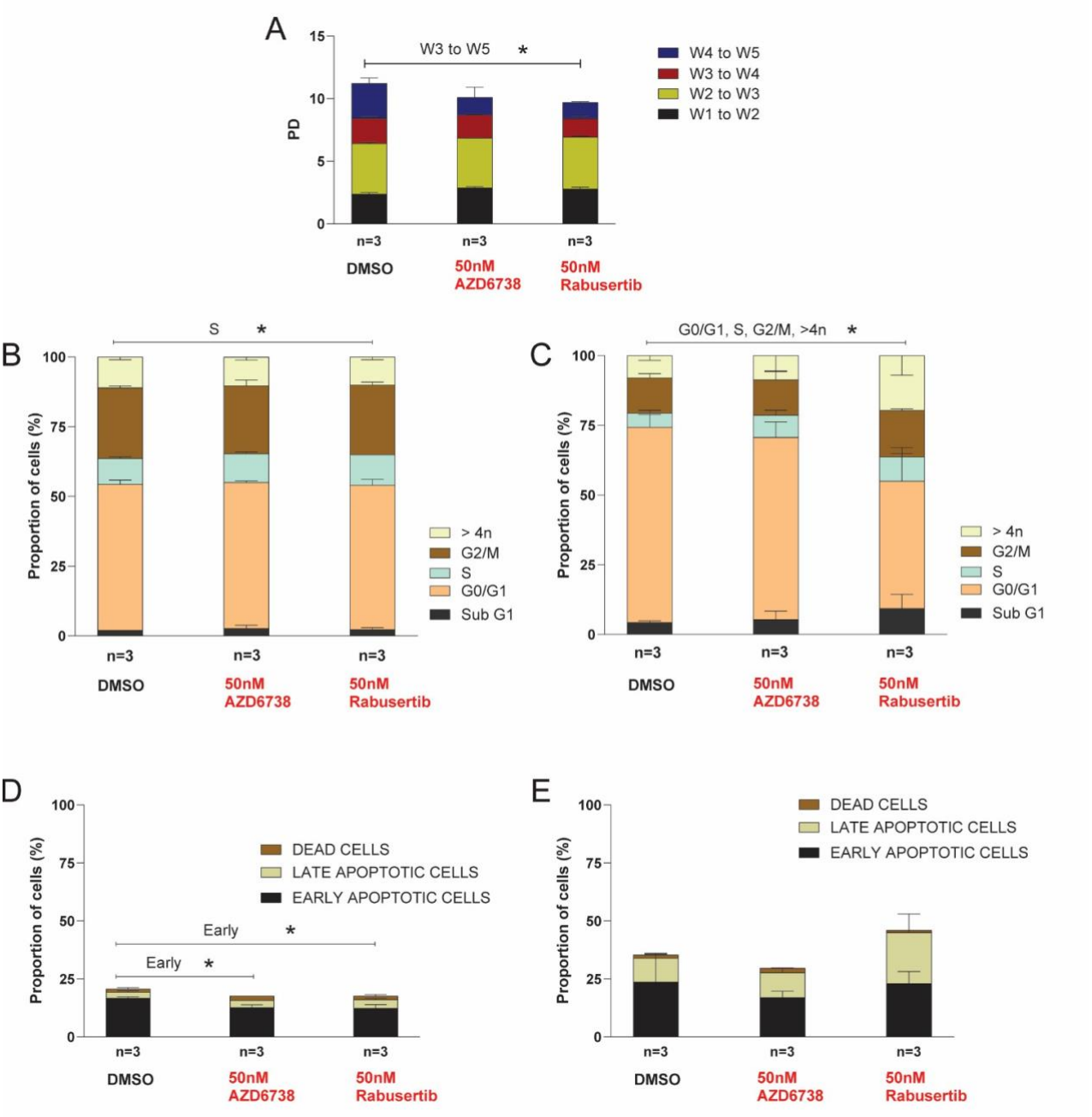

Figure 4.7: Cell growth, cell cycle and apoptosis analysis of DN-hTERT HCT116 cells treated with 50nM AZD6738 and 50nM Rabusertib in Experiment 2. The figure shows the PD each week of treatment (A), the cell cycle distribution at Week 4 of treatment (B), the cell cycle distribution at Week 5 of treatment (C), the apoptotic levels at Week 4 of treatment (D) and the apoptotic levels at Week 5 of treatment (E). Apoptosis was analysed using Annexin-V/propidium iodide (PI) staining. Cells are classified as early apoptotic when they are Annexin V positive and PI negative, late apoptotic when they are Annexin V and PI positive and dead when they are Annexin V negative and PI positive. P values were obtained using Student's t-test (2 tailed, equal variances, n=3) and * indicates $p < 0.05$.

In the third experiment, there was a growth reduction in cells treated with the two inhibitors compared to control cells during deep crisis (W4 to W5, figure 4.8.A.) Cells treated with AZD6738 grew ~1PD less than control cells (p=0.1) and cells treated with Rabusertib grew ~2PD less than control cells (p=0.006). Cells treated with Rabusertib also grew less (~0.5PD) than control cells during early crisis (W3 to W4, p=0.02), but the primary impact was evident during deep crisis. This confirms that the two inhibitors reduced cell growth during crisis, particularly Rabusertib.

We compared cell cycle progression at the end of Week 4 of treatment (day 59) (figure 4.8.B) and during deep crisis (day 73) (figure 4.8.C). Before deep crisis, the cell cycle distribution amongst the samples was similar, with Rabusertib-treated cells having a higher percentage of cells in sub G1 phase (p=0.047) and S phase (p=0.02) and a lower percentage of cells in >4n phase (p=0.02). In all samples, most cells were in G0/G1 phase (>57%), a lower percentage of cells was in the S, G2/M and >4n phase (~40% combined) and a very low percentage of cells was in the sub G1 phase (~2%). During deep crisis, there was a difference in cell cycle distribution between control cells and inhibitor treated cells. There were more inhibitor-treated-cells in S phase (1-2% increase), >4n phase (~5% increase) and sub G1 phase (3-5% increase) and less cells in G1 phase (10-14% decrease) compared to control cells, but there was no difference in the number of the cells that were in G2 phase (~20%). The differences were more pronounced in Rabusertib-treated cells (more cells in sub G1 phase, p=0.005 and less cells in G1 phase, p=0.02 compared to control cells). This showed that both inhibitors changed cell cycle progression during deep crisis, particularly Rabusertib.

We compared apoptosis at the end of Week 4 of treatment (day 59) (figure 4.8.D) and during deep crisis (day 73) (figure 4.8.E). Before deep crisis, apoptotic levels were relatively low (26-31%) and Rabusertib-treated cells had slightly higher late apoptosis (~3% higher) than control cells (not significant, p=0.14). During deep crisis, there was an increase in the apoptotic levels (both early and late apoptotic cells) between control cells (28%) and Rabusertib-treated cells (41%), although not significant (p=0.057 and p=0.13). There was also an increase in apoptosis (both early, p=0.005 and late apoptotic cells, p=0.055) in AZD6738-treated cells (38%) compared to control cells. This showed that both inhibitors increased apoptosis during deep crisis, particularly Rabusertib.

In conclusion, Experiment 3 confirmed that in early crisis, the inhibitors exerted only mild effects on cell growth, cell cycle progression and apoptosis, while in deep crisis, both inhibitors decreased cell growth and affected cell cycle progression (particularly Rabusertib). While in Experiment 2 only Rabusertib increased apoptosis, in Experiments 1 and 3 both inhibitors increased apoptotic levels in deep crisis.

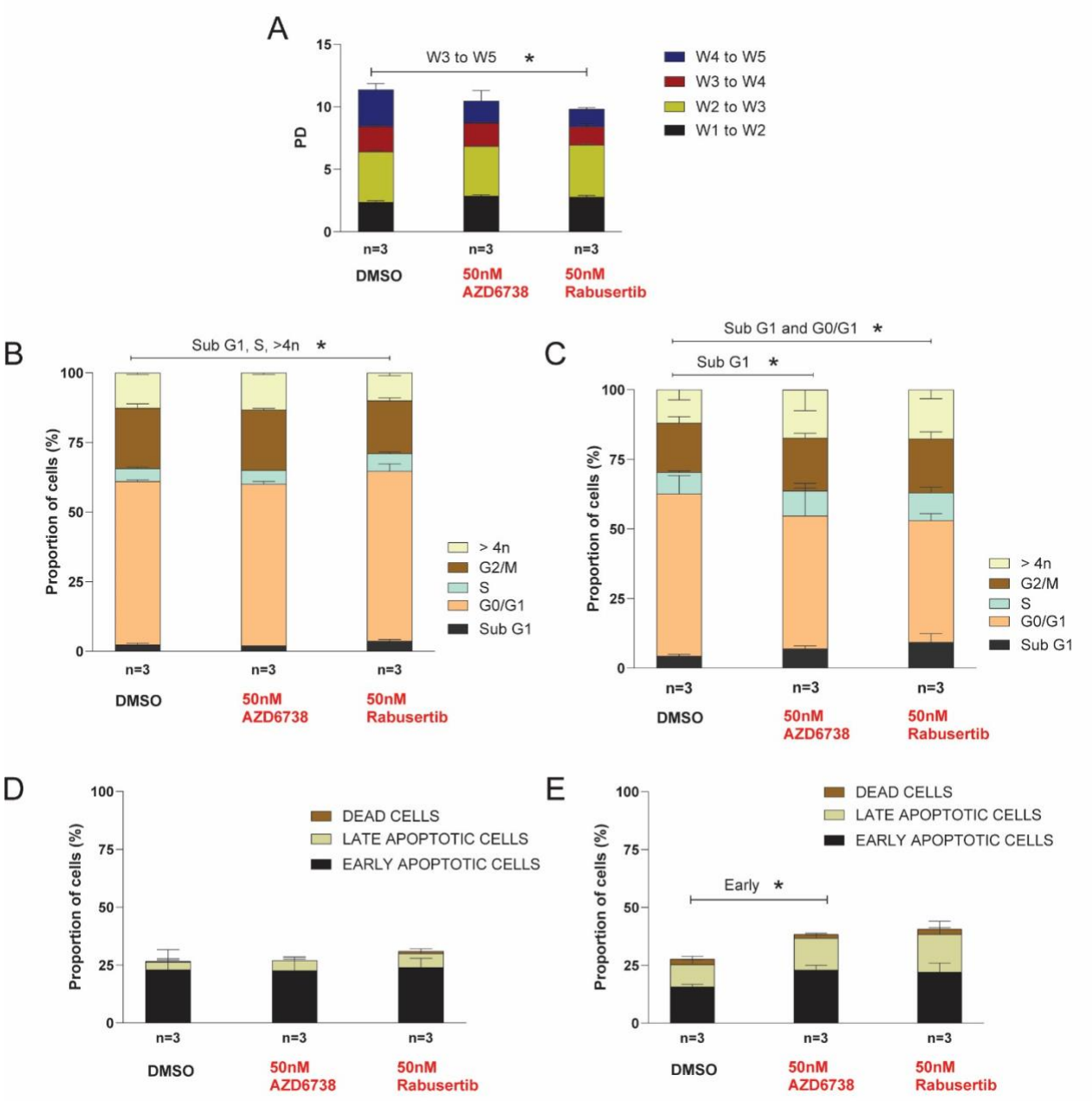

Figure 4.8: Cell growth, cell cycle and apoptosis analysis of DN-hTERT HCT116 cells treated with 50nM AZD6738 and 50nM Rabusertib in Experiment 3. The figure shows the PD each week of treatment (A), the cell cycle distribution at Week 4 of treatment (B), the cell cycle distribution at Week 5 of treatment (C), the apoptotic levels at Week 4 of treatment (D) and the apoptotic levels at Week 5 of treatment (E). Apoptosis was analysed using Annexin-V/propidium iodide (PI) staining. Cells are classified as early apoptotic when they are Annexin V positive and PI negative, late apoptotic when they are Annexin V and PI positive and dead when they are Annexin V negative and PI positive. P values were obtained using Student's t-test (2 tailed, equal variances, n=3) and * indicates $p < 0.05$.

4.4.5 Assessing the effect of Rabusertib and AZD6738 on telomere erosion

Telomere length analysis was undertaken to assess if the two inhibitors affected the rate of telomere erosion during crisis. The telomere length of the 17p telomeres of DN-hTERT HCT116 cells at the third week (day 52, PD~49) of administration of the inhibitor, when they started entering early crisis, was compared to the fifth week (days 66-73, PD~53) of administration of the inhibitor, when they were in deep crisis (figure 4.9.A,B). As expected, the telomeres of cells in late crisis were slightly shorter compared to those in early crisis (figure 4.9.G). This result confirms that HCT116 DN-hTERT cells entered crisis induced by telomere erosion.

In the previous chapter, we showed that 50nM AZD6738 and 50nM Rabusertib did not affect telomere erosion during early crisis (figure 3.25). In this experiment, during early crisis, the telomeres of the inhibitor-treated cells were equally short to the control cells (~1.7kb, p=0.25 for AZD6738-treated cells and p=0.9 for Rabusertib-treated cells). This confirms that neither of the inhibitors affected the rate of telomere erosion during early crisis (figure 4.9.A,G).

During late crisis, the telomeres of the inhibitor-treated cells were almost the same length as the control cells in all three experiments (figure 4.9.B,G). In experiments 1 and 3, AZD6738-treated cells had a slightly longer telomere length compared to control cells. This might be because some cells treated with AZD6738 might have started escaping crisis, increasing the overall telomere length of the sample analysed, as escape from crisis is accompanied by the re-activation or increase of the telomerase reverse transcriptase, which synthesises new telomeric nucleotide repeats (von Morgen and Maciejowski, 2018).

To further address differences between the samples, the telomere length distributions were displayed as scatter plots with the standard deviation (figure 4.9.C-F). As cells started entering crisis (Week 3), samples displayed a bimodal distribution and similar heterogeneity (figure 4.9C). In the first experiment of late crisis samples (Week 5), bimodal telomere length distributions were not apparent in the different samples (figure 4.9D). Although heterogeneity appeared to be similar across the samples, two of the control samples had one very long telomere. In the second experiment of late crisis samples, bimodal telomere length distributions were also not apparent in the different samples (figure 4.9E). Overall,

differences in heterogeneity were minimal and two AZD6738 samples had one very long telomere. In the third experiment of late crisis samples, bimodal telomere length distributions were much less apparent than the previous repeats (figure 4.9F). Overall, the heterogeneity was higher than the previous experiments, with many samples containing telomeres that were longer than 3kb. The samples from the third experiment were obtained a few days deeper into crisis compared to the previous experiments, so some cells might have started escaping crisis and lengthening their telomeres. In all of the experiments, the two inhibitors did not affect heterogeneity in late crisis.

Overall, the results from the three experiments showed that neither of the inhibitors affected the rate of telomere erosion during early or late crisis.

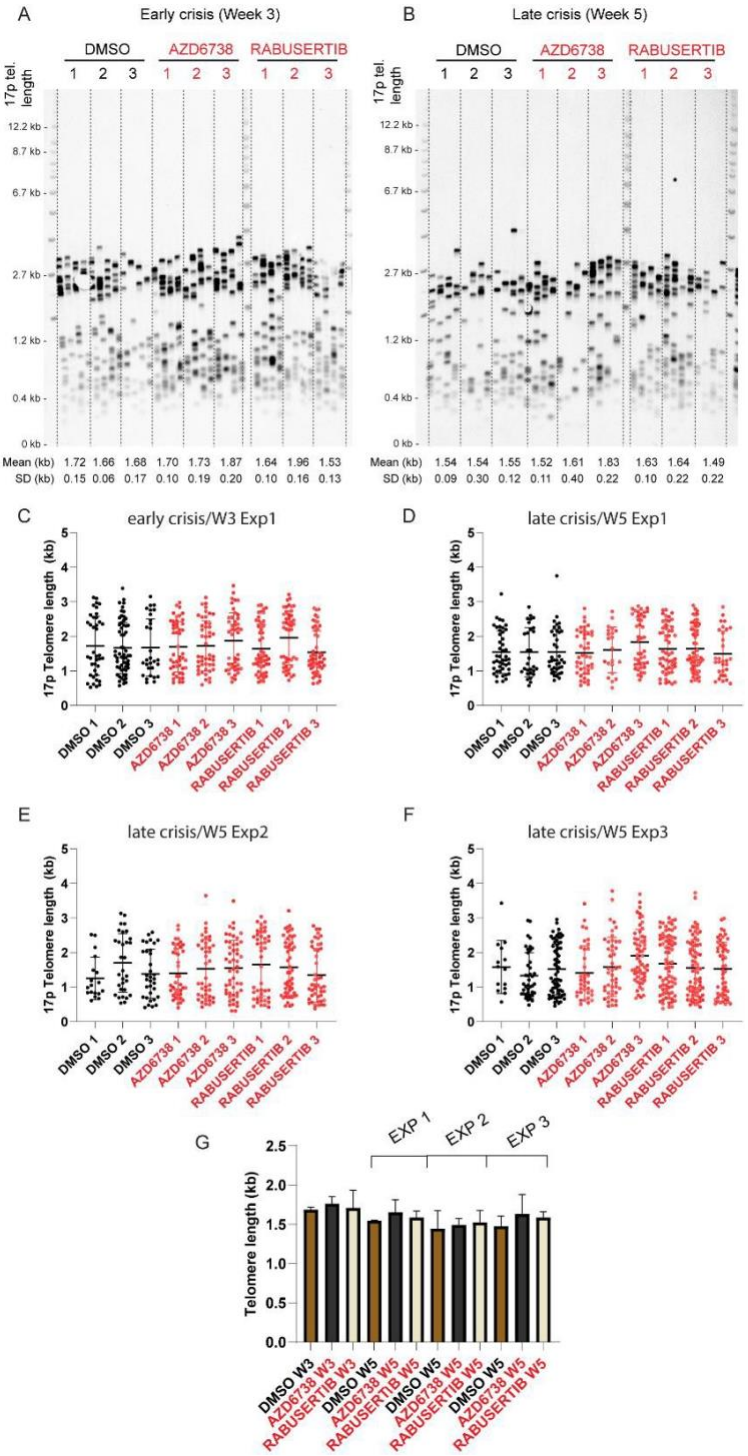

Figure 4.9: STELA of the 17p telomeres from DN-hTERT HCT116 cells treated with 50nM AZD6738 and 50nM Rabusertib. The figure shows the STELA analysis at early crisis (day 52) (A), the STELA analysis at deep crisis (experiment 1, day 66) (B), the scatterplots from early crisis (day 52) (C) and late crisis in Experiment 1 (day 66) (D), Experiment 2 (day 70) (E) and Experiment 3 (day 73) (F) and the mean telomere length per sample during early crisis (W3) and during late crisis (W5) for all three experiments (G). DMSO is used as a control sample. P values were obtained using Student's t-test (2 tailed, equal variances, n=3).

4.4.6 Assessing the effect of Rabusertib and AZD6738 on genomic instability

Crisis is characterised by the presence of telomere fusion events. We conducted a simplified telomere fusion assay to determine whether the two inhibitors affected the frequencies of telomere fusion events between two chromosome ends during crisis. We used primers that target the 17p and XpYp telomere-adjacent DNA to detect fusion between these telomeres. Telomere fusion events were readily detected in the cells undergoing (early and late) crisis, confirming the occurrence of telomere crisis (figure 4.10.A,B). As expected, more telomere fusion events were detected during late crisis (Week 5) compared to early crisis (Week 3). Overall, the number of fusions observed in early crisis was slightly higher in the inhibitor-treated cells compared to control cells, but the difference was not significant (p=0.25 for AZD6738 and p=0.12 for Rabusertib) (figure 4.10.G).

During late crisis, the number of fusions observed in experiments 2 and 3 was much higher in the Rabusertib-treated cells (32 and 34 respectively) compared to control cells (7 and 3 respectively) (p=0.015, Experiment 2 and p=0.004, Experiment 3) (figure 4.10B,E,F,G). We did not observe this difference in the first experiment (figure 4.10D,G), as the control cells had a higher number of fusion events compared to control cells in the other two experiments. A possible explanation is that as the control cells in Experiments 2 and 3 cells were harvested and analysed a few days later than Experiment 1, they might have already started escaping crisis at the time of analysis, which reduced the number of fusion events (as telomerase would have elongated the telomeres).

The increase in telomere fusion events in the inhibitor-treated cells during late crisis could either be a result of the biological activity of the inhibitors (e.g. by increasing DNA damage) or the escape of control cells from crisis which would decrease telomere fusion, as explained above. The latter hypothesis seems more likely as the fusion number of Rabusertib-treated cells remained very similar in all three repeats (32-34) and we know that they do not escape crisis. However, in both control cells and AZD6738-treated cells, which escape crisis, there was a reduction in fusion events. For example, in experiment 1, there were 34 fusion events in AZD6738-treated cells, while in experiments 2 and 3 this number dropped to 22 and 13 respectively. In experiments 2 and 3, where cells were collected a few days later in crisis compared to experiment 1, some of these cells might have already started escaping crisis, restoring the length of the telomeres and decreasing fusions. In that

case, the difference in the number of fusion events between inhibitor-treated and control cells would be due to a decrease in fusion in control cells rather than an increase in fusion in inhibitor-treated cells.

To further examine potential differences between the samples, the size of the telomere fusion molecules may indicate different types of fusion events (for example the presence of insertions or deletions will lead to longer or shorter fusion molecules). Thus telomere fusion length events were quantified and displayed as scatter plots (figure 4.10 C-F). There were more fusion products with a size of >10kb in early crisis cells, leading to higher heterogeneity compared to deep crisis cells. These long fusion products were probably fusions with insertion and they were observed mostly in inhibitor-treated cells, with very few observed in the control cells (figure 4.10.C). In addition, the mean fusion length was lower in early crisis cells (3.7-5.7kb) compared to cells that had entered deep crisis (4.9-6.5kb, experiment 1, figure 4.10.D), although the further the cells were in late crisis, the lower the mean fusion length became (4-4.7kb, experiment 3, figure 4.10.F) indicating an increase in deletion or a reduction in insertion events.

In conclusion, cells treated with Rabusertib (and to a lesser degree AZD6738) exhibited a higher number of fusion events during deep crisis, but it is unclear as to whether this increase was caused by the inhibitor increasing DNA damage, or whether it was due to a failure or delay to escape crisis.

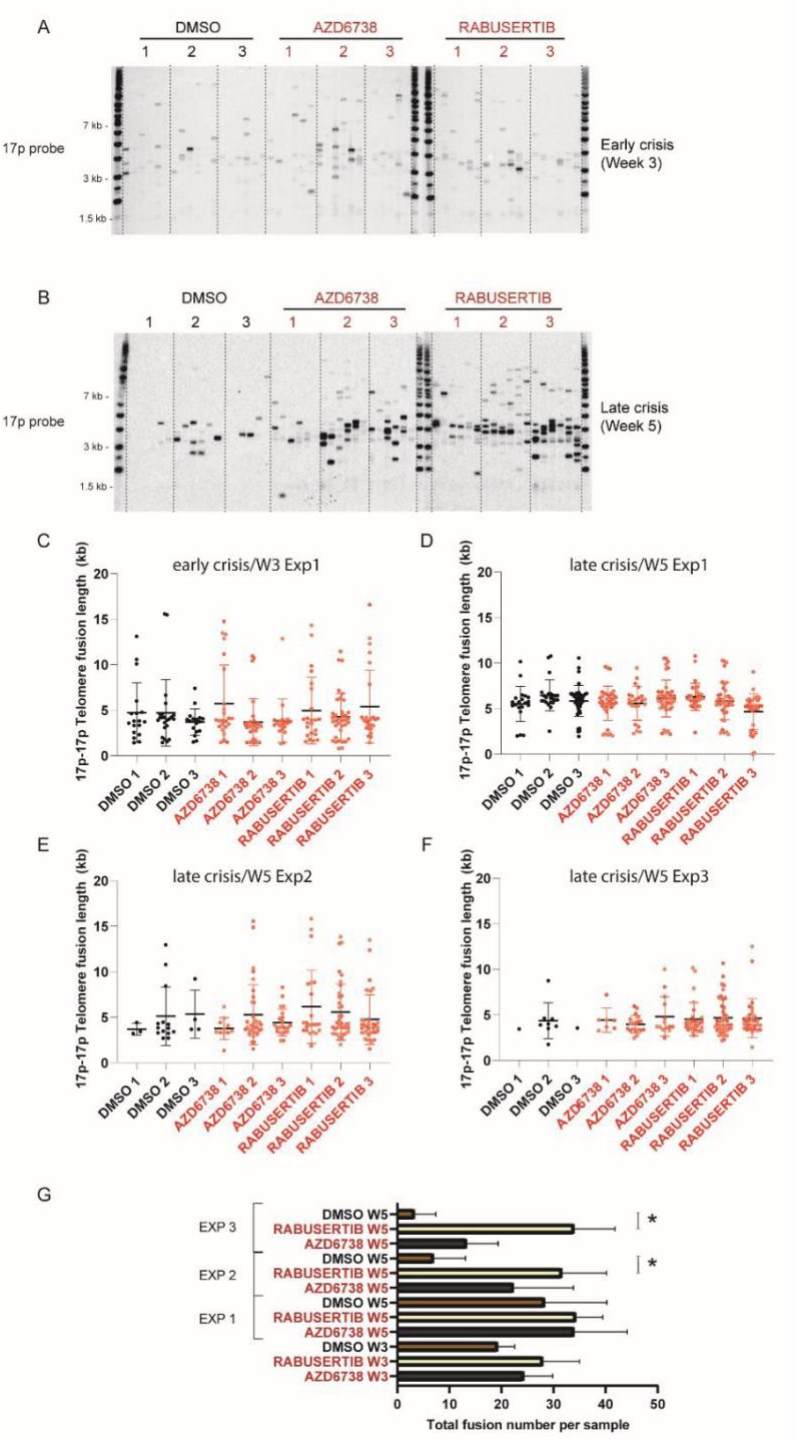

Figure 4.10: Telomere fusion analysis in DN-hTERT HCT116 cells treated with 50nM AZD6738 and 50nM Rabusertib. The figure shows the fusion analysis at early crisis (day 52), (A), at deep crisis (day 70, experiment 2) (B), the scatterplots from early crisis (day 52) (C) and late crisis in Experiment 1 (day 66) (D), Experiment 2 (day 70) (E) and Experiment 3 (day 73) (F) and the mean total fusion number per sample during early crisis (W3) and during late crisis (W5) for all three experiments (G). DMSO is used as a control sample. P values were obtained using Student's t-test (2 tailed, equal variances, n=3) and * indicates $p < 0.05$.

4.4.7 Assessing the effect of Rabusertib and AZD6738 on DDR protein status

4.4.7.1 Assessing DDR protein expression levels in WT-HCT116 cells

As previously mentioned, we hypothesise that the two inhibitors affect the ability of DN-hTERT HCT116 cells to escape telomere crisis by elevating DNA damage which synergises with telomere damage. To test this hypothesis, we examined the levels and phosphorylation of some key proteins that play an important role in the DNA damage response pathway (CHK1, CHK2, p53, H2AX). CHK1 phosphorylation at S345 by ATR and CHK1 autophosphorylation at S296 are induced following DNA damage (Liu et al, 2000; Okita et al, 2012). CHK2 is phosphorylated by ATM at T68, leading to a conformational change, as a result of DNA damage (Zannini et al, 2014). Gamma-H2AX is a phosphorylated form (S139) of the histone variant H2AX, which forms when DNA double-strand breaks occur and its detection is considered a specific and sensitive molecular marker for identifying DNA damage (Mah et al, 2010).

Bleomycin is a glycopeptide antibiotic, which oxidatively damages DNA by binding to metal ions to create reactive oxygen species and triggers G2/M phase cell cycle arrest by inducing phosphorylation of Chk1 and Chk2 (Petering and Antholine, 1990; Jang et al, 2008; Bacevic et al, 2017). We first used Western Blot analysis to assess how DDR protein levels were affected in WT-HCT116 cells following bleomycin treatment in the presence of Rabusertib and AZD6738. By comparing the expression profile between WT-HCT116 and DN-hTERT HCT116 cells, we set to understand if the inhibitor mechanism of action changes when cells undergo crisis. We tested the antibodies and Western blot condition in the WT-HCT116 cells by including two untreated samples (lanes 2,4, figure 4.11A) and two samples treated with 50µg/ml bleomycin for 1.5 hours (lanes 1,3). CHK1-S296, CHK1-S345, CHK2-T68, Gamma H2AX and p53 levels appeared to increase in bleomycin-treated cells compared to untreated cells, as expected. CHK1 and CHK2 levels appeared to remain similar across all samples (figure 4.11A).

Following DNA damage, ATR phosphorylates CHK1 at S345 resulting in CHK1 autophosphorylation at S296. Parsels et al (2011) showed that increased CHK1 phosphorylation at S345 is a pharmacodynamic biomarker of CHK1 inhibition. Chen et al

(2015) demonstrated that decreased CHK1 phosphorylation at S345 and increased Gamma H2AX expression can be used as biomarkers for ATR inhibition.

We analysed DDR protein levels in WT-HCT116 cells following treatment with AZD6738 and Rabusertib (figure 4.11.B,C). We included an untreated sample, a sample treated with 50µg/ml bleomycin for 0.5 hour, and samples treated with 50nM or 5 µM inhibitor for 0.5 hour or 24 hours (with/without bleomycin). The WT-HCT116 cells from two experiments were cultured, lysed and sonicated under the same conditions.

In both experiments, CHK1-S296 levels increased in cells treated only with 5µM AZD6738 compared to untreated cells (lane 3 versus lane 8, figure 4.11.B,C). In both experiments, there was higher CHK1-S296 expression in cells treated both with 5µM AZD6738 (for 0.5 hour) and bleomycin compared to cells treated only with bleomycin (lane 2 versus lane 7, figure 4.11.B,C). Treatment with Rabusertib and bleomycin appeared to decrease CHK1-S296 levels compared to cells treated only with bleomycin in the first experiment (lane 1,2 versus lane 7, figure 4.11.B). The results on CHK1-S296 expression in cells treated with Rabusertib were inconclusive in the second experiment, as the signal was too weak and difficult to quantify (figure 4.11.C).

In both experiments, there was a higher CHK1-S345 expression in the cells treated only with 5µM AZD6738/5µM Rabusertib compared to untreated cells (lane 3 versus lane 8, figure 4.11.B,C). In addition, in both experiments, CHK1-S345 levels increased in cells treated both with 5µM AZD6738/5µM Rabusertib and bleomycin compared to cells treated only with bleomycin (lane 1,2 versus lane 7). The difference in CHK1-S296 and CHK1-S345 observed above was not due to a difference in CHK1 levels, as CHK1 levels appeared to remain similar across all samples in both experiments (figure 4.11.B,C).

In both experiments, CHK2-T68 and Gamma H2AX expression levels followed the same pattern. While there was little to no CHK2-T68 and Gamma H2AX signal in cells that were not treated with bleomycin (lanes 3,6 and 8), all bleomycin-treated cells showed an increase (lanes 1,2,4,5 and 7), which appeared to be similar across all bleomycin-treated samples. Interestingly, in the first experiment, the levels of both proteins were higher in the cells treated only with 5µM AZD6738 compared to untreated cells (lane 3 versus lane 8, figure 4.11.B). This was also observed in the second experiment, although the signal was much

weaker (figure 4.11.C). We could not determine if the same result occurred in 5µM Rabusertib-treated cells compared to untreated cells, as the signal was fainter. However, there was an upregulation of CHK2-T68 levels in 5µM Rabusertib-treated cells (lane 3 versus lane 8, first experiment) and 50nM Rabusertib-treated cells compared to untreated cells (lane 6 versus lane 8, second experiment) (figure 4.11.B,C). The difference in CHK2-T68 and Gamma-H2AX observed above was not due to a difference in the level of the proteins, as CHK2 and H2AX levels appeared to remain similar across all samples (except for a decrease in CHK2 observed in cells treated with 5µM inhibitor for 24hr (with bleomycin, lane 1, figure 4.11.B,C).

P53 levels appeared to increase in cells treated only with bleomycin and in all cells treated with 50nM AZD6738/50nM Rabusertib, compared to untreated cells (lanes 4-7 versus lane 8, figure 4.11.C). However, there was not an increased P53 expression in any of the cells treated with 5µM AZD6738/5µM Rabusertib, compared to untreated cells (lanes 1-3 versus lane 8).

In conclusion, we have shown that treatment with 5µM AZD6738 increased CHK2-T68, Gamma H2AX, CHK1-S345 and CHK1-S296 expression levels in WT-HCT116 cells. 5µM Rabusertib increased CHK1-S345 and CHK2-T68 expression levels and decreased CHK1-S296 levels in WT-HCT116 cells. We have also demonstrated that treatment with 5µM AZD6738 or 5µM Rabusertib and bleomycin increased CHK1-S345 levels, compared to treatment with bleomycin alone. Elevation of CHK1-S345 expression following treatment with Rabusertib was consistent with what we expected, based on the known molecular biology of CHK1. While treatment with AZD6738 was expected to produce higher Gamma H2AX levels, we did not expect to see higher CHK1-S345 and CHK1-S296 levels. These phosphorylation events indicate that CHK1, downstream of ATR, which is being inhibited, remained active.

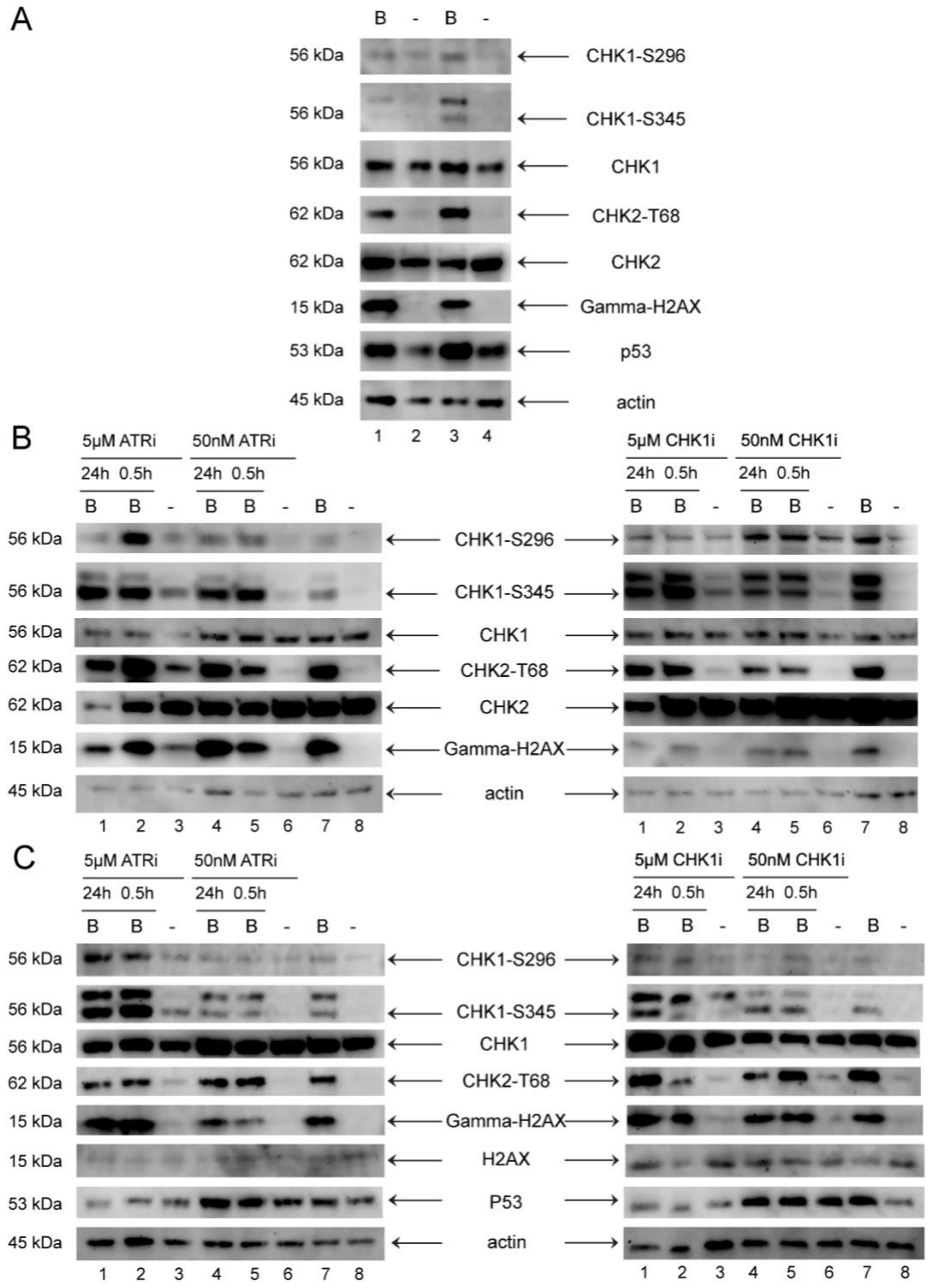

Figure 4.11: Western Blot showing levels of protein expression in WT-HCT116. (A) The figure shows levels of DDR protein expression in WT-HCT116 treated with 50μg/ml bleomycin. (B, C) The figures show levels of DDR protein expression in WT-HCT116 treated with 5μM or 50nM inhibitor (AZD6738 and Rabusertib) for 0.5 hour or 24 hours, with or without 50μg/ml bleomycin. The cells without bleomycin (lanes 3 and 6) were treated with inhibitor for 24hr. Actin expression was used as loading control.

4.4.7.2 Assessing DDR protein expression levels in DN-hTERT HCT116 cells

To assess the status of DDR proteins in DN-hTERT HCT116 cells undergoing crisis, we conducted two Western Blot experiments using deep crisis cells from Experiment 2 (figure 4.12.A) and Experiment 3 (figure 4.12.B). The DN-hTERT HCT116 cells from both experiments were cultured, lysed and sonicated under the same conditions. However, cells from Experiment 2 were harvested at day 70 and cells from Experiment 3 were harvested at day 73. In both experiments, we included DN-hTERT HCT116 untreated or treated with 50µg/ml bleomycin for 0.5 hour as controls.

In both experiments, CHK1-S345 and CHK1-S296 bands were very weak, except for an increased expression in the bleomycin-treated sample (lane 11), as expected. Given the weak signal of the bands, we were not able to determine how the two inhibitors affected CHK1 phosphorylation levels in DN-hTERT HCT116 cells. This could be because a concentration of 50nM might be too low to produce a visible difference in band intensity, as in WT-HCT116 cells the differences were also not detectable at the same concentration (figure 4.11.B,C).

In both experiments, no differences in Gamma H2AX levels were detected between inhibitor-treated cells and untreated cells, but there was increased expression in the bleomycin-treated sample (lane 11), as expected. There were also no differences in CHK2-T68 expression between the inhibitor-treated cells and the DMSO-treated cells, although surprisingly, there was an increased expression in untreated cells (lane 12, figure 4.12A,B). While it was unlikely that DDR was activated in untreated cells, as evidenced by the absence of upregulation in Gamma H2AX levels, it is possible that upregulation of CHK2-T68 expression was due to intrinsic cellular properties.

In both experiments, CHK2 levels appeared to be similar in all samples, except for a reduction in bleomycin-treated cells, which was probably due to loading less protein as indicated by the actin levels (lane 11, figure 4.12.A). In the first experiment, CHK1, H2AX and p53 expression appeared to be similar across the samples, which was not the case in the

second experiment. The differences observed in the second experiment might be attributed to uneven loading as indicated by the variation in the actin levels.

As our results were inconclusive, we decided to investigate LC3B levels in deep crisis cells from Experiment 2 (figure 4.12.C) and Experiment 3 (figure 4.12.D) in order to understand how the inhibitors affect autophagy during crisis. LC3B is a universal-marker of autophagy and conversion of LC3B-I to LC3B-II is crucial for autophagosome formation in order to activate autophagy (Satyavarapu et al, 2018). Nassour et al (2019) showed that autophagy is essential for cell death during telomere-driven crisis and loss of autophagy is needed for escape from crisis. In both of these Western Blot experiments, we included an untreated WT-HCT116 sample and a WT-HCT116 sample treated with 50μg/ml bleomycin for 0.5 hour as controls. In one of the experiments, LC3B-I levels appeared to be lower in DN-hTERT HCT116 cells compared to WT cells, while the LC3-B-II levels appeared to be similar in all samples (figure 4.12.D). This indicated that in that experiment the conversion of LC3B-I to LC3-B-II was higher in DN-hTERT HCT116 cells, which suggests higher autophagy levels. However, in the other experiment, both LC3B-I and LC3B-II levels appeared to be lower in WT cells compared to DN-hTERT HCT116 cells, leading to inconclusive results (figure 4.12.C). Overall, no differences were detected between the inhibitor-treated and control DN-hTERT samples (lanes 1-6 versus lanes 7-9).

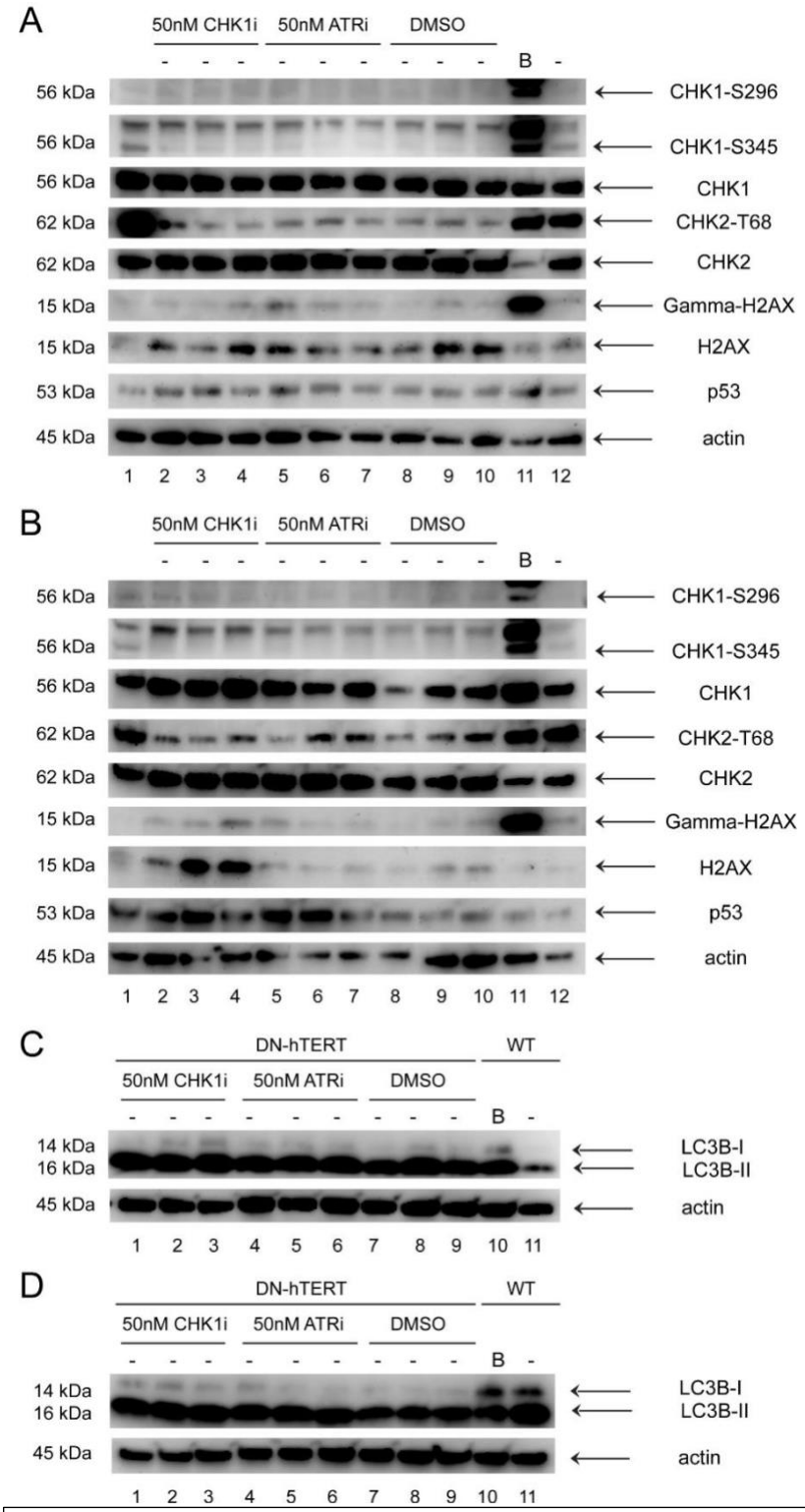

Figure 4.12: Western Blot showing levels of protein expression in DN-hTERT HCT116. (A,B) The figures show levels of DDR protein expression in DN-hTERT HCT116 from Experiments 2 and 3 respectively, as well as untreated DN-hTERT HCT116 or treated with 50µg/ml bleomycin. (C,D) The figures show levels of LC3B in DN-hTERT HCT116 from Experiments 2 and 3 respectively, as well as untreated WT HCT116 or treated with 50µg/ml bleomycin. Actin expression was used as loading control.

4.5 Discussion

4.5.1 Rabusertib and AZD6738 affect the ability of HCT116 cells to escape a telomere crisis

In the previous chapter, DDR inhibitors Rabusertib (CHK1i) and AZD6738 (ATRi) impaired the ability of DN-hTERT expressing HCT116 cells to escape a telomere-induced crisis. To confirm that, we set up a triplicate experiment (n=3) in which DN-hTERT HCT116 cells were treated with 50nM Rabusertib and 50nM AZD6738. All three samples treated with Rabusertib failed to escape crisis (figure 4.1.A), while all three samples treated with AZD6738 escaped crisis more slowly than control cells (figure 4.2A). Before cells entered crisis, the inhibitors did not strongly influence cell growth, cell cycle progression and apoptosis. When AZD6738-treated cells entered early crisis (day 56), there was higher apoptosis compared to control cells (figure 4.2B). This suggests that AZD6738 may slow down escape from crisis by increasing apoptosis during crisis. When AZD6738-treated cells escaped crisis, they still maintained high apoptotic levels and an altered cell cycle for a longer time compared to control cells. However, it was not possible to determine whether it was because of direct biological effects of AZD6738 or due to a delayed escape from crisis (caused by AZD6738). In the latter scenario, not all telomeres would have been elongated enough to restore telomere stability, thus causing high apoptotic levels due to DDR activation.

In the previous chapter, both inhibitors showed high potency and experiments demonstrated that Rabusertib (12.5nM, 25nM and 50nM) (figure 3.16) and AZD6738 (12.5nM, 25nM and 50nM) (figure 3.23) prevented cells from escaping crisis. In total, there have been four experiments in which Rabusertib-treated cells have consistently failed to escape crisis. This confirms that Rabusertib influences the ability of the cells to escape crisis. In the previous chapter, there were two experiments in which cells treated with AZD6738 (12.5nM, 25nM and 50nM) failed to escape crisis. In this triplicate experiment, it was the first time that AZD6738-treated cells escaped crisis. The fact that cells treated with 50nM AZD6738 managed to escape crisis albeit slowly and have previously failed twice to escape crisis further strengthens the hypothesis that treatment with a higher concentration of the inhibitor could kill cells during crisis.

Harata et al (2023) confirmed that AZD6738 inhibits Chk1 Ser345 phosphorylation, which is an ATR substrate (IC_{50} of 0.074μM) and in doing so, it inhibits DNA damage repair leading to accumulation of DNA damage and apoptosis. AZD6738 is known to specifically inhibit the G2/M checkpoint by suppressing DNA damage-dependent activation of ATR (Suzuki et al, 2022). P53 mutant cancer cells are expected to be particularly sensitive to AZD6738, as they are dependent on the G2/M checkpoint for cell repair since P53 plays an essential role in the G1/S checkpoint. However several studies have shown no significant differences in sensitivity to AZD6738 between P53 mutant and P53 functional cell lines (Harata et al, 2023; Dillon et al, 2017). The reason for this is thought to be that WT-HCT 116 cells accumulate damage in the S phase and failure of its repair at the G2/M checkpoint results in cell death (Harata et al, 2023). However, Wilson et al (2022) showed that AZD6738 induces potent ATM-dependent signalling as a result of 'on target' ATR inhibition and suggested that complete suppression of ATM activity may be needed for sensitivity to ATR inhibition. Hence, it is possible that while AZD6738 inhibited ATR to increase cell death, because of G2/M checkpoint inhibition, this was partly counteracted by compensatory ATM signalling and as a consequence, not all cells were killed during crisis.

King et al (2014) demonstrated that Rabusertib inactivates the G2/M DNA damage checkpoint and inhibits phosphorylation of CHK1 substrates without supressing direct phosphorylation of CHK1 by ATR. Wang et al (2014) showed that Rabusertib inhibits autophosphorylation of CHK1 at Ser296 and provokes the DNA damage response increasing apoptosis and autophagy. Specifically, they found that Rabusertib activates the whole spectrum of the DNA damage response pathway and suggested that the inhibitor may induce the DSB response independently of CHK1 inhibition. Hence, it is possible that Rabusertib killed crisis cells (which were already experiencing telomere damage) by inducing further DNA damage, both dependently and independently of CHK1 inhibition, leading to cell death by apoptosis and autophagy. To examine these hypotheses, we examined cell cycle progression, apoptosis, telomere stability and DNA damage response of cells treated with these inhibitors during deep crisis.

4.5.2 Rabusertib and AZD6738 only affect cells with short dysfunctional telomeres

To first understand if the two inhibitors only have an effect on cells undergoing crisis, we set up an experiment in which we treated WT-HCT116 cells with 50nM Rabusertib and 50nM AZD6738 for 111 days. We have previously used these concentrations to treat WT-HCT116 cells for a period of two weeks and there was no difference in cell growth (figure 3.1E, figure 3.2A). In this experiment, the two inhibitors at the aforementioned concentration did not affect cell growth, cell cycle progression or apoptosis in WT-HCT116 cells (figures 4.4, 4.5). This is consistent with other studies in literature (Paculova et al, 2017; Harata et al, 2023; Suzuki et al, 2022; Dillon et al, 2017). This confirms that the inhibitors selectively affect only cells undergoing crisis with short dysfunctional telomeres and not healthy cells with long telomeres.

To understand how the inhibitors function, we need to know the timepoint in which they affect the properties of the cells. We treated DN-hTERT HCT116 cells with the two inhibitors (n=3) and harvested cells during deep crisis for analysis. We performed the experiment three times and each time the cells were harvested deeper into crisis. The three experiments showed that neither of the inhibitors affected strongly cell growth, cell cycle progression and apoptosis prior to crisis (figures 4.6, 4.7, 4.8). Unlike these three experiments, the previous triplicate experiment showed that cells treated with 50nM AZD6738 had an altered cell cycle progression and increased apoptosis in the fourth week of treatment (day 56) (figure 4.2). This is because the cells analysed from the triplicate experiment (figures 4.1-4.3) were at PD 53 (deeper in crisis), while cells analysed in the three experiments (figures 4.6-4.8) were at PD 51-52. All experiments showed that Rabusertib decreased cell growth and affected cell cycle progression by decreasing cell accumulation in G0/G1 phase during deep crisis, with AZD6738 having a milder similar effect. The change in the cell cycle is consistent with the proposed effect of Rabusetib, resulting in a reduction in the cell population in G0/G1 phase due to G2/M phase arrest (Wang et al, 2014). The second experiment showed that only Rabusertib increased apoptosis during late crisis, while the first and third experiments showed that both inhibitors increased apoptotic levels. A possible explanation that in the second experiment AZD6738-treated cells did not have higher apoptosis, is that some of the cells might have

started escaping crisis. In conclusion, both inhibitors (mainly Rabusertib) affect cellular properties by reducing cell growth, decreasing the G0/G1 phase population and increasing apoptosis in deep crisis. Our results suggest that these changes start appearing around PD 52-53.

We also assessed the telomere length of the 17p telomeres of DN-hTERT HCT116 cells in early and late crisis (n=3) to determine telomere erosion. Neither of the inhibitors affected the rate of telomere erosion during early or late crisis (figure 4.9). A few differences in the mean telomere length observed in late crisis between the control and AZD6738-treated cells were attributed to earlier escape from crisis. In the previous chapter, the two inhibitors at the aforementioned concentration did not affect telomere erosion during early crisis (figure 3.25), which is consistent with the findings of this experiment (figure 4.9). During early crisis, telomeres displayed a bimodal distribution, which became less apparent in late crisis and is consistent with STELA experiments using WT-HCT116 cells shown by Jones et al (2014). This is to be expected, as cells in deep crisis have experienced telomere shortening. Also, if some cells have started escaping crisis, some telomeres might have been lengthened by telomerase, which make the bimodal distribution less apparent.

We also examined total chromosomal telomere fusion events in DN-hTERT HCT116 cells in early crisis and late crisis (n=3) to determine genomic instability. We found that there was no difference in the number of fusion events before deep crisis but cells treated with Rabusertib (and to a lesser degree AZD6738) exhibited a higher number of fusion events during deep crisis (figure 4.10). This could be either because the inhibitors increased telomere fusion or because control cells underwent reduced telomere fusion events by escaping crisis. Before deep crisis, there were more fusion products with a size of >10kb, indicating fusions were occurring with less deletion or more insertion events and these were observed mostly in inhibitor-treated cells (figure 4.10). We also observed that the mean fusion length was longer as cells were entering deep crisis and became shorter as cells went deeper into crisis. This is likely because there was a change in the fusion spectrum towards increased deletions during late crisis.

Jones et al (2014) suggested that the relative proportions of inter-chromosomal to intra-chromosomal fusions affect the ability of human cells to escape crisis. Ngo et al (2018) showed that there was an increase in intra-chromosomal fusion relative to inter-chromosomal fusion in cells (treated with PARPi) that failed to escape crisis, which was the opposite to what was observed by Jones et al (in cells that lacked LIG3). Future telomere fusion assay experiments on cells treated with Rabusertib can also examine the ratio of inter-chromosomal to intra-chromosomal fusions to determine if this factor influences escape from crisis.

4.5.3 AZD6738 and Rabusertib activate the DNA Damage Response

We investigated the molecular mechanism by which AZD6738 and Rabusertib influence the ability of cells to escape a telomere crisis by performing Western Blot analysis in WT-HCT116 (figure 4.11) and DN-hTERT HCT116 cells (figure 4.12). Following bleomycin treatment of WT-HCT116 cells, CHK1-S296, CHK1-S345, CHK2-T68, Gamma H2AX and total p53 levels appeared to increase compared to untreated cells, while CHK1 and CHK2 levels appeared to remain similar across all samples (figure 4.11.A). The activation of the DNA damage response pathway, indicated by the upregulation of DDR proteins was expected, because bleomycin is an agent that induces DNA double-strand breaks (Palii et al, 2008). Bacevic et al (2017) showed that WT-HCT116 cells treated with 10µg/ml bleomycin for 24hours showed increased CHK2-T68 and total p53 expression (the other markers were not tested), but no change in CHK1 and CHK2 levels. Palii et al (2008) showed that WT-HCT116 cells treated with 10 µg/ml bleomycin for 4 hours exhibited increased CHK1-S345, CHK2-T68 and total p53 expression while no differences were detected in CHK1 and CHK2 levels. The results from both the aforementioned studies are consistent with our results and indicate that the inclusion of a bleomycin-treated sample is a reliable control to study DDR protein levels.

In WT-HCT116 cells, 5µM AZD6738 increased CHK2-T68, Gamma H2AX, CHK1-S345 and CHK1-S296 levels and combined AZD6738 and bleomycin treatment increased CHK1-S345 levels, compared to treatment with bleomycin alone (figure 4.11.B,C). Moiseeva et al (2019) examined the molecular mechanism of AZD6738 by treating 293T (human embryonic kidney) and U20S (human osteosarcoma) cells with 5µM AZD6738 for 1 hour. They observed that AZD6739 inhibited both CHK1 autophosphorylation at S296 and CHK1 phosphorylation at S345. Vendetti et al (2015) also examined the molecular mechanisms of AZD6738 by

treating three NSCLC cell lines (H23, H460, A549) with 0.3µM or 1µM AZD6738 for 24 hours. They showed that AZD6738 decreased CHK1 S345 phosphorylation and increased p53 and gamma H2AX levels, while CHK1 levels did not change. While we detected an increase in CHK2-T68 and Gamma H2AX expression, indicative of the activation of the DNA damage response, we did not detect a reduction in CHK1-S345 and CHK1-S296 levels, which showed that CHK1 was still active. This does not necessarily mean that the inhibitor failed to inhibit ATR as CHK1 acts downstream of both ATR and ATM kinase. It is possible that following ATR inhibition, ATM was upregulated to compensate for ATR loss, which phosphorylated CHK1 at S345 resulting in CHK1 autophosphorylation of S296. This is supported by the upregulation of ATM downstream effector CHK2-T68. Similarly to our study, Isono et al (2022) also observed increased CHK1-S345 levels in three bladder cancer cell lines (J82, T24 and UM-UC-3) treated with 1µM AZD6738 (alone or with gemcitabine) for 24 hours. In addition, Wallez et al (2018) found elevated levels of ATM and DNA-PK activation in pancreatic ductal adenocarcinoma cell lines treated with 2µM AZD6738 (alone or with gemcitabine) for 30 hours. As DNA-PK can also phosphorylate CHK1 independently of ATR, pCHK1 might not necessarily act as a reliable biomarker of ATR inhibition by AZD6738 (Wallez et al, 2018). Overall, our results suggest that AZD6738 acted in two ways, firstly by activating the DNA damage response, as indicated by an increased Gamma H2AX and CHK2-T68 expression and secondly by upregulating CHK1 activity, as indicated by an increase in CHK1-S345 and CHK1-S296 levels, which was likely a result of potent ATM activation following ATR inhibition. We propose that impairing the ATR-CHK1 pathway increased DNA damage (as indicated by the activation of the DDR and an increase in apoptosis), which synergised with telomere damage to initially kill the cells. However, it is likely that after a while, ATM expression was upregulated to re-activate CHK1 activity which allowed escape from crisis by facilitating the repair of the DNA damage.

In WT-HCT116 cells, 5µM Rabusertib increased CHK1-S345 and CHK2-T68 expression levels and combined Rabusertib and bleomycin treatment increased CHK1-S345 levels, compared to treatment with bleomycin alone (figure 4.11.B,C). One of the experiments also showed that combined Rabusertib and bleomycin treatment decreased CHK1-S296 levels compared to cells treated only with bleomycin (figure 4.11.B). The other experiment produced a faint CHK1-S296 signal and the result was inconclusive (figure 4.11.C). Wang et al (2014)

examined the molecular mechanism of Rabusertib by treating A549 (lung carcinoma epithelial) and H1299 (non-small cell lung cancer) cells with different concentrations of LY2603618 (Rabusertib) (1-20μM) for 24 hours. They observed that Rabusertib inhibited CHK1 autophosphorylation at S296 (although the signal was very weak) and increased CHK1 phosphorylation at S345 in human cancer cells. They also observed that Rabusertib increased Gamma-H2AX (and gamma H2AX foci formation), total p53 and CHK2-T68 levels, while it did not impact total CHK1 and CHK2 levels. Our results were consistent with these findings, as we detected increased CHK1-S345 and CHK2-T68 and decreased CHK1-S296 expression. The only observation that we were not able to confirm was an increase in Gamma-H2AX expression, as the signal of the non-bleomycin-treated cells was too weak to reach a conclusion. Increase in CHK1 (S345) expression following CHK1 inhibition has been shown in other studies and is due to DNA damage buildup that amplifies ATR/ATM signalling, which in turn upregulates phosphorylation of CHK1 (S345), CHK2 (T68) and H2AX (Parsels et al, 2011). Another observation from Wang et al (2014) was that 1μM Rabusertib did not block completely CHK1(S296) phosphorylation and suggested that the inhibitor may activate the DDR response independently of CHK1 inhibition. In our experiment, 5μM Rabusertib was also not enough to completely inhibit CHK1(S296) phosphorylation (figure 4.11.B), yet we observed the activation of several DNA damage response factors, further reinforcing this hypothesis. Overall, our results suggest that Rabusertib acted by firstly reducing CHK1 activity, as indicated by the elevation of DNA-damage regulated phosphorylation of CHK1 (S345) and reduction of CHK1-S296 autophosphorylation and secondly by triggering the DNA damage response, as indicated by an increased CHK2-T68 expression. We propose that impairing the ATR-CHK1 pathway increased DNA damage (as indicated by the activation of the DDR and an increase in apoptosis), which synergised with telomere damage to kill the cells.

These results may explain why Rabusertib was more efficient at preventing cells from escaping crisis. We have confirmed that both AZD6738 and Rabusertib increased DNA damage as they activated the DNA damage response. However, Rabusertib reduced CHK1 activity (as the concentration was not high enough to inhibit it), while AZD6738 upregulated CHK1 activity, most probably due to compensation by ATM and DNA-PK upregulation. Hence, it is reasonable to conclude that it might be easier for AZD6738-treated cells to

repair their DNA damage since CHK1 will activate the downstream effectors. In other words, Rabusertib appears to be a more specific inhibitor of the ATR-CHK1 pathway, as it inhibits downstream AZD6738, allowing less opportunities for compensating mechanisms to take place.

In DN-hTERT HCT116 cells, we could not determine how CHK1-S345 and CHK1-S296 expression was affected by inhibitor treatment, as little to no signal was detected (figure 4.12). No differences were detected in CHK2, Gamma H2AX and CHK2-T68 levels between the inhibitor-treated cells and the control cells. The results on CHK1, H2AX and p53 expression were inconclusive as they appeared to be similar across the samples in the first experiment, but there were differences detected in the second experiment. It is likely that those differences could be due to uneven loading, as actin levels varied in the second experiment. Overall, the inhibitor concentration appeared to be a very low concentration to detect clear differences and patterns between the samples.

We investigated LC3B expression in both WT and DN-hTERT HCT116 cells and found out that they both transitioned from LC3-I to LC3-II, which is a hallmark of autophagy as the lipidated form LC3-II is needed for the full formation of autophagosomes. Interestingly, one experiment showed that the conversion to LC3-II was more efficient in DN-hTERT HCT116 cells, as in these cells there was barely detectable LC3-I, unlike WT cells (figure 4.12.D). This indicates that telomere erosion might induce autophagy in colorectal cancer cells, but another experiment did not support this, necessitating the repetition of the study (figure 4.12.C). Nassour et al (2019) showed that not only telomere damage during telomere crisis triggers autophagy, but also autophagy is required for cell death in crisis as its suppression enabled cells to bypass crisis. This suggests that treatment with an inhibitor that induces autophagy will increase the chances of failure to escape crisis, while treatment with an inhibitor that inhibits autophagy might have the opposite effect. No differences in autophagy were detected between inhibitor-treated cells and control DN-hTERT HCT116 cells. Wang et al (2014) showed that Rabusertib stimulated transition of LC3-I to LC3-II and induced autophagy. However, this was detectable only when lung cancer cells were treated with concentrations higher than 5μM Rabusertib in their Western Blot analysis, explaining why a concentration of 50nM was not able to produce a visible change in our Western Blot. Bowler et al (2020) found that 1μM AZD6738 treatment of OE21 (human esophageal

squamous cell carcinoma) cells did not produce any changes in LC3 or p62 levels (loss of p62 is also a marker of autophagy). To the best of our knowledge, this is the only study that has investigated how AZD6738 affects autophagy and the results showed that it did not influence the process. This might provide a second explanation to why Rabusertib was more effective at blocking escape from crisis. Induction of autophagy from Rabusertib treatment might synergise with induction of autophagy from telomere damage to kills cells during crisis, an advantage that AZD6738 might not be able to offer.

Some limitations from the Western Blot experiments include the lack of repeats, the inability to confirm ATR inhibition by AZD6738 and the fact that the concentration of the inhibitor was too low to produce differences in band intensity that would be visible in a Western Blot experiment. Some markers (CHK2, H2AX, p53) were only tested in one of the two experiments, so including more repeats (e.g. n=3) would have provided stronger evidence to support our results. In order to confirm that increased CHK1 activity due to AZD6738 treatment was caused by a compensatory pathway activation rather than lack of ATR specificity, we should have tested for ATM or DNA-PK activation. Future experiments can include the study of ATM-S1981, ATM, DNA-PKcs-S2056, DNA-PKcs, RPA-S33 (downstream target of ATR, ATM and DNA-PK) and RPA-S4/8 (downstream target of DNA-PK activation) expression in AZD6738-treated WT-HCT116 cells. Future Western Blot experiments could also include more DDR proteins, such as total ATR, ATR-S428, p53-S15 and CHK1-S317 to get a further understanding of the inhibitors' molecular mechanisms. As protein level changes caused by 50nM AZD6738/Rabusertib treatment may have been missed due to low detection sensitivity, future Western blot experiments can include DN-hTERT HCT116 samples treated with 5µM AZD6738/Rabusertib to understand the molecular mechanism of the drugs. Alternatively, more sensitive methods could be used, such as flow cytometry, which would provide greater precision.

Another limitation is that we only included one autophagy marker. While LC3 is a commonly used marker of autophagy, increased levels of LC3-II may be observed either because of elevated formation of autophagosomes or blockage of autophagosome degradation, as autophagy is a multistep process (Bowler et al, 2020). Future experiments could include p62, as loss of its expression is another commonly used marker of autophagy. Increased p62 and increased levels of LC3-II would suggest blockage in autophagy (Klionsky et al, 2016).

However, in our experiment all LC3-II levels seemed similar and our conclusion was made taking into account the different LC3-I levels, which indicated different conversion rates. It would also be interesting to confirm that the two inhibitors increase apoptosis during crisis by testing the expression of apoptosis markers, such as cleaved forms of caspase 3, caspase 9, caspase 8 and PARP.

4.5.4 Conclusion

In this chapter we have shown that 50nM Rabusertib and 50nM AZD6738 affected the ability of the cells to escape a telomere crisis. Both inhibitors specifically affected cell growth, cell cycle progression, apoptosis and potentially telomere fusion during late crisis but not prior to crisis. Neither of the inhibitors affected telomere erosion during deep crisis or before. Both inhibitors only affected cells with short dysfunctional telomeres. While both inhibitors activated the DNA damage response, our results suggested that Rabusertib reduced CHK1 activity, while AZD6738 had an opposite effect. Overall, we provide the first demonstration that the ATR-CHK1 pathway plays an important role in keeping the cells alive during crisis and our data supports further clinical evaluation of Rabusertib as a potential treatment for patients with pre-cancerous lesions exhibiting short dysfunctional telomeres.

Chapter 5

Assessing the effect of Rabusertib (CHK1i) and AZD6738 (ATRi) on fibroblast cells

5.1 Abstract

Telomere crisis is a cellular state caused by telomere erosion leading to genomic instability and cell death and escape of cells from crisis contributes to tumorigenesis. ATR and its downstream effector CHK1 regulate DNA damage cell cycle checkpoints to inhibit cell cycle progression of cells with damaged DNA amongst other functions. In this chapter we assess how two inhibitors, Rabusertib, which is a CHK1 inhibitor (CHK1i) and AZD6738, which is an ATR inhibitor (ATRi) affect primary human fibroblast cells with short and long telomeres.

We used primary fibroblast cells (HCA2 and IMR90) that undergo a well-defined period of crisis from which they do not escape. We treated these cells with NU7441, Rabusertib and AZD6738 and the effects of these drugs on cell growth, cell cycle and apoptosis were monitored during crisis. We also assessed how Rabusertib and AZD6738 affected cell growth, cell cycle progression and apoptosis in a mixed primary fibroblast population with shorter and longer telomeres and used allele-specific STELA to identify the presence of the fibroblast types in the population at different stages of treatment.

50nM Rabusertib (CHK1i) slowed down cell growth, altered cell cycle progression and increased apoptosis in both IMR90 and HCA2 fibroblasts undergoing telomere crisis while 50nM AZD6738 (ATRi) only had a minimal effect on IMR90 cells and no effect on HCA2 cells. Treatment with 50nM and 100nM Rabusertib also decreased cell growth in HCA2 cells with shorter telomeres, but not in IMR90 cells with longer telomeres and 100nM Rabusertib specifically increased apoptosis in HCA2 cells with shorter telomeres.

In conclusion, fibroblasts undergoing crisis are sensitive to 50nM Rabusertib, but not to 50nM AZD6738. These results suggest the use of CHK1 inhibitors instead of ATR inhibitors to impair the ATR-CHK1 pathway and support the concept that Rabusertib may be able to therapeutically target lesions that exhibit short dysfunctional telomeres.

5.2 Introduction

Telomere crisis is a state caused by critical telomere shortening and results in increased cell death and genomic instability. Some cells will re-activate telomerase reverse transcriptase to heal short telomeres and enable DNA proliferation, leading to escape from telomere crisis, which contributes to tumorigenesis as these cells have an altered genome (von Morgen and Maciejowski, 2018). In the previous chapter, we established that inhibition of ATR and CHK1 affect escape of HCT116 cells from telomere crisis. In this chapter, we investigate how ATR and CHK1 inhibition affect primary fibroblast cells with short and long telomeres.

ATR is activated by genotoxic stress and single-strand DNA, which arises from either replicative stress or resected DNA double-strand breaks (Carrassa and Damia, 2017). It is essential for cell viability and is a regulator of the intra S-phase checkpoint and the G2/M cell cycle checkpoint to prevent cells with DNA damage from entering mitosis (Carrassa and Damia, 2017). ATR is also involved in origin firing suppression, inter-strand crosslink repair, meiosis, telomere stability and response to mechanical and osmotic stress (Saldivar et al, 2017). ATR is also needed to maintain stability of specific chromosomal parts (common fragile sites) during DNA replication (Saldivar et al, 2017).

AZD6738 is the first ATR inhibitor to be described with *in vivo* data, has high solubility and bioavailability. It is very potent and selective and was developed by AstraZeneca (Barnieh et al, 2021; Foote et al, 2018). It inhibits activation of ATR and has been widely studied preclinically in different tumour types as monotherapy or in combination with other agents (Suzuki et al, 2022). There are numerous phase I and II studies either currently recruiting or preparing to recruit, as monotherapy or combined with radiotherapy, olaparib, acalabrutinib, gemcitabine, durvalumab, carboplatin and paclitaxel, in multiple cancers (Foote et al, 2018). Preliminary results from these studies are promising, demonstrating rapid absorption and significant ATR inhibition (Foote et al, 2018).

ATR phosphorylates its downstream effector CHK1 at S317 and S345, triggering its autophosphorylation at S296 and subsequent activation (Neizer-Ashun and Bhattacharya, 2020). CHK1 is crucial for G2 cell cycle arrest to allow for DNA repair and plays a role in

homologous recombination by recruiting RAD51 to the DNA damage site and facilitating its interaction with BRCA2 (Neizer-Ashun and Bhattacharya, 2021; Carrassa and Damia, 2017). CHK1 is also involved in the mitotic spindle checkpoint to prevent chromosomal instability and aneuploidy, origin firing suppression, embryo development, gene transcription, somatic cell viability maintenance, hematopoietic stem and progenitor cell development and expansion (Carrassa and Damia, 2017; Zhang and Hunter, 2014; Neizer-Ashun and Bhattacharya, 2021). It has been shown that the ATR and ATM pathways cross-talk and when there is DNA damage, ATM can activate CHK1 (Weber and Ryan, 2015).

Rabusertib is a very selective and highly potent CHK1 inhibitor developed by Eli Lilly and Company and produces an identical phenotype to that caused by genetic knockdown of CHK1 (Klaeger et al, 2017; King et al, 2014). It decreases CHK1 autophosphorylation on Serine 296 and inhibits phosphorylation of CHK1 substrates without affecting phosphorylation of CHK1 by ATR (King et al, 2014). It has completed seven trials and Phase I studies have assessed the safety and maximum tolerable dose of Rabusertib in combination with pemetrexed, cisplatin and gemcitabine (Weiss et al, 2013; Calvo et al, 2016; Doi et al, 2015). However, phase II studies appeared to be less promising, as Rabusertib did not show a significant effect in the overall survival of cancer patients, when combined with gemcitabine or pemetrexed (Laquente et al, 2017; Scagliotti et al, 2016).

Fibroblasts are mesenchymal cells that originate from the embryonic mesoderm tissue, they generate and preserve the extracellular matrix in connective tissues and play a role in tissue remodelling, would healing, inflammation, angiogenesis and cancer (Kendall and Fenghali-Bostwich, 2014). IMR-90 is a diploid fibroblast cell line that comes from human (female) foetal lung characterised by Nichols et al (1977) and these cells have been used as model fibroblasts in many studies (Ehler et al, 1996; Monroe et al, 2020). They share many features of differentiated smooth muscle cells, such as an elongated and slender shape and longitudinal alignment of their actin-attachment sites (Ehler et al, 1996). HCA2 is a diploid fibroblast cell line that comes from human neonatal foreskin and is a well-characterised model of human neonatal fibroblasts (Young and Smith, 2001; Liu and Hornsby, 2007; Lopez et al, 2012).

In the previous chapter, we showed that 50nM Rabusertib (CHK1i) prevented cells from escaping crisis and 50nM AZD6738 (ATRi) dramatically slowed down escape from crisis

(figures 4.1, 4.2). To further examine the effect of these inhibitors on cells undergoing crisis, we tested their impact on cell growth, cell cycle progression and apoptotic levels in primary fibroblasts undergoing crisis. These cells have been modified to express the human papilloma virus (HPV)16 E6E7 oncoproteins, which block the function of p53 and pRb leading to bypass of senescence and entry into crisis (Capper et al, 2017). However, these cells do not usually escape crisis, unlike HCT116 cells described in previous chapters. Testing the DDR inhibitors in these cells will provide an interesting model for understanding if they can specifically kill primary human cells undergoing crisis. We also included NU7441 (DNA-PKi) in our study, which prevented cells from escaping crisis at the concentrations of 1 μM and 1.5 μM in the experiments of Chapter 1.

This study is divided into two stages. In the first stage, we treated HCA2 and IMR90 cells with different concentrations of Rabusertib, AZD6738 and NU7441 from an early passage until they progressed into deep crisis. We assessed how the three inhibitors affected the properties of the cells such as cell growth, cell cycle progression and apoptosis before they entered crisis (long telomeres) and when they were in deep crisis (short telomeres). In the second stage, we treated a mixed population of early and late passage primary human fibroblasts with Rabusertib and AZD6738 in a series of three experiments. In the first two experiments, we examined a mixed population of early passage HCA2 cells and late passage IMR90 cells and in the third experiment we examined a mixed population of late passage HCA2 cells and early passage IMR90 cells. We monitored how the two inhibitors affected cellular properties in early and late passage cells and whether these inhibitors can selectively kill late passage fibroblast cells experiencing telomere crisis.

5.3 Aims

In this chapter, we focus on the DDR inhibitors Rabusertib (CHK1i), AZD6738 (ATRi) and NU7441 (DNA-PKi), which prevented HCT116 cells from escaping crisis in the previous chapters. We hypothesise that these inhibitors may selectively kill late passage fibroblast cells experiencing telomere crisis. To test this, we treated HCA2 and IMR90 cells with the inhibitors and the properties of the cells (cell growth, cell cycle progression, apoptosis) were studied during crisis.

The aims of this chapter are to:

- Establish if the three inhibitors affect cell growth, cell cycle progression and apoptosis in primary human fibroblasts during different stages of crisis
- Establish a method to identify HCA2 and IMR90 cells individually in a mixed population
- Assess if the inhibitors can induce cell death in fibroblasts undergoing crisis but not in younger cells
- Evaluate how the inhibitors affect cell growth, cell cycle progression and apoptosis in a mixed population of early passage HCA2 cells and late passage IMR90 cells
- Examine how the inhibitors affect cell growth, cell cycle progression and apoptosis in a mixed population of late passage HCA2 cells and early passage IMR90 cells

5.4 Results

The purpose of the experiments detailed in this chapter was to establish whether the DDR inhibitors Rabusertib (CHK1i), AZD6738 (ATRi) and NU7441 (DNA-PKi) specifically affected cells undergoing crisis. To achieve this, we undertook experiments in which younger cells were mixed with older cells undergoing crisis in the presence of the DDRi. To determine whether the inhibitors could specifically affect the different cell populations, we chose two fibroblast cultures previously characterised for XpYp telomere-adjacent sequence polymorphism (Baird et al, 2003).

As shown in figure 5.1, HCA2 cells exhibit a homozygous AT haplotype and IMR90 cells exhibit a homozygous GC haplotype. HCA2 and IMR90 cells are homozygous for two different XpYp telomere-adajcent haplotypes that could be utilised with allele-specific STELA to allow the presence of individual fibroblast cultures to be detected in a mixed population. This is because the bands that appear on the AT allele correspond to HCA2 cells, while bands that appear on the GC allele correspond to IMR90 cells. The results would indicate whether the inhibitors selectively influence and potentially reduce the presence of crisis cells in a mixed population of younger and crisis cells.

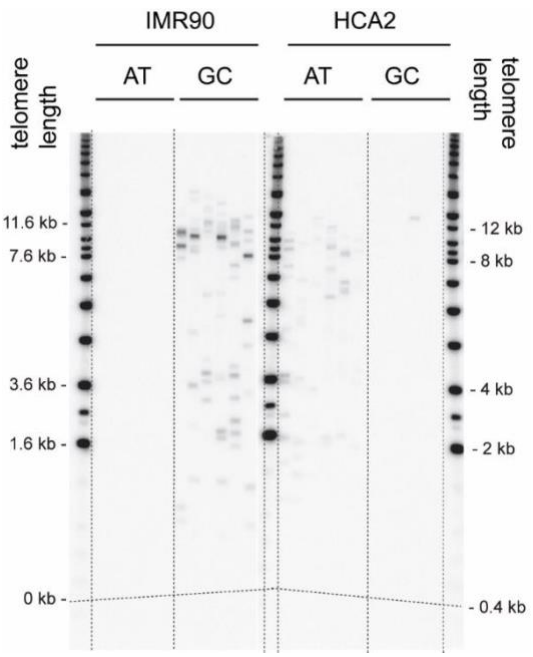

Figure 5.1: Allele-specific STELA analysis. The figure shows the allele-specific STELA analysis of young HCA2 (homozygous AT haplotype) and young IMR90 (homozygous GC haplotype).

5.4.1 Assessing the effect of DDR inhibitors on IMR90 cells during crisis

The experiment included one control sample treated with DMSO and two samples each treated with NU7441, AZD6738 and Rabusertib. Treatment started when cells were at PD 61.32, when they started entering early crisis and terminated when cell growth stopped at PD 76.5 in control cells during deep/late crisis. Figure 5.2.A shows the growth curve of IMR90 cells treated during early and deep crisis (from PD 61.32 until PD 76.5 for control cells), with day 0 of treatment marking the start of treatment. Previous experiments conducted in our lab have shown that IMR90 cells start entering early crisis around PD 61 and deep crisis around PD 71, with cell growth ceasing around PD 78. The inhibitors were added every two or three days at the same time for all samples. At days 16, 34, 60 and 77 of treatment, the cells were counted and cell-cycle and apoptosis assays were performed to determine the growth rate, cell cycle progression and cell death respectively.

From the start of treatment (day 0, start of early crisis) to day 16 (PD 69.3, early crisis), cells treated with AZD6738 exhibited similar cell growth to control cells, while cells treated with NU7441 (140,000-230,000 cells) and Rabusertib (170,000-380,000 cells) had a lower cell count compared to control cells (800,000 cells) (figure 5.2.A). From day 16 (PD 69.3 for control cells) to day 34 (PD 72.2 for control cells, deep crisis), cells treated with AZD6738, 12.5nM Rabusertib and 250nM NU7441 exhibited a similar cell growth to control cells, while cells treated with 50nM Rabusertib and 1000nM NU7441 exhibited very little cell growth and considerably lower to control cells. During deep crisis, from day 34 (PD 72.2 for control cells) to day 77 (PD 76.5 for control cells), cell growth declined in control cells, as they started showing signs of deep crisis (large, multinucleated and surrounded by precipitate) and cells treated with AZD6738 had a similar cell growth to control cells. However, cells treated with both concentrations of NU7441 and 12.5 Rabusertib showed very little cell growth, while cells treated with 50nM Rabusertib almost doubled (from 497,000 to 1,117,000). In conclusion, 50nM Rabusertib and 1000nM NU7441 had the strongest impact on cell growth in IMR90 cells from early to deep crisis, whereas 12.5nM Rabusertib and 250nM NU7441 also reduced cell growth to a lesser degree.

At day 34, cells treated with 50nM Rabusertib and 1000nM NU7441 had a considerably altered cell cycle distribution compared to control cells (figure 5.2.B). While cells treated with 250nM NU7441 had a similar cell cycle distribution compared to control cells, the

distribution of 1000nM NU7441-treated cells was completely altered (31% less cells in G0/G1 phase, 3% more cells in S phase, 18% more cells in G2/M phase and 8% more cells in >4N phase). Cells treated with both concentrations of AZD6738, showed a different cell cycle distribution compared to control cells (5-7% less cells in G0/G1 phase and 4-5% more cells in G2/M phase), although it was not dramatically different. While cells treated with 12.5nM Rabusertib had 5% less cells in G0/G1 phase and 5% more cells in G2/M phase compared to control cells, the distribution of 50nM Rabusertib-treated cells was completely altered (32% less cells in G0/G1 phase, 8% more cells in S phase, 11% more cells in G2/M phase and 13% more cells in >4N phase).

At day 60 or 77, no cell samples were collected for NU7441-treated cells due to the low cell number and no dramatic differences were observed between other inhibitor-treated cells and control cells. Cells treated with both concentrations of AZD6738 had 2-3% less cells in G0/G1 phase and 1-3% more cells in G2/M phase compared to control cells. Cells treated with 12.5nM Rabusertib had 2% less cells in G0/G1 phase, 4% less cells in S phase and 7% more cells in G2/M phase, while unexpectedly, cells treated with 50nM Rabusertib had 5% more cells in G0/G1 phase compared to control cells. Overall, 50nM Rabusertib and 1000nM NU7441 strongly affected cell cycle distribution in IMR90 cells undergoing crisis (at day 34) and that may contribute to the dramatic decline in cell growth that was observed from day 16 to day 34.

Apoptosis levels were relatively high at day 34 (>32%) and even higher at day 77 (>61%) as cells were in deep crisis (figure 5.2.C). No cell samples were collected from 1000nM NU7441 -treated cells at day 34 and only cell samples from control cells and AZD6738-treated cells were collected at day 77 (due to low cell number). At day 34, cells treated with 250nM NU7441 (32%) and 12.5nM AZD6738 (45%) did not exhibit higher apoptosis compared to control cells (49%), while cells treated with 50nM AZD6738 (54%), 12.5nM Rabusertib (57%) and 50nM Rabusertib (71%) exhibited higher apoptosis. At day 60 or 77, cells treated with 12.5nM AZD6738 (61%) and 50nM Rabusertib (63%) did not exhibit higher apoptosis compared to control cells (70%), while cells treated with 50nM AZD6738 (75%) exhibited slightly higher apoptosis. Overall, 50nM Rabusertib increased apoptosis in IMR90 cells undergoing crisis (day 34).

In conclusion, both concentrations of Rabusertib and NU7441 inhibited cell growth during crisis, 50nM Rabusertib and 1000nM NU7441 had a strong effect on cell cycle distribution and 50nM Rabusertib strongly increased apoptosis in IMR90 cells undergoing crisis. However, AZD6738 did not strongly affect cell growth, cell cycle progression or apoptosis in IMR90 cells undergoing crisis.

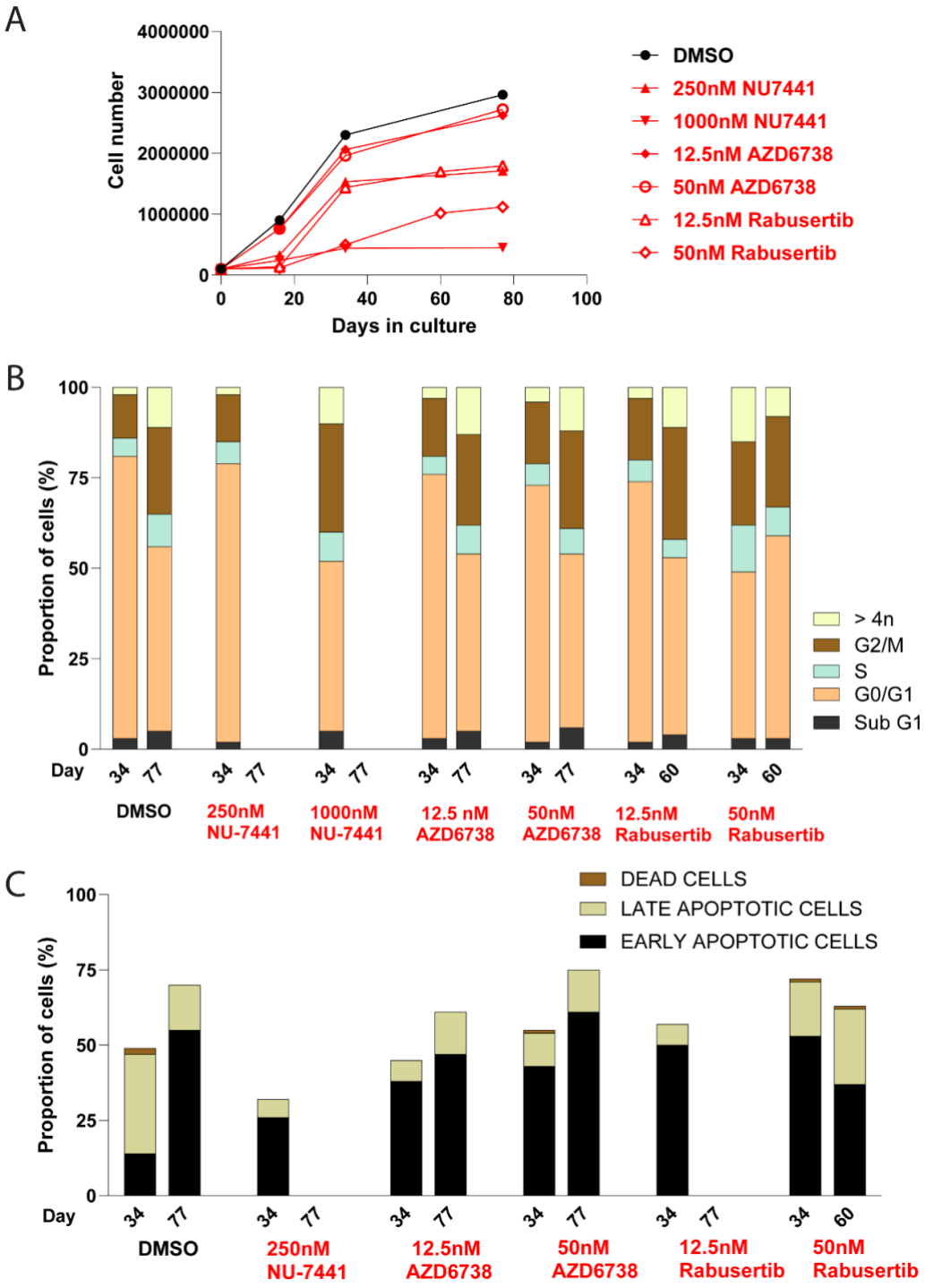

Figure 5.2: Cell growth, cell cycle and apoptosis analysis of IMR90 cells treated with NU7441, AZD6738 and Rabusertib during deep crisis. The figure shows the growth curve (A), the cell cycle progression (B) and the apoptotic levels (C) of IMR90 treated with DMSO and three DDR inhibitors. Apoptosis was analysed using Annexin-V/propidium iodide (PI) staining. Cells are classified as early apoptotic when they are Annexin V positive and PI negative, late apoptotic when they are Annexin V and PI positive and dead when they are Annexin V negative and PI positive.

5.4.2 Assessing the effect of DDR inhibitors on HCA2 cells during crisis

The experiment included one control sample treated with DMSO and two samples each treated with NU7441, AZD6738 and Rabusertib. Treatment started when cells were at PD 38.42, when they started entering early crisis and terminated when cell growth stopped at PD 58.47 in control cells during deep/late crisis. Figure 5.3.A shows the growth curve of HCA2 cells treated during early and deep crisis (from PD 38.42 until PD 58.47 for control cells), with day 0 of treatment corresponding to the start of the treatment. Previous experiments conducted in our lab have shown that HCA2 cells start entering early crisis around PD 33 and deep crisis around PD 53, with cell growth ceasing around PD 63. The inhibitors were added every two or three days at the same time for all samples. At days 16, 34, 60 and 77 of treatment, the cells were counted and cell-cycle and apoptosis assays were performed to determine the growth rate, cell cycle progression and cell death respectively.

From the start of treatment (day 0, start of early crisis) to day 16 (PD 46.17, early crisis), cells treated with both concentrations of AZD6738 and 12.5nM Rabusertib had a similar cell count to control cells, while cells treated with 250nM NU7441 (500,000 cells), 1000nM NU7441 (230,000) and 50nM Rabusertib (280,000 cells) had a lower cell count compared to control cells (780,000 cells) (figure 5.3.A). From day 16 (PD 46.17 for control cells) to day 34 (PD 50 for control cells), cells treated with AZD6738 and 12.5nM Rabusertib exhibited a similar cell growth to control cells, cells treated with 250nM NU7441 had a slower cell growth and cells treated with 50nM Rabusertib and 1000nM NU7441 exhibited almost no cell growth. During the start of deep crisis, from day 34 (PD 50 for control cells) to day 60 (PD 55 for control cells), cell growth slightly declined in control cells and cells treated with AZD6738 and Rabusertib had similar cell growth to control cells. On the other hand, cells treated with 250nM NU7441 and 1000nM NU7441 (which were not passaged due to low cell number) showed reduced cell growth. During deep crisis, from day 60 (PD 55 for control cells) to day 77 (PD 58.47 for control cells), cell growth declined in control cells as they started showing signs of deep crisis (large, multinucleated and surrounded by precipitate). All cells showed similar cell growth to control cells, except for an increase in cell growth in 50nM Rabusertib-treated cells, which could be either because cells started developing resistance or due to a pipetting error when passaging. In conclusion, 50nM Rabusertib,

250nM NU7441 and 1000nM NU7441 strongly reduced cell growth in HCA2 cells from early to deep crisis.

At day 34, no differences in cell cycle distribution were detected between inhibitor-treated cells and control cells, except for cells treated with 50nM Rabusertib (12% less cells in G0/G1 phase, 5% more cells in S phase and 6% more cells in >4N phase) (figure 5.3.B). At day 60, no differences in cell cycle distribution were detected between inhibitor-treated cells and control cells, except for cells treated with both concentrations of Rabusertib (5-7% less cells in G0/G1 phase, 4% more cells in G2/M phase and 2% more cells in >4N phase). Similarly, at day 77, there were differences in cell cycle distribution between Rabusertib-treated cells and control cells (7-10% less cells in G0/G1 phase, 4-5% more cells in G2/M phase and 3-4% more cells in >4N phase). No 1000nM NU7441-treated cell samples were collected at days 34 and 60, due to a low cell number. Overall, 12.5nM and 50nM Rabusertib strongly affected cell cycle in HCA2 cells undergoing telomere crisis.

Apoptosis levels were high at day 60 (>49%) and even higher at day 77 (>72%) as cells were in deep crisis (figure 5.3.C). Unfortunately, the DMSO sample at day 34 was lost, whereas the rest of the cell samples that were not collected for analysis were due to a low cell number. At day 60, cells treated with 50nM AZD6738 (62%), 12.5nM Rabusertib (71%) and 50nM Rabusertib (61%) exhibited higher apoptosis compared to control cells (57%). At day 77, cells treated with 250nM NU7441 (81%), 1000nM NU7441 (80%) and 50nM AZD6738 (80%) exhibited only slightly higher apoptosis compared to control cells (78%). Overall, 50nM AZD6738 and 12.5nM and 50nM Rabusertib had the strongest effect in increasing apoptosis in HCA2 cells undergoing crisis.

In conclusion, 50nM Rabusertib, 250nM NU7441 and 1000nM NU7441 decreased cell growth in HCA2 cells during crisis, while 12.5nM and 50nM Rabusertib had a strong effect on cell cycle distribution and increased apoptosis. Overall, in both experiments (figures 5.2 and 5.3), 50nM Rabusertib, dramatically reduced cell growth, altered the cell cycle and increased cell death in primary fibroblasts undergoing crisis.

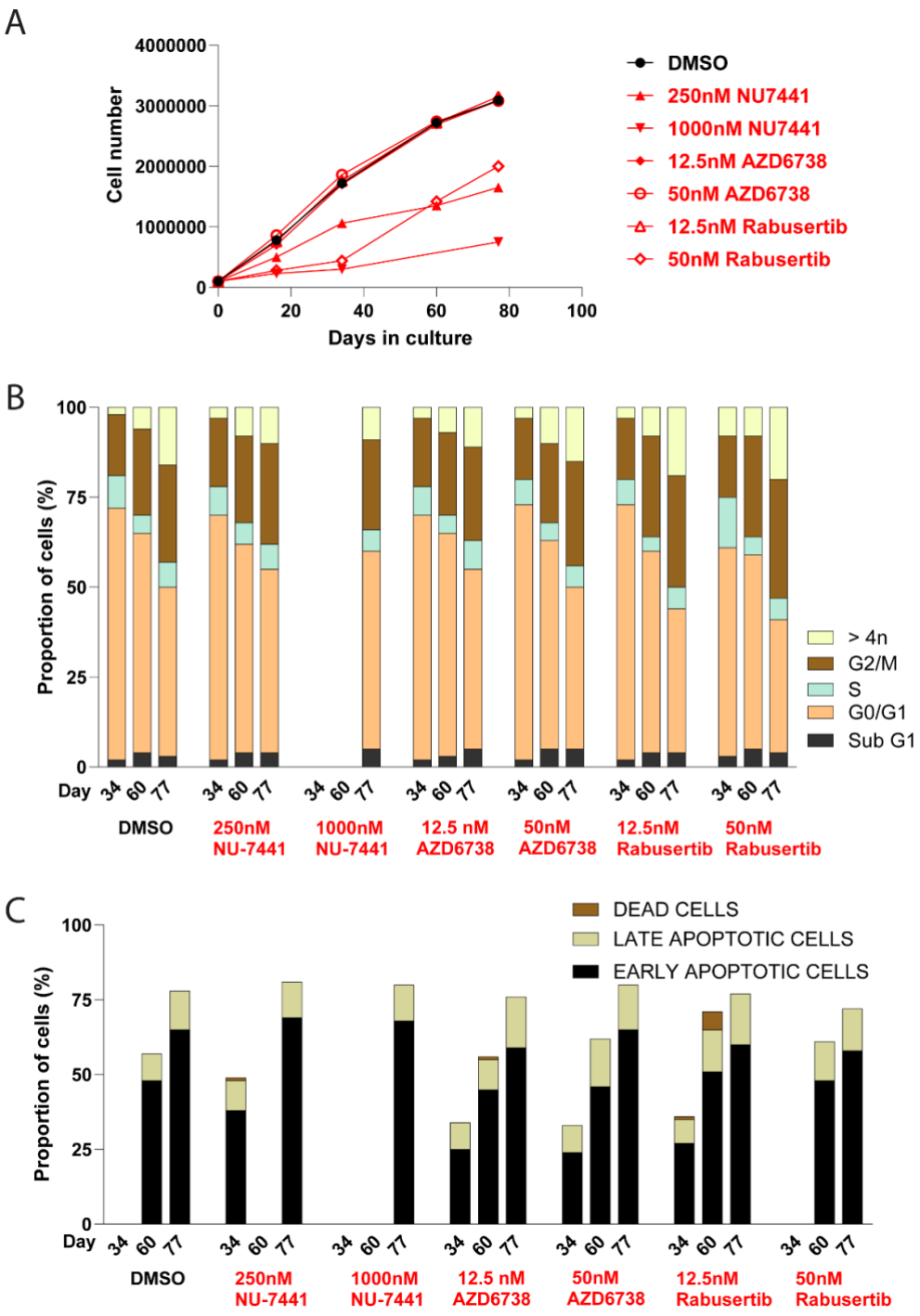

Figure 5.3: Cell growth, cell cycle and apoptosis analysis of HCA2 cells treated with NU7441, AZD6738 and Rabusertib during deep crisis. The figure shows the growth curve (A), the cell cycle progression (B) and the apoptotic levels (C) of HCA2 treated with DMSO and three DDR inhibitors. Apoptosis was analysed using Annexin-V/propidium iodide (PI) staining. Cells are classified as early apoptotic when they are Annexin V positive and PI negative, late apoptotic when they are Annexin V and PI positive and dead when they are Annexin V negative and PI positive.

5.4.3. Assessing the effect of DDR inhibitors on a mixed fibroblast population with short and long telomeres

In the previous experiment, we showed that 50nM Rabusertib killed fibroblast cells during telomere crisis. To further test if Rabusertib affects specifically old cells undergoing telomere crisis, we examined the effect of the inhibitor in a mixed population of old and young cells. We performed a series of three experiments, where we mixed young HCA2 cells with old IMR90 cells or the reverse. We tested the impact of NU7441, Rabusertib and AZD6738 on cell growth, cell cycle progression and apoptotic levels in HCA2 cells alone, in IMR90 cells alone and in the mixed population. Testing the DDR inhibitors in mixed primary human fibroblasts will provide a model for simulating a real-life scenario, where tissues consist of old and young cells with varying telomere lengths. In addition, we monitored the presence of IMR90 and HCA2 cells in the mixed-cell samples by using allele-specific STELA. HCA2 cells have a homozygous AT haplotype, whereas IMR90 cells have a homozygous GC haplotype, allowing the detection of these cells when they are mixed together.

5.4.3.1 Short-term treatment of young HCA2 cells mixed with old IMR90 cells

The first experiment included 7-day treatment of three cell populations, each having an untreated and a DMSO-treated sample serving as controls and two samples each treated with NU7441, AZD6738 and Rabusertib. The first population was made of younger HCA2 cells (PD~41, early crisis), the second population was made of older IMR90 cells (PD~65, early crisis estimated to be approaching deep crisis at the end of treatment) and the third population was made of the young HCA2 cells mixed with the older IMR90 cells (in a 1:2 ratio). The inhibitors were added every two or three days at the same time for all samples. At day 7 of treatment, the cells were counted, and cell-cycle and apoptosis assays were performed to determine the growth rate, cell cycle progression and cell death respectively. A sample from the mixed cells was also collected for STELA analysis.

In HCA2 cells, AZD6738-treated samples had similar cell growth to control cells (figure 5.4.A). Samples treated with Rabusertib (660,000-700,000 cells) and 500nM NU7441 (700,000 cells) had a small decrease in cell growth compared to control cells (850,000), while 1000nM NU7441-treated cells had the lowest cell growth (480,000 cells). In IMR90 cells, inhibitor-treated samples had similar cell growth to control cells, except for a reduced

cell growth in 1000nM NU7441-treated cells (figure 5.4.B). In mixed cells, AZD6738-treated and 25nM Rabusertib-treated samples had similar cell growth to control cells (figure 5.4.C). However, cells treated with 50nM Rabusertib (2,800,000 cells), 500nM NU7441 (2,600,000 cells) and 1000nM NU7441 (2,000,000 cells) had a decreased cell growth compared to control cells (3,400,000). Overall, the cell growth pattern of the mixed-cell population was more similar to the HCA2 population, as younger HCA2 cells were expected to outgrow the older IMR90 cells. This is confirmed by the cell count, as the inoculation number of IMR90 cells (75000) was higher than the HCA2 cells (56000), yet after a week there are >2.5 times more untreated HCA2 cells (850,000, figure 5.4.A) compared to untreated IMR90 cells (320,000, figure 5.4.B).

HCA2 cells had a different cell cycle distribution compared to IMR90 cells (figure 5.5). In untreated IMR90 cells, there were 13% less cells in G0/G1 phase, 9% more cells in G2/M phase and 3% more cells in >4N phase compared to untreated HCA2 cells. In addition, the cell cycle progression profile of IMR90 cells is indicative of cells undergoing deep crisis (figure 5.5.B). The cell cycle distribution of the mixed population is similar to HCA2 cells, because they make up the majority of the mixed population. There were no visible differences in cell cycle distribution between control cells and inhibitor-treated cells in any of the populations.

Due to a low cell count, no apoptosis analysis was performed in IMR90 cells (figure 5.6). Apoptotic levels in all HCA2 samples (14-22%) and mixed cells (16-31%) were relatively low. Overall, there was a small increase in apoptosis in the mixed-cell population compared to HCA2 cells, which is thought to be due to the presence of IMR90 cells, as they are expected to exhibit higher apoptotic levels in deep crisis (figure 5.2.C). It is not known why control cells in the mixed-cell population have higher apoptosis than some inhibitor-treated cells, but as this is not reflected in either the growth curve or the cell cycle distribution, these cells could have been stressed prior to the apoptosis analysis.

Overall, 1000nM NU7441 affected cell growth in both younger HCA2 and older IMR90 cells. No differences in cell cycle progression and apoptosis were reported in the 7-day treatment. This is thought to be because the treatment period was too short to observe substantial differences and we decided to conduct follow-up experiments with an increased treatment period.

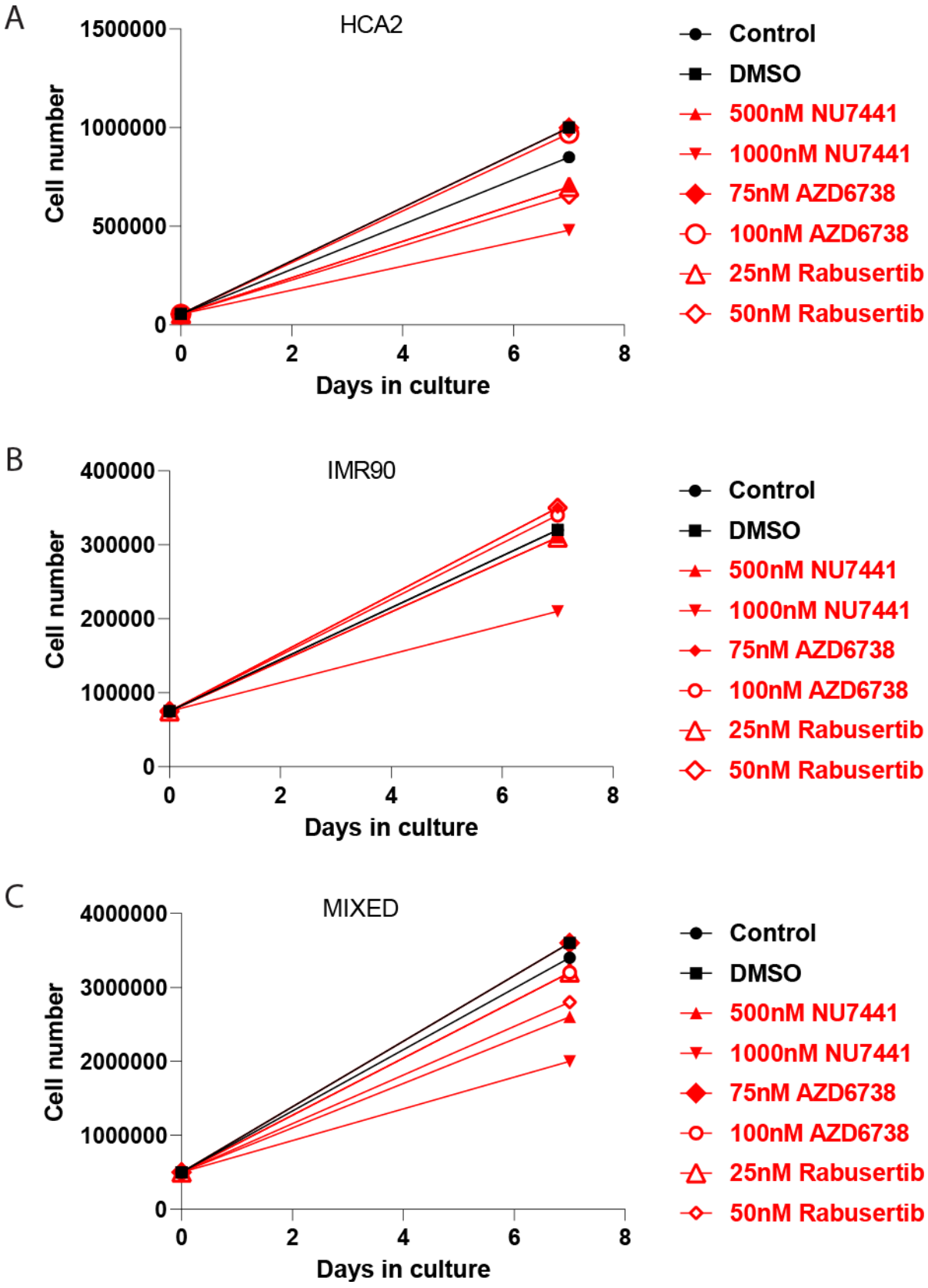

Figure 5.4: Cell growth of HCA2, IMR90 and mixed cells treated with NU7441, AZD6738 and Rabusertib. The figure shows the growth curve of HCA2 (A), IMR90 (B) and mixed HCA2 with IMR90 (C) treated with DMSO and three DDR inhibitors for 7 days.

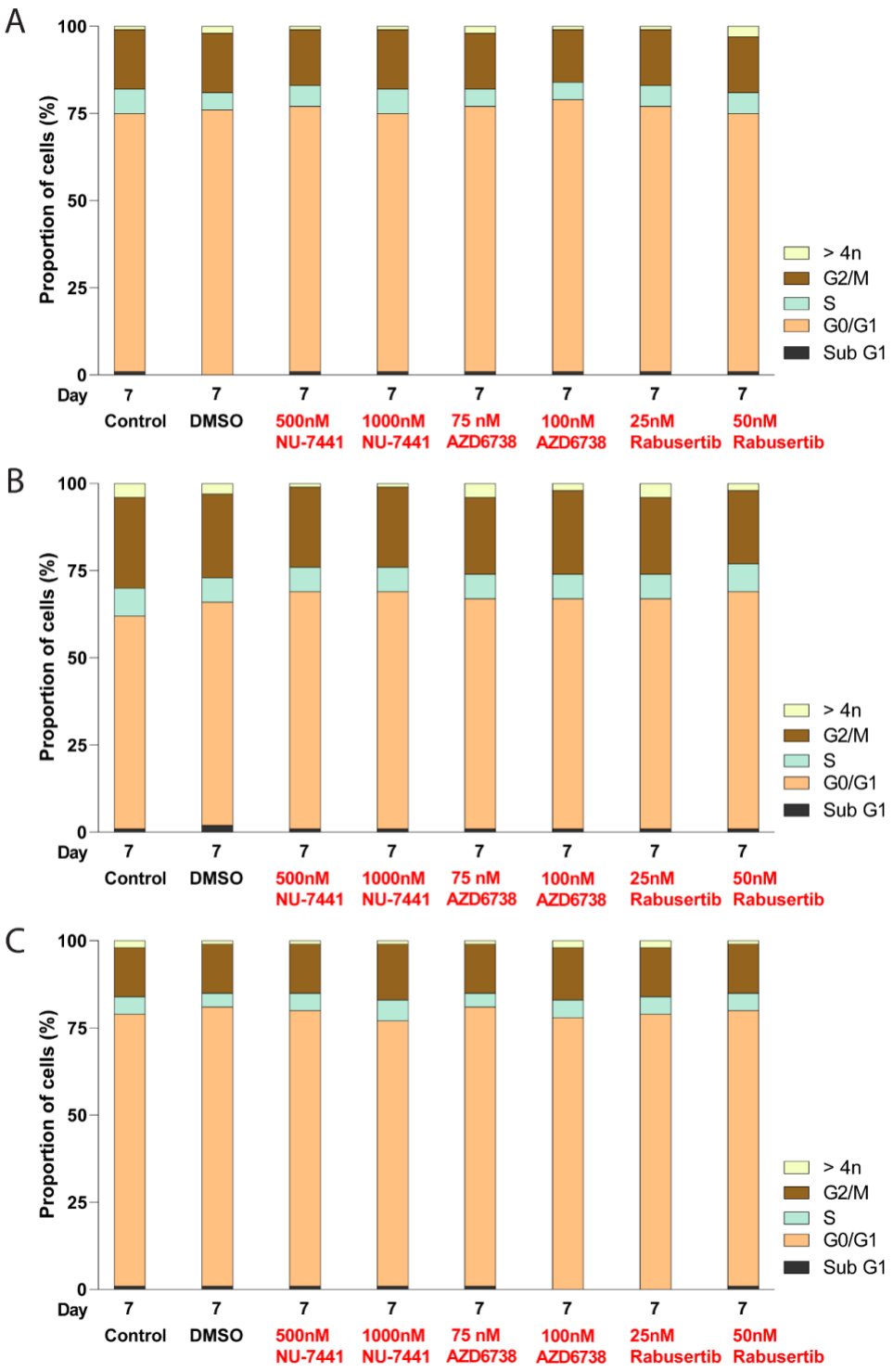

Figure 5.5: Cell cycle analysis of HCA2, IMR90 and mixed cells treated with NU7441, AZD6738 and Rabusertib. The figure shows the cell cycle distribution of HCA2 (A), IMR90 (B) and mixed HCA2 with IMR90 (C) treated with DMSO and three DDR inhibitors for 7 days.

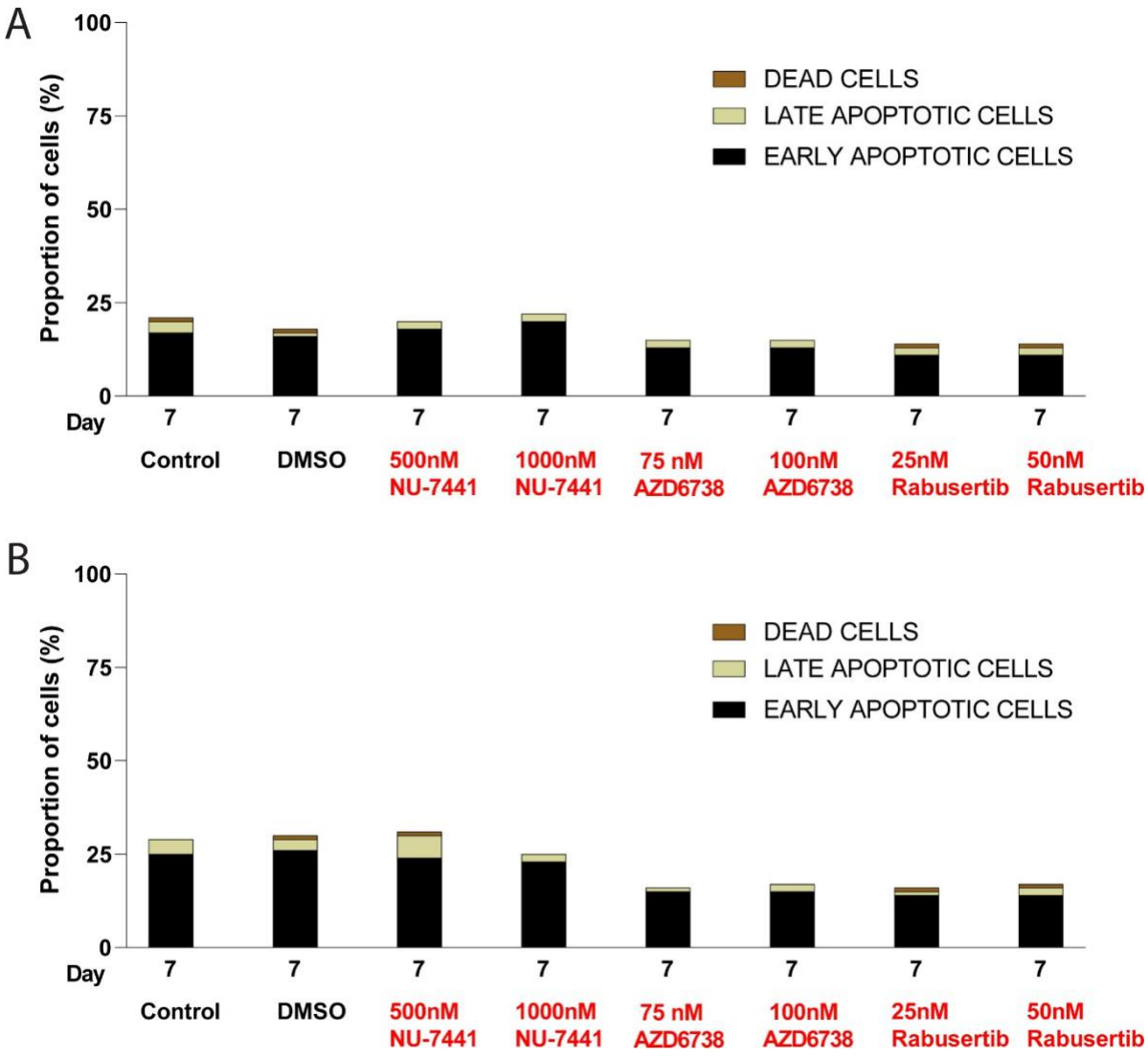

Figure 5.6: Apoptosis analysis of HCA2 and mixed cells treated with NU7441, AZD6738 and Rabusertib. The figure shows the apoptotic levels of HCA2 (A) and mixed HCA2 with IMR90 (B) treated with DMSO and three DDR inhibitors for 7 days. Apoptosis was analysed using Annexin-V/propidium iodide (PI) staining. Cells are classified as early apoptotic when they are Annexin V positive and PI negative, late apoptotic when they are Annexin V and PI positive and dead when they are Annexin V negative and PI positive.

Allele-specific STELA was used to monitor the proportions of younger (HCA2) and crisis (IMR90) cells in the mixed population. Consistent with the 1:2 initial ratio in week 0 (start of treatment), there were more IMR90 cells than HCA2 cells as indicated by the number of bands detected on the GC and AT allele respectively (figure 5.7.A). After 7 days of treatment (Week 1), we could detect more bands on the AT allele (young HCA2 cells) than on the GC allele (crisis IMR90 cells), which indicated that young HCA2 cells have started to outgrow the old IMR90 cells, which were growing more slowly because they were deeper in crisis (figure 5.7.B). We could not detect any substantial differences in the number of the bands across the samples, so the impact of the inhibitors on each type of cells within the sample was inconclusive (the ratio of AT/GC bands is 2.5 for control cells, 1.33 for DMSO-treated cells, 3.53 and 1.23 for NU7441-treated cells, 1.79 and 1.4 for AZD6738-treated cells and 1.63 and 1.56 for Rabusertib-treated cells). However, we established a proof of principle that allele-specific STELA technique could be used to identify the individual types of fibroblasts within the mixed population. We have shown that even though the starting population had a much lower number of HCA2 cells, they eventually represented the majority of the cells after the first week of treatment.

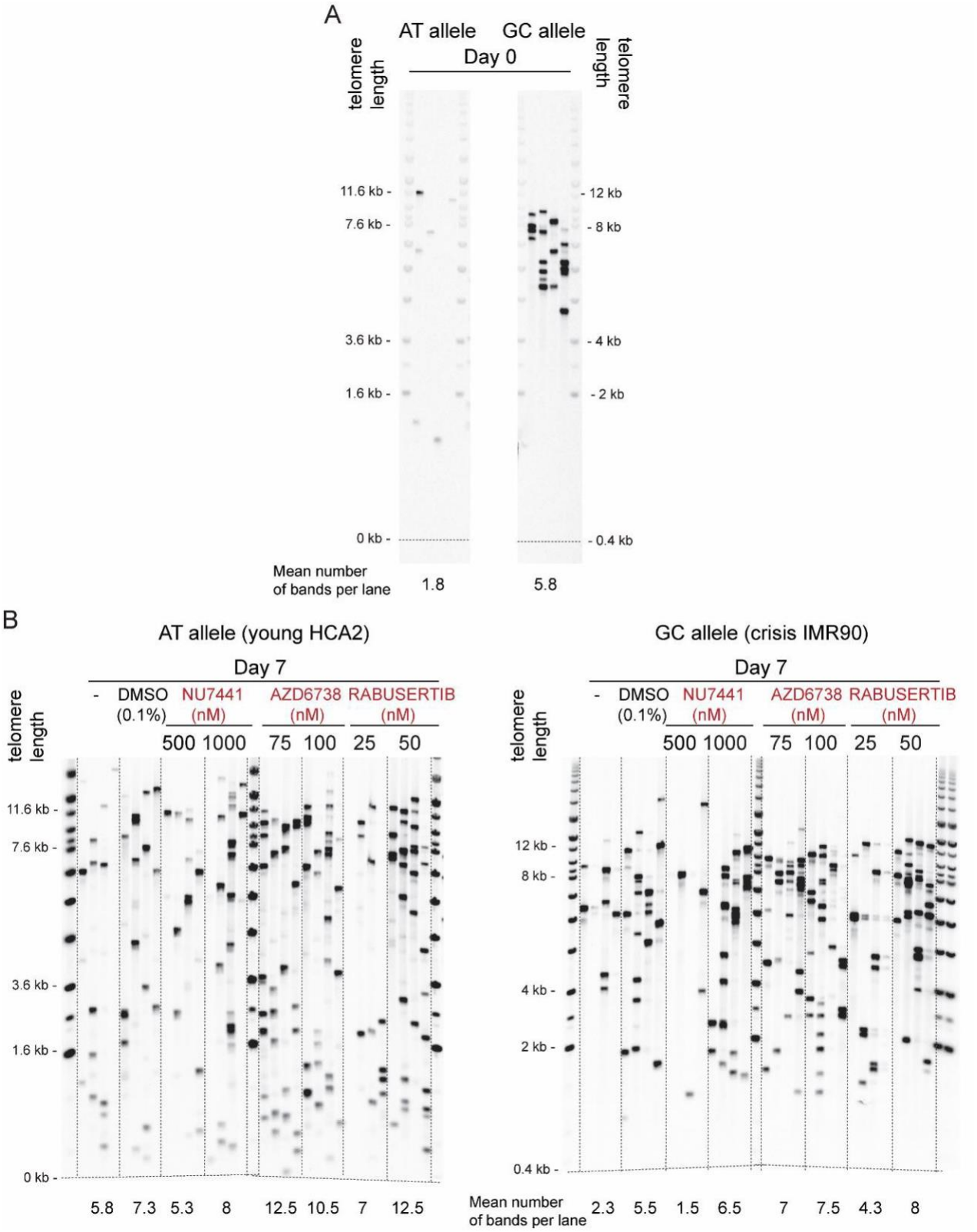

Figure 5.7: Allele-specific STELA analysis of young HCA2 (homozygous AT haplotype) mixed with old IMR90 (homozygous GC haplotype). The figure shows the allele-specific STELA analysis (the AT allele is shown on the left, the GC allele on the right) of the mixed population before (A) and after one week of treatment (B).

5.4.3.2 Long-term treatment of young HCA2 cells mixed with old IMR90 cells

Following the first experiment, we decided to increase the duration of the mixed-cell population treatment to monitor how the DDR inhibitors affect IMR90 cells deeper in crisis. This time we also initiated the experiment with older IMR90 cells compared to the previous experiment (PD~70 instead of PD~65). In addition, we increased the concentrations of some inhibitors. The second experiment included four populations. The first population was made of younger HCA2 cells (PD~41, early crisis) and the second population was made of older IMR90 cells (PD~70, deep crisis) and they were treated for 7 days (control samples). The third and the fourth population was made of younger HCA2 cells mixed with older IMR90 cells (in a 1:2 ratio) and treated for 7 and 21 days respectively. Each population had an untreated and a DMSO-treated sample serving as controls and two samples each treated with NU7441, AZD6738 and Rabusertib. The inhibitors were added every two or three days at the same time for all samples. At day 7 and 21 (for the last population) of treatment, the cells were counted and cell-cycle and apoptosis assays were performed to determine the growth rate, cell cycle progression and cell death respectively. A sample from the mixed cells was also collected for STELA analysis.

In young HCA2 cells, all treated samples had similar cell growth to control cells except for cells treated with 1000nM NU7441, which showed a decreased cell growth (figure 5.8.A). In the crisis IMR90 cells, there were not any major differences in cell growth between inhibitor-treated samples and control cells, except for a reduced cell growth in 1000nM NU7441-treated cells (figure 5.8.B). While untreated HCA2 cells demonstrated similar cell growth to the first experiment (~800,000 cells), IMR90 cell growth (in untreated cells) almost halved (180,000 cells in this experiment compared to 320,000 cells in the first experiment, figure 5.8A,B), consistent with these cells being deeper in crisis. In the first 7 days of the mixed-cell treatment, 1000nM NU7441 had the strongest impact on cell growth (figure 5.8.C). After 21 days of treatment, 1000nM NU7441 slowed down cell growth the most, followed by 200nM AZD6738 and 500nM NU7441 (figure 5.8.D).

IMR90 cells had a different cell cycle distribution compared to HCA2 cells (less cells in G0/G1 phase and more cells in G2, S and >4N phase), which was indicative of them being in deep crisis, but no major differences were observed between the samples (figure 5.9). At day 7, there were no major differences in cell cycle distribution among the mixed-cell samples, but

at day 21, 50nM Rabusertib-treated cells had an altered cell cycle compared to control cells (7% less cells in G0/G1 phase, 4% more cells in G2 phase and 3% more cells in >4N phase).

Due to a low cell count, no apoptosis analysis was performed in IMR90 cells or mixed cells at day 21 (figure 5.10). Apoptotic levels in all HCA2 samples (9-16%) and mixed cells (12-21%) were relatively low and no major differences were observed between the samples. The small increase in apoptosis in the mixed-cell population compared to HCA2 cells is thought to be due to the presence of older IMR90 cells.

Overall, 1000nM NU7441 affected cell growth in all cells (as observed in the first experiment), while Rabusertib mildly affected the cell cycle distribution of the mixed population.

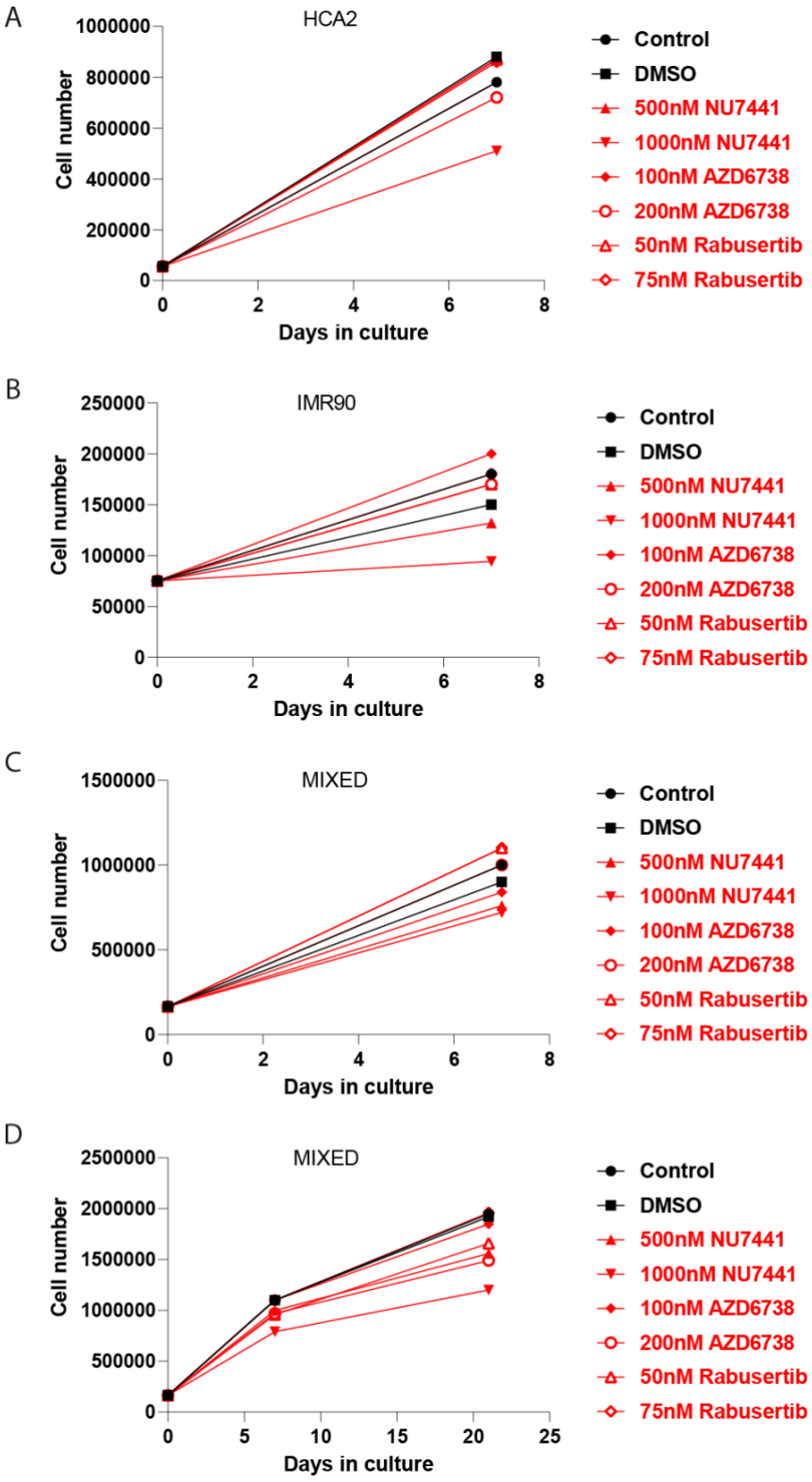

Figure 5.8: Cell growth of HCA2, IMR90 and mixed cells treated with NU7441, AZD6738 and Rabusertib. The figure shows the growth curve of HCA2 (A), IMR90 (B) and mixed HCA2 with IMR90 treated for 7 (C) and 21 days (D) respectively.

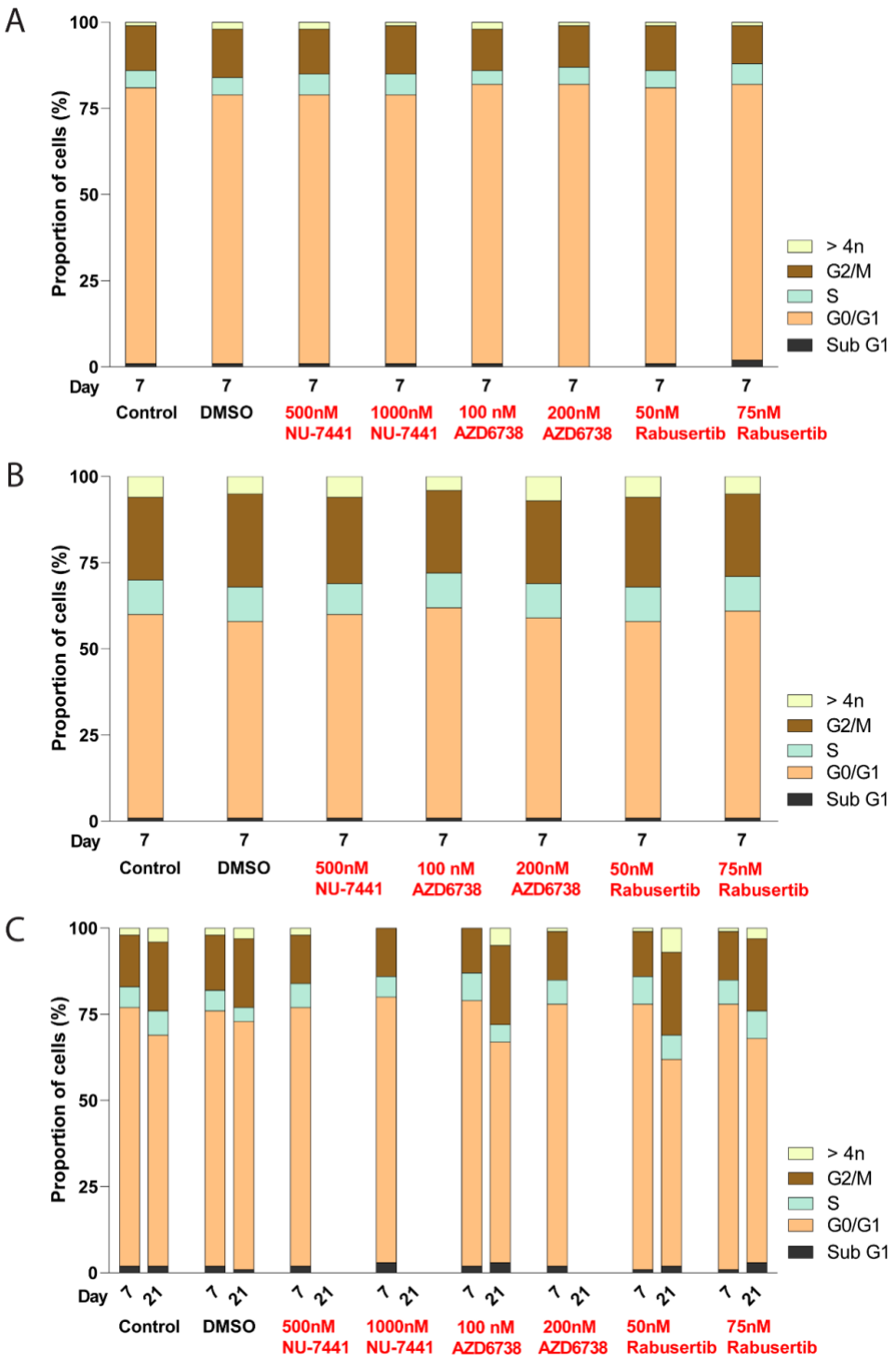

Figure 5.9: Cell cycle analysis of HCA2, IMR90 and mixed cells treated with NU7441, AZD6738 and Rabusertib. The figure shows the cell cycle distribution of HCA2 (A), IMR90 (B) and mixed HCA2 with IMR90 (C) treated with DMSO and three DDR inhibitors.

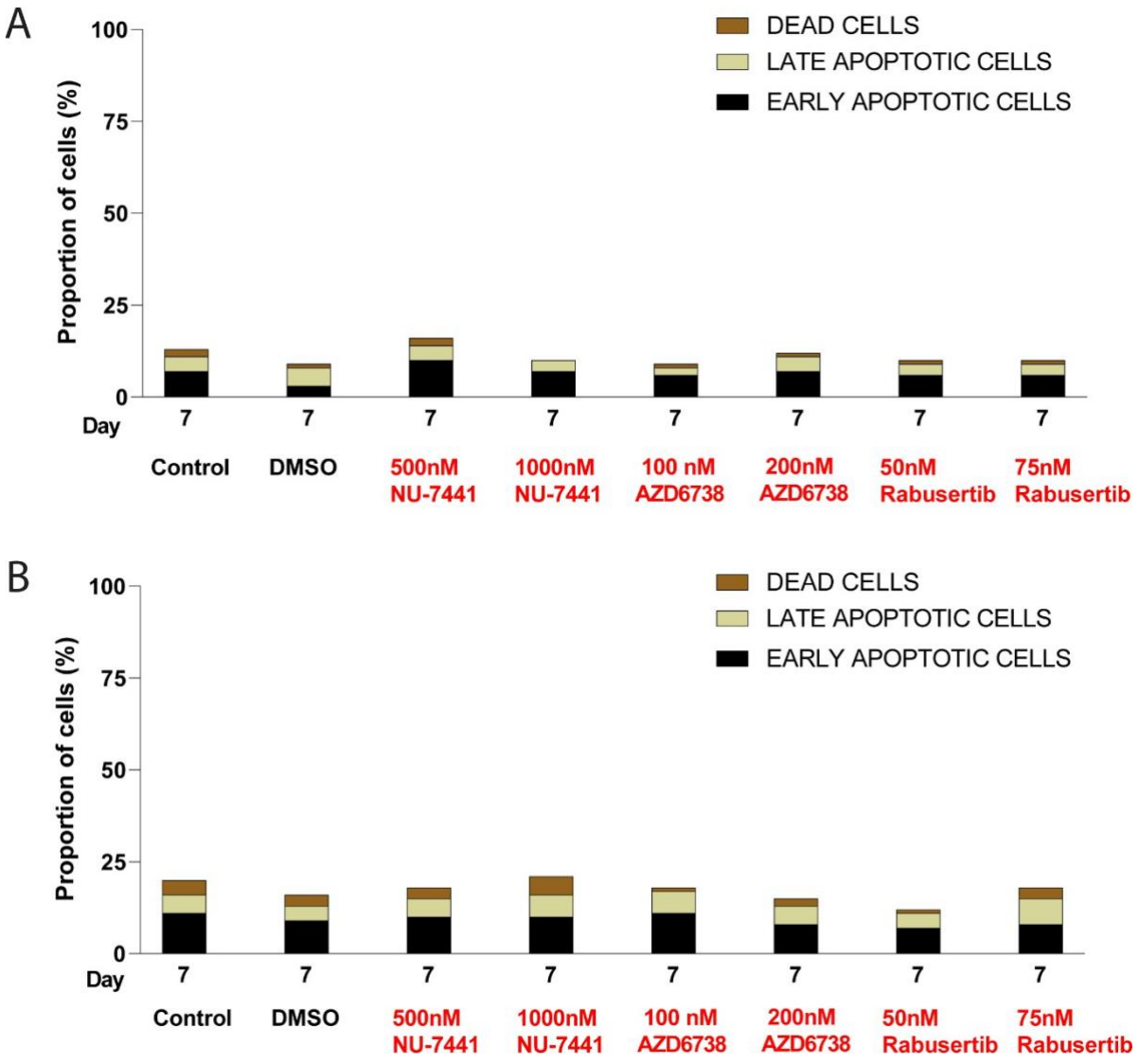

Figure 5.10: Apoptosis analysis of HCA2 and mixed cells treated with NU7441, AZD6738 and Rabusertib. The figure shows the apoptotic levels of HCA2 (A) and mixed HCA2 with IMR90 (B) treated with DMSO and three DDR inhibitors for 7 days. Apoptosis was analysed using Annexin-V/propidium iodide (PI) staining. Cells are classified as early apoptotic when they are Annexin V positive and PI negative, late apoptotic when they are Annexin V and PI positive and dead when they are Annexin V negative and PI positive.

We next conducted allele-specific STELA to determine the relative proportions of the young and old cells, also examining their telomere length distributions. Consistent with the initiating 1:2 cellular ratio, in week 0, there were more IMR90 cells than HCA2 cells, as indicated by the number of bands detected on the GC and AT alleles respectively (figure 5.11.B). After 7 days of treatment (Week 1), (1.2 up to 2.4 times) more bands were observed on the AT allele (young HCA2 cells) than on the GC allele (crisis IMR90 cells). As this was also observed in the DMSO control, it was apparent that the young HCA2 cells had outgrown the old IMR90 cells (figure 5.11.A). This is similar to the observesation from the last experiment (figure 5.8), as IMR90 cells were growing more slowly because they were deeper in crisis. No substantial differences in the number of the bands across the samples could be identified after a week of treatment, so the impact of the inhibitors on each type of cells within the sample was inconclusive (the ratio of AT/GC bands is 1.7 for control cells, 1.45 for DMSO-treated cells, 1.97 and 2.43 for NU7441-treated cells, 1.97 and 1.95 for AZD6738-treated cells and 1.2 and 1.63 for Rabusertib-treated cells).

After 21 days of treatment (Week 3), the number of bands detected on the AT allele (figure 5.11.B) had increased compared to Week 1 (figure 11.A), which indicated that the number of HCA2 cells had increased in the mixed-cell population. On the other hand, there were almost no bands at all detected on the GC allele, included the DMSO treated control (figure 11.B). This indicated that IMR90 cells had almost disappeared in the mixed-cell population.

Here, we have demonstrated that allele-specific STELA can be used to identify the presence of individual types of fibroblasts (that are homozygous) within the mixed population and we have confirmed that even though the starting population had a much lower number of HCA2 cells, the latter eventually replaced the IMR90 cells after three weeks of treatment. This is because by the end of day 21 of treatment, most IMR90 cells would have entered late crisis and died or were unable to grow.

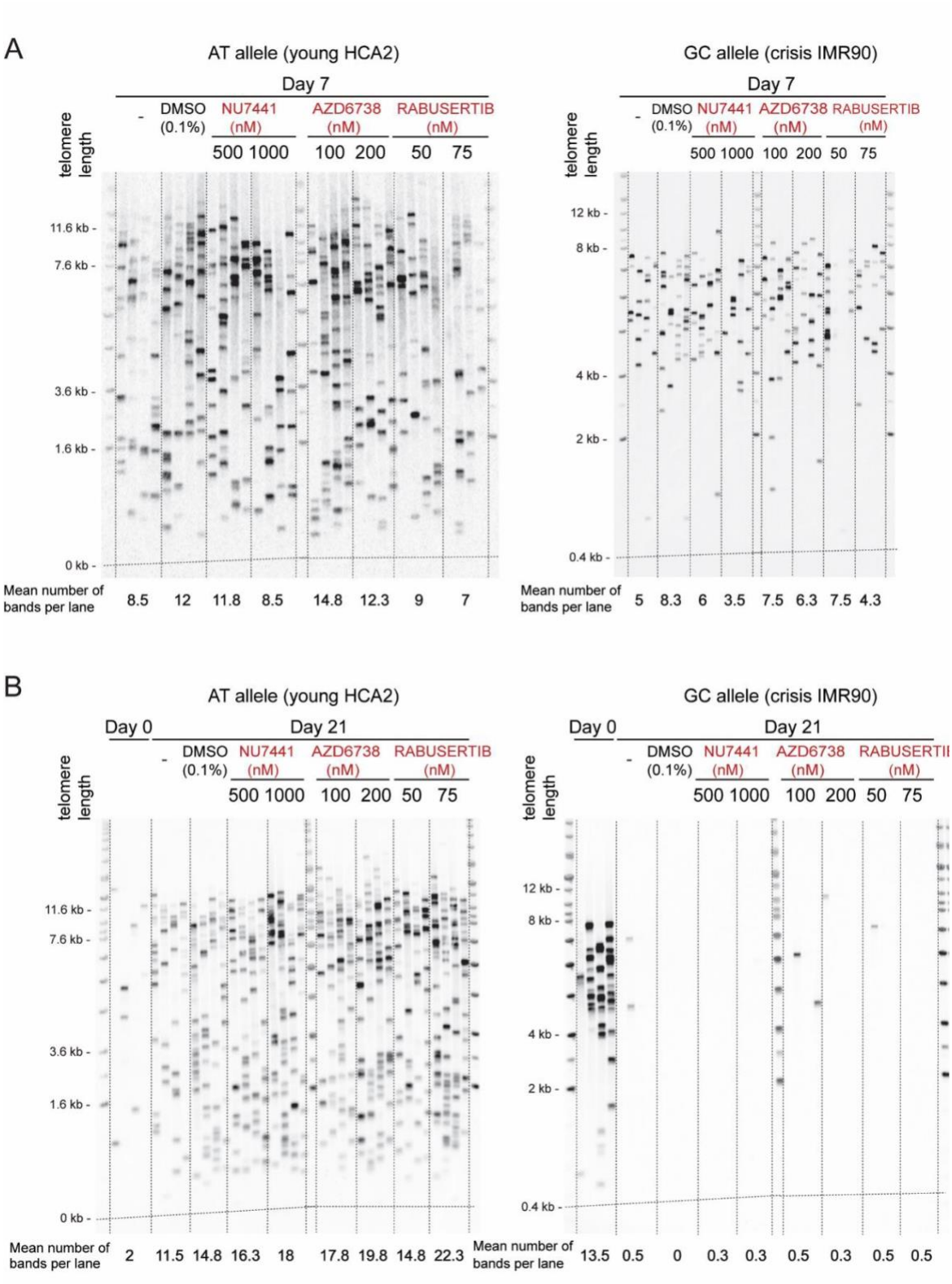

Figure 5.11: Allele-specific STELA analysis of young HCA2 (homozygous AT haplotype) mixed with old IMR90 (homozygous GC haplotype). The figure shows the allele-specific STELA analysis (the AT allele is shown on the left, the GC allele on the right) of the mixed population after one week of treatment (A) and after three weeks of treatment (B).

5.4.3.3 Long-term treatment of old HCA2 cells mixed with young IMR90 cells

Following the second experiment, we decided on the reversed mixed-cell population consisting of crisis HCA2 cells and young IMR90 cells. For this experiment, we did not include NU7441 but included three concentrations of AZD6738 and Rabusertib. The third experiment included three populations. The first population contained younger IMR90 cells (PD~63.9, entering early crisis) and the second population contained older HCA2 cells (PD~46.12, entering deep crisis) and they were treated for 32 days. The third population contained young IMR90 cells mixed with the old HCA2 cells (in a ratio of 1:2) and treated for 32 days. Each population had an untreated and a DMSO-treated sample serving as controls and three samples each treated with AZD6738 and Rabusertib. The inhibitors were added every two or three days at the same time for all samples. At day 10, 20 and 32 of treatment, the cells were counted and cell-cycle and apoptosis assays were performed to determine the growth rate, cell cycle progression and cell death respectively. A sample from the mixed cells was also collected for STELA analysis.

In IMR90 cells, all treated samples had similar cell growth to control cells except for cells treated with 500nM AZD6738 (5,000,000 cells), which showed a decreased cell growth compared to control cells (8,600,000) and cells treated with 500nM Rabusertib, which did not grow at all (figure 5.12.A). In HCA2 cells, 50nM AZD6738 did not affect cell growth and 50nM Rabusertib and 100nM AZD6738 reduced cell growth (1,360,000 and 1,430,000 compared to 1,660,000 control cells respectively) (figure 5.12.B). 100nM Rabusertib and 500nM AZD6738 reduced cell growth further (1,020,000 and 930,000 compared to 1,660,000 control cells respectively) and 500nM Rabusertib eliminated cell growth completely. In mixed cells, all treated samples had similar cell growth to control cells except for cells treated with 500nM AZD6738 (6,800,000 cells), which showed a decreased cell growth compared to control cells (8,800,000) and cells treated with 500nM Rabusertib, which showed no growth (figure 5.12.C). The growth curve of the mixed population is almost identical to IMR90 cells, since they represent the majority of the mixed population. Even though at day 0 the inoculation number was higher in HCA2 cells compared to IMR90 cells, at day 32 there were 8,600,000 untreated IMR90 cells and 1,660,000 untreated HCA2 cells (more than five times less).

HCA2 cells had a considerably different cell distribution compared to IMR90 cells (less cells in G0/G1 phase and more cells in G2, S and >4N phase), which was indicative that they were in deep crisis (figure 5.13). IMR90 cells treated with 100nM Rabusertib and 500nM AZD6739 had a slightly altered cell cycle distribution compared to control cells at all days (less cells in G0/G1 phase and more cells in G2, S and >4N phase). The most dramatic difference was observed in cells treated with 500nM Rabusertib at day 32 (less cells in G0/G1 phase and more cells in G2, S and >4N phase). HCA2 cells treated with 500nM Rabusertib and 500nM AZD6739 had an altered cell cycle distribution compared to control cells at day 10 and 20 respectively (less cells in G0/G1 phase and more cells in G2 and >4N phase).

Mixed cells treated with 50nM and 100nM Rabusertib and 500nM AZD6738 had a slightly altered cell cycle distribution at day 32 (less cells in G0/G1 phase and more cells in G2 and S phase), while cells treated with 500nM Rabusertib were affected dramatically, in a similar way to younger IMR90 cells. Overall, only the higher concentrations of AZD6738 and Rabusertib had a strong effect on cell cycle.

In IMR90 cells, apoptotic levels were relatively low (<32%) (figure 5.14.A). At day 10, 50nM Rabusertib, 100nM Rabusertib and 500nM AZD6738 slightly increased apoptosis by 6%, 3% and 6% respectively. At day 20, no major differences were observed between the IMR90 samples, while at day 32, all Rabusertib-treated samples increased apoptosis by 20%, 14% and 13%. In HCA2 cells, apoptotic levels were slightly higher compared to IMR90 cells, as they were in deep crisis (16% higher apoptosis in untreated HCA2 cells compared to untreated IMR90 cells at day 32) (figure 5.14.B). No 500nM Rabusertib-treated sample was collected due to the very low cell number. At day 10, 100nM Rabusertib strongly increased apoptosis by 23%. At day 20, 50nM and 100nM Rabusertib samples increased apoptosis by 4% and 29% respectively. At day 32, 50nM and 100nM Rabusertib and 100nM AZD6738 increased apoptosis by 6%, 18% and 10% respectively. In mixed cells, none of the AZD6738 concentrations affected apoptosis, while Rabusertib increased apoptosis at day 32 (by 28% when treated with 50nM and 43% when treated with 100nM) (figure 5.14.C). Overall, we have shown that Rabusertib increased apoptosis more in old IMR90 cells and the mixed-cell population compared to young IMR90 cells.

In conclusion, 50nM and 100nM Rabusertib did not have an impact on cell growth in IMR90 and mixed cells but decreased cell growth in HCA2 cells. It also increased apoptosis in all

cells but did not have a strong effect on cell cycle distribution. On the other hand, 50nM AZD6738 had no impact on cell growth, cell cycle and apoptosis in any of the cell populations, but 100nM AZD6738 slightly decreased cell growth and increased apoptosis only in HCA2 cells. 500nM AZD6738 decreased cell growth in all cell populations, but had a bigger impact on the cell cycle of HCA2 cells.

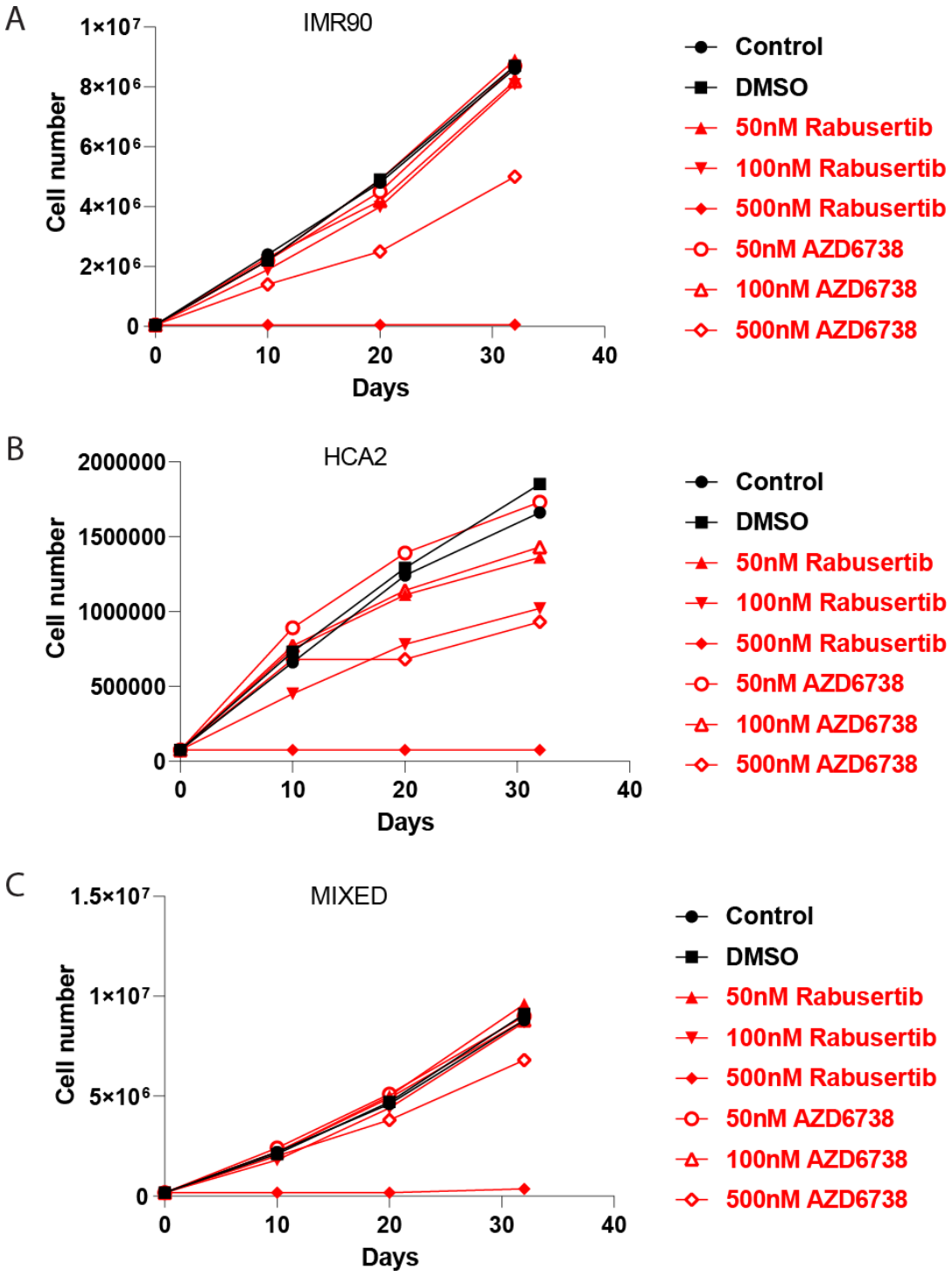

Figure 5.12: Cell growth of IMR90, HCA2 and mixed cells treated with AZD6738 and Rabusertib.

The figure shows the growth curve of IMR90 (A), HCA2 (B) and mixed HCA2 with IMR90 (C) treated for 32 days.

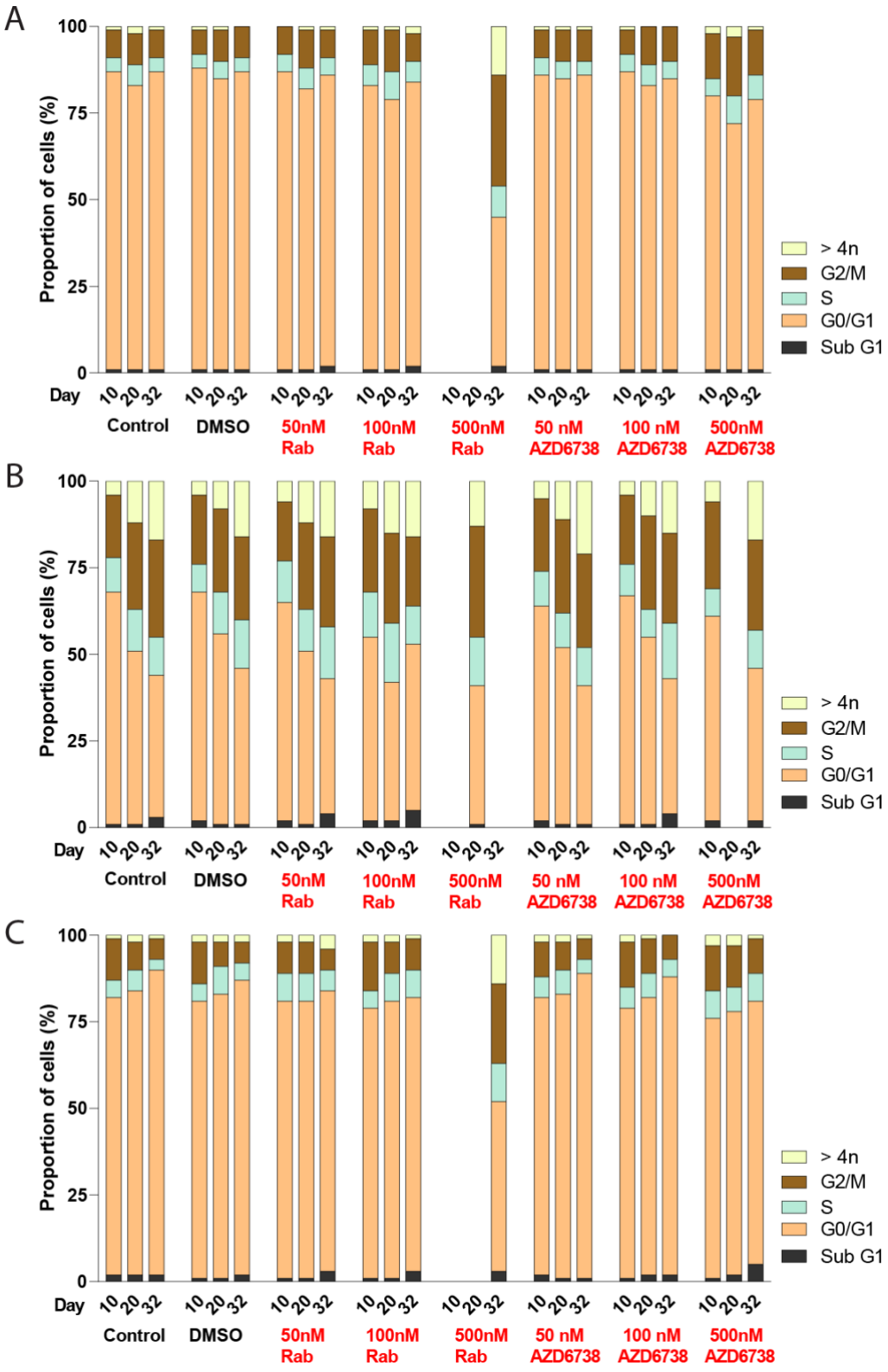

Figure 5.13: Cell cycle analysis of IMR90, HCA2 and mixed cells treated with AZD6738 and Rabusertib. The figure shows the cell cycle distribution of IMR90 (A), HCA2 (B) and mixed HCA2 with IMR90 (C) treated for 32 days.

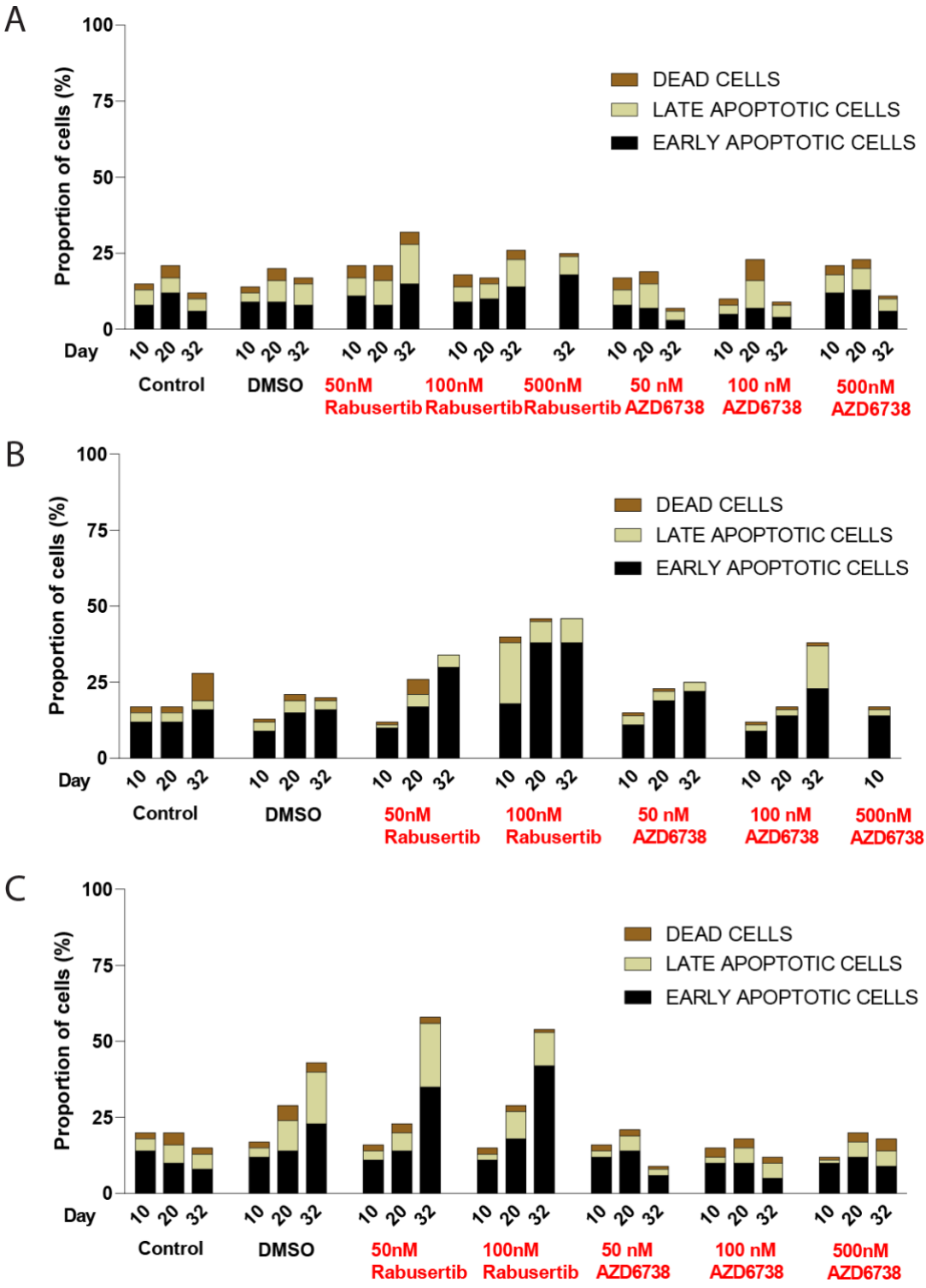

Figure 5.14: Apoptosis analysis of IMR90, HCA2 and mixed cells treated with AZD6738 and Rabusertib. The figure shows the apoptotic levels of IMR90 (A), HCA2 (B) and mixed HCA2 with IMR90 (C) treated with DMSO and two DDR inhibitors for 32 days. Apoptosis was analysed using Annexin-V/propidium iodide (PI) staining. Cells are classified as early apoptotic when they are Annexin V positive and PI negative, late apoptotic when they are Annexin V and PI positive and dead when they are Annexin V negative and PI positive.

We performed allele-specific STELA to assess the relative proportions of young and old cells in the mixed population. Consistent with the initiating 1:2 cellular ratio in week 0, there were more HCA2 cells than IMR90 cells as indicated by the number of bands detected on the AT and GC allele respectively (figure 5.15.C). After 10 days of treatment, there were still more bands on the AT allele (HCA2 cells) compared to the GC allele (IMR90 cells). No substantial differences in the number of the bands across the samples could be identified after ten days of treatment, so the impact of the inhibitors on each type of cells within the sample was not obvious (the ratio of AT/GC bands is 1.94 for control cells, 1.2 for DMSO-treated cells, 1.05, 1.8 and 1.67 for AZD6738-treated cells and 0.78 and 0.74 for Rabusertib-treated cells).

After 20 days of treatment, there were almost no bands at all detected on the AT allele (figure 5.15.B), which indicated that HCA2 cells had almost disappeared in the mixed-cell population. This is in accordance with the last experiment, where we observed the elimination of old IMR90 cells after 21 days of treatment (figure 5.11B). However, in this experiment, AZD6738-treated samples contained a higher number of bands on the AT allele compared to all other samples, indicating that AZD6738 may unexpectedly prolong the life of HCA2 cells undergoing crisis.

After 32 days of treatment, there were almost no bands at all detected on the AT allele (HCA2 cells) even in cells treated with AZD6738 (figure 5.15.C). However, many bands were detected on the GC allele (IMR90 cells). As expected, most HCA2 cells died or could not grow as a result of being in late crisis and the mixed population contained almost exclusively young IMR90 cells.

We have once again used allele-specific STELA to identify the presence of individual types of fibroblasts within the mixed population and we have confirmed that even though the starting population had a much lower number of IMR90 cells, they eventually replaced the HCA2 cells after 32 days of treatment. However, the effect, if any, of the AZD6738 and Rabusertib treatments could not be established.

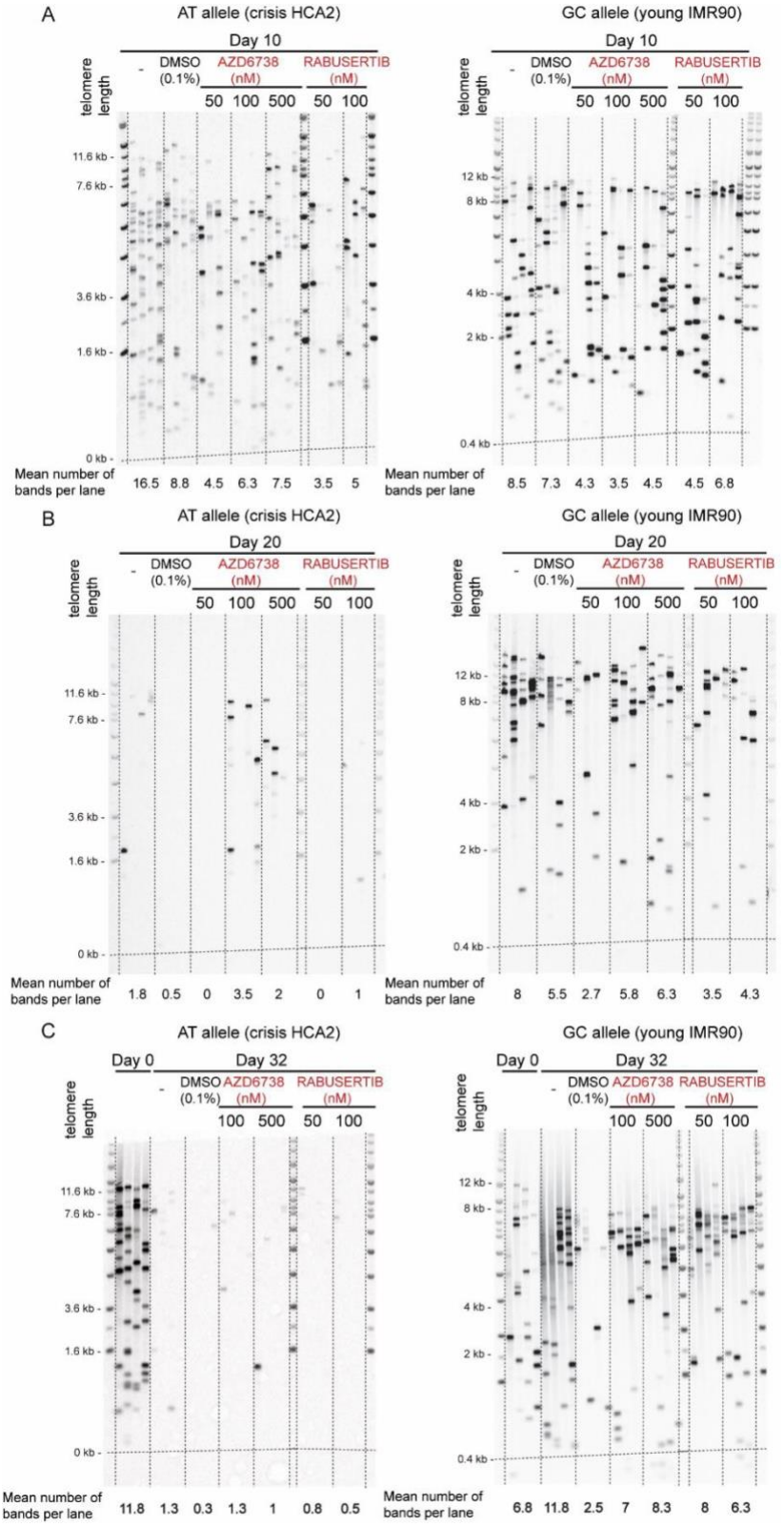

Figure 5.15: Allele-specific STELA analysis of old HCA2 (homozygous AT haplotype) mixed with young IMR90 (homozygous GC haplotype). The figure shows the allele-specific STELA analysis (the AT allele is shown on the left, the GC allele on the right) of the mixed population at day 10 of treatment (A), at day 20 of treatment (B) and at day 32 of treatment (C).

5.5 Discussion

5.5.1 Fibroblasts undergoing a telomere crisis are sensitive to Rabusertib

In the previous chapter, we demonstrated that 50nM Rabusertib prevented DN-hTERT HCT116 cells from escaping a telomere-induced crisis. Untreated HCT116 DN-hTERT cells reproducibly escape crisis by re-activating telomerase, which lengthens telomeres and stops telomere fusions (figures 4.1 and 4.2; Ngo et al, 2018). This prompted us to investigate how 50nM Rabusertib would affect telomere crisis in primary human cells. To test this, we examined primary IMR90 and HCA2 fibroblasts that bypass senescence and enter crisis but do not escape. Other studies have also used primary human fibroblasts to model telomere crisis (Nassour et al, 2019; Davoli and de Lange, 2012).

Treatment of IMR90 cells undergoing crisis with 50nM Rabusertib drastically reduced cell growth by ~62.23% from the onset of early crisis (PD 61.32) to the end of the experiment (PD 76.5 for control cells, late crisis, figure 5.2.A). This reduction was evident even before deep crisis, with a striking ~87% decrease in cell growth during early crisis (PD 69.3 for control cells). Even at a lower concentration of 12.5nM, Rabusertib induced a ~39.41% decrease in cell growth compared to control cells during crisis. Treatment with 50nM Rabusertib altered IMR90 cell cycle during crisis, showing 32% less cells in G0/G1 phase, 8% more cells in S phase, 11% more cells in G2 phase and 13% more cells in >4N phase at day 34 (figure 5.2.B). Similar trends were observed with 12.5nM Rabusertib at day 19 and 61 of treatment. In addition, at the same day, treatment with 50nM Rabusertib increased apoptosis by 22%, while 12.5nM Rabusertib increased apoptosis by 8% compared to control cells (figure 5.2.C).

Treatment of HCA2 cells undergoing crisis with 50nM Rabusertib drastically reduced cell growth by ~35.27% from the onset of early crisis (PD 38.42) to the end of the experiment (PD 58.47 for control cells, late crisis, figure 5.3.A). The inhibitor had also reduced cell growth even before deep crisis, showing ~64.1% reduction in cell growth during early crisis (PD 46.17 for control cells). In contrast, 12.5nM Rabusertib had no effect on cell growth. Interestingly, both in IMR90 and HCA2 cells undergoing crisis, 50nM Rabusertib had a similar

effect to 250nM NU7441, demonstrating the potency and efficiency of the inhibitor. Treatment with 50nM Rabusertib also altered the cell cycle of HCA2 cells undergoing crisis (figure 5.3.B). For example, at day 34 of treatment, there were 12% less cells in G0/G1 phase, 5% more cells in S phase and 6% more cells in >4N phase compared to control cells. Similar, but milder effects were observed with 12.5nM Rabusertib. Additionally, 50nM Rabusertib increased apoptosis by 4% at day 60 in crisis IMR90 cells, while 12.5nM Rabusertib increased apoptosis by 14% at day 60 compared to control cells (figure 5.3.C). Our results from the previous chapter showed that 50nM Rabusertib influenced DN-hTERT HCT116 cells during crisis by decreasing cell growth, altering cell cycle progression similarly to fibroblasts and increasing apoptosis, consistent with its effects on primary fibroblasts in crisis.

In the first and second mixing experiments, treatment with 50nM Rabusertib did not affect cell growth, cell cycle progression or apoptosis in older IMR90 cells (figures 5.4-5.10). However, a caveat of these experiments is that the effect of Rabusertib on older IMR90 cells was only monitored for 7 days, which did not provide enough time to see the full impact of Rabusertib on these cells. In the third mixing experiment, treatment with 50nM Rabusertib did not affect the growth of younger IMR90 cells or mixed cells, but it decreased the cell growth of older HCA2 cells by ~18.07% (figure 5.12). Treatment with 100nM Rabusertib also specifically decreased the growth of older HCA2 cells by ~ 38.55%. Treatment with 50nM Rabusertib did not have an effect on cell cycle progression but increased apoptosis in all populations (figure 5.14). Treatment with 100nM Rabusertib specifically increased apoptosis in older HCA2 cells (by 23% at day 10, 29% at day 20 and 18% at day 32), but not in the other populations. Overall, we have shown that 50nM Rabusertib and 100nM Rabusertib selectively reduced growth in cells with shorter telomeres and 100nM Rabusertib selectively increased apoptosis in these cells. However, we could not detect specific killing of older fibroblasts in a mixed population (further discussed below).

The observation that primary fibroblasts with short dysfunctional telomeres are sensitive to Rabusertib support the hypothesis that the ATR-CHK1 pathway is essential for cell survival during crisis. As CHK1 is mainly responsible for inducing repair during S-phase replication, CHK1 inhibition as a single agent is thought to be toxic to cells in S phase by increasing endogenous replication stress (Warren and Eastman, 2020). This is supported by our results,

as Rabusertib increased G2/M accumulation and increased apoptosis in primary fibroblasts. In the previous chapter we showed that 5μM Rabusertib increased CHK1-S345 and CHK2-T68 and decreased CHK1-S296 levels. This supports previous findings that Rabusertib reduces CHK1 autophosphorylation at S296 and upregulates CHK1 phosphorylation at S345 in human cancer cells, by the amplification of ATR/ATM signalling (Wang et al, 2014). The fact that 50nM Rabusertib reduced but did not inhibit CHK1 S296 autophosphorylation suggests that the inhibitor may also activate the DDR in other yet-to-be-understood pathways (Wang et al, 2014).

5.5.2 Fibroblasts undergoing a telomere crisis are not sensitive to AZD6738

In the previous chapter, we demonstrated that 50nM AZD6738 slowed down DN-hTERT HCT116 cells from escaping a telomere-induced crisis. We have shown that 50nM AZD6738 only affects colorectal cancer cells with short dysfunctional telomeres and not wild-type cells and that provides a clue that the ATR-CHK1 pathway plays an important role in keeping the cells alive during a telomere-induced crisis. In this study, we set to understand how 50nM AZD6738 would affect primary human fibroblasts undergoing crisis.

Treatment of IMR90 cells undergoing crisis with 50nM AZD6738 had a minimal overall effect, showing only an 8.11% decrease in cell growth by the end of the experiment (PD 76.5 for control cells, late crisis, figure 5.2.A). The inhibitor slightly affected the cell cycle at day 34, with 5-7% less cells in G0/G1 phase and 4-5% more cells in G2/M phase compared to control cells, but had no impact at day 77 (figure 5.2.B). In addition, there was a slight 5% increase in apoptosis at both day 34 and 77 in crisis IMR90 cells (figure 5.2.C). Treatment with 50nM AZD6738 also minimally impacted HCA2 cells undergoing crisis, showing no effect on cell growth compared to control cells by the end of the experiment (PD 58.47 for control cells, late crisis, figure 5.3.A). In addition there was no effect on the cell cycle and only a slight increase in apoptosis by 5% at day 60 and by 2% at day 77 (figure 5.3.C). Our results from the previous chapter showed that 50nM AZD6738 affected DN-hTERT HCT116 cells during crisis by decreasing cell growth, altering cell cycle progression and by potentially increasing apoptosis (in two out of three experiments) (figures 4.6-4.8). However, these

effects were not as strong as those induced by 50nM Rabusertib. In this chapter, we demonstrate similar but milder changes in crisis IMR90 cells, but not in crisis HCA2 cells.

The mixing experiments consistently showed that 50nM AZD6738 did not affect cell growth, cell cycle or apoptosis in younger cells, crisis cells and mixed young-crisis cells (figure 5.4-5.15). Treatment with 100nM AZD6738 did not affect older IMR90 cells in the seven-day treatment, but in the 32-day treatment, it slightly decreased cell growth by approximately 13.86% and increased apoptosis by 10% at day 32 in older HCA2 cells (figures 5.12-5.14). Treatment with 500nM AZD6738 decreased cell growth and altered cell cycle progression in all populations. As suggested in the previous chapter, in future experiments, it may be useful to investigate higher concentrations of 50nM AZD6738 in their ability to influence cells undergoing a telomere crisis. However, given the high potency of the inhibitor, it would be difficult to find the appropriate concentration that has a strong effect on cells undergoing crisis and is not toxic to wild-type cells. We have shown that a concentration of 100nM AZD6738 only has a weak effect on cells undergoing deep crisis and a high concentration of 500nM AZD6738 is expected to be toxic for all cells and not only cells undergoing crisis (figure 3.2).

In the previous chapter, we tried to answer why AZD6738 did not prevent cells from escaping crisis but only slowed them down. When we investigated the expression of molecular DNA damage markers, we observed that in WT-HCT116 cells, 5µM AZD6738 increased CHK1-S345 and CHK1-S296 levels, indicating that CHK1 was still active despite inhibiting ATR. We hypothesised that after ATR inhibition, ATM was upregulated to compensate for ATR loss, which phosphorylated CHK1 at S345 leading to CHK1 autophosphorylation at S296. This hypothesis was also supported by the upregulation of ATM downstream effector CHK2-T68. Min et al, (2017) assessed AZD6738 on gastric cancer cells and in a xenograft mouse model and proposed that ATM activation is the main mechanism of resistance to AZD6738, as they observed that the ATM-CHK2 signalling was activated when ATR was inhibited. Other studies have observed increased CHK1-S345 levels or upregulation of ATM in cancer cells after AZD6738 treatment (Isono et al, 2022; Wallez et al, 2018). These findings also extend to other ATR inhibitors. For example, Reaper et al (2011) used VE-821, another highly selective ATR inhibitor to show that impairing ATM

signalling increases sensitivity to ATR inhibition because in the absence of ATR, ATM is activated as a compensatory response. They proposed a model in which ATR suppression leads to activation of an S phase checkpoint by ATM that restricts replication and the production of DSBs. Lee and Dutta (2021) also showed that ATM activates CHK1 leading to phosphorylation of ASF1A (S166) and NHEJ repair in G1 phase at DNA double strand breaks. It is likely that in this study, fibroblasts undergoing crisis were not sensitive to AZD6738 because ATM was upregulated to compensate for ATR loss.

Ditano et al (2021) compared sensitivity of multiple cell lines to MK-8776 (CHK1i) and AZD6738 and found out that there was a different profile of sensitivity between ATRi and CHK1i. They reported that ATM knockout cells were strongly sensitive to ATRi and were much less efficient at arresting in S phase, while even low levels of ATM expression did not confer sensitivity to ATRi. However, no such observations were made in regards to CHK1 inhibition. Although there are studies that show that ATM inhibition combined with CHK1 inhibition induces synthetic lethality in cancer cells (Tozaki et al, 2023), association between CHK1i resistance and upregulation of ATM is reported less frequently in literature (Ando et al, 2019).

Given these observations, using ATR inhibitors to inhibit CHK1 in cells undergoing crisis may be accompanied by risk as it might have the opposite effect, due to ATM upregulation. In this case, ATR inhibitors would have to be used in conjunction with ATM inhibitors to ensure that DNA is not repaired when ATR is inactivated. In fact, Min et al, (2017) found that ATR inhibition by AZD6738 is synthetically lethal with ATM deficiency in gastric cancer cells. Instead, using CHK1 inhibitors to inhibit CHK1 may a be more direct and efficient way to achieve the desirable result. The observations of this study – that fibroblasts undergoing deep crisis are sensitive to 50nM Rabusertib but not to 50nM AZD6738 even though they inhibit the same pathway – further support our hypothesis.

5.5.3 Allele-specific STELA offers the potential to identify cells within a mixed population

To investigate the influence of the inhibitors specifically in older fibroblasts with shorter telomeres compared to younger fibroblasts with longer telomeres in a mixed-cell

population, we carried out allele-specific STELA. We used heterozygosities (−427G/A and −415C/T in DNA adjacent to the XpYp telomere) to detect the AT haplotype and the GC haplotype (Baird et al, 2003). As HCA2 cells are homozygous for the AT haplotype and IMR90 cells are homozygous for the GC haplotype (figure 5.1), their detection is possible because PCR amplification of the AT allele can only be derived from HCA2 cells and PCR amplification of the GC allele can only be derived from IMR90 cells. In addition, STELA is quantifiable through band counting, which increases sensitivity in our analysis.

In all mixing experiments, we started (day 0) with more old (in deep crisis) cells than young (in early crisis) cells, which was indicated by the number of bands detected on the AT and GC allele (figures 5.7, 5.11 and 5.15). After approximately a week of treatment, there was a similar number of bands in the AT and the GC allele indicating that the amount of each type of cells was approximately equal in the mixed sample. After three or more weeks of treatment, older cells almost disappeared as bands would be barely detectable on the appropriate allele, while younger cells made up almost the entire sample. This was expected, as younger cells would grow faster, while older cells could not grow as a result of being in late crisis. These observations confirmed the initial ratio of older to younger cells and that older cells would be deeper in crisis compared to younger cells, due to their limited growth that ceased after three weeks as predicted by their PD, validating the use of this technique to identify the cell populations.

However, no striking differences were detected between the inhibitor-treated samples and the control cells in any of the experiments. Overall, there was a slight variation in the number of bands, such as DMSO-treated cells sometimes having less bands compared to untreated cells, which could be a result of the random sampling of single telomeres. The only clear observation was that at day 20 in mixing experiment 3, there were more live old HCA2 cells treated with AZD6738 than control cells. Intriguingly, AZD6738 not only did not affect cells undergoing crisis, but it may also prolong their survival, possibly through re-activation of ATM as discussed earlier. In future experiments, STELA analysis could be performed more frequently to cover more timepoints. For example in figure 5.15, between day 10 and the following analysis at day 20, the older cells had almost disappeared entirely from the mixed sample. A STELA analysis between day 10 and 20 would have shed more light on the effect of the inhibitors on the older cell population. In addition, future studies

can also perform Western Blot analysis on the fibroblasts to confirm the molecular mechanisms of the inhibitors and verify the upregulation of ATM following ATR inhibition.

The methodology we used is designed to identify cells in the mixed population, based on our knowledge of the genotypes of HCA2 and IMR90, and allele-specific STELA is an established method for allele differentiation. A limitation of this technique is that it would not be able to accurately identify cells that have a heterozygous haplotype. However, allele-specific STELA could be used to analyse other polymorphic loci throughout the genome. Another way to identify the cells in the mixing experiments could be by using allele-specific qPCR. In this approach, allele-specific qPCR primers and fluorophores are designed for the AT and GC haplotypes. The fluorescence signal is measured during qPCR to quantify the amount of each allele, allowing for identification of HCA2 and IMR90 cells (Lee et al, 2016). In addition, labelling the cells with dyes could have been used as a method for detecting the cells. In this approach, HCA2 and IMR90 cells are labelled with different genotype-specific dyes and fluorescence microscopy is used to visualise these dyes (Pradhan et al, 2023).

5.5.4 Conclusion

In this study we have shown that 50nM Rabusertib (CHK1i) reduced cell growth, altered cell cycle distribution and elevated apoptosis in primary fibroblasts undergoing telomere crisis. The same concentration also appeared to reduce cell growth in HCA2 fibroblasts with shorter telomeres but not in IMR90 fibroblasts with longer telomeres, while 100nM Rabusertib acted specifically to elevate apoptosis only in HCA2 cells with shorter telomeres. Primary fibroblasts undergoing telomere crisis did not appear to be sensitive to 50nM AZD6738 (ATRi), which also did not affect cells with shorter telomeres differently compared to cells with longer telomeres. While both inhibitors target the same pathway (ATR-CHK1), which is crucial for keeping cells alive during crisis, it is likely that when ATR is inhibited, CHK1 activity is restored by ATM. These observations suggest that the use of CHK1 inhibitors instead of ATR inhibitors may be more effective to kill cells undergoing a telomere crisis.

Chapter 6

General Discussion

6.1 Summary

The aim of this thesis was to investigate the ability of eight DDR inhibitors, targeting different DDR pathways, to inhibit escape from a telomere-driven crisis and determine how they affect the cells during crisis.

Chapter 3 investigated which of these inhibitors influenced cell viability during crisis in colorectal cancer cells. We identified three inhibitors that did not have any impact; 6-0H-DOPA (RAD52i), RI-1 (RAD51i) and Adavosertib (WEE1i) and three inhibitors that may eliminate cells during crisis; Rabusertib (CHK1i), AZD6738 (ATRi) and NU7441 (DNA-PKi). Our study of L189 (LIG1,3,4i) and KU-60019 (ATMi) activity on escape from telomere crisis was inconclusive. We selected 50nM Rabusertib and 50nM AZD6738 to further investigate in the following chapter, due to their promising activity at such a low concentration.

Chapter 4 confirmed that 50nM Rabusertib and 50nM AZD6738 influenced the ability of the HCT116 cells to escape a telomere crisis and assessed their mechanism of action. We found that Rabusertib (and AZD6738 to a lesser degree) affected cell growth, cell cycle progression, apoptosis and telomere fusion during late crisis. The inhibitors did not have an impact on telomere length before or during crisis. We also showed that the action of both inhibitors was specific to cells undergoing crisis, as they had no effect on WT cells. Both inhibitors activated the DNA damage response, although unexpectedly, AZD6738 increased CHK1 activity. The fact that AZD6738 slowed down escape from crisis, but did not completely kill cells experiencing crisis, along with the observation that CHK1 activity was upregulated, suggest that a compensatory mechanism may have been activated following ATR inhibition.

Chapter 5 examined how Rabusertib and AZD6738 affected primary fibroblasts undergoing crisis. We determined that Rabusertib decreased cell growth, altered cell cycle progression and increased apoptosis in primary fibroblasts undergoing telomere crisis, while AZD6738 did not have a strong effect. Rabusertib also reduced cell growth and increased apoptosis in older HCA2 fibroblasts but not in younger IMR90 fibroblasts in a mixed population of young

and old fibroblasts. These results confirmed that although both inhibitors target the ATR-CHK1 pathway, CHK1 inhibition was more effective than ATR inhibition for impairing cell viability during crisis.

6.2 Discussion

6.2.1. NU7441 may impair escape of DN-HCT116 cells from crisis while 6-OH-DOPA, RI-1 and Adavosertib showed no impact

HCT116 DN-hTERT cells treated with 0.3µM and 1µM 6-OH-DOPA escaped crisis and 6-OH-DOPA did not affect cell growth, cell cycle progression or apoptosis before crisis (figure 3.11). After escape from crisis, 6-OH-DOPA slightly decreased cell growth (by ~5PD) and slightly increased apoptosis (by 8-10%) compared to control cells. 6-OH-DOPA inhibits RAD52, which plays a role in single strand annealing and DNA replication and is a non-essential accessory factor of homologous recombination (Rossi et al, 2021; Balboni et al, 2023). It has been demonstrated that BRCA2-deficient cells require RAD52 to survive as it assumes the role of BRCA2 when it is not active (Balboni et al, 2023). As RAD52 inhibition has mostly been shown to selectively kill BRCA-deficient cancer cells (Chandramouly et al, 2015) and HCT116 cells are BRCA-proficient, RAD52 inhibition would neither have inhibited HR nor sufficiently increased DNA damage during crisis. Testing concentrations higher than 1µM 6-OH-DOPA might not be practical for drug administration.

HCT116 DN-hTERT cells treated with 1.5µM RI-1 escaped crisis and RI-1 did not influence cell growth, cell cycle progression or apoptosis prior to crisis (figure 3.18). RI-1 inhibits RAD51, which is important for maintaining genomic stability and overcoming replication stress and is the principal catalyst of HR (Wassing and Esashi, 2021). However, it has been demonstrated that alterations in the RAD51 pathway do not have a significant impact on the effectiveness of double-strand break repair (DSBR) in mammalian cells, as cells shift to a different DSBR pathway that does not involve RAD51, such as SSA (Lambert and Lopez, 2000). An alternative hypothesis would be that homologous recombination is not crucial for maintaining cell viability during crisis. Testing RI-1 concentrations higher than 1.5µM might not be practical for drug administration.

HCT116 DN-hTERT cells treated with 50nM, 75nM and 100nM Adavosertib escaped crisis and Adavosertib reduced cell growth, altered cell cycle progression and increased apoptotic levels prior to crisis (figures 3.5, 3.21). Adavosertib inhibits WEE1, which is crucial for G2/M checkpoint regulation to inhibit mitotic entry after DNA damage (Bukhari et al, 2022). It has

been demonstrated that resistance to Adavosertib could arise by a decrease in CDK1 levels (the substrate for WEE1 inhibition) or elevation of CHK1 (via mTOR and PERK pathways) to reestablish G2/M arrest (Gomez et al, 2022). In support of this hypothesis, we observed a striking accumulation of 50nM Adavosertib-treated cells in G2/M phase, after escape from crisis, indicating that G2/M arrest had been restored (figure 3.6.C). Testing concentrations higher than 100nM Adavosertib, which reduced cell growth prior to crisis, would be challenging as higher concentrations might kill cells before entering crisis.

HCT116 DN-hTERT cells treated with 0.5µM NU7441 escaped crisis, while cells treated with 1µM and 1.5µM NU7441 failed to escape (figures 3.4, 3.15, 3.24). NU7441 had a concentration-dependent effect on cell growth, altered cell cycle progression and increased apoptosis prior to crisis. NU7441 inhibits DNA-PKcs, an essential component of NHEJ that facilitates the processing and ligation of double-strand breaks (Mohiuddin and Kang, 2019). In addition, DNA-PK contributes to other cell survival and proliferation pathways, it is crucial for maintaining telomeres by aiding telomere end-capping and preventing fusion and it may influence cell cycle machinery in response to DNA damage (Yang et al, 2016; Mohiuddin and Kang, 2019). Our results showed that NU7441 may influence the ability of DN-hTERT HCT116 cells to escape a telomere-driven crisis, indicating that the function of DNA-PK is important for cell survival during telomere crisis. However, we did not investigate NU7441 further, as other inhibitors appeared promising at lower concentrations. Future experiments could confirm if NU7441 prevents cells from escaping a telomere-driven crisis.

Overall, 1µM 6-0H-DOPA, 1.5µM RI-1 and 100nM Adavosertib failed to prevent cells from escaping crisis, indicating that RAD51, RAD52 and WEE1 are not essential for maintaining cell viability during a telomere-driven crisis. Alternatively, the inhibitors might not have been active in these cells, so future studies will be needed to test their molecular function. In addition, 1µM NU7441 may kill cells experiencing a telomere crisis, though additional experiments are required for confirmation.

6.2.2 AZD6738 impaired escape of DN-HCT116 cells from crisis but did not strongly affect fibroblasts undergoing crisis

AZD6738 inhibits ATR, which is important in regulating the intra S-phase and G2/M cell cycle checkpoint and modulating the DNA replication stress response (Sundar et al, 2017). Our experiments showed that HCT116 DN-hTERT cells treated with 50nM AZD6738 either failed to escape crisis (figure 3.23) or escaped crisis more slowly than control cells (figure 4.2). AZD6738 did not strongly affect cell growth, cell cycle progression or apoptotic levels prior to crisis. However, when AZD6738-treated cells escaped crisis, they exhibited high apoptotic levels and an altered cell cycle for a longer period compared to control cells. It is likely that treatment with a higher concentration of the inhibitor may completely kill cells undergoing crisis.

Treatment of IMR90 cells undergoing crisis with 50nM AZD6738 did not strongly influence cell growth (8.11% decrease compared to control cells), cell cycle progression and apoptosis (figure 5.2). Similarly, treatment of HCA2 cells undergoing crisis with 50nM AZD6738 also failed to strongly affect cell growth, cell cycle progression and apoptosis (figure 5.3). Treatment with 100nM AZD6738 only slightly decreased cell growth in HCA2 cells undergoing crisis by approximately 13.86% and increased apoptosis by 10% (figures 5.12 and 5.14). Treatment with 500nM AZD6738 decreased cell growth in both younger and older fibroblasts, due to drug toxicity. Intriguingly, we observed that in a mixed population of younger IMR90 and older HCA2 fibroblasts, older cells treated with AZD6738 survived better than control cells at day 20 of treatment (figure 5.15). This is suggestive of a resistance mechanism that the fibroblasts might have developed after treatment.

Treatment of WT-HCT116 cells with 50nM AZD6738 for 111 days did not affect cell growth, cell cycle progression or apoptosis (figure 4.5), as confirmed by other studies in literature (Harata et al, 2023; Dillon et al, 2017). As shown by our previous observations, we confirmed that treatment of DN-hTERT HCT116 cells with 50nM AZD6738 did not have a strong effect on cell growth, cell cycle progression and apoptosis prior to deep crisis, but had a mild effect on them during crisis (figures 4.6-4.8). The inhibitor did not affect the rate of telomere erosion before or during crisis, but it may slightly increase fusion during crisis

(figures 4.9, 4.10). These observations suggest that AZD6738 acted selectively on cells undergoing crisis at the time of crisis by mildly affecting cellular properties (cell growth, cell cycle, cell death).

In WT-HCT116 cells, 5µM AZD6738 elevated CHK2-T68, Gamma H2AX, CHK1-S345 and CHK1-S296 expression and combined AZD6738 and bleomycin treatment elevated CHK1-S345 levels, compared to treatment with bleomycin alone (figure 4.11 B,C). Increased CHK2-T68 and Gamma H2AX suggested that AZD6738 activated the DNA damage response. However, it has been demonstrated in literature that AZD6738 suppresses both CHK1 autophosphorylation at S296 and CHK1 phosphorylation at S345, which we did not detect (Moiseeva et al, 2019; Vendetti et al, 2015). The most likely explanation that CHK1 was still active would be an upregulation of ATM, as a compensation for ATR loss, which phosphorylated and activated CHK1. This hypothesis was also supported by the increase of ATM downstream effector CHK2-T68 expression (figure 4.11). However, multiple studies have shown that ATR inhibition (by AZD6738 or other inhibitors) triggers strong ATM-dependent signalling to compensate for ATR inhibition, which would re-activate the cell cycle checkpoints and allow for DNA repair (Min et al, 2017; Isono et al, 2022; Wallez et al, 2018; Reaper et al, 2011). We propose that impairing the ATR-CHK1 pathway elevated DNA damage which in combination with telomere damage, initially killed the cells. However, following a possible ATM upregulation, CHK1 expression was increased which allowed escape from crisis by repairing the DNA damage. As even reduced ATM expression does not confer sensitivity to ATRi, complete suppression of ATM activity would be necessary for sensitivity to ATR inhibition (Ditano et al, 2021). This means that AZD6738 would have to be used with an ATM inhibitor to avoid activation of CHK1 activity.

Overall, AZD6738 increased DNA damage, but it increased CHK1 activity, which possibly led to repair of DNA damage that it initially caused. Despite the seeming emergence of resistance to AZD6738, the ATR inhibitor dramatically slowed down escape of DN-HCT116 cells from crisis and maintained high levels of apoptosis after escape. This provides strong evidence that the ATR-CHK1 pathway is crucial for cell survival during a telomere-driven crisis.

6.2.3 Rabusertib killed DN-HCT116 cells experiencing crisis and reduced the growth of fibroblasts undergoing crisis

Rabusertib inhibits CHK1, which is downstream of ATR (in the same pathway) and modulates the intra S-phase and G2/M cell cycle checkpoint (King et al, 2013). Our experiments showed that HCT116 DN-hTERT cells treated with 50nM Rabusertib, as well as concentrations as low as 12.5nM Rabusertib, consistently failed to escape crisis (figures 3.15, 3.20, 4.1). Rabusertib did not affect cell growth or cell cycle progression strongly, but in some experiments, it slightly increased apoptotic levels just before cells entered crisis.

Treatment of IMR90 cells undergoing crisis with 50nM Rabusertib strongly decreased cell growth by 61.32% compared to control cells and even 12.5nM Rabusertib decreased cell growth by 39.41% compared to control cells (figure 5.2). 50nM Rabusertib also had a strong effect on cell cycle distribution (32% less cells in G0/G1 phase) and strongly increased apoptosis (by 22%) in IMR90 cells undergoing crisis. Treatment of HCA2 cells undergoing crisis with 50nM Rabusertib decreased cell growth by 35.27% compared to control cells, altered the cell cycle distribution (12% less cells in G0/G1 phase) and slightly increased apoptosis (figure 5.3). Treatment with 50nM Rabusertib and 100nM Rabusertib selectively decreased the cell growth of older HCA2 cells by approximately 18.07% and 38.55% respectively, while they did not affect younger IMR90 cells. Treatment with 100nM Rabusertib also selectively increased apoptosis (by 18-29%) in older HCA2 cells, but not in younger IMR90 cells. However, we could not detect specific killing of older fibroblasts in a mixed population of younger and older fibroblast cells undergoing crisis.

Treatment of WT-HCT116 cells with 50nM Rabusertib for 111 days did not affect cell growth, cell cycle progression or apoptosis (figure 4.4), as confirmed by other studies in literature (Paculova et al, 2017; Suzuki et al, 2022). As shown by our previous observations, we confirmed that treatment of DN-hTERT HCT116 cells with 50nM Rabusertib did not have a strong effect on cell growth, cell cycle progression and apoptosis prior to crisis (figures 4.6-4.8). However, Rabusertib decreased cell growth, affected cell cycle progression and increased apoptosis during crisis (figures 4.6-4.8). The inhibitor did not affect the rate of telomere erosion before or during crisis but cells treated with Rabusertib experienced a

higher number of fusion events during crisis compared to control cells (figures 4.9, 4.10). These observations suggest that the inhibitor acted selectively on cells undergoing crisis at the time of crisis by affecting cellular properties (cell growth, cell cycle, cell death and possibly telomere dynamics).

In WT-HCT116 cells, 5μM Rabusertib elevated CHK1-S345 and CHK2-T68 expression levels and combined Rabusertib and bleomycin treatment elevated CHK1-S345 expression, compared to treatment with bleomycin alone (figure 4.11.B,C). Combined Rabusertib and bleomycin treatment reduced CHK1-S296 expression compared to cells treated only with bleomycin in one of the two experiments, while the other experiment was inconclusive (figure 4.11.B). Our results are similar to other studies investigating the molecular mechanism of Rabusertib (Wang et al, 2014). Elevation of CHK1 (S345) levels following CHK1 inhibition happens because the DNA damage buildup amplifies ATR/ATM signalling, which consequently upregulates phosphorylation of CHK1 (S345), CHK2 (T68) and H2AX (Parsels et al, 2011). Interestingly, it has been observed that 1μM Rabusertib does not block completely CHK1(S296) phosphorylation, indicating that the inhibitor may activate the DDR regardless of CHK1 inhibition (Wang et al, 2014). According to our results, 5μM Rabusertib also did not completely supress CHK1(S296) phosphorylation (figure 4.11.B). We propose that Rabusertib activated the DDR response and impaired the ATR-CHK1 pathway, which increased DNA damage and killed cells undergoing crisis that were already experiencing telomere damage.

One of two experiments showed that the conversion of LC3-I to LC3-II was more efficient in DN-hTERT HCT116 cells compared to WT cells (figure 4.12.D), indicating that telomere damage during crisis may trigger autophagy, which has been already demonstrated in literature (Nassour et al, 2019). Although we did not detect any differences in autophagy between inhibitor-treated cells and control DN-hTERT HCT116 cells, it has been shown that Rabusertib induces autophagy (Wang et al, 2014). It is possible that autophagy triggered by Rabusertib and autophagy triggered during telomere crisis, synergised to kills cells undergoing crisis.

Studies have shown that Rabusertib suppresses autophosphorylation of CHK1 at Ser296, inhibiting phosphorylation of CHK1 substrates and the activation of G2/M DNA damage

checkpoint, leading to apoptosis and autophagy (King et al, 2014; Wang et al, 2014). In addition, CHK1 inhibition as monotherapy is considered to be cytotoxic in S phase by increasing endogenous replication stress (Warren and Eastman, 2020). Interestingly, CHK1 has also been shown to participate in DNA resection at dysfunctional telomeres, so it is possible that Rabusertib may increase DNA damage by impairing DNA resection (Holstein et al, 2017). Rabusertib may also trigger the DNA damage response independently of CHK1 inhibition (e.g. via MAPK signalling pathway) (Wang et al, 2014).

Overall, CHK1 inhibition killed DN-HCT116 cells undergoing crisis and was cytotoxic to fibroblasts undergoing crisis. These results further support that the ATR-CHK1 pathway is essential for keeping cells alive during a telomere-driven crisis. We have shown that Rabusertib was more efficient at killing cells experiencing a telomere crisis compared to AZD6738.

The transition from normal to cancerous cells is thought to happen through a multistep process that allows them to bypass at least two proliferative barriers: senescence (M1) and crisis (M2) (Nassour et al, 2021). Senolytics are drugs that specifically target and eliminate senescent cells by inducing apoptosis (Kirkland et al, 2017; Kirkland and Tchkonia, 2020). While many drugs with senolytic properties have been reported, only two drugs (olaparib, rucaparib) were previously described to selectively eliminate cells experiencing telomere crisis (Ngo et al, 2018). In our study, we demonstrated that another drug, Rabusertib, exhibits this property, acting as a crisolytic agent.

6.3 Future Directions

6.3.1 Future studies with ATRi

In order to explore the full potential of AZD6738, future research could examine concentrations higher than 50nM but lower than 150nM, which increases toxicity in WT cells. In addition, to verify that the elevated CHK1 activity resulting from AZD6738 treatment was due to a compensatory mechanism, instead of lack of ATR specificity, future Western Blot experiments could be conducted. The experiments could test for ATM or DNA-PK activation by including markers such as ATM-S1981, ATM, DNA-PKcs-S2056 and DNA-PKcs. The inclusion of more DDR markers (total ATR, ATR-S428, p53-S15 and CHK1-S317) could shed more light on the molecular mechanism of the inhibitor.

6.3.2 Future studies with CHK1i

In our study we only studied one cancer cell line. Future studies could investigate the effect of CHK1 inhibition on different cancer cell lines. We also used HCT116 cells, which are cancer cells that have been driven back to telomere crisis and escape. Hence, it would be important to assess whether Rabusertib would have the same effect on human precancerous cells undergoing a telomere crisis, extending beyond primary human fibroblasts. Studies could also be extended to pre-cancerous cells with eroded telomeres from early-stage patients.

Rabusertib was tested in clinical trials for pancreatic cancer and non small cell lung carcinoma, but was discontinued because it did not show any clinical advantage when used in combination with pemetrexed or gemcitabine (Gorecki et al, 2021). If future studies confirm the activity of Rabusertib in human pre-cancerous cells with eroded telomeres, further clinical evaluation of Rabusertib may be continued as a potential treatment for patients in the early stages of tumour progression. Alternatively, CHK1 inhibitor prexasertib can be used in further studies, as it has entered trials as a monotherapy with promising potential (Gorecki et al, 2021).

6.3.3 Future studies with other DDRi

Previous studies from our lab have shown that HCT116 cells undergoing crisis require i) LIG3 activity, which is considered necessary for A-NHEJ and ii) PARP1 activity, which also participates in A-NHEJ and in SSBR and telomere maintenance (Jones et al, 2014; Ngo et al, 2018). Here, we have demonstrated that HCT116 cells undergoing crisis require ATR-CHK1 activity. Hence, future research can target other components of A-NHEJ, SSBR and ATR-CHK1, such as XRCC1 and CDC25 phosphatases.

In this study, DNA-PKi NU7441, consistently prevented cells from escaping crisis at a concentration of 1 μM and 1.5 μM. Although we did not focus on this inhibitor due to other inhibitors being promising at a lower concentration, future studies could investigate the effect of DNA-PK inhibition on crisis. This could be studied using more potent inhibitors, such as AZD7648, which is highly selective and currently undergoing trials (Fok et al, 2019).

6.3.4 Future studies with TMM inhibitors

The activation of telomere maintenance mechanisms (TMM) is essential for escaping crisis. The main mechanism involves the reactivation of the reverse transcriptase telomerase, while a subset of cancer cells uses alternative lengthening of telomeres (ALT) (Nassour et al, 2021). Hence, targeting TMM could be vital for inhibiting the escape from crisis, as these mechanisms immortalise cancer cells. Imetelstat inhibits telomerase by binding to the telomerase RNA component TERC and it has progressed to clinical trials, showing promising clinical efficacy in essential thrombocythemia, myelofibrosis and lower-risk myelodysplastic syndrome (Claude and Decottignies, 2020; Recagni et al, 2020; Platzbecker et al, 2023). On the other hand, the limited knowledge about ALT has constrained the development of ALT inhibitors, but it has been shown that ATRX acts as an ALT inhibitor in the context of telomere dysfunction (Geiller et al, 2022; Recagni et al, 2020). Future studies exploring Imetelstat in the context of telomere crisis could offer valuable insights.

6.4 Conclusions

6.4.1 Project Conclusions

In summary, the data shown in this thesis demonstrated that:

- RAD51, RAD52 and WEE1 inhibition did not stop cells from escaping a telomere crisis
- ATR and CHK1 inhibition impaired escape from a telomere crisis, indicating the importance of the ATR-CHK1 pathway in cell survival during crisis
- ATR and CHK1 inhibition did not affect WT-HCT116 cells, unlike cells undergoing crisis
- Although CHK1 and ATR inhibition did not have a strong impact on cell growth, cell cycle progression and apoptosis prior to crisis, CHK1 inhibition (and to a lesser degree ATR inhibition) decreased cell growth, affected cell cycle progression and increased apoptosis during crisis
- ATR and CHK1 inhibition did not affect telomere erosion before or during crisis.
- ATR and CHK1 inhibition did not affect the number of fusion events before crisis, but CHK1 inhibition may increase telomere fusion during crisis
- Primary fibroblasts undergoing crisis were sensitive to CHK1 inhibition, but not to ATR inhibition
- CHK1 inhibition selectively reduced cell growth and increased apoptosis in older fibroblasts undergoing crisis, but not in younger fibroblasts
- ATR and CHK1 inhibition activated the DNA damage response
- Unexpectedly, ATR inhibition led to an upregulation of CHK1 activity, possibly by ATM
- Autophagy levels may be higher when cells are experiencing crisis

6.4.2 General Conclusion

Escape from a telomere-driven crisis is considered to promote cancer progression. We have shown that one of the pathways that contribute to escape from crisis is the ATR-CHK1 pathway, which regulates the intra S-phase and the G2/M cell cycle checkpoints amongst other functions. We have demonstrated that CHK1 inhibition selectively kills cells undergoing crisis and is more effective than ATR inhibition. We propose that CHK1 inhibition

increases DNA damage, which synergises with telomere damage generated during crisis to kill the cells. These findings suggest an intervention that could selectively sensitise cells with short and dysfunctional telomeres to therapy, offering an alternative therapy approach in the early stages of tumour progression.

Appendices

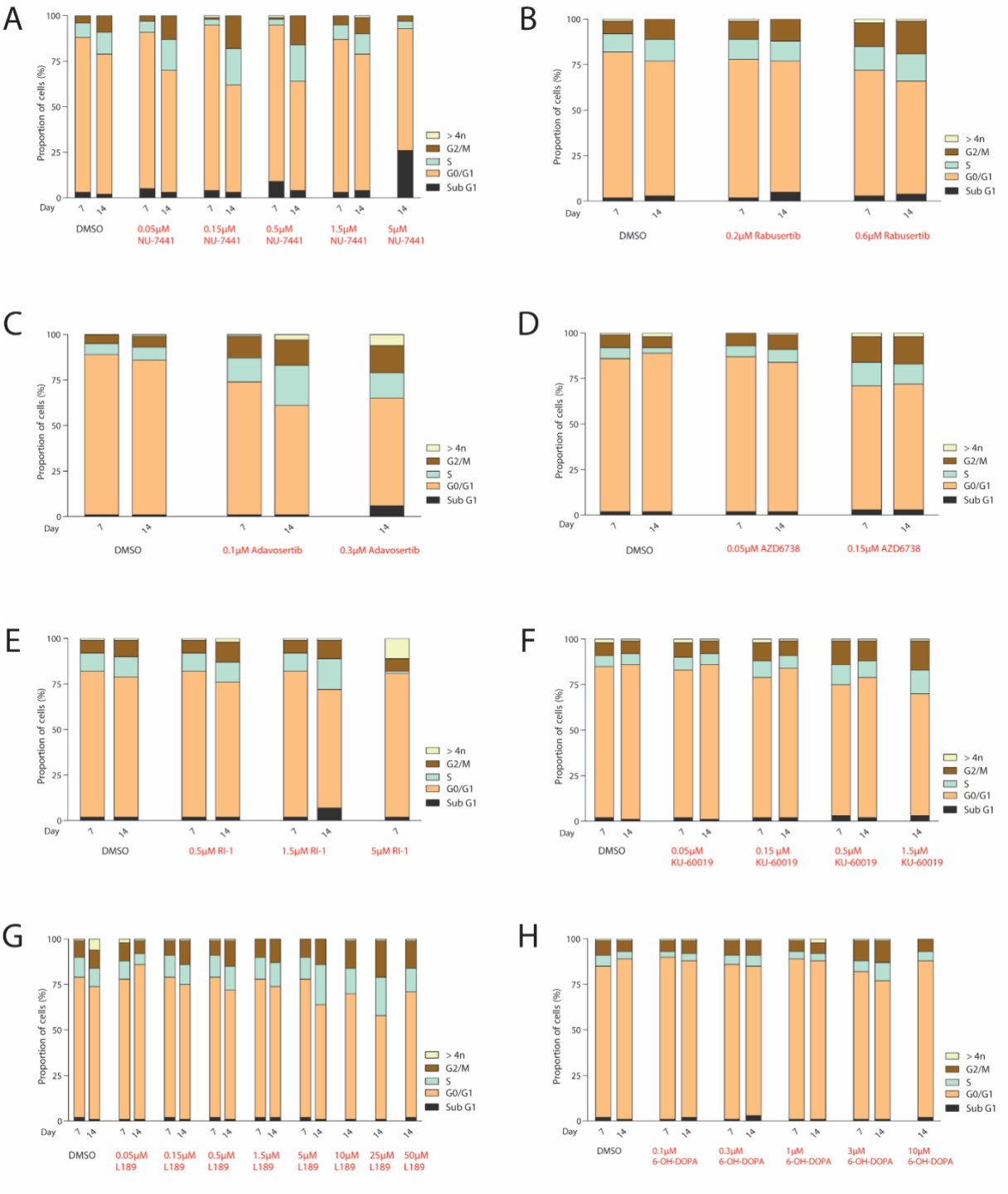

Appendix 1: Cell cycle analysis of WT-HCT116 cells treated with DDR inhibitors. The figure shows the cell cycle distribution of WT-HCT116 cells treated with DMSO and NU7441 (A), Rabusertib (B), Adavosertib (C), AZD6738 (D), RI-1 (E), KU-60019 (F), L189 (G) and 6-OH-DOPA (H).

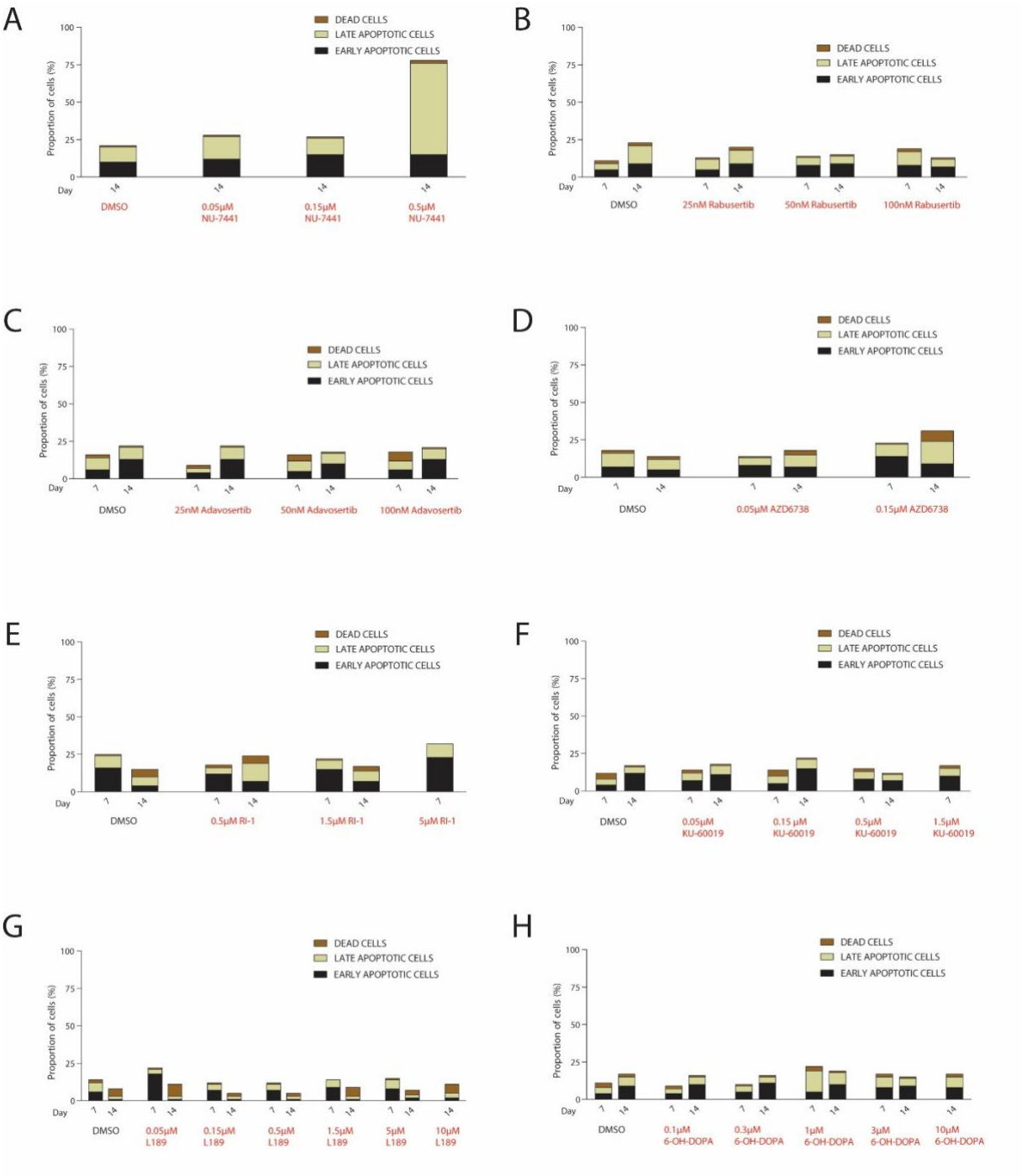

Appendix 2: Apoptosis analysis of WT-HCT116 cells treated with DDR inhibitors. The figure shows the apoptotic levels of WT-HCT116 cells treated with DMSO and NU7441 (A), Rabusertib (B), Adavosertib (C), AZD6738 (D), RI-1 (E), KU-60019 (F), L189 (G) and 6-OH-DOPA (H). Apoptosis was analysed using Annexin-V/propidium iodide (PI) staining. Cells are classified as early apoptotic when they are Annexin V positive and PI negative, late apoptotic when they are Annexin V and PI positive and dead when they are Annexin V negative and PI positive.

References

Abbotts, R., & Wilson, D. M. (2017). Coordination of DNA single Strand Break Repair. *Free Radical Biology and Medicine*, *107*, 228–244. https://doi.org/10.1016/j.freeradbiomed.2016.11.039

Agostini, L. C., Jain, A., Shupp, A., Nevler, A., McCarthy, G., Bussard, K. M., Yeo, C. J., & Brody, J. R. (2021). Combined targeting of PARG and WEE1 causes decreased cell survival and DNA damage in an S-phase–dependent manner. *Molecular Cancer Research*, *19*(2), 207–214. https://doi.org/10.1158/1541-7786.mcr-20-0708

Aguilar-Morante, D., Juul Elbæk, K., Frias, A., & Hamerlik, P. (2018). RDNA-16. the role of RAD52 in genomic instability and therapeutic resistance of malignant gliomas. *Neuro-Oncology*, *20*(suppl_6), vi224–vi224. https://doi.org/10.1093/neuonc/noy148.930

Alcaraz-Sanabria, A., Nieto-Jiménez, C., Corrales-Sánchez, V., Serrano-Oviedo, L., Andrés-Pretel, F., Montero, J. C., Burgos, M., Llopis, J., Galán-Moya, E. M., Pandiella, A., & Ocaña, A. (2017). Synthetic lethality interaction between Aurora kinases and CHEK1 inhibitors in ovarian cancer. *Molecular Cancer Therapeutics*, *16*(11), 2552–2562. https://doi.org/10.1158/1535-7163.mct-17-0223

Anand, R. P., Lovett, S. T., & Haber, J. E. (2013). Break-induced DNA replication. *Cold Spring Harbor Perspectives in Biology*, *5*(12). https://doi.org/10.1101/cshperspect.a010397

Ando, K., Nakamura, Y., Nagase, H., Nakagawara, A., Koshinaga, T., Wada, S., & Makishima, M. (2019). Co-inhibition of the DNA damage response and Chk1 enhances apoptosis of neuroblastoma cells. *International Journal of Molecular Sciences*, *20*(15), 3700. https://doi.org/10.3390/ijms20153700

Artandi, S. E., Chang, S., Lee, S.-L., Alson, S., Gottlieb, G. J., Chin, L., & DePinho, R. A. (2000). Telomere dysfunction promotes non-reciprocal translocations and epithelial cancers in mice. *Nature*, *406*(6796), 641–645. https://doi.org/10.1038/35020592

Bačević, K., Lossaint, G., Achour, T. N., Georget, V., Fisher, D., & Dulić, V. (2017). Cdk2 strengthens the intra-S checkpoint and counteracts cell cycle exit induced by DNA damage. *Scientific Reports*, *7*(1). https://doi.org/10.1038/s41598-017-12868-5

Baird, D. M., Rowson, J., Wynford-Thomas, D., & Kipling, D. (2003). Extensive allelic variation and ultrashort telomeres in senescent human cells. *Nature Genetics*, *33*(2), 203–207. https://doi.org/10.1038/ng1084

Balboni, B., Rinaldi, F., Previtali, V., Ciamarone, A., Girotto, S., & Cavalli, A. (2023). Novel insights into RAD52's structure, function, and druggability for synthetic lethality and innovative anticancer therapies. *Cancers*, *15*(6), 1817. https://doi.org/10.3390/cancers15061817

Balbous, A., Cortes, U., Guilloteau, K., Rivet, P., Pinel, B., Duchesne, M., Godet, J., Boissonnade, O., Wager, M., Bensadoun, R. J., Chomel, J.-C., & Karayan-Tapon, L. (2016). A radiosensitizing effect of RAD51 inhibition in glioblastoma stem-like cells. *BMC Cancer*, *16*(1). https://doi.org/10.1186/s12885-016-2647-9

Barnes, R. P., Fouquerel, E., & Opresko, P. L. (2019). The impact of oxidative DNA damage and stress on telomere homeostasis. *Mechanisms of Ageing and Development*, *177*, 37–45. https://doi.org/10.1016/j.mad.2018.03.013

Barnieh, F. M., Loadman, P. M., & Falconer, R. A. (2021). Progress towards a clinically-successful ATR inhibitor for cancer therapy. *Current Research in Pharmacology and Drug Discovery*, *2*, 100017. https://doi.org/10.1016/j.crphar.2021.100017

Barrett, J. H., Iles, M. M., Dunning, A. M., & Pooley, K. A. (2015). Telomere length and common disease: Study design and Analytical Challenges. *Human Genetics*, *134*(7), 679–689. https://doi.org/10.1007/s00439-015-1563-4

Barthel, F. P., Wei, W., Tang, M., Martinez-Ledesma, E., Hu, X., Amin, S. B., Akdemir, K. C., Seth, S., Song, X., Wang, Q., Lichtenberg, T., Hu, J., Zhang, J., Zheng, S., & Verhaak, R. G. (2017). Systematic analysis of telomere length and somatic alterations in 31 cancer types. *Nature Genetics*, *49*(3), 349–357. https://doi.org/10.1038/ng.3781

Beard, W. A., Horton, J. K., Prasad, R., & Wilson, S. H. (2019). Eukaryotic base excision repair: New approaches Shine light on mechanism. *Annual Review of Biochemistry*, *88*(1), 137–162. https://doi.org/10.1146/annurev-biochem-013118-111315

Berte, N., Piée-Staffa, A., Piecha, N., Wang, M., Borgmann, K., Kaina, B., & Nikolova, T. (2016). Targeting homologous recombination by pharmacological inhibitors enhances the killing response of glioblastoma cells treated with alkylating drugs. *Molecular Cancer Therapeutics*, *15*(11), 2665–2678. https://doi.org/10.1158/1535-7163.mct-16-0176

Biddlestone-Thorpe, L., Sajjad, M., Rosenberg, E., Beckta, J. M., Valerie, N. C. K., Tokarz, M., Adams, B. R., Wagner, A. F., Khalil, A., Gilfor, D., Golding, S. E., Deb, S., Temesi, D. G., Lau, A., O'Connor, M. J., Choe, K. S., Parada, L. F., Lim, S. K., Mukhopadhyay, N. D., & Valerie, K. (2013). ATM kinase inhibition preferentially sensitizes p53-mutant glioma to ionizing radiation. *Clinical Cancer Research*, *19*(12), 3189–3200. https://doi.org/10.1158/1078-0432.ccr-12-3408

Blackford, A. N., & Jackson, S. P. (2017). ATM, ATR, and DNA-PK: The Trinity at the heart of the DNA damage response. *Molecular Cell*, *66*(6), 801–817. https://doi.org/10.1016/j.molcel.2017.05.015

Bonilla, B., Hengel, S. R., Grundy, M. K., & Bernstein, K. A. (2020). *rad51* gene family structure and function. *Annual Review of Genetics*, *54*(1), 25–46. https://doi.org/10.1146/annurev-genet-021920-092410

Bowler, E., Skwarska, A., Wilson, J. D., Ramachandran, S., Bolland, H., Easton, A., Ostheimer, C., Hwang, M.-S., Leszczynska, K. B., Conway, S. J., & Hammond, E. M. (2020). Pharmacological inhibition of ATR can block autophagy through an ATR-independent mechanism. *iScience*, *23*(11), 101668. https://doi.org/10.1016/j.isci.2020.101668

Brambati, A., Barry, R. M., & Sfeir, A. (2020). DNA polymerase theta (polθ) – an error-prone polymerase necessary for genome stability. *Current Opinion in Genetics & Development*, *60*, 119–126. https://doi.org/10.1016/j.gde.2020.02.017

Brambati, A., Sacco, O., Porcella, S., Heyza, J., Kareh, M., Schmidt, J. C., & Sfeir, A. (2023). Rhino directs MMEJ to repair DNA breaks in mitosis. *Science*, *381*(6658), 653–660. https://doi.org/10.1126/science.adh3694

Brunner, A., Suryo Rahmanto, A., Johansson, H., Franco, M., Viiliäinen, J., Gazi, M., Frings, O., Fredlund, E., Spruck, C., Lehtiö, J., Rantala, J. K., Larsson, L.-G., & Sangfelt, O. (2020). PTEN and DNA-PK determine sensitivity and recovery in response to WEE1 inhibition in human breast cancer. *eLife*, *9*. https://doi.org/10.7554/elife.57894

Budke, B., Logan, H. L., Kalin, J. H., Zelivianskaia, A. S., Cameron McGuire, W., Miller, L. L., Stark, J. M., Kozikowski, A. P., Bishop, D. K., & Connell, P. P. (2012). RI-1: A chemical inhibitor of RAD51 that disrupts homologous recombination in human cells. *Nucleic Acids Research*, *40*(15), 7347–7357. https://doi.org/10.1093/nar/gks353

Bukhari, A. B., Chan, G. K., & Gamper, A. M. (2022). Targeting the DNA damage response for cancer therapy by inhibiting the kinase WEE1. *Frontiers in Oncology*, *12*. https://doi.org/10.3389/fonc.2022.828684

Calvo, E., Braiteh, F., Von Hoff, D., McWilliams, R., Becerra, C., Galsky, M. D., Jameson, G., Lin, J., McKane, S., Wickremsinhe, E. R., Hynes, S. M., Bence Lin, A., Hurt, K., & Richards, D. (2016). Phase I study of Chk1 inhibitor ly2603618 in combination with gemcitabine in patients with solid tumors. *Oncology*, *91*(5), 251–260. https://doi.org/10.1159/000448621

Calvo, E., Chen, V. J., Marshall, M., Ohnmacht, U., Hynes, S. M., Kumm, E., Diaz, H. B., Barnard, D., Merzoug, F. F., Huber, L., Kays, L., Iversen, P., Calles, A., Voss, B., Lin, A. B., Dickgreber, N., Wehler, T., & Sebastian, M. (2014). Preclinical analyses and phase I

evaluation of ly2603618 administered in combination with pemetrexed and cisplatin in patients with advanced cancer. *Investigational New Drugs*, *32*(5), 955–968. https://doi.org/10.1007/s10637-014-0114-5

Capper, R., Britt-Compton, B., Tankimanova, M., Rowson, J., Letsolo, B., Man, S., Haughton, M., & Baird, D. M. (2007). The nature of telomere fusion and a definition of the critical telomere length in human cells. *Genes & Development*, *21*(19), 2495–2508. https://doi.org/10.1101/gad.439107

Carrassa, L., & Damia, G. (2017). DNA damage response inhibitors: Mechanisms and potential applications in cancer therapy. *Cancer Treatment Reviews*, *60*, 139–151. https://doi.org/10.1016/j.ctrv.2017.08.013

Cesare, A. J., & Karlseder, J. (2012). A three-state model of telomere control over human proliferative boundaries. *Current Opinion in Cell Biology*, *24*(6), 731–738. https://doi.org/10.1016/j.ceb.2012.08.007

Chakravarti, D., LaBella, K. A., & DePinho, R. A. (2021). Telomeres: History, health, and hallmarks of aging. *Cell*, *184*(2), 306–322. https://doi.org/10.1016/j.cell.2020.12.028

Chandramouly, G., McDevitt, S., Sullivan, K., Kent, T., Luz, A., Glickman, J. F., Andrake, M., Skorski, T., & Pomerantz, R. T. (2015). Small-molecule disruption of RAD52 rings as a mechanism for precision medicine in BRCA-deficient cancers. *Chemistry & Biology*, *22*(11), 1491–1504. https://doi.org/10.1016/j.chembiol.2015.10.003

Chen, Q., Cai, D., Li, M., & Wu, X. (2017). The homologous recombination protein rad51 is a promising therapeutic target for cervical carcinoma. *Oncology Reports*, *38*(2), 767–774. https://doi.org/10.3892/or.2017.5724

Chen, T., Middleton, F. K., Falcon, S., Reaper, P. M., Pollard, J. R., & Curtin, N. J. (2014). Development of pharmacodynamic biomarkers for ATR inhibitors. *Molecular Oncology*, *9*(2), 463–472. https://doi.org/10.1016/j.molonc.2014.09.012

Chen, X., Zhong, S., Zhu, X., Dziegielewska, B., Ellenberger, T., Wilson, G. M., MacKerell, A. D., & Tomkinson, A. E. (2008). Rational design of human DNA ligase inhibitors that target cellular DNA replication and Repair. *Cancer Research*, *68*(9), 3169–3177. https://doi.org/10.1158/0008-5472.can-07-6636

Chiba, K., Lorbeer, F. K., Shain, A. H., McSwiggen, D. T., Schruf, E., Oh, A., Ryu, J., Darzacq, X., Bastian, B. C., & Hockemeyer, D. (2017). Mutations in the promoter of the telomerase gene *tert* contribute to tumorigenesis by a two-step mechanism. *Science*, *357*(6358), 1416–1420. https://doi.org/10.1126/science.aao0535

Choi, W., & Lee, E. S. (2022). Therapeutic targeting of DNA damage response in cancer. *International Journal of Molecular Sciences*, *23*(3), 1701. https://doi.org/10.3390/ijms23031701

Claude, E., & Decottignies, A. (2020). Telomere maintenance mechanisms in cancer: Telomerase, ALT or lack thereof. *Current Opinion in Genetics & Development*, *60*, 1–8. https://doi.org/10.1016/j.gde.2020.01.002

Coppé, J.-P., Desprez, P.-Y., Krtolica, A., & Campisi, J. (2010). The senescence-associated secretory phenotype: The dark side of tumor suppression. *Annual Review of Pathology: Mechanisms of Disease*, *5*(1), 99–118. https://doi.org/10.1146/annurev-pathol-121808-102144

Cortés-Ciriano, I., Lee, J.-K., Xi, R., Jain, D., Jung, Y. L., Yang, L., Gordenin, D., Klimczak, L. J., Zhang, C.-Z., Pellman, D. S., & Park, P. J. (2020). *Comprehensive Analysis of Chromothripsis in 2,658 Human Cancers Using Whole-Genome Sequencing*. https://doi.org/10.1101/333617

Counter, C. M., Avilion, A. A., LeFeuvre, C. E., Stewart, N. G., Greider, C. W., Harley, C. B., & Bacchetti, S. (1992). Telomere shortening associated with chromosome instability is arrested in immortal cells which express telomerase activity. *The EMBO Journal*, *11*(5), 1921–1929. https://doi.org/10.1002/j.1460-2075.1992.tb05245.x

Davoli, T., & de Lange, T. (2012). Telomere-driven tetraploidization occurs in human cells undergoing crisis and promotes transformation of mouse cells. *Cancer Cell*, *21*(6), 765–776. https://doi.org/10.1016/j.ccr.2012.03.044

de Lange, T. (2018). Shelterin-mediated telomere protection. *Annual Review of Genetics*, *52*(1), 223–247. https://doi.org/10.1146/annurev-genet-032918-021921

Deckbar, D., Birraux, J., Krempler, A., Tchouandong, L., Beucher, A., Walker, S., Stiff, T., Jeggo, P., & Löbrich, M. (2007). Chromosome breakage after G2 checkpoint release. *The Journal of Cell Biology*, *176*(6), 749–755. https://doi.org/10.1083/jcb.200612047

Demanelis, K., Jasmine, F., Chen, L. S., Chernoff, M., Tong, L., Shinkle, J., Sabarinathan, M., Lin, H., Ramirez, E., Oliva, M., Kim-Hellmuth, S., Stranger, B. E., Ardlie, K. G., Aguet, F., Ahsan, H., Doherty, J., Kibriya, M. G., & Pierce, B. L. (2020). *Determinants of Telomere Length across Human Tissues*. https://doi.org/10.1101/793406

Dilley, R. L., & Greenberg, R. A. (2015). Alternative telomere maintenance and cancer. *Trends in Cancer*, *1*(2), 145–156. https://doi.org/10.1016/j.trecan.2015.07.007

Dillon, M. T., Barker, H. E., Pedersen, M., Hafsi, H., Bhide, S. A., Newbold, K. L., Nutting, C. M., McLaughlin, M., & Harrington, K. J. (2017). Radiosensitization by the ATR inhibitor

AZD6738 through generation of acentric micronuclei. *Molecular Cancer Therapeutics*, *16*(1), 25–34. https://doi.org/10.1158/1535-7163.mct-16-0239

Dillon, M. T., Bergerhoff, K. F., Pedersen, M., Whittock, H., Crespo-Rodriguez, E., Patin, E. C., Pearson, A., Smith, H. G., Paget, J. T. E., Patel, R. R., Foo, S., Bozhanova, G., Ragulan, C., Fontana, E., Desai, K., Wilkins, A. C., Sadanandam, A., Melcher, A., McLaughlin, M., & Harrington, K. J. (2019). ATR inhibition potentiates the radiation-induced inflammatory tumor microenvironment. *Clinical Cancer Research*, *25*(11), 3392–3403. https://doi.org/10.1158/1078-0432.ccr-18-1821

Ditano, J. P., & Eastman, A. (2021). Comparative activity and off-target effects in cells of the Chk1 inhibitors MK-8776, SRA737, and ly2606368. *ACS Pharmacology & Translational Science*, *4*(2), 730–743. https://doi.org/10.1021/acsptsci.0c00201

Do, K., Wilsker, D., Ji, J., Zlott, J., Freshwater, T., Kinders, R. J., Collins, J., Chen, A. P., Doroshow, J. H., & Kummar, S. (2015). Phase I study of single-agent Azd1775 (MK-1775), a wee1 kinase inhibitor, in patients with refractory solid tumors. *Journal of Clinical Oncology*, *33*(30), 3409–3415. https://doi.org/10.1200/jco.2014.60.4009

Doi, T., Yoshino, T., Shitara, K., Matsubara, N., Fuse, N., Naito, Y., Uenaka, K., Nakamura, T., Hynes, S. M., & Lin, A. B. (2015). Phase I study of Ly2603618, a Chk1 inhibitor, in combination with gemcitabine in Japanese patients with solid tumors. *Anti-Cancer Drugs*, *26*(10), 1043–1053. https://doi.org/10.1097/cad.0000000000000278

Dylgjeri, E., & Knudsen, K. E. (2022). DNA-pkcs: A targetable protumorigenic protein kinase. *Cancer Research*, *82*(4), 523–533. https://doi.org/10.1158/0008-5472.can-21-1756

Ehler, E., Babiychuk, E., & Draeger, A. (1996). Human Foetal Lung (IMR-90) cells: Myofibroblasts with smooth muscle-like contractile properties. *Cell Motility and the Cytoskeleton*, *34*(4), 288–298. https://doi.org/10.1002/(sici)1097-0169(1996)34:4<288::aid-cm4>3.0.co;2-4

Elbakry, A., & Löbrich, M. (2021). Homologous recombination subpathways: A tangle to resolve. *Frontiers in Genetics*, *12*. https://doi.org/10.3389/fgene.2021.723847

Ellenberger, T., & Tomkinson, A. E. (2008). Eukaryotic DNA ligases: Structural and functional insights. *Annual Review of Biochemistry*, *77*(1), 313–338. https://doi.org/10.1146/annurev.biochem.77.061306.123941

Fok, J. H., Ramos-Montoya, A., Vazquez-Chantada, M., Wijnhoven, P. W., Follia, V., James, N., Farrington, P. M., Karmokar, A., Willis, S. E., Cairns, J., Nikkilä, J., Beattie, D., Lamont, G. M., Finlay, M. R., Wilson, J., Smith, A., O'Connor, L. O., Ling, S., Fawell, S. E., … Cadogan, E. B. (2019). AZD7648 is a potent and selective DNA-PK inhibitor that enhances radiation,

chemotherapy and Olaparib activity. *Nature Communications*, *10*(1). https://doi.org/10.1038/s41467-019-12836-9

Foote, K. M., Nissink, J. W., McGuire, T., Turner, P., Guichard, S., Yates, J. W., Lau, A., Blades, K., Heathcote, D., Odedra, R., Wilkinson, G., Wilson, Z., Wood, C. M., & Jewsbury, P. J. (2018). Discovery and characterization of AZD6738, a potent inhibitor of ataxia telangiectasia mutated and RAD3 related (ATR) kinase with application as an anticancer agent. *Journal of Medicinal Chemistry*, *61*(22), 9889–9907. https://doi.org/10.1021/acs.jmedchem.8b01187

Fouquerel, E., & Opresko, P. L. (2017). Convergence of the Nobel fields of telomere biology and dna repair. *Photochemistry and Photobiology*, *93*(1), 229–237. https://doi.org/10.1111/php.12672

Gachechiladze, M., Škarda, J., Soltermann, A., & Joerger, M. (2017). RAD51 as a potential surrogate marker for DNA repair capacity in solid malignancies. *International Journal of Cancer*, *141*(7), 1286–1294. https://doi.org/10.1002/ijc.30764

Geiller, H. E., Harvey, A., Jones, R. E., Grimstead, J. W., Cleal, K., Hendrickson, E. A., & Baird, D. M. (2022). ATRX modulates the escape from a telomere crisis. *PLOS Genetics*, *18*(11). https://doi.org/10.1371/journal.pgen.1010485

Geng, W., Tian, D., Wang, Q., Shan, S., Zhou, J., Xu, W., & Shan, H. (2019). DNA-PKcs inhibitor increases the sensitivity of gastric cancer cells to radiotherapy. *Oncology Reports*. https://doi.org/10.3892/or.2019.7187

Ghosh, D., & Raghavan, S. C. (2021). Nonhomologous end joining: New accessory factors fine tune the machinery. *Trends in Genetics*, *37*(6), 582–599. https://doi.org/10.1016/j.tig.2021.03.001

Ghosh, G., Wang, V. Y., Huang, D., & Fusco, A. (2012). NF-KB regulation: Lessons from structures. *Immunological Reviews*, *246*(1), 36–58. https://doi.org/10.1111/j.1600-065x.2012.01097.x

Giardini, M. A., Segatto, M., da Silva, M. S., Nunes, V. S., & Cano, M. I. (2014). Telomere and telomerase biology. *Progress in Molecular Biology and Translational Science*, 1–40. https://doi.org/10.1016/b978-0-12-397898-1.00001-3

Gire, V. (2004). Dysfunctional telomeres at senescence signal cell cycle arrest via CHK2. *Cell Cycle*, *3*(10), 1217–1220. https://doi.org/10.4161/cc.3.10.1167

Golding, S. E., Rosenberg, E., Valerie, N., Hussaini, I., Frigerio, M., Cockcroft, X. F., Chong, W. Y., Hummersone, M., Rigoreau, L., Menear, K. A., O'Connor, M. J., Povirk, L. F., van Meter, T.,

& Valerie, K. (2009). Improved ATM kinase inhibitor KU-60019 radiosensitizes glioma cells, compromises insulin, Akt and ERK prosurvival signaling, and inhibits migration and invasion. *Molecular Cancer Therapeutics*, *8*(10), 2894–2902. https://doi.org/10.1158/1535-7163.mct-09-0519

Gomez, M. K., Illuzzi, G., Colomer, C., Churchman, M., Hollis, R. L., O'Connor, M. J., Gourley, C., Leo, E., & Melton, D. W. (2020). Identifying and overcoming mechanisms of PARP inhibitor resistance in homologous recombination repair-deficient and repair-proficient high grade serous ovarian cancer cells. *Cancers*, *12*(6), 1503. https://doi.org/10.3390/cancers12061503

González-Gualda, E., Baker, A. G., Fruk, L., & Muñoz-Espín, D. (2020). A guide to assessing cellular senescence *in vitro* and *in vivo*. *The FEBS Journal*, *288*(1), 56–80. https://doi.org/10.1111/febs.15570

Gorecki, L., Andrs, M., & Korabecny, J. (2021). Clinical candidates targeting the ATR–chk1–wee1 axis in cancer. *Cancers*, *13*(4), 795. https://doi.org/10.3390/cancers13040795

Gottifredi, V., & Wiesmüller, L. (2020). Current understanding of RAD52 functions: Fundamental and therapeutic insights. *Cancers*, *12*(3), 705. https://doi.org/10.3390/cancers12030705

Groelly, F. J., Fawkes, M., Dagg, R. A., Blackford, A. N., & Tarsounas, M. (2022). Targeting DNA damage response pathways in cancer. *Nature Reviews Cancer*, *23*(2), 78–94. https://doi.org/10.1038/s41568-022-00535-5

Gunes, C., Avila, A. I., & Rudolph, K. L. (2018). Telomeres in cancer. *Differentiation*, *99*, 41–50. https://doi.org/10.1016/j.diff.2017.12.004

Guo, Z., Deshpande, R., & Paull, T. T. (2010). ATM activation in the presence of oxidative stress . *Cell Cycle*, *9*(24), 4805–4811. https://doi.org/10.4161/cc.9.24.14323

Harata, S., Suzuki, T., Takahashi, H., Hirokawa, T., Kato, A., Watanabe, K., Yanagita, T., Ushigome, H., Shiga, K., Ogawa, R., Mitsui, A., Kimura, M., Matsuo, Y., & Takiguchi, S. (2023). AZD6738 promotes the tumor suppressive effects of trifluridine in colorectal cancer cells. *Oncology Reports*, *49*(3). https://doi.org/10.3892/or.2023.8489

Hatch, E. M. (2018). Nuclear envelope rupture: Little holes, big openings. *Current Opinion in Cell Biology*, *52*, 66–72. https://doi.org/10.1016/j.ceb.2018.02.001

Hayashi, M. T., Cesare, A. J., Rivera, T., & Karlseder, J. (2015). Cell death during crisis is mediated by mitotic telomere deprotection. *Nature*, *522*(7557), 492–496. https://doi.org/10.1038/nature14513

Hirai, H., Iwasawa, Y., Okada, M., Arai, T., Nishibata, T., Kobayashi, M., Kimura, T., Kaneko, N., Ohtani, J., Yamanaka, K., Itadani, H., Takahashi-Suzuki, I., Fukasawa, K., Oki, H., Nambu, T., Jiang, J., Sakai, T., Arakawa, H., Sakamoto, T., … Kotani, H. (2009). Small-molecule inhibition of wee1 kinase by MK-1775 selectively sensitizes p53-deficient tumor cells to DNA-damaging agents. *Molecular Cancer Therapeutics*, *8*(11), 2992–3000. https://doi.org/10.1158/1535-7163.mct-09-0463

Hoang, S. M., & O'Sullivan, R. J. (2020). Alternative lengthening of telomeres: Building bridges to connect chromosome ends. *Trends in Cancer*, *6*(3), 247–260. https://doi.org/10.1016/j.trecan.2019.12.009

Holstein, E., Ngo, H., Lawless, C., Banks, P., Greetham, M., Wilkinson, D. J., & Lydall, D. (2017). Systematic analysis of the DNA damage response network in telomere defective budding yeast. *G3: Genes, Genomes, Genetics*, *7*(7), 2375–2389. https://doi.org/10.1534/g3.117.042283

Hopkins, J. L., Lan, L., & Zou, L. (2022). DNA repair defects in cancer and therapeutic opportunities. *Genes & Development*, *36*(5–6), 278–293. https://doi.org/10.1101/gad.349431.122

Hu, J., Hwang, S. S., Liesa, M., Gan, B., Sahin, E., Jaskelioff, M., Ding, Z., Ying, H., Boutin, A. T., Zhang, H., Johnson, S., Ivanova, E., Kost-Alimova, M., Protopopov, A., Wang, Y. A., Shirihai, O. S., Chin, L., & DePinho, R. A. (2012). Antitelomerase therapy provokes alt and mitochondrial adaptive mechanisms in cancer. *Cell*, *148*(4), 651–663. https://doi.org/10.1016/j.cell.2011.12.028

Huang, R., & Zhou, P.-K. (2021). DNA damage repair: Historical perspectives, mechanistic pathways and clinical translation for targeted cancer therapy. *Signal Transduction and Targeted Therapy*, *6*(1). https://doi.org/10.1038/s41392-021-00648-7

Huang, X., Tran, T., Zhang, L., Hatcher, R., & Zhang, P. (2005). DNA damage-induced mitotic catastrophe is mediated by the Chk1-dependent mitotic exit DNA damage checkpoint. *Proceedings of the National Academy of Sciences*, *102*(4), 1065–1070. https://doi.org/10.1073/pnas.0409130102

Isono, M., Okubo, K., Asano, T., & Sato, A. (2022). Ataxia telangiectasia and RAD3-related inhibition by AZD6738 enhances gemcitabine-induced cytotoxic effects in bladder cancer cells. *PLOS ONE*, *17*(4). https://doi.org/10.1371/journal.pone.0266476

Jafri, M. A., Ansari, S. A., Alqahtani, M. H., & Shay, J. W. (2016). Roles of telomeres and telomerase in cancer, and advances in telomerase-targeted therapies. *Genome Medicine*, *8*(1). https://doi.org/10.1186/s13073-016-0324-x

Jahagirdar, D., Purohit, S., & Sharma, N. K. (2019). Combinatorial use of DNA ligase inhibitor L189 and temozolomide potentiates cell growth arrest in Hela. *Current Cancer Therapy Reviews*, *15*(1), 65–73. https://doi.org/10.2174/1573394714666180216150332

Jang, S., Ryu, S. M., Lee, J., Lee, H., Hong, S.-H., Ha, K.-S., Park, W. S., Han, E.-T., & Yang, S.-R. (2019). Bleomycin inhibits proliferation via Schlafen-mediated cell cycle arrest in mouse alveolar epithelial cells. *Tuberculosis and Respiratory Diseases*, *82*(2), 133. https://doi.org/10.4046/trd.2017.0124

Jiang, Y. (2022). Contribution of microhomology to genome instability: Connection between DNA repair and replication stress. *International Journal of Molecular Sciences*, *23*(21), 12937. https://doi.org/10.3390/ijms232112937

Jin, J., Fang, H., Yang, F., Ji, W., Guan, N., Sun, Z., Shi, Y., Zhou, G., & Guan, X. (2018). Combined inhibition of ATR and WEE1 as a novel therapeutic strategy in triple-negative breast cancer. *Neoplasia*, *20*(5), 478–488. https://doi.org/10.1016/j.neo.2018.03.003

Jin, M. H., & Oh, D.-Y. (2019). ATM in DNA repair in cancer. *Pharmacology & Therapeutics*, *203*, 107391. https://doi.org/10.1016/j.pharmthera.2019.07.002

Jones, R. E., Oh, S., Grimstead, J. W., Zimbric, J., Roger, L., Heppel, N. H., Ashelford, K. E., Liddiard, K., Hendrickson, E. A., & Baird, D. M. (2014). Escape from telomere-driven crisis is DNA ligase III dependent. *Cell Reports*, *8*(4), 1063–1076. https://doi.org/10.1016/j.celrep.2014.07.007

K. NAMBIAR, D., MISHRA, D., & P. SINGH, R. (2023). Targeting DNA repair for cancer treatment: Lessons from PARP inhibitor trials. *Oncology Research*, *31*(4), 405–421. https://doi.org/10.32604/or.2023.028310

Karlseder, J. (2020). Suppression of genomic instability by replicative senescence and Crisis. *Genome Instability & Disease*, *1*(3), 143–150. https://doi.org/10.1007/s42764-020-00013-y

Kendall, R. T., & Feghali-Bostwick, C. A. (2014). Fibroblasts in fibrosis: Novel roles and mediators. *Frontiers in Pharmacology*, *5*. https://doi.org/10.3389/fphar.2014.00123

Kim, H., Min, A., Im, S., Jang, H., Lee, K. H., Lau, A., Lee, M., Kim, S., Yang, Y., Kim, J., Kim, T. Y., Oh, D., Brown, J., O'Connor, M. J., & Bang, Y. (2016). Anti-tumor activity of the ATR inhibitor AZD6738 in HER2 positive breast cancer cells. *International Journal of Cancer*, *140*(1), 109–119. https://doi.org/10.1002/ijc.30373

Kim, H.-Y., Cho, Y., Kang, H., Yim, Y.-S., Kim, S.-J., Song, J., & Chun, K.-H. (2016). Targeting the Wee1 kinase as a molecular targeted therapy for gastric cancer. *Oncotarget*, *7*(31), 49902–

49916. https://doi.org/10.18632/oncotarget.10231

Kim, S. T., Smith, S. A., Mortimer, P., Loembé, A.-B., Cho, H., Kim, K.-M., Smith, C., Willis, S., Irurzun-Arana, I., Berges, A., Hong, J. Y., Park, S. H., Park, J. O., Park, Y. S., Lim, H. Y., Kang, W.

K., Kozarewa, I., Pierce, A. J., Dean, E., & Lee, J. (2021). Phase I study of Ceralasertib (AZD6738), a novel DNA damage repair agent, in combination with weekly paclitaxel in refractory cancer. *Clinical Cancer Research*, *27*(17), 4700–4709. https://doi.org/10.1158/1078-0432.ccr-21-0251

King, C., Diaz, H., Barnard, D., Barda, D., Clawson, D., Blosser, W., Cox, K., Guo, S., & Marshall, M. (2013). Characterization and preclinical development of ly2603618: A selective and potent Chk1 inhibitor. *Investigational New Drugs*, *32*(2), 213–226. https://doi.org/10.1007/s10637-013-0036-7

Kirkland, J. L. (2017). The path toward translating senolytic drugs into clinical treatments. *Innovation in Aging*, *1*(suppl_1), 743–743. https://doi.org/10.1093/geroni/igx004.2681

Kirkland, J. L., & Tchkonia, T. (2020). Senolytic drugs: From discovery to translation. *Journal of Internal Medicine*, *288*(5), 518–536. https://doi.org/10.1111/joim.13141

Klaeger, S., Heinzlmeir, S., Wilhelm, M., Polzer, H., Vick, B., Koenig, P.-A., Reinecke, M., Ruprecht, B., Petzoldt, S., Meng, C., Zecha, J., Reiter, K., Qiao, H., Helm, D., Koch, H., Schoof, M., Canevari, G., Casale, E., Depaolini, S. R., … Kuster, B. (2017). The target landscape of clinical kinase drugs. *Science*, *358*(6367). https://doi.org/10.1126/science.aan4368

Klionsky *et al*, (2016). Guidelines for the use and interpretation of assays for monitoring autophagy. *Autophagy*, 12(1), 1-222. doi: 10.1080/15548627.2015.1100356.

Kong, A., & Mehanna, H. (2021). WEE1 inhibitor: Clinical development. *Current Oncology Reports*, *23*(9). https://doi.org/10.1007/s11912-021-01098-8

Kopa, P., Macieja, A., Gulbas, I., Pastwa, E., & Poplawski, T. (2019). Inhibition of DNA-PK potentiates the synergistic effect of NK314 and etoposide combination on human glioblastoma cells. *Molecular Biology Reports*, *47*(1), 67–76. https://doi.org/10.1007/s11033-019-05105-x

Krejci, L., Altmannova, V., Spirek, M., & Zhao, X. (2012). Homologous recombination and its regulation. *Nucleic Acids Research*, *40*(13), 5795–5818. https://doi.org/10.1093/nar/gks270

Kumari, R., & Jat, P. (2021). Mechanisms of cellular senescence: Cell cycle arrest and senescence associated secretory phenotype. *Frontiers in Cell and Developmental Biology*, *9*. https://doi.org/10.3389/fcell.2021.645593

Kwok, M., Davies, N., Agathanggelou, A., Smith, E., Oldreive, C., Petermann, E., Stewart, G., Brown, J., Lau, A., Pratt, G., Parry, H., Taylor, M., Moss, P., Hillmen, P., & Stankovic, T. (2016). ATR inhibition induces synthetic lethality and overcomes chemoresistance in TP53- or ATM-defective chronic lymphocytic leukemia cells. *Blood*, *127*(5), 582–595. https://doi.org/10.1182/blood-2015-05-644872

Kwon, M., Kim, G., Kim, R., Kim, K.-T., Kim, S. T., Smith, S., Mortimer, P. G., Hong, J. Y., Loembé, A.-B., Irurzun-Arana, I., Koulai, L., Kim, K.-M., Kang, W. K., Dean, E., Park, W.-Y., & Lee, J. (2022). Phase II study of ceralasertib (AZD6738) in combination with durvalumab in patients with advanced gastric cancer. *Journal for ImmunoTherapy of Cancer*, *10*(7). https://doi.org/10.1136/jitc-2022-005041

Lambert, S. (2000). Characterization of mammalian RAD51 double strand break repair using non-lethal dominant-negative forms. *The EMBO Journal*, *19*(12), 3090–3099. https://doi.org/10.1093/emboj/19.12.3090

Laquente, B., Lopez-Martin, J., Richards, D., Illerhaus, G., Chang, D. Z., Kim, G., Stella, P., Richel, D., Szcylik, C., Cascinu, S., Frassineti, G. L., Ciuleanu, T., Hurt, K., Hynes, S., Lin, J., Lin, A. B., Von Hoff, D., & Calvo, E. (2017). A phase II study to evaluate ly2603618 in combination with gemcitabine in pancreatic cancer patients. *BMC Cancer*, *17*(1). https://doi.org/10.1186/s12885-017-3131-x

Lavin, M. F., & Yeo, A. J. (2020). Clinical potential of ATM inhibitors. *Mutation Research/Fundamental and Molecular Mechanisms of Mutagenesis*, *821*, 111695. https://doi.org/10.1016/j.mrfmmm.2020.111695

Lecona, E., & Fernandez-Capetillo, O. (2018). Targeting ATR in cancer. *Nature Reviews Cancer*, *18*(9), 586–595. https://doi.org/10.1038/s41568-018-0034-3

Lee, H. B., Schwab, T. L., Koleilat, A., Ata, H., Daby, C. L., Cervera, R. L., McNulty, M. S., Bostwick, H. S., & Clark, K. J. (2016). Allele-specific quantitative PCR for accurate, rapid, and cost-effective genotyping. *Human Gene Therapy*, *27*(6), 425–435. https://doi.org/10.1089/hum.2016.011

Lee, K. Y., & Dutta, A. (2021). Chk1 promotes non-homologous end joining in G1 through direct phosphorylation of ASF1A. *Cell Reports*, *34*(4), 108680. https://doi.org/10.1016/j.celrep.2020.108680

Leijen, S., van Geel, R. M. J. M., Pavlick, A. C., Tibes, R., Rosen, L., Razak, A. R., Lam, R., Demuth, T., Rose, S., Lee, M. A., Freshwater, T., Shumway, S., Liang, L. W., Oza, A. M., Schellens, J. H. M., & Shapiro, G. I. (2016). Phase I study evaluating wee1 inhibitor AZD1775 as monotherapy and in combination with gemcitabine, cisplatin, or carboplatin in patients with advanced solid tumors. *Journal of Clinical Oncology*, *34*(36), 4371–4380.

https://doi.org/10.1200/jco.2016.67.5991

Lewis, C. W., Jin, Z., Macdonald, D., Wei, W., Qian, X. J., Choi, W. S., He, R., Sun, X., & Chan, G. (2017). Prolonged mitotic arrest induced by WEE1 inhibition sensitizes breast cancer cells to paclitaxel. *Oncotarget*, *8*(43), 73705–73722. https://doi.org/10.18632/oncotarget.17848

Lheureux, S., Cristea, M. C., Bruce, J. P., Garg, S., Cabanero, M., Mantia-Smaldone, G., Olawaiye, A. B., Ellard, S. L., Weberpals, J. I., Wahner Hendrickson, A. E., Fleming, G. F., Welch, S., Dhani, N. C., Stockley, T., Rath, P., Karakasis, K., Jones, G. N., Jenkins, S., Rodriguez-Canales, J., … Oza, A. M. (2021). Adavosertib plus gemcitabine for platinum-resistant or platinum-refractory recurrent ovarian cancer: A double-blind, randomised, placebo-controlled, phase 2 trial. *The Lancet*, *397*(10271), 281–292. https://doi.org/10.1016/s0140-6736(20)32554-x

Li, K., Yan, H., Guo, W., Tang, M., Zhao, X., Tong, A., Peng, Y., Li, Q., & Yuan, Z. (2018). ATM inhibition induces synthetic lethality and enhances sensitivity of PTEN-deficient breast cancer cells to cisplatin. *Experimental Cell Research*, *366*(1), 24–33. https://doi.org/10.1016/j.yexcr.2018.03.006

Liao, C., Talluri, S., Zhao, J., Mu, S., Kumar, S., Shi, J., Buon, L., Munshi, N. C., & Shammas, M. A. (2022). RAD51 is implicated in DNA damage, chemoresistance and immune dysregulation in solid tumors. *Cancers*, *14*(22), 5697. https://doi.org/10.3390/cancers14225697

Lieber, M. R. (2010). The mechanism of double-strand DNA break repair by the nonhomologous DNA end-joining pathway. *Annual Review of Biochemistry*, *79*(1), 181–211. https://doi.org/10.1146/annurev.biochem.052308.093131

Lin, T. T., Letsolo, B. T., Jones, R. E., Rowson, J., Pratt, G., Hewamana, S., Fegan, C., Pepper, C., & Baird, D. M. (2010). Telomere dysfunction and fusion during the progression of chronic lymphocytic leukemia: Evidence for a telomere crisis. *Blood*, *116*(11), 1899–1907. https://doi.org/10.1182/blood-2010-02-272104

Liu, D., & Hornsby, P. J. (2007). Senescent human fibroblasts increase the early growth of xenograft tumors via matrix metalloproteinase secretion. *Cancer Research*, *67*(7), 3117–3126. https://doi.org/10.1158/0008-5472.can-06-3452

Liu, Q., Guntuku, S., Cui, X.-S., Matsuoka, S., Cortez, D., Tamai, K., Luo, G., Carattini-Rivera, S., DeMayo, F., Bradley, A., Donehower, L. A., & Elledge, S. J. (2000). Chk1 is an essential kinase that is regulated by ATR and required for the G2/m DNA damage checkpoint. *Genes & Development*, *14*(12), 1448–1459. https://doi.org/10.1101/gad.14.12.1448

Lo, A. W. l., Sabatier, L., Fouladi, B., Pottier, G., Ricoul, M., & Mumane, J. P. (2002). DNA amplification by breakage/fusion/bridge cycles initiated by spontaneous telomere loss in a human cancer cell line. *Neoplasia*, *4*(6), 531–538. https://doi.org/10.1038/sj.neo.7900267

Lok, B. H., & Powell, S. N. (2012). Molecular pathways: Understanding the role of RAD52 in homologous recombination for therapeutic advancement. *Clinical Cancer Research*, *18*(23), 6400–6406. https://doi.org/10.1158/1078-0432.ccr-11-3150

Lopez, M. F., Tollervey, J., Krastins, B., Garces, A., Sarracino, D., Prakash, A., Vogelsang, M., Geesman, G., Valderrama, A., Jordan, I. K., & Lunyak, V. V. (2012). Depletion of nuclear histone H2A variants is associated with chronic DNA damage signaling upon drug-evoked senescence of human somatic cells. *Aging*, *4*(11), 823–842. https://doi.org/10.18632/aging.100507

Maciejowski, J., & de Lange, T. (2017). Telomeres in cancer: Tumour suppression and genome instability. *Nature Reviews Molecular Cell Biology*, *18*(3), 175–186. https://doi.org/10.1038/nrm.2016.171

Maciejowski, J., Li, Y., Bosco, N., Campbell, P. J., & de Lange, T. (2015). Chromothripsis and Kataegis induced by telomere crisis. *Cell*, *163*(7), 1641–1654. https://doi.org/10.1016/j.cell.2015.11.054

Mah, L.-J., El-Osta, A., & Karagiannis, T. C. (2010). ГH2AX: A sensitive molecular marker of DNA damage and Repair. *Leukemia*, *24*(4), 679–686. https://doi.org/10.1038/leu.2010.6

Marechal, A., & Zou, L. (2013). DNA damage sensing by the ATM and ATR kinases. *Cold Spring Harbor Perspectives in Biology*, *5*(9). https://doi.org/10.1101/cshperspect.a012716

Marteijn, J. A., Lans, H., Vermeulen, W., & Hoeijmakers, J. H. (2014). Understanding nucleotide excision repair and its roles in cancer and ageing. *Nature Reviews Molecular Cell Biology*, *15*(7), 465–481. https://doi.org/10.1038/nrm3822

Matheson, C. J., Backos, D. S., & Reigan, P. (2016). Targeting wee1 kinase in cancer. *Trends in Pharmacological Sciences*, *37*(10), 872–881. https://doi.org/10.1016/j.tips.2016.06.006

Matt, S., & Hofmann, T. G. (2016). The DNA damage-induced cell death response: A roadmap to kill cancer cells. *Cellular and Molecular Life Sciences*, *73*(15), 2829–2850. https://doi.org/10.1007/s00018-016-2130-4

McCabe, N., Hanna, C., Walker, S. M., Gonda, D., Li, J., Wikstrom, K., Savage, K. I., Butterworth, K. T., Chen, C., Harkin, D. P., Prise, K. M., & Kennedy, R. D. (2015). Mechanistic rationale to target PTEN-deficient tumor cells with inhibitors of the DNA damage response kinase ATM. *Cancer Research*, *75*(11), 2159–2165. https://doi.org/10.1158/0008-5472.can-14-3502

McNeely, S., Beckmann, R., & Bence Lin, A. K. (2014). Chek again: Revisiting the development of Chk1 inhibitors for cancer therapy. *Pharmacology & Therapeutics*, *142*(1), 1–10. https://doi.org/10.1016/j.pharmthera.2013.10.005

Meng, X., Gao, J. Z., Gomendoza, S. M., Li, J. W., & Yang, S. (2021). Recent advances of WEE1 inhibitors and statins in cancers with P53 mutations. *Frontiers in Medicine*, *8*. https://doi.org/10.3389/fmed.2021.737951

Min, A., Im, S.-A., Jang, H., Kim, S., Lee, M., Kim, D. K., Yang, Y., Kim, H.-J., Lee, K.-H., Kim, J. W., Kim, T.-Y., Oh, D.-Y., Brown, J., Lau, A., O'Connor, M. J., & Bang, Y.-J. (2017). Azd6738, a novel oral inhibitor of ATR, induces synthetic lethality with ATM deficiency in gastric cancer cells. *Molecular Cancer Therapeutics*, *16*(4), 566–577. https://doi.org/10.1158/1535-7163.mct-16-0378

Mir, S. M., Samavarchi Tehrani, S., Goodarzi, G., Jamalpoor , Z., Jahanbakhsh, A., Khelghati, N., Qujeq, D., & Maniati, M. (2020). shelterin complex at telomeres: Implications in ageing . *Clinical Interventions in Aging*, *Volume 15*, 827–839. https://doi.org/10.2147/cia.s256425

Mitchell, T. J., Turajlic, S., Rowan, A., Nicol, D., Farmery, J. H. R., O'Brien, T., Martincorena, I., Tarpey, P., Angelopoulos, N., Yates, L. R., Butler, A. P., Raine, K., Stewart, G. D., Challacombe, B., Fernando, A., Lopez, J. I., Hazell, S., Chandra, A., Chowdhury, S., … Campbell, P. J. (2018). Timing the landmark events in the evolution of clear cell renal cell cancer: Tracerx renal. *Cell*, *173*(3). https://doi.org/10.1016/j.cell.2018.02.020

Mjelle, R., Hegre, S. A., Aas, P. A., Slupphaug, G., Drabløs, F., Sætrom, P., & Krokan, H. E. (2015). Cell cycle regulation of human DNA repair and chromatin remodeling genes. *DNA Repair*, *30*, 53–67. https://doi.org/10.1016/j.dnarep.2015.03.007

Mohiuddin, I. S., & Kang, M. H. (2019). DNA-PK as an emerging therapeutic target in cancer. *Frontiers in Oncology*, *9*. https://doi.org/10.3389/fonc.2019.00635

Moiseeva, T. N., Yin, Y., Calderon, M. J., Qian, C., Schamus-Haynes, S., Sugitani, N., Osmanbeyoglu, H. U., Rothenberg, E., Watkins, S. C., & Bakkenist, C. J. (2019). An ATR and Chk1 kinase signaling mechanism that limits origin firing during unperturbed DNA replication. *Proceedings of the National Academy of Sciences*, *116*(27), 13374–13383. https://doi.org/10.1073/pnas.1903418116

Monroe, J. D., Moolani, S. A., Irihamye, E. N., Speed, J. S., Gibert, Y., & Smith, M. E. (2020). RNA-seq analysis of Cisplatin and the monofunctional platinum(ii) complex, Phenanthriplatin, in A549 non-small cell lung cancer and IMR90 lung fibroblast cell lines. *Cells*, *9*(12), 2637. https://doi.org/10.3390/cells9122637

Montpetit, A. J., Alhareeri, A. A., Montpetit, M., Starkweather, A. R., Elmore, L. W., Filler, K., Mohanraj, L., Burton, C. W., Menzies, V. S., Lyon, D. E., & Jackson-Cook, C. K. (2014). Telomere length. *Nursing Research*, *63*(4), 289–299. https://doi.org/10.1097/nnr.0000000000000037

Moynahan, M. E., & Jasin, M. (2010). Mitotic homologous recombination maintains genomic stability and suppresses tumorigenesis. *Nature Reviews Molecular Cell Biology*, *11*(3), 196–207. https://doi.org/10.1038/nrm2851

Nassour, J., Aguiar, L. G., Correia, A., Schmidt, T. T., Mainz, L., Przetocka, S., Haggblom, C., Tadepalle, N., Williams, A., Shokhirev, M. N., Akincilar, S. C., Tergaonkar, V., Shadel, G. S., & Karlseder, J. (2023). Telomere-to-mitochondria signalling by ZBP1 mediates replicative crisis. *Nature*, *614*(7949), 767–773. https://doi.org/10.1038/s41586-023-05710-8

Nassour, J., Radford, R., Correia, A., Fusté, J. M., Schoell, B., Jauch, A., Shaw, R. J., & Karlseder, J. (2019). Autophagic cell death restricts chromosomal instability during replicative crisis. *Nature*, *565*(7741), 659–663. https://doi.org/10.1038/s41586-019-0885-0

Nassour, J., Schmidt, T. T., & Karlseder, J. (2021). Telomeres and cancer: Resolving the paradox. *Annual Review of Cancer Biology*, *5*(1), 59–77. https://doi.org/10.1146/annurev-cancerbio-050420-023410

Narita, M. (2019). Crisis management by Autophagy. *Nature Structural & Molecular Biology*, *26*(3), 151–152. https://doi.org/10.1038/s41594-019-0195-0

Neizer-Ashun, F., & Bhattacharya, R. (2021). Reality chek: Understanding the biology and clinical potential of CHK1. *Cancer Letters*, *497*, 202–211. https://doi.org/10.1016/j.canlet.2020.09.016

Neurohr, G. E., Terry, R. L., Lengefeld, J., Bonney, M., Brittingham, G. P., Moretto, F., Miettinen, T. P., Vaites, L. P., Soares, L. M., Paulo, J. A., Harper, J. W., Buratowski, S., Manalis, S., van Werven, F. J., Holt, L. J., & Amon, A. (2019). Excessive cell growth causes cytoplasm dilution and contributes to senescence. *Cell*, *176*(5). https://doi.org/10.1016/j.cell.2019.01.018

Ngo, G. H. P., & Lydall, D. (2015). The 9-1-1 checkpoint clamp coordinates resection at DNA double strand breaks. *Nucleic Acids Research*, *43*(10), 5017–5032. https://doi.org/10.1093/nar/gkv409

Ngo, G. H. P., Balakrishnan, L., Dubarry, M., Campbell, J. L., & Lydall, D. (2014). The 9-1-1 checkpoint clamp stimulates DNA resection by DNA2-Sgs1 and EXO1. *Nucleic Acids Research*, *42*(16), 10516–10528. https://doi.org/10.1093/nar/gku746

Ngo, G., Hyatt, S., Grimstead, J., Jones, R., Hendrickson, E., Pepper, C., & Baird, D. (2018). PARP inhibition prevents escape from a telomere-driven crisis and inhibits cell immortalisation. *Oncotarget*, *9*(101), 37549–37563. https://doi.org/10.18632/oncotarget.26499

Nichols, W. W., Murphy, D. G., Cristofalo, V. J., Toji, L. H., Greene, A. E., & Dwight, S. A. (1977). Characterization of a new human diploid cell strain, IMR-90. *Science*, *196*(4285), 60–63. https://doi.org/10.1126/science.841339

Nickoloff, J. A., Sharma, N., Taylor, L., Allen, S. J., & Hromas, R. (2021). The safe path at the fork: Ensuring replication-associated DNA double-strand breaks are repaired by homologous recombination. *Frontiers in Genetics*, *12*. https://doi.org/10.3389/fgene.2021.748033

Nik-Zainal, S., Alexandrov, L., Wedge, D., Van Loo, P., Raine, K., Jones, D. R., Futreal, P. A., Campbell, P. J., & Stratton, M. R. (2012). 604 cancer genomics, epigenetics and genomic instability. Mutational processes shaping the genomes of twenty-one breast cancers. *European Journal of Cancer*, *48*. https://doi.org/10.1016/s0959-8049(12)71258-3

Norris, K., Hillmen, P., Rawstron, A., Hills, R., Baird, D. M., Fegan, C. D., & Pepper, C. (2019). Telomere length predicts for outcome to FCR chemotherapy in CLL. *Leukemia*, *33*(8), 1953–1963. https://doi.org/10.1038/s41375-019-0389-9

O'Connor, M. J. (2015). Targeting the DNA damage response in cancer. *Molecular Cell*, *60*(4), 547–560. https://doi.org/10.1016/j.molcel.2015.10.040

O'Sullivan, R. J., Arnoult, N., Lackner, D. H., Oganesian, L., Haggblom, C., Corpet, A., Almouzni, G., & Karlseder, J. (2014). Rapid induction of alternative lengthening of telomeres by depletion of the histone chaperone ASF1. *Nature Structural & Molecular Biology*, *21*(2), 167–174. https://doi.org/10.1038/nsmb.2754

Ohtani, N. (2022). The roles and mechanisms of senescence-associated secretory phenotype (SASP): Can it be controlled by senolysis? *Inflammation and Regeneration*, *42*(1). https://doi.org/10.1186/s41232-022-00197-8

Okita, N., Minato, S., Ohmi, E., Tanuma, S., & Higami, Y. (2012). DNA damage-induced Chk1 autophosphorylation at SER296 is regulated by an intramolecular mechanism. *FEBS Letters*, *586*(22), 3974–3979. https://doi.org/10.1016/j.febslet.2012.09.048

Olovnikov, A. M. (1996). Telomeres, telomerase, and aging: Origin of the theory. *Experimental Gerontology*, *31*(4), 443–448. https://doi.org/10.1016/0531-5565(96)00005-8

Paculová, H., Kramara, J., Šimečková, Š., Fedr, R., Souček, K., Hylse, O., Paruch, K., Svoboda, M., Mistrík, M., & Kohoutek, J. (2017). BRCA1 or CDK12 loss sensitizes cells to Chk1 inhibitors. *Tumor Biology*, *39*(10), 101042831772747.

https://doi.org/10.1177/1010428317727479

Palii, S. S., Van Emburgh, B. O., Sankpal, U. T., Brown, K. D., & Robertson, K. D. (2008). DNA methylation inhibitor 5-aza-2'-deoxycytidine induces reversible genome-wide DNA damage that is distinctly influenced by DNA methyltransferases 1 and 3b. *Molecular and Cellular Biology*, *28*(2), 752–771. https://doi.org/10.1128/mcb.01799-07

Palm, W., & de Lange, T. (2008). How shelterin protects mammalian telomeres. *Annual Review of Genetics*, *42*(1), 301–334. https://doi.org/10.1146/annurev.genet.41.110306.130350

Parsels, L. A., Qian, Y., Tanska, D. M., Gross, M., Zhao, L., Hassan, M. C., Arumugarajah, S., Parsels, J. D., Hylander-Gans, L., Simeone, D. M., Morosini, D., Brown, J. L., Zabludoff, S. D., Maybaum, J., Lawrence, T. S., & Morgan, M. A. (2011). Assessment of chk1 phosphorylation as a pharmacodynamic biomarker of Chk1 inhibition. *Clinical Cancer Research*, *17*(11), 3706–3715. https://doi.org/10.1158/1078-0432.ccr-10-3082

Pearl, L. H., Schierz, A. C., Ward, S. E., Al-Lazikani, B., & Pearl, F. M. (2015). Therapeutic opportunities within the DNA damage response. *Nature Reviews Cancer*, *15*(3), 166–180. https://doi.org/10.1038/nrc3891

Pećina-Šlaus, N., Kafka, A., Salamon, I., & Bukovac, A. (2020). Mismatch repair pathway, genome stability and cancer. *Frontiers in Molecular Biosciences*, *7*. https://doi.org/10.3389/fmolb.2020.00122

Peddibhotla, S., Lam, M. H., Gonzalez-Rimbau, M., & Rosen, J. M. (2009). The DNA-damage effector checkpoint kinase 1 is essential for chromosome segregation and cytokinesis. *Proceedings of the National Academy of Sciences*, *106*(13), 5159–5164. https://doi.org/10.1073/pnas.0806671106

Petering, D. H., Byrnes, R. W., & Antholine, W. E. (1990). The role of redox-active metals in the mechanism of action of Bleomycin. *Chemico-Biological Interactions*, *73*(2–3), 133–182. https://doi.org/10.1016/0009-2797(90)90001-4

Phan, L. M., & Rezaeian, A.-H. (2021). ATM: Main features, signaling pathways, and its diverse roles in DNA damage response, tumor suppression, and cancer development. *Genes*, *12*(6), 845. https://doi.org/10.3390/genes12060845

Pilié, P. G., Tang, C., Mills, G. B., & Yap, T. A. (2018). State-of-the-art strategies for targeting the DNA damage response in cancer. *Nature Reviews Clinical Oncology*, *16*(2), 81–104. https://doi.org/10.1038/s41571-018-0114-z

Pismataro, M. C., Astolfi, A., Barreca, M. L., Pacetti, M., Schenone, S., Bandiera, T., Carbone,

A., & Massari, S. (2023). Small molecules targeting DNA polymerase theta (polθ) as promising synthetic lethal agents for precision cancer therapy. *Journal of Medicinal Chemistry*, *66*(10), 6498–6522. https://doi.org/10.1021/acs.jmedchem.2c02101

Platzbecker, U., Santini, V., Fenaux, P., Sekeres, M. A., Savona, M. R., Madanat, Y. F., Díez-Campelo, M., Valcárcel, D., Illmer, T., Jonášová, A., Bělohlávková, P., Sherman, L. J., Berry, T., Dougherty, S., Shah, S., Xia, Q., Sun, L., Wan, Y., Huang, F., … Zeidan, A. M. (2023). Imetelstat in patients with lower-risk myelodysplastic syndromes who have relapsed or are refractory to erythropoiesis-stimulating agents (IMerge): A multinational, randomised, double-blind, placebo-controlled, phase 3 trial. *The Lancet*. https://doi.org/10.1016/s0140-6736(23)01724-5

Pradhan, S., Apaydin, S., Bucevičius, J., Gerasimaitė, R., Kostiuk, G., & Lukinavičius, G. (2023). Sequence-specific DNA labelling for fluorescence microscopy. *Biosensors and Bioelectronics*, *230*, 115256. https://doi.org/10.1016/j.bios.2023.115256

Reaper, P. M., Griffiths, M. R., Long, J. M., Charrier, J.-D., MacCormick, S., Charlton, P. A., Golec, J. M., & Pollard, J. R. (2011). Selective killing of ATM- or p53-deficient cancer cells through inhibition of ATR. *Nature Chemical Biology*, *7*(7), 428–430. https://doi.org/10.1038/nchembio.573

Recagni, M., Bidzinska, J., Zaffaroni, N., & Folini, M. (2020). The role of alternative lengthening of telomeres mechanism in cancer: Translational and therapeutic implications. *Cancers*, *12*(4), 949. https://doi.org/10.3390/cancers12040949

Restelli, V., Lupi, M., Chilà, R., Vagni, M., Tarantelli, C., Spriano, F., Gaudio, E., Bertoni, F., Damia, G., & Carrassa, L. (2019). DNA damage response inhibitor combinations exert synergistic antitumor activity in aggressive B-cell lymphomas. *Molecular Cancer Therapeutics*, *18*(7), 1255–1264. https://doi.org/10.1158/1535-7163.mct-18-0919

Roake, C. M., & Artandi, S. E. (2020). Regulation of human telomerase in homeostasis and disease. *Nature Reviews Molecular Cell Biology*, *21*(7), 384–397. https://doi.org/10.1038/s41580-020-0234-z

Rose, M., Burgess, J. T., O'Byrne, K., Richard, D. J., & Bolderson, E. (2020). PARP inhibitors: Clinical relevance, mechanisms of action and tumor resistance. *Frontiers in Cell and Developmental Biology*, *8*. https://doi.org/10.3389/fcell.2020.564601

Rossi, M. J., DiDomenico, S. F., Patel, M., & Mazin, A. V. (2021). RAD52: Paradigm of synthetic lethality and new developments. *Frontiers in Genetics*, *12*. https://doi.org/10.3389/fgene.2021.780293

Saldivar, J. C., Cortez, D., & Cimprich, K. A. (2017). The essential kinase ATR: Ensuring faithful duplication of a challenging genome. *Nature Reviews Molecular Cell Biology*, *18*(10), 622–636. https://doi.org/10.1038/nrm.2017.67

Satyavarapu, E. M., Das, R., Mandal, C., Mukhopadhyay, A., & Mandal, C. (2018). Autophagy-independent induction of LC3B through oxidative stress reveals its non-canonical role in Anoikis of Ovarian Cancer Cells. *Cell Death & Disease*, *9*(10). https://doi.org/10.1038/s41419-018-0989-8

Scagliotti, G., Kang, J. H., Smith, D., Rosenberg, R., Park, K., Kim, S.-W., Su, W.-C., Boyd, T. E., Richards, D. A., Novello, S., Hynes, S. M., Myrand, S. P., Lin, J., Smyth, E. N., Wijayawardana, S., Lin, A. B., & Pinder-Schenck, M. (2016). Phase II evaluation of LY2603618, a first-generation Chk1 inhibitor, in combination with pemetrexed in patients with advanced or metastatic non-small cell lung cancer. *Investigational New Drugs*, *34*(5), 625–635. https://doi.org/10.1007/s10637-016-0368-1

Shay, J. W. (2013). Are short telomeres predictive of advanced cancer? *Cancer Discovery*, *3*(10), 1096–1098. https://doi.org/10.1158/2159-8290.cd-13-0506

Shay, J. W. (2016). Role of telomeres and telomerase in aging and cancer. *Cancer Discovery*, *6*(6), 584–593. https://doi.org/10.1158/2159-8290.cd-16-0062

Shay, J. W., & Wright, W. E. (2019). Telomeres and telomerase: Three decades of progress. *Nature Reviews Genetics*, *20*(5), 299–309. https://doi.org/10.1038/s41576-019-0099-1

Sobinoff, A. P., & Pickett, H. A. (2017). Alternative lengthening of telomeres: DNA repair pathways converge. *Trends in Genetics*, *33*(12), 921–932. https://doi.org/10.1016/j.tig.2017.09.003

Sullivan, K., Cramer-Morales, K., McElroy, D. L., Ostrov, D. A., Haas, K., Childers, W., Hromas, R., & Skorski, T. (2016). Identification of a small molecule inhibitor of RAD52 by structure-based selection. *PLOS ONE*, *11*(1). https://doi.org/10.1371/journal.pone.0147230

Sun, Y., McCorvie, T. J., Yates, L. A., & Zhang, X. (2019). Structural basis of homologous recombination. *Cellular and Molecular Life Sciences*, *77*(1), 3–18. https://doi.org/10.1007/s00018-019-03365-1

Sunada, S., Kanai, H., Lee, Y., Yasuda, T., Hirakawa, H., Liu, C., Fujimori, A., Uesaka, M., & Okayasu, R. (2016). Nontoxic concentration of dna-pk inhibitor NU7441 radio-sensitizes lung tumor cells with little effect on double strand break repair. *Cancer Science*, *107*(9), 1250–1255. https://doi.org/10.1111/cas.12998

Sundar, R., Brown, J., Ingles Russo, A., & Yap, T. A. (2017). Targeting ATR in cancer medicine. *Current Problems in Cancer*, *41*(4), 302–315. https://doi.org/10.1016/j.currproblcancer.2017.05.002

Suzuki, T., Hirokawa, T., Maeda, A., Harata, S., Watanabe, K., Yanagita, T., Ushigome, H., Nakai, N., Maeda, Y., Shiga, K., Ogawa, R., Mitsui, A., Kimura, M., Matsuo, Y., Takahashi, H., & Takiguchi, S. (2022). ATR inhibitor AZD6738 increases the sensitivity of colorectal cancer cells to 5-fluorouracil by inhibiting repair of DNA damage. *Oncology Reports*, *47*(4). https://doi.org/10.3892/or.2022.8289

Tao, Y., Leteur, C., Yang, C., Zhang, P., Castedo, M., Pierré, A., Golsteyn, R. M., Bourhis, J., Kroemer, G., & Deutsch, E. (2009). Radiosensitization by Chir-124, a selective Chk1 inhibitor: Effects of p53 and cell cycle checkpoints. *Cell Cycle*, *8*(8), 1196–1205. https://doi.org/10.4161/cc.8.8.8203

Tomkinson, A. E., & Della-Maria, J. A. (2013). DNA ligases: Mechanism and functions. *Encyclopedia of Biological Chemistry*, 28–32. https://doi.org/10.1016/b978-0-12-378630-2.00303-0

Tozaki, Y., Aoki, H., Kato, R., Toriuchi, K., Arame, S., Inoue, Y., Hayashi, H., Kubota, E., Kataoka, H., & Aoyama, M. (2023). The combination of ATM and Chk1 inhibitors induces synthetic lethality in colorectal cancer cells. *Cancers*, *15*(3), 735. https://doi.org/10.3390/cancers15030735

van Harten, A. M., Buijze, M., van der Mast, R., Rooimans, M. A., Martens-de Kemp, S. R., Bachas, C., Brink, A., Stigter-van Walsum, M., Wolthuis, R. M., & Brakenhoff, R. H. (2019). Targeting the cell cycle in head and neck cancer by chk1 inhibition: A novel concept of Bimodal Cell Death. *Oncogenesis*, *8*(7). https://doi.org/10.1038/s41389-019-0147-x

Van Linden, A. A., Baturin, D., Ford, J. B., Fosmire, S. P., Gardner, L., Korch, C., Reigan, P., & Porter, C. C. (2013). Inhibition of wee1 sensitizes cancer cells to antimetabolite chemotherapeutics *in vitro* and *in vivo*, independent of p53 functionality. *Molecular Cancer Therapeutics*, *12*(12), 2675–2684. https://doi.org/10.1158/1535-7163.mct-13-0424

Vecchio, D., Daga, A., Carra, E., Marubbi, D., Raso, A., Mascelli, S., Nozza, P., Garrè, M. L., Pitto, F., Ravetti, J. L., Vagge, S., Corvò, R., Profumo, A., Baio, G., Marcello, D., & Frosina, G. (2014). Pharmacokinetics, pharmacodynamics and efficacy on pediatric tumors of the glioma radiosensitizer ku60019. *International Journal of Cancer*, *136*(6), 1445–1457. https://doi.org/10.1002/ijc.29121

Vendetti, F. P., Lau, A., Schamus, S., Conrads, T. P., O'Connor, M. J., & Bakkenist, C. J. (2015). The orally active and bioavailable ATR kinase inhibitor AZD6738 potentiates the anti-tumor

effects of cisplatin to resolve ATM-deficient non-small cell lung cancer*in vivo*. *Oncotarget*, *6*(42), 44289–44305. https://doi.org/10.18632/oncotarget.6247

Wallez, Y., Dunlop, C. R., Johnson, T. I., Koh, S.-B., Fornari, C., Yates, J. W. T., Bernaldo de Quirós Fernández, S., Lau, A., Richards, F. M., & Jodrell, D. I. (2018). The ATR inhibitor AZD6738 synergizes with gemcitabine *in vitro* and *in vivo* to induce pancreatic ductal adenocarcinoma regression. *Molecular Cancer Therapeutics*, *17*(8), 1670–1682. https://doi.org/10.1158/1535-7163.mct-18-0010

Wang, F.-Z., Fei, H., Cui, Y.-J., Sun, Y.-K., Li, Z.-M., Wang, X.-Y., Yang, X.-Y., Zhang, J.-G., & Sun, B.-L. (2014). The checkpoint 1 kinase inhibitor LY2603618 induces cell cycle arrest, DNA damage response and autophagy in cancer cells. *Apoptosis*, *19*(9), 1389–1398. https://doi.org/10.1007/s10495-014-1010-3

Warren, N. J., & Eastman, A. (2019). Comparison of the different mechanisms of cytotoxicity induced by checkpoint kinase I inhibitors when used as single agents or in combination with DNA damage. *Oncogene*, *39*(7), 1389–1401. https://doi.org/10.1038/s41388-019-1079-9

Wassing, I. E., Graham, E., Saayman, X., Rampazzo, L., Ralf, C., Bassett, A., & Esashi, F. (2021). The rad51 recombinase protects mitotic chromatin in human cells. *Nature Communications*, *12*(1). https://doi.org/10.1038/s41467-021-25643-y

WATSON, J. D. (1972). Origin of concatemeric T7DNA. *Nature New Biology*, *239*(94), 197–201. https://doi.org/10.1038/newbio239197a0

Weber, A. M., & Ryan, A. J. (2015). ATM and ATR as therapeutic targets in cancer. *Pharmacology & Therapeutics*, *149*, 124–138. https://doi.org/10.1016/j.pharmthera.2014.12.001

Wehler, T., Thomas, M., Schumann, C., Bosch-Barrera, J., Viñolas Segarra, N., Dickgreber, N. J., Dalhoff, K., Sebastian, M., Corral Jaime, J., Alonso, M., Hynes, S. M., Lin, J., Hurt, K., Bence Lin, A., Calvo, E., & Paz-Ares, L. (2017). A randomized, phase 2 evaluation of the Chk1 inhibitor, ly2603618, administered in combination with pemetrexed and cisplatin in patients with advanced nonsquamous non-small cell lung cancer. *Lung Cancer*, *108*, 212–216. https://doi.org/10.1016/j.lungcan.2017.03.001

Weiss, G. J., Donehower, R. C., Iyengar, T., Ramanathan, R. K., Lewandowski, K., Westin, E., Hurt, K., Hynes, S. M., Anthony, S. P., & McKane, S. (2012). Phase I dose-escalation study to examine the safety and tolerability of Ly2603618, a checkpoint 1 kinase inhibitor, administered 1 day after Pemetrexed 500 mg/M2 every 21 days in patients with cancer. *Investigational New Drugs*, *31*(1), 136–144. https://doi.org/10.1007/s10637-012-9815-9

Wilson, Z., Odedra, R., Wallez, Y., Wijnhoven, P. W. G., Hughes, A. M., Gerrard, J., Jones, G. N., Bargh-Dawson, H., Brown, E., Young, L. A., O'Connor, M. J., & Lau, A. (2022). ATR inhibitor AZD6738 (ceralasertib) exerts antitumor activity as a monotherapy and in combination with chemotherapy and the PARP inhibitor Olaparib. *Cancer Research*, *82*(6), 1140–1152. https://doi.org/10.1158/0008-5472.can-21-2997

Yanai, M., Makino, H., Ping, B., Takeda, K., Tanaka, N., Sakamoto, T., Yamaguchi, K., Kodani, M., Yamasaki, A., Igishi, T., & Shimizu, E. (2017). *DNA-PK inhibition by NU7441 enhances chemosensitivity to topoisomerase inhibitor in non-small cell lung carcinoma cells by blocking DNA damage repair*. Yonago acta medica, 60(1), 9-15.

Yang, C., Wang, Q., Liu, X., Cheng, X., Jiang, X., Zhang, Y., Feng, Z., & Zhou, P. (2016). NU7441 enhances the radiosensitivity of liver cancer cells. *Cellular Physiology and Biochemistry*, *38*(5), 1897–1905. https://doi.org/10.1159/000445551

Yue, X., Bai, C., Xie, D., Ma, T., & Zhou, P.-K. (2020). DNA-pkcs: A multi-faceted player in DNA damage response. *Frontiers in Genetics*, *11*. https://doi.org/10.3389/fgene.2020.607428

Zannini, L., Delia, D., & Buscemi, G. (2014). CHK2 kinase in the DNA damage response and beyond. *Journal of Molecular Cell Biology*, *6*(6), 442–457. https://doi.org/10.1093/jmcb/mju045

Zenvirt, S., Kravchenko-Balasha, N., & Levitzki, A. (2010). Status of p53 in human cancer cells does not predict efficacy of CHK1 kinase inhibitors combined with chemotherapeutic agents. *Oncogene*, *29*(46), 6149–6159. https://doi.org/10.1038/onc.2010.343

Zhang, B., Wu, H., Hao, J., Wu, Y., & Yang, B. (2020). Inhibition of DNA-pkcs activity re-sensitizes uveal melanoma cells to radio- and chemotherapy. *Biochemical and Biophysical Research Communications*, *522*(3), 639–646. https://doi.org/10.1016/j.bbrc.2019.11.133

Zhang, Y., & Hunter, T. (2013). Roles of Chk1 in Cell Biology and Cancer therapy. *International Journal of Cancer*, *134*(5), 1013–1023. https://doi.org/10.1002/ijc.28226

Zhao, F., Kim, W., Kloeber, J. A., & Lou, Z. (2020). DNA end resection and its role in DNA replication and DSB repair choice in mammalian cells. *Experimental & Molecular Medicine*, *52*(10), 1705–1714. https://doi.org/10.1038/s12276-020-00519-1

Zhao, J., Niu, X., Li, X., Edwards, H., Wang, G., Wang, Y., Taub, J. W., Lin, H., & Ge, Y. (2016). Inhibition of Chk1 enhances cell death induced by the BCL-2-selective inhibitor ABT-199 in acute myeloid leukemia cells. *Oncotarget*, *7*(23), 34785–34799. https://doi.org/10.18632/oncotarget.9185

Zhao, Q., Guan, J., Zhang, Z., Lv, J., Wang, Y., Liu, L., Zhou, Q., & Mao, W. (2017). Inhibition of RAD51 sensitizes breast cancer cells with wild-type PTEN to Olaparib. *Biomedicine & Pharmacotherapy*, *94*, 165–168. https://doi.org/10.1016/j.biopha.2017.07.090

Zhao, Y., Thomas, H. D., Batey, M. A., Cowell, I. G., Richardson, C. J., Griffin, R. J., Calvert, A. H., Newell, D. R., Smith, G. C. M., & Curtin, N. J. (2006). Preclinical evaluation of a potent novel DNA-dependent protein kinase inhibitor NU7441. *Cancer Research*, *66*(10), 5354–5362. https://doi.org/10.1158/0008-5472.can-05-4275